o. SE-7
o. 58

LOW COST SOLAR ARRAY PROJECT
Large Area Silicon Sheet Task

Dist. Category UC-63
DOE/JPL 954654-79/7

SILICON WEB PROCESS DEVELOPMENT

ANNUAL REPORT

April 1978-April 1979

C. S. Duncan, R. H. Hopkins, R. G. Seidensticker,
J. P. McHugh, F. E. Hill, M. E. Heimlich, J. M. Driggers
Westinghouse Research & Development Center
Pittsburgh, Pennsylvania 15235

Contract No. NAS 954654

"The JPL Low-Cost Silicon Solar Array Project is sponsored by the U. S. Department of Energy and forms part of the Solar Photovoltaic Conversion Program to initiate a major effort toward the development of low-cost solar arrays. This work was performed for the Jet Propulsion Laboratory, California Institute of Technology by agreement between NASA and DOE."

Westinghouse R&D Center
1310 Beulah Road
Pittsburgh, Pennsylvania 15235

LOW COST SOLAR ARRAY PROJECT
Large Area Silicon Sheet Task

SILICON WEB PROCESS DEVELOPMENT

ANNUAL REPORT

April 1978-April 1979

C. S. Duncan, R. H. Hopkins, R. G. Seidensticker,
J. P. McHugh, F. E. Hill, M. E. Heimlich, J. M. Driggers
Westinghouse Research & Development Center
Pittsburgh, Pennsylvania 15235

Contract No. NAS 954654

"The JPL Low-Cost Silicon Solar Array Project is sponsored by the U. S. Department of Energy and forms part of the Solar Photovoltaic Conversion Program to initiate a major effort toward the development of low-cost solar arrays. This work was performed for the Jet Propulsion Laboratory, California Institute of Technology by agreement between NASA and DOE."

Westinghouse R&D Center
1310 Beulah Road
Pittsburgh, Pennsylvania 15235

TECHNICAL CONTENT STATEMENT

"This report was prepared as an account of work sponsored by the United States Government. Neither the United States nor the United States Department of Energy, nor any of their employees, nor any of their contractors, subcontractors, or their employees, makes any warranty, express or implied, or assumes any legal liability or responsibility for the accuracy, completeness or usefulness of any information, apparatus, product or process disclosed, or represents that its use would not infringe privately owned rights."

TABLE OF CONTENTS

TABLE OF CONTENTS (Cont.)

LIST OF FIGURES

LIST OF FIGURES (Cont.)

LIST OF FIGURES (Cont.)

LIST OF FIGURES (Cont.)

LIST OF TABLES

1. SUMMARY

Silicon dendritic web, a single crystal ribbon shaped during growth by crystallographic forces and surface tension (rather than dies), is a highly promising base material for efficient low cost solar cells. The form of the product—smooth, flexible strips 100 to 200μm thick—conserves expensive silicon and facilitates automation of crystal growth and the subsequent manufacturing of solar cells. These characteristics, coupled with the highest demonstrated ribbon solar cell efficiency-15.5%-make silicon web a leading candidate to achieve, or better, the 1986 Low Cost Solar Array (LSA) Project cost objective of 50 cents per peak watt of photovoltaic output power.

The main objectives of the Phase II Web Program, technology development to significantly increase web output rate and to show the feasibility for simultaneous melt replenishment and growth, have largely been accomplished. Recently, web output rates of 23.6cm^2/min, nearly three times the 8cm^2/min maximum rate of a year ago, were achieved. We now have grown webs 4cm wide or greater, e.g. Figure 1, on a number of occasions. Moreover, these wide webs are free from the rippled texture accompanying growth of the widest Phase I ribbons.

These results have important economic, as well as technologic implications, viz. Figure 2. At the 23.6cm^2/min demonstrated output rate, the projected silicon web wafer plus polysilicon cost is about 12.8 cents per watt, or more than 3 cents per watt below the LSA 1986 cost goal of 16 cents per watt. Even if the future cost of polysilicon falls only to $25/kg, the projected web wafer plus polysilicon cost is 17 cents per watt, or within 1 cent of the LSA objective.

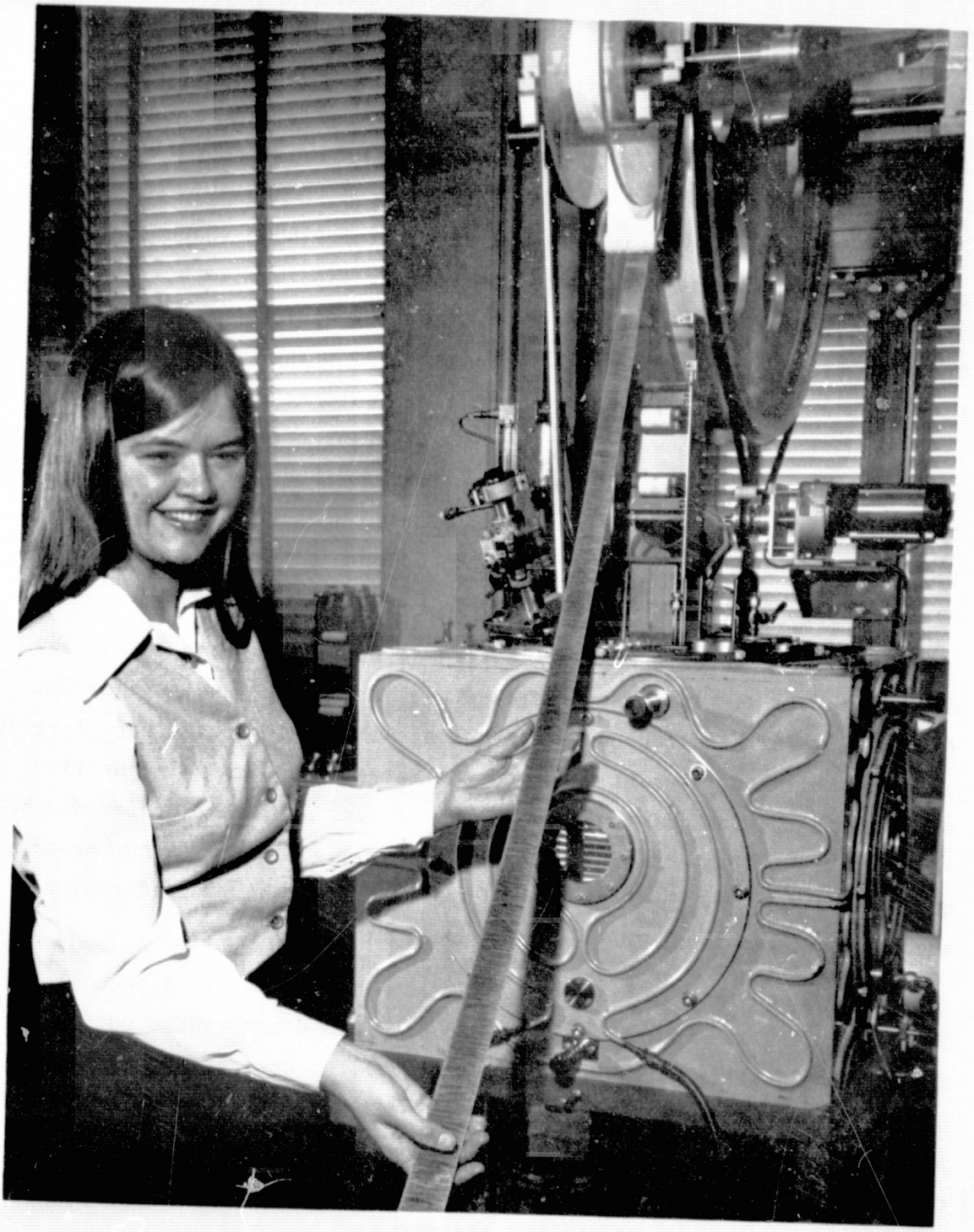

Figure 1 Maria Heimlich displays a 4cm wide silicon web crystal recently grown as part of the DOE/JPL Web Development Program.

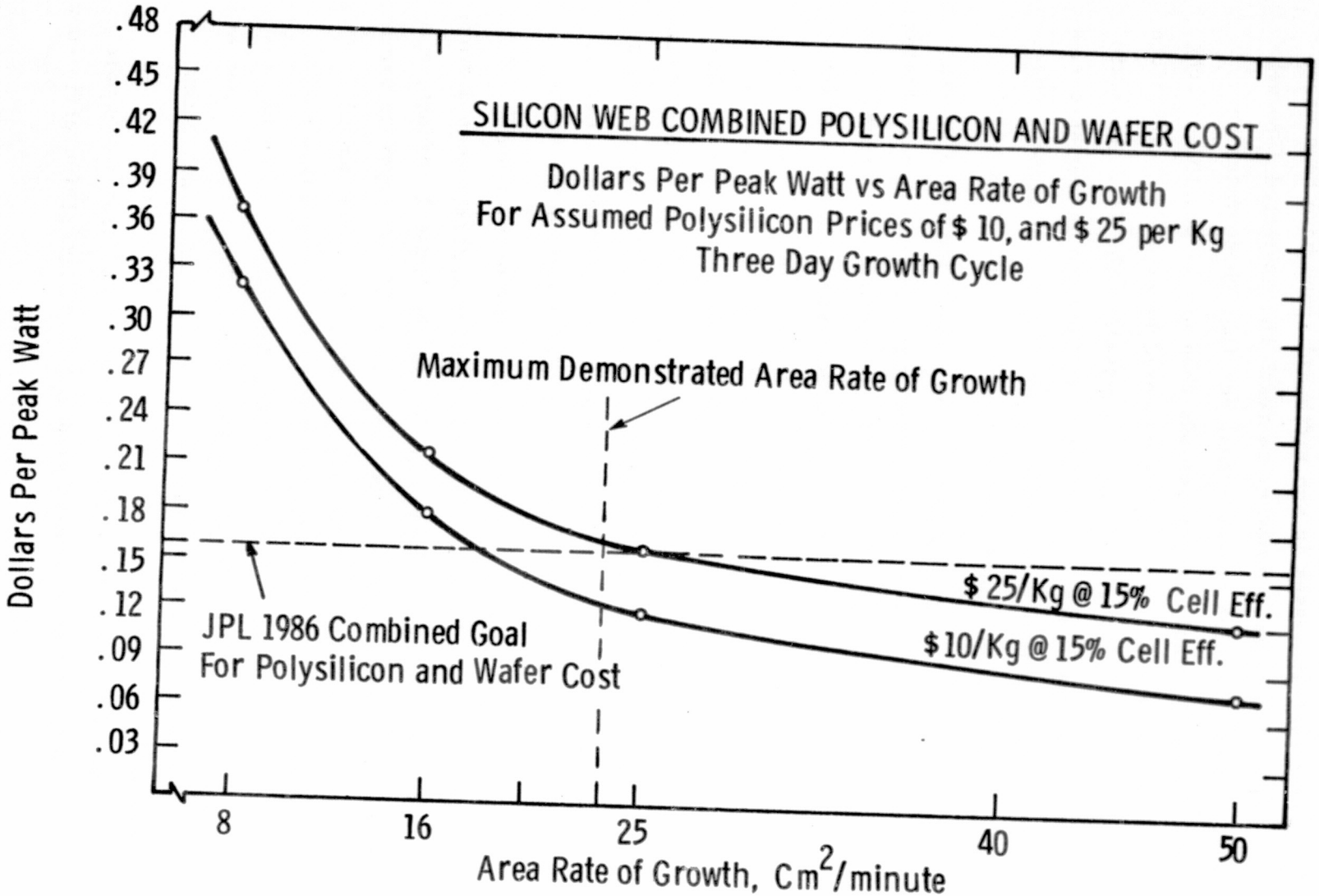

Figure 2 Projected silicon web wafer plus polycrystalline silicon price as a function of web output rate. Present maximum demonstrated output rate is indicated by the vertical dashed line.

Significant increases in web width and speed have been made during the Phase II program. However, to reach the projected 1986 web costs requires not only high output rates, but that these rates be sustainable for considerably longer periods than now is possible. Long term high output operation currently is hampered by depletion of silicon from the crucible as liquid transforms to crystal. The fall in liquid level reduces web growth rate and promotes an increase in web stress, a precursor to ribbon bending. Thus melt replenishment and closed loop level control are critical requirements for further web development.

A first step in establishing the necessary long term growth stability, development of melt replenishment technology, has been tested and shown feasible during this program. The feedstock, pelletized silicon, is injected into the melt from a programmable, mechanically-actuated pellet feeder while concurrently pulling a web crystal. The system employs a unique two compartment crucible design in which the melting pellets are separated from the growing web by a quartz barrier. A key result of these experiments was the demonstration that solar cells fabricated on the replenished material were just as efficient as cells fabricated on typical webs growth without melt replenishment. The feeding technique apparently introduces no undesirable contaminants.

Besides the important developments in output rate and replenishment technology, characterization studies indicate that average web solar cell efficiency has increased during the Phase II effort, and that further improvements can be expected. Over 180 web crystals grown under a variety of conditions typifying the range of experimental parameters studied in Phase II have been fabricated into solar cells. The average cell efficiency (AM1, AR coated) for the 740 cells was 13%, about 1% higher than the efficiency average during Phase I. As part of a companion program (JPL 95473), solar cells fabricated on web grown during the past year exhibited 15.5% AM1 conversion efficiency, the highest yet for any ribbon solar cell material. The first one square foot area web demonstration modules produced 11.5% conversion efficiency.

Most of the major technical requirements to produce silicon web suitable for low cost solar cells have now been demonstrated. These include output rate, cell efficiency, ribbon thickness, and tolerance to impurities (likely in solar grade silicon) sufficient to meet the 1986 LSA cost objectives. Future activity must be aimed at the development of an operational melt replenishment system and closed loop growth system controls so that high web output rates can be sustained for prolonged periods with a minimum of operator intervention.

2. INTRODUCTION

Silicon dendritic web is a single crystal silicon ribbon material with unique advantages for the manufacture of low cost solar cells. Shaped by the interplay of natural crystallographic and surface tension forces, rather than potentially contaminating dies, the web produces solar cells with excellent conversion efficiency. For example, during the past year an AM1 efficiency of 15.5% was demonstrated, so far the highest value reported for a ribbon material. The web process also conserves expensive silicon: the ribbons are thin as grown, 100 to 200 μm, and the facet-smooth surfaces require no costly cutting or etching before cell fabrication. Because impurities are rejected from the ribbon during crystal growth, it is feasible to use cheaper, less pure "solar" grades of silicon as feedstock for the web process. Finally, long flexible web strips facilitate automation of both crystal growth and the subsequent cell manufacturing operations. Taken together, these characteristics make the web process a leading candidate to achieve or better the 1986 Low Cost Solar Array (LSA) Project cost objectives of 50 cents per peak watt of photovoltaic output power.

Development of web technology has continued under Westinghouse funding, and under the auspices of the Department of Energy and the Jet Propulsion Laboratory, as part of the LSA Project, JPL Contract 954654. By the end of Phase I of that contract (April 1978) a number of important results had been obtained.[1] For example, web crystals over 3 cm wide had been grown (4 cm in very short segments) and a maximum web area output rate of 8 cm^2/min had been demonstrated. Stable growth of thin ($\leq$150μm) ribbons was readily achievable. Even in webs grown from silicon melts purposely contaminated with up to 40 parts per million of Cr, Mn, Fe or Ni, the crystal structure and cell performance were unimpaired so that the use of a "solar" grade feedstocks is feasible. Finally, web

solar cells, though unoptimized with respect to performance or material quality yielded efficiencies as high as 14.5% AM1 with a 12% average efficiency for all Phase I cells made and tested.

The Phase I study yielded significant improvements in web technology and also identified the requirements, or critical process developments, to achieve the 1986 cost objectives. These were derived from an economic analysis of the web process by the JPL SAMICS-IPEG approach.[1] Briefly, that analysis showed the web process can achieve the 1986 JPL wafer plus polycrystalline silicon cost goal at an area output rate of 25 cm^2/min, a polysilicon price of $25/kg, and 15% cell conversion efficiency assuming automated continuous growth for periods up to about 65 hours. When the polysilicon price falls to $10/kg, the projected wafer plus silicon cost for web is about $.04/watt below the JPL 1986 objective.

Clearly, improvements in output rate and in the ability to grow web for extended time periods were required. Because of its large leverage on system costs, an increase in cell efficiency was also desirable. For this reason development of technology to raise the output of the web process-to 25 cm^2/min became a major objective of the Phase II program described in this annual report. A second key objective of the Phase II study was to show the feasibility of melt replenishment so that stable growth conditions can be maintained for practical periods. This is the first step toward achieving a fully automated growth system. The material produced as part of the development effort was to be 100 to 200 μm thick, exhibit dislocation densities of 10^4 cm^{-2} or less and possess quality sufficient for the fabrication of 12% efficient solar cells.

The Phase II program approach utilized both active and passive thermal trimming and special growth lid designs to increase web width and growth velocity while minimizing stress in the material. Development of these techniques is an interactive process in which computer simulation of the growing ribbon is coupled with empirical evaluation of system parameters and hardware to improve web output rate.

Development of melt replenishment capability included investigations of mechanical and thermal requirements to feed pelletized silicon to the melt while simultaneously growing web crystal. The impact of changes in growth system parameters on web seeding and web quality were monitored by structural, electrical, and device measurements to assure that the material remains compatible with the fabrication of efficient solar cells. Finally, the economic analysis was updated to reflect the progress in web technology development.

The Phase II effort has been quite successful. We recently achieved an output rate of 23.6 cm^2/min, nearly three times the maximum value attained during the Phase I program and very close to our goal of 25 cm^2/min. Long webs over 4 cm wide were grown on a number of occasions. Not only are these recent webs wider than the earlier cr tals, but they also are free from the ripples often encountered in the widest Phase I material.[1]

At 23.6 cm^2/min the projected web polysilicon plus wafer costs is \$0.17 per watt (about a penny a watt above the 1986 target) with \$25/kg silicon, and \$0.13 per watt, or 3 cents below the 1986 goal, with \$10/kg silicon. The same assumptions regarding cell efficiency and growth cycle time described above hold for these calculations.

To achieve the projected costs requires that the web be grown at high output rates for prolonged times. We cannot yet do this; the falling melt level and ensuing changes in thermal environment produced as liquid transforms to web eventually reduces growth speed and promotes web deformation. A first step in eliminating this difficulty, introduction of melt replenishment technology, has been successfully tested as part of this program. The system employs a mechanically-actuated pellet feeder by which 1 to 2 mm sized silicon pellets can be inserted at a programmed rate into the liquid to maintain the level constant. A two compartment crucible in which the melt is self-leveling keeps the injected pellets from the growing web as they melt. Web crystals grown with simultaneous melt replenishment have yielded the same high average cell efficiencies as crystals grown without replenishment.

Besides improvements in web output rate and replenishment technology, characterization experiments on over 180 webs grown during Phase II indicate a general increase to 13% AM1 in average cell conversion efficiency compared with the 12% average efficiency typifying the Phase I study. This is despite the fact that no "standard" growth procedures are now employed-crystals are grown under a variety of conditions depending on the parameters being tested, e.g. to improve output rate. Web cell efficiencies as high as 15.5% and module efficiencies up to 11.5% were demonstrated as part of a companion program (JPL 954873). We expect these erficiencies will increase still further with improvement in cell processing and module fabrication.

The remaining sections of this annual report provide an overall picture of the results from over 380 experimental runs conducted as part of Phase II web development program. For specific details readers may consult previous quarterly reports,[2-4] the Growth Run Summary in Appendix 2, or the appended paper entitled, "Silicon Ribbon Growth by the Dendritic Web Process, a detailed discussion of the origin and control of stress in web crystals, the tolerance of web growth to impurities and recent backsurface field solar cell results.

3. PROGRESS IN WEB TECHNOLOGY DEVELOPMENT

3.1 Enhancement in Silicon Web Output Rate

Web crystals are grown from silicon held molten in a quartz crucible, Figure 3 , which is heated inductively through a molybdenum susceptor. System heat flow is controlled by a slotted molybdenum susceptor lid and heat shields through which the growing web also passes. The lid and shields shape the liquid isotherms so the center region is supercooled while the periphery remains hot enough to prevent freezing at the quartz crucible-melt interface. These elements in combination with thermal trimmers placed above the shields also define the temperature profile in the web crystal itself.

The rate at which liquid silicon is converted to web single crystal is determined by the product of the web width and growth velocity. Crystal width depends dominantly on the lateral temperature profile in the liquid while the dissipation of the latent heat of fusion controls the growth velocity. As we have noted before, the growth slot width, bevel angle, and lid thickness (and the level of the liquid in the cavity) have profound effects on web growth velocity, while the slot length, area and hole size are more important for controlling the melt temperature profile.[1,4]

As wider and wider web was grown, it became clear that the limitation to further width increase was no longer imposed by the melt profile. Instead stresses caused the wider crystals to deform, and structure to degrade.[4] For this reason a computer model of the stress in web was developed and verified to guide the implementation of thermal trimming elements which minimize web stress. Section 3.1.1 describes the model development and stress measurements in web; sections 3.1.2 and 3.1.3., respectively, highlight studies to improve web width and speed, while experiments coupling increases in web width and speed to maximize output rate are the subject of section 3.1.4.

Dwg. 7686A17

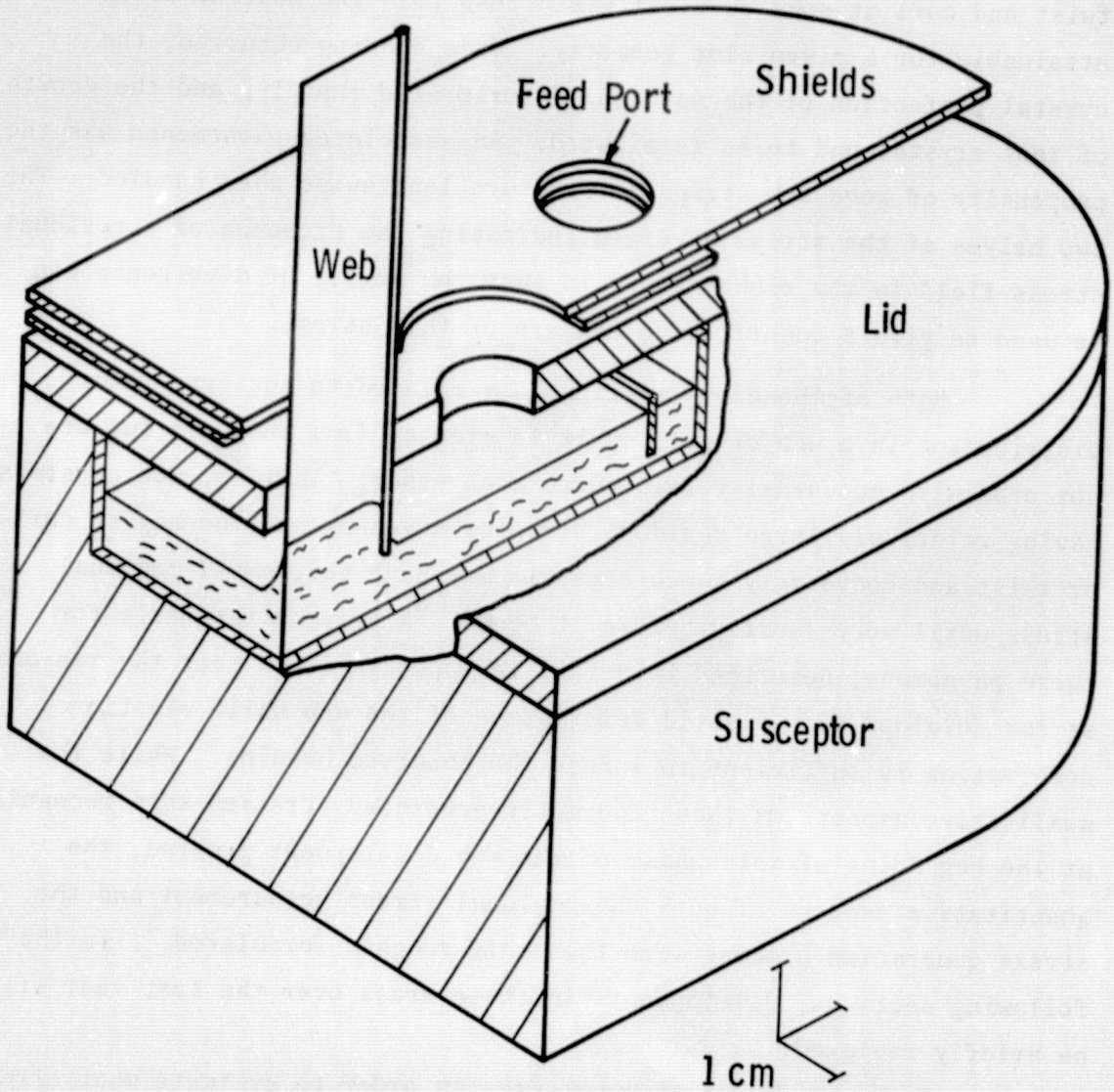

Figure 3 Schematic section of susceptor for web growth fitted with an "RE-1" lid

3.1.1 Stress Modeling and Measurements

At the end of the Phase I program we had clearly identified a major impact of thermal stress on web crystals: the tendency of web to twist and curl at some critical width less than the maximum width attainable for a given slot geometry. Once bending occurred, the crystal perfection of the material deteriorated rapidly, and the growth of that crystal had to be terminated. An associated phenomenon was the propensity of some web strips to fracture lengthwise when handled. The two halves of the strips diverged, indicating the presence of a residual stress field in the ribbons, and in fact the degree of divergence can be used to give a quantitative measure of this stress.[1]

Both of these observations are related to the temperature distribution in a web crystal as it is growing from the melt but are not otherwise necessarily related to each other. That is, web crystals having relatively large residual stresses may show no tendency to curl or twist and conversely a web crystal may have very small residual stress until very shortly before it bends. A proposed rationale for these phenomena, described in detail in Appendix 1, is that the residual stress develops from plastic deformation of the web while elastic deformation is sufficient to induce the observed bending. While the qualitative aspects of these thermally-generated stresses were recognized at the beginning of this phase of the web development program, the quantitative aspects of both the residual stress measurement and the stress generation process were then only roughly formulated.[1] In the following sections, developments in these areas over the last year will be briefly reviewed.

Residual Stress Measurements. In order to evaluate what effects changes in susceptor lid geometry had on the residual stress in web crystals, some technique for quantitative stress measurement was needed. The so called "split width" technique was chosen for its simplicity and moderate precision despite the drawback that it is destructive and gives only an average stress level, not a stress distribution. In this method a length of web crystal, usually about 20cm, is split lengthwise down

the middle. If residual stress present, both pieces curve and the curvature is evaluated by measuring the separation of the two halves as a function of length. Usually the crystal splits completely and the two pieces must be repositioned for the measurements; however,errors introduced by this procedure can be minimized by proper treatment of the data.

The average residual stress in the material can be determined by analogy to the stresses generated by bending a beam to a uniform curvature. For a beam of width W, bent to a radius of curvature R, The stress at the edges is given by

$$\sigma = \pm\frac{EW}{2R} \tag{1}$$

where E is Young's modulus.

The radius of curvature can be expressed as

$$R = \frac{\left[1 + \left(\frac{dy}{dx}\right)^2\right]^{3/2}}{\frac{d^2y}{dx^2}} \tag{2}$$

$$\approx 1 \Big/ \frac{d^2y}{dx^2} \text{ if } \frac{dy}{dx} \ll 1 \tag{3}$$

so that

$$\sigma \approx \frac{EW}{2}\frac{d^2y}{dx^2}. \tag{4}$$

Since dy/dx in split web crystals is very small ($\sim 10^{-3}$), Eq.(4) is the appropriate formulation.

In practice, the web sample is scribed with a diamond tool and fractured lengthwise; accidently split crystals have been utilized as well. One half of the pair is taped to a plastic strip and the second half is fitted to it at one end and lightly taped in place.

Longitudinal alignment is simple by means of small nicks on the crystal which act as fiducial marks. Angular and lateral positioning is more difficult, but those errors can be compensated to a great extent by the statistical treatment of the data. The total split width is measured with a filar micrometer eyepiece; the longitudinal position determined by 1 cm lines scribed on the plastic mounting strip. The raw width-length data-usually 18 to 26 data pairs-is then fit to a quadratic form using regression analysis:

$$y = \alpha_0 + \alpha_1 x + \alpha_2 x^2. \qquad (5)$$

The systematic errors in mounting the crystal strips appear in α_0 and α_1, whereas the second derivative is computed from α_2. The final equation is

$$\sigma_{res} = \frac{EW}{4} \alpha_2 \qquad (6)$$

where W is the total ribbon width, α_2 is defined by Eq. 5 and we have used the value $E = 1.9 \times 10^{12}$ dynes/cm^2 for Young's Modulus.[5] The usual result of the regression analysis is a high degree of correlation ($r^2 \approx .998$) and a reasonable standard error for the α_2 coefficient ($\sim 20\%$). In low residual stress samples ($\sigma \approx 10^6$ dynes/cm^2), the uncertainty in α_2 approaches 100% indicating that this stress is about the limit of resolution for the technique.

Typical stress data for a number of crystals are collected in Table 1. In all cases the lid and shield configuration was the RE-1 configuration shown in Figure 4. (Dwg. 1703B17) In addition to the group of data for the unmodified configuration, two other groups of data are presented: (1) crystals grown from an RE1 lid with the addition of a hot aftertrimmer and (2) crystals grown from an RE-1 lid with a cold aftertrimmer. These represent two types of thermal trimming which were tested as means to reduce the stress, and hence, deformation in web crystals.

TABLE 1

STRESS MEASURED IN WEB CRYSTALS GROWN
WITH DIFFERENT THERMAL TRIMMING GEOMETRIES

SAMPLE	$10^6\sigma$ dynes/cm^2	W^2 cm^2	10^6 σ/W^2
RE-1 LID ALONE			
RE1-1	16.3	2.657	6.1
RE3-6.4	7.6	3.208	2.4
RE7-2.5	36.5	4.335	8.4
RE54-1.3	3.45	3.574	0.97
RE56-1.2	0.83	3.600	0.23
RE57-1.2	8.04	3.769	2.13
J80-2.16	3.00	3.920	0.77
J84-4.3	1.46	3.869	0.38
RE-1 LID WITH AFTERHEATER			
J82-3.2	127	3.857	32.9
J85-1.4	67.8	4.562	14.8
J85-2.5	65.6	4.170	15.7
RE-1 LID WITH COLD AFTERTRIMMER			
J106-1.6	-4.87	4.012	-1.21
J018-1.3	28.2	4.272	-6.61
J115-1.4	13.8	3.38	4.08
J116-2.4	-36.8	3.686	-10.0
J117-1	10.9	4.306	2.5

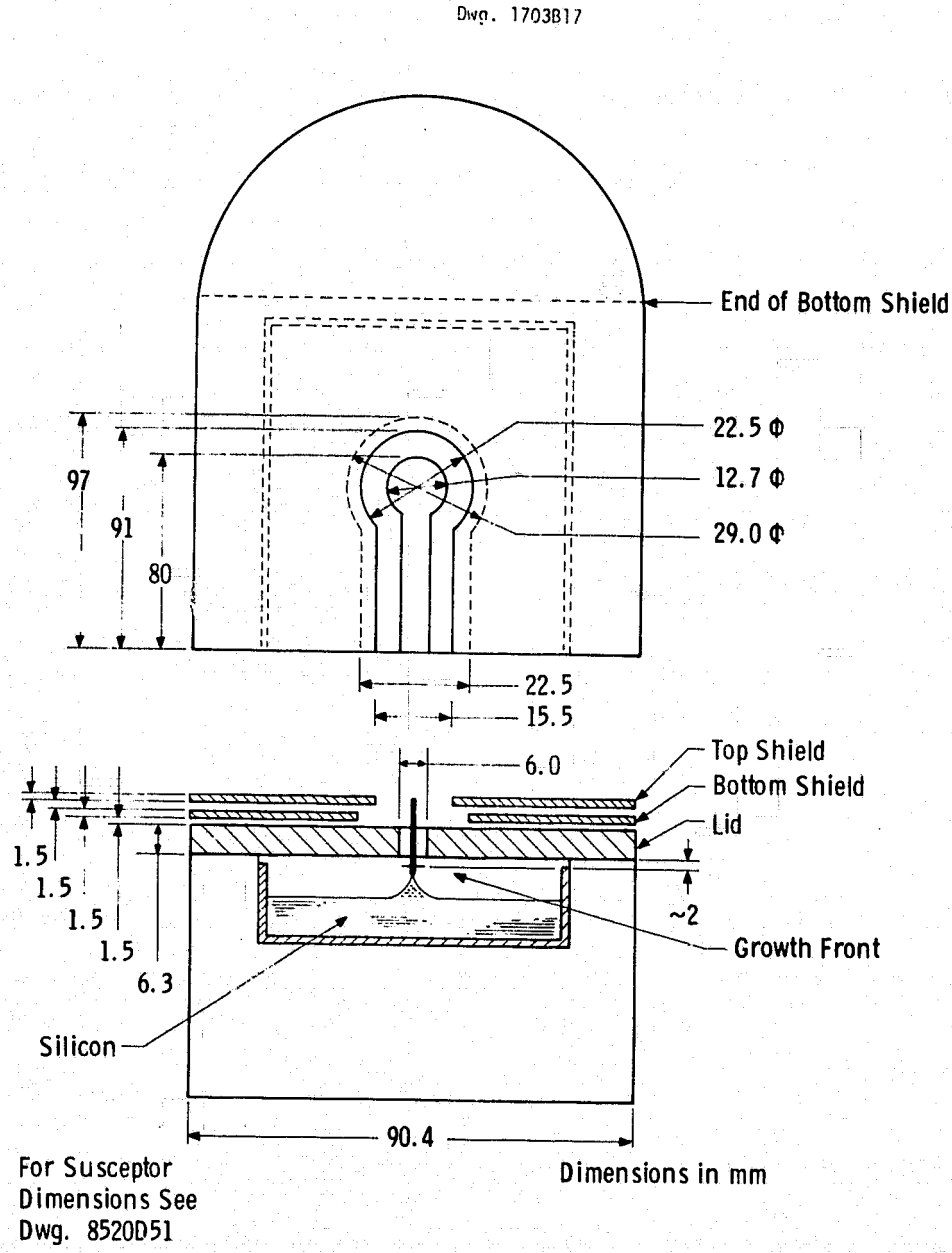

Figure 4 RE1 Growth Lid Configuration (schematic)

Inspection of the data is sufficient to reveal that the use of a hot aftertrimmer dramatically increases the residual stress while the cold aftertrimmer gives results which are similar to those with no aftertrimmer, (at least insofar as the residual stress is concerned; we take up effects due to elastic bending later.)

The stress data in the table are given both as the total stress as calculated from Eq. (6) and also as a "specific stress" σ/W^2. The latter quantity appears to be a parameter which is more nearly characteristic of the growth conditions than simply the stress itself. A wide web sample and a narrow web sample can have markedly differing stress values, however σ/W^2 is nearly the same for the two samples, and characterizes the growth geometry.

Stress Modeling. The empirical data clearly illustrate how the growth geometry may profoundly effect the residual stress in web crystals; however, they give little insight as to how the stresses develop. For this reason, we developed mathematical models to portray the physical situation involved. The goal of this work was to understand the origin of the thermal stress and to develop low stress designs for the growth system including e.g the use of after-trimmers.

The analytical approach employed for the modeling was the finite element method.[6] Although this approach is particularly useful for complex geometries, the mechanics of the available computer code made it very simple to input arbitrary temperature distributions and material properties for the simple half strip geometry used to represent the web. A number of element geometries were evaluated; however, most of the model runs were done with a geometry comprised of rectangular elements uniform in length along the longitudinal crystal axis (Z-direction) but varied in width transverse to the crystal, Figure 5. The elements were narrower at the edge with the intent of obtaining better longitudinal stress resolution. (Recent evidence suggests that a nearly square, uniform element may give somewhat better results; for the most part, the difference between the two geometries is minimal. Problems

Curve 716729-A

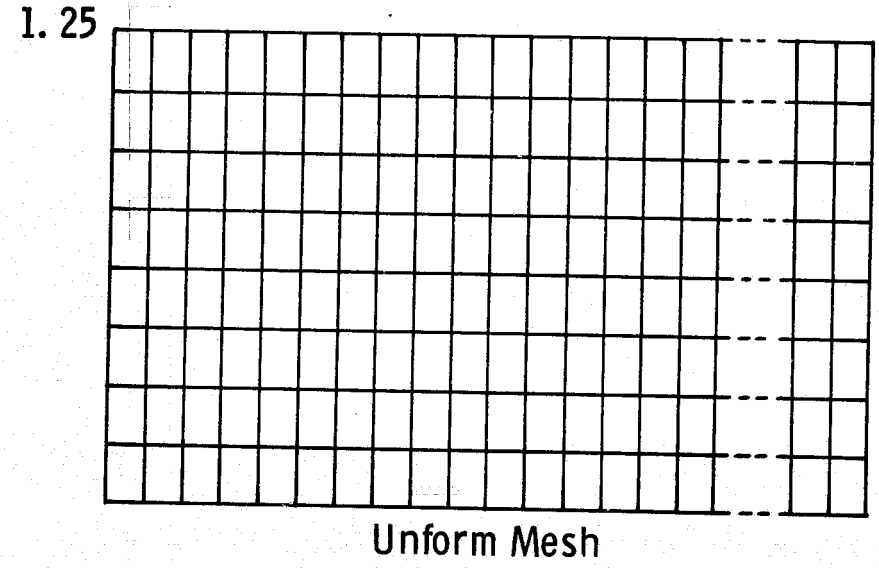

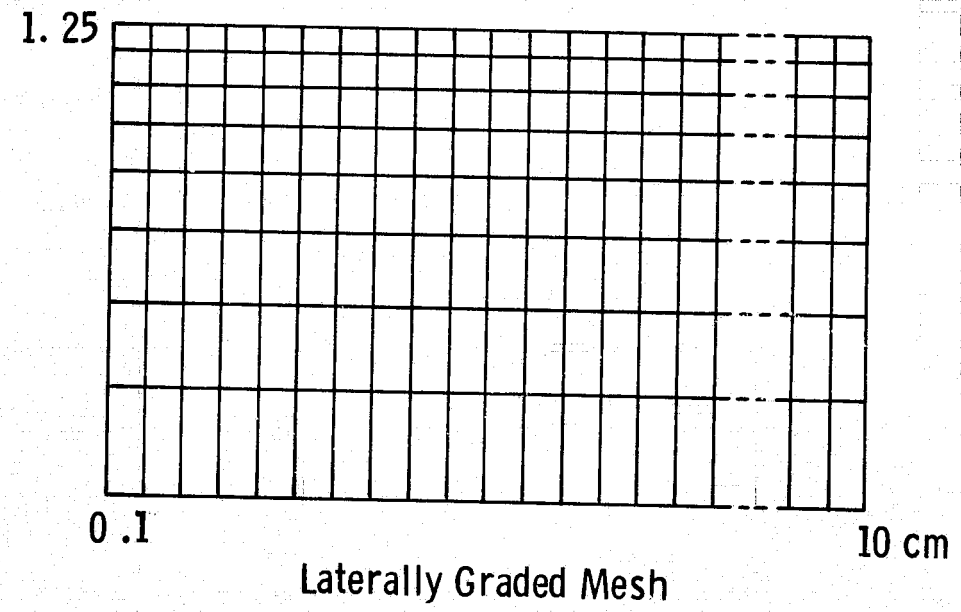

Figure 5 Rectangular Grid Elements used in Stress Model Calculations

arise only when very small stress levels are being computed. The variation evidently arises when taking the difference between two large numbers, and for these cases greater precision is achieved when the elements are more nearly square.) For further general description of the model see Appendix 1.

Low Stress Temperature Profiles. At the inception of the stress modeling work, the computer program used with the model was checked by running the special case of a linear temperature profile with temperature independent material parameters. Thermal stress theory predicts that the resulting stresses in the ribbon should be zero,[7] and in fact the calculated stresses, while not zero were quite small. The same temperature profile was then run with a temperature dependent thermal expansion (as is the case for silicon); the resulting stress fields increased markedly as might be expected. The model was then assumed to be operative, and further effort was applied to the modeling of temperature profiles appropriate to specific lid designs. Near the end of the current program phase, however, it became necessary to obtain a better definition of an "ideal" profile; clearly it was not simply a linear profile.

For silicon, the thermal expansion coefficient is given by[8]

$$\alpha = 2.552\text{x}10^{-6} + 1.953\text{x}10^{-9}T - 9.03\text{x}10^{-15}T^2. \qquad (7)$$

When we modeled a ribbon with a linear temperature profile but with this quadratic expansivity, small but real stresses were calculated. Indeed, using the approximate equation[9]

$$\sigma_{ZZ} = \frac{\alpha E}{6}(C^2-3y^2)\frac{d^2T}{dZ^2} \qquad (8)$$

(C = ribbon half width and y = lateral coordinate), it was possible to calculate an effective d^2T/dZ^2 from the value of σ_{ZZ}. It was found that

$$\left.\frac{d^2T}{dZ^2}\right|_{eff.} = \frac{1}{\alpha}\frac{d^2}{dZ^2}(\alpha T). \tag{9}$$

This suggests that the zero stress temperature profile is given by

$$\frac{d^2}{dZ^2}(\alpha T) = 0 = \frac{d^2T}{dZ^2}\left(\alpha + T\frac{d\alpha}{dT}\right) + 2\frac{d\alpha}{dT}\left(\frac{dT}{dZ}\right)^2 \tag{10}$$

For the case where $\alpha = \alpha_0 + \alpha\ T$, this equation reduces to

$$(a+T)\frac{d^2T}{dZ^2} + \left(\frac{dT}{dZ}\right)^2 = 0 \tag{11}$$

where $a = \alpha_0/2\alpha_1$. Equation (11) has the solution

$$T - a = \sqrt{b_1 Z + b_2} \tag{12}$$

This form of temperature profile was modeled in combination with the thermal expansivity, Eq. 7, and the result was a null stress field over most of the ribbon.

With the curved temperature profile given by Eq. 12, all the stress and shear components were zero over most of the ribbon with the exception of the ribbon ends where modest lateral and longitudinal stresses were calculated. To investigate this end effect phenomena further, several additional runs were made using various element sizes and types in the model. The results of these runs indicated that "end effect" stresses were an artifact of the analysis resulting from computing the differences of two large numbers in the computer program. These errors tended to be absolute in nature rather than relative, so that for the large stresses calculated in the lid analyses, only small percentage errors resulted. This conclusion was verified by running some previously analyzed temperature profiles and finding only a 10 to 20 percent change in the calculated stresses. Future modeling runs will be done using a modified element geometry to reduce the end effects; however, the basic conclusions derived from the previous runs are still valid at least on a comparative basis.

The analysis of a "low stress temperature profile" gave important directions for lid and aftertrimmer design. Rather than strive for a linear temperature profile in the growing web, the model indicates that a sub-linear profile is desired over at least a portion of the crystal. This obviously cannot be an extensive region; however, it can be obtained in limited portions, and in fact is one of the inherent characteristics of the RE-1 configuration which has demonstrated low stress growth, viz Table 1.

Thermal Trimming. An important application of the thermal stress modeling was to evaluate the effect on stress of the vertical thermal profile (e.g due to an aftertrimmer or extra shields placed above the susceptor and lid assembly) in the web. The temperature distribution in the web was modeled using an expanded version of the thermal model detailed in Appendix 6.5 of reference 1. Three situations were investigated: (1) Hot aftertrimmers at various positions and temperatures; (2) no after trimmer; and (3) a cold after trimmer at various positions. Temperature distributions for typical examples of these situations are shown in Figure 6; TAS is the aftertrimmer temperature and its position is indicated in the figure. The temperature profile near the growth front is changed only slightly between the three cases; the greatest effect is several centimeters up the ribbon. The hot aftertrimmer results in a relatively hot, uniform temperature region as might be expected. The cold aftertrimmer, which has the physical effect of shielding the web from the hot upper surface of the lid assembly, generates a more linear profile. The longitudinal (σ_{ZZ}) and lateral (σ_{YY}) components of the resulting thermal stresses are plotted in Figures 7 and 8.

The model calculations can be used qualitatively to rationalize the stress data (Table 1) obtained for webs growth with different thermal trimming configurations. The largest stresses are predicted for the hot aftertrimmers and the smallest for the cold aftertrimmer. In Figure 8, portions of the curves are dashed; in that region, the calculated stresses exceed the silicon yield stress estimated from the work of Graham et al.[10]

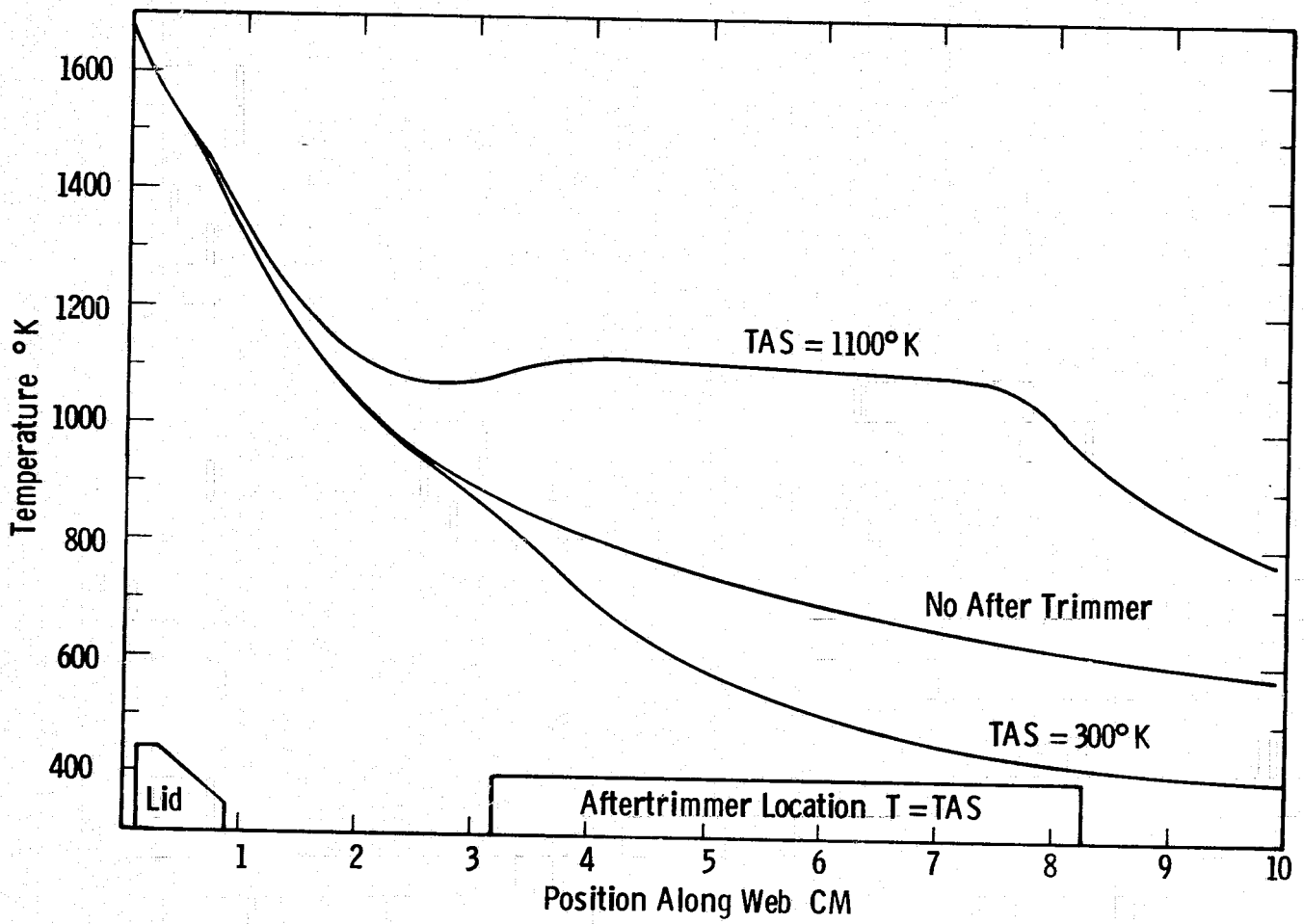

Figure 6 Computed longitudinal temperature profiles in silicon web crystals. Temperature as a function of position along web for three cases: no aftertrimmer, 300°K aftertrimmer (TAS - 300°K), and 1100°K aftertrimmer (TAS = 1100°K).

Curve 716352-A

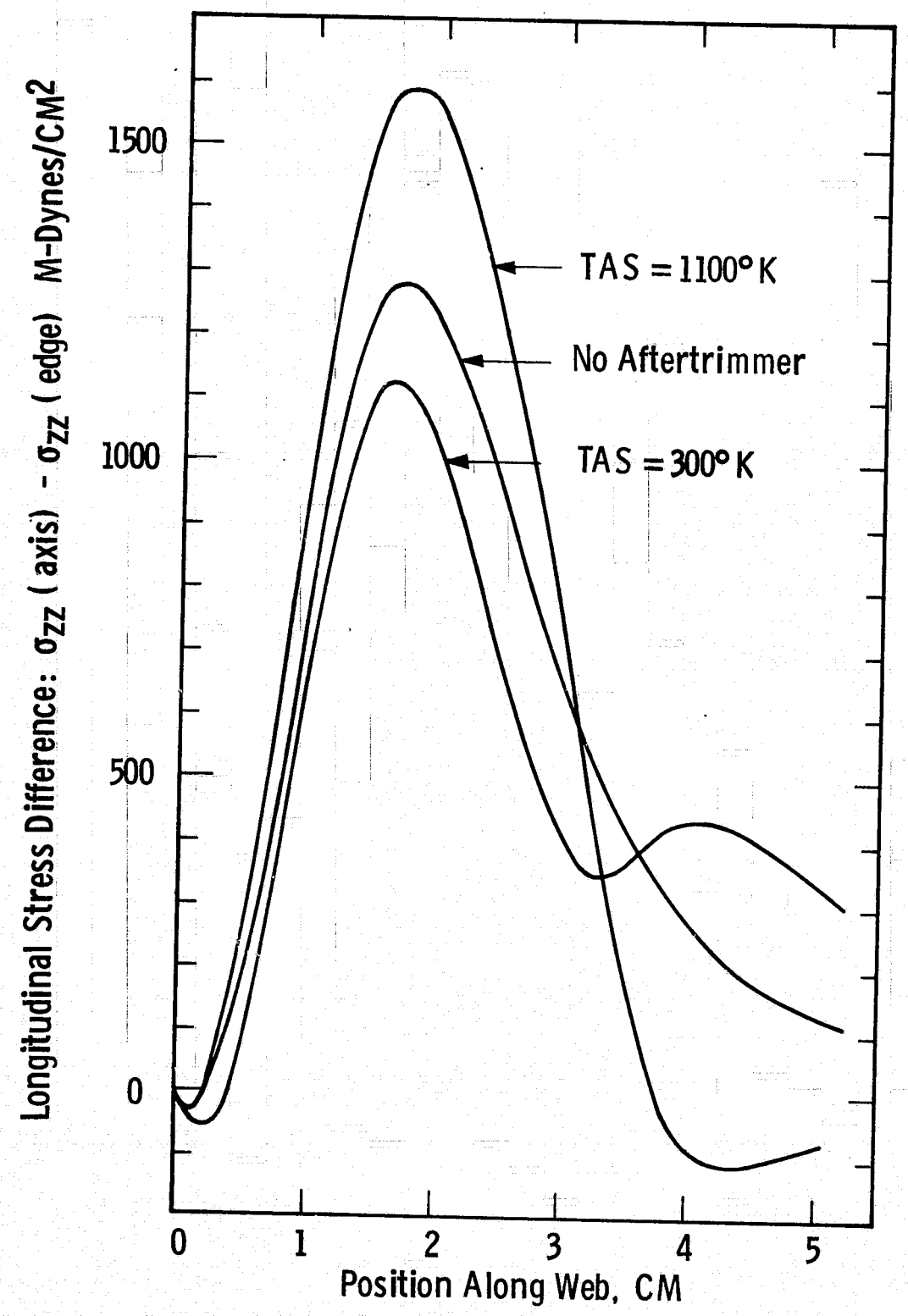

Figure 7 Computed variation in longitudinal stress difference (σ_{ZZ} axis-σ_{ZZ} edge) as a function of position above the crystal-liquid interface for three cases: no aftertrimmer, 300°K after trimmer, and 1100°K after trimmer.

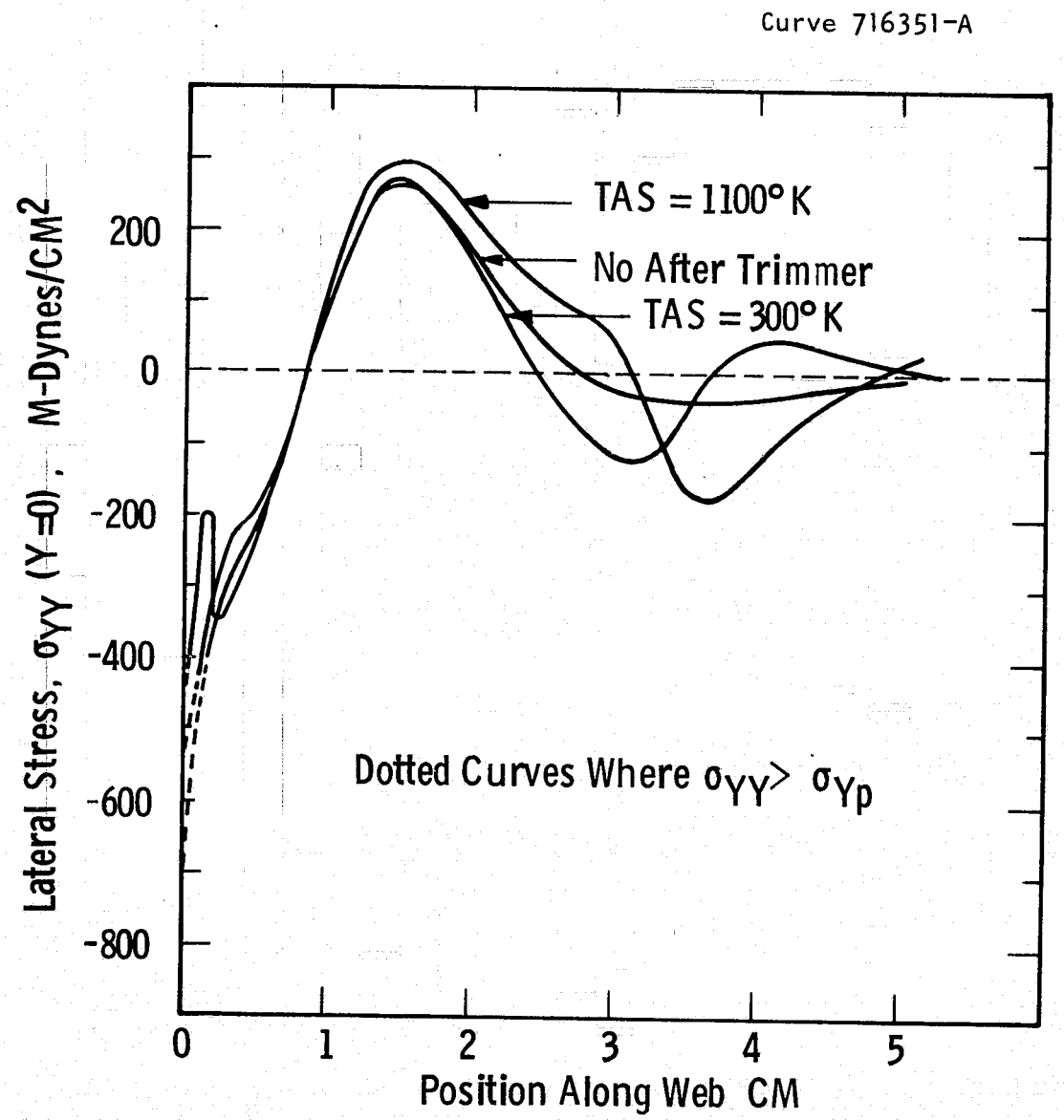

Figure 8 Computed lateral stress distribution in silicon web crystals. Lateral stress (σ_{YY}) at web centerline as a function of position above the crystal-liquid interface. Curves are dotted at positions were σ_{YY} exceeds the silicon yield stress (σ_{YP}).

A second aspect of the modeling was the prediction that the stresses, particularly lateral stress, are sensitive to the position of the melt with respect to the lid. (see Appendix 1 for details). The calculations indicate that as the melt level changes the stress in the web may also change. Thus,the stress distribution and hence ultimate web width can be very dependent on the melt level during growth as well as on the lid geometry and thermal trimmer profile. Since we now do not replenish the melt in most of our runs we may, in fact, be negating the beneficial effects of low stress lids and thermal trimmers designed to provide the wide web.

In summary both experimental results and computer simulation indicate that afterheaters placed above the susceptor lid raise rather than reduce the residual stress in web crystals. Afterheaters per se are not a viable technique to promote the growth of wide web crystals. Instead, analyses show that a susceptor lid designed for low stress (no plastic deformation) coupled with a cold aftertrimmer (to minimize elastic bending of the web above the lid) should promote conditions for wide web growth.

Since one effect of the cold trimmer is to shield the growing web from the hot lid assembly, alternatives to the cold trimmer are modifications to the top shielding or some combination of shielding plus the cold trimmer. As we show below,this approach works and has recently produced long web crystals 4 cm wide with improved structure.

Finally, the model studies imply that control of the melt level in the web growth system is important if the benefits of low stress lids and thermal trimmers are to be fully achieved. If the melt is depleted by crystal growth, stress levels rise and web deformation is expected.

3.1.2 Thermal Geometry for Wide Web Growth

As we have pointed out,[1,4] the shape of the thermal profile in the liquid controls web width unless thermal stress causes premature deformation of the ribbon. The essential features of the process are depicted in Figure 9. Heat loss from the meniscus, perturbs the thermal field near the tip of the bordering dendrite so that there is slightly more growth on the outer edge than on the inner edge. This causes a small deviation of the growth direction from the preferred [211] direction and the crystal widens so long as there is a uniform temperature profile in the melt. When the widening web reaches a region of increasing melt temperature as shown in the figure, the intrinsic lateral temperature gradient in the liquid counteracts the temperature gradient created by the meniscus heat loss. The web then ceases to widen and continues to grow at a steady state.

Thus, if the melt profile is too steeply concave upward wide web cannot be grown. Web width was limited by this effect at the beginning of the development program. Through a design program based on experimental development aided by computer simulations, susceptor/ crucible/ lid designs, which demonstrated flat melt temperature profiles over regions approximately 60 mm in length, were achieved (See Appendix 1). With sufficiently flat melt profiles available, aftertrimming elements were then applied to the system to minimize ribbon deformation. The following two sections describe the general experimental aspects of lid design and thermal aftertrimming, respectively.

3.1.2.1 Lid Design

To a large extent the shape and dimensions of the lid slot controls the temperature profile in the liquid. By proper design this profile can be made flat to a few tenths of a degree over a distance corresponding to the desired web width. While the number of potential designs is large, certain constraints limit the number of practical choices[1]:

Dwg. 6438A24

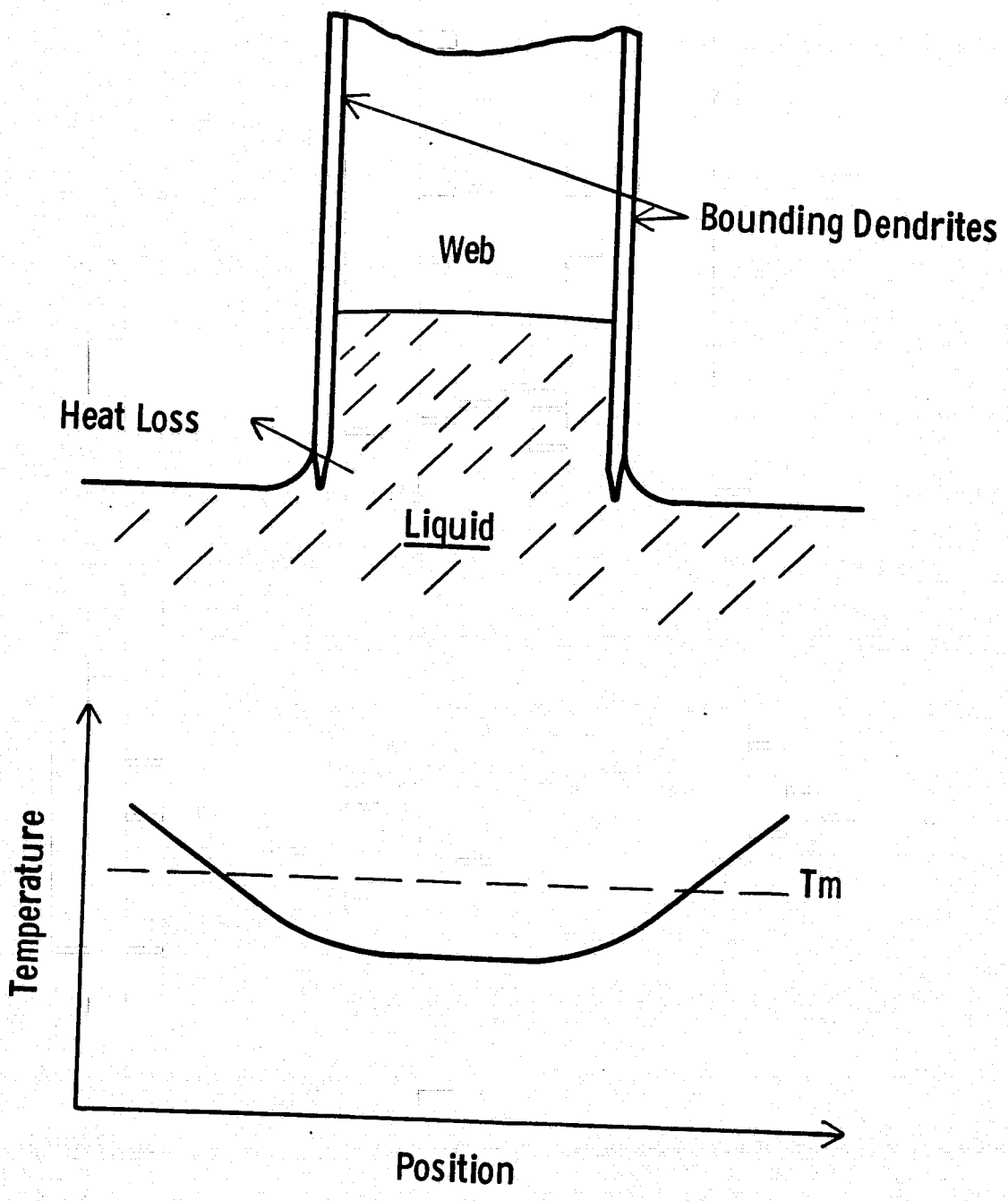

Figure 9 Schematic illustration of a growing web compared with temperature profile at melt surface.

(1) The temperature difference (ΔT) between the center of the melt and the crucible wall must be large enough so that the silicon-crucible interface temperature remains above the melting point of Si when the melt is undercooled for growth.

(2) Convective flow and any resulting temperature fluctuations in the melt must be low. Thus, the center to edge ΔT should not be substantially larger than necessary to satisfy (1).

(3) The growth region should be the coldest region of the melt with a smoothly varying profile to the walls.

(4) Any oxide generated by the reaction of the molten silicon with the quartz crucible must be managed so that it does not circulate in regions of the system where it can interfere with growth.

(5) Convective gas flow should be minimized so that thermal perturbations remain small near the crystal-meniscus interface region.

Excessive deviations from conditions (1) and (3) promote "ice" nucleation; variance from (2) and (5) may induce spontaneous pull out, while point (4) is self explanatory. These considerations though not overriding do enter into lid design considerations.

There are two major configurational aspects of lid slot geometry. The first is the horizontal two dimensional shape, i.e. length, width, size of dogbone holes (if any) etc. These primarily dictate the distribution of heat loss from the melt and, therefore, the melt temperature distribution. The second is dimensional shape in the vertical direction, i.e. lid thickness, bevels, etc. which controls the heat losses from the web near the interface region and upward, and therefore the vertical temperature distribution in the growing web. This is important since the vertical temperature distribution affects web stress levels, and thus indirectly impacts web width.

In addition to slot geometry itself, the configuration and number of shields above the lid also contribute to controlling the vertical and melt temperature distributions (viz Section 3.1.1)and are in a very practical sense a part of the lid configuration. Thus in our terminology, lid configuration refers to the combination of lid and top shields.

From a width point of view the two most successful lid configurations tested so far are illustrated in Figures 4 and 10. While the two configurations at first appear quite different, inspection of the figures shows that the two-dimensional slot geometries are identical for each. Specifically, the slots measure 80 mm long overall, 6 mm wide with 12.7 mm diameter dogbone holes. The thicker, beveled slot for the lid in Figure 10 has advantages over that of Figure 4 in terms of growth speed and stress induced deformation, which will be discussed later. In terms of melt temperature profile the lids are essentially identical, producing a flat growth zone greater than 5 cm wide, viz profile A, Figure 11. Webs 3 to 3.5 cm wide could be grown repeatably with these lids, web deformation limiting further widening.

Other slot geometry configurations have been tested both to gather data for imput to the thermal modeling work and to test the effect of variations in lid design on growth behavior. For example, a straight 80x6 mm slot produced web 2.6 cm wide. The melt profile was dipped several degrees over a distance of 4.5 cm as measured by a dendrite probe of the melt surface. (profile B, Figure 11).

Changing the slot to 83 mm x 6 mm with 9.5 mm dia. dogbone holes, produced a 3.5 cm web width. If the dogbone holes are made too large, there is a strong tendency to nucleate free floating ice in the dogbone region. For example, when the dogbone holes were increased to 15.9 mm dia.,there were some growth problems in this respect. Melt profiles were measured by the dendrite probe method[1] and the results were consistent with the general expectation, i.e. the flatness in the melt profile improved as the slot geometry progressed from no hole to larger dogbone holes.

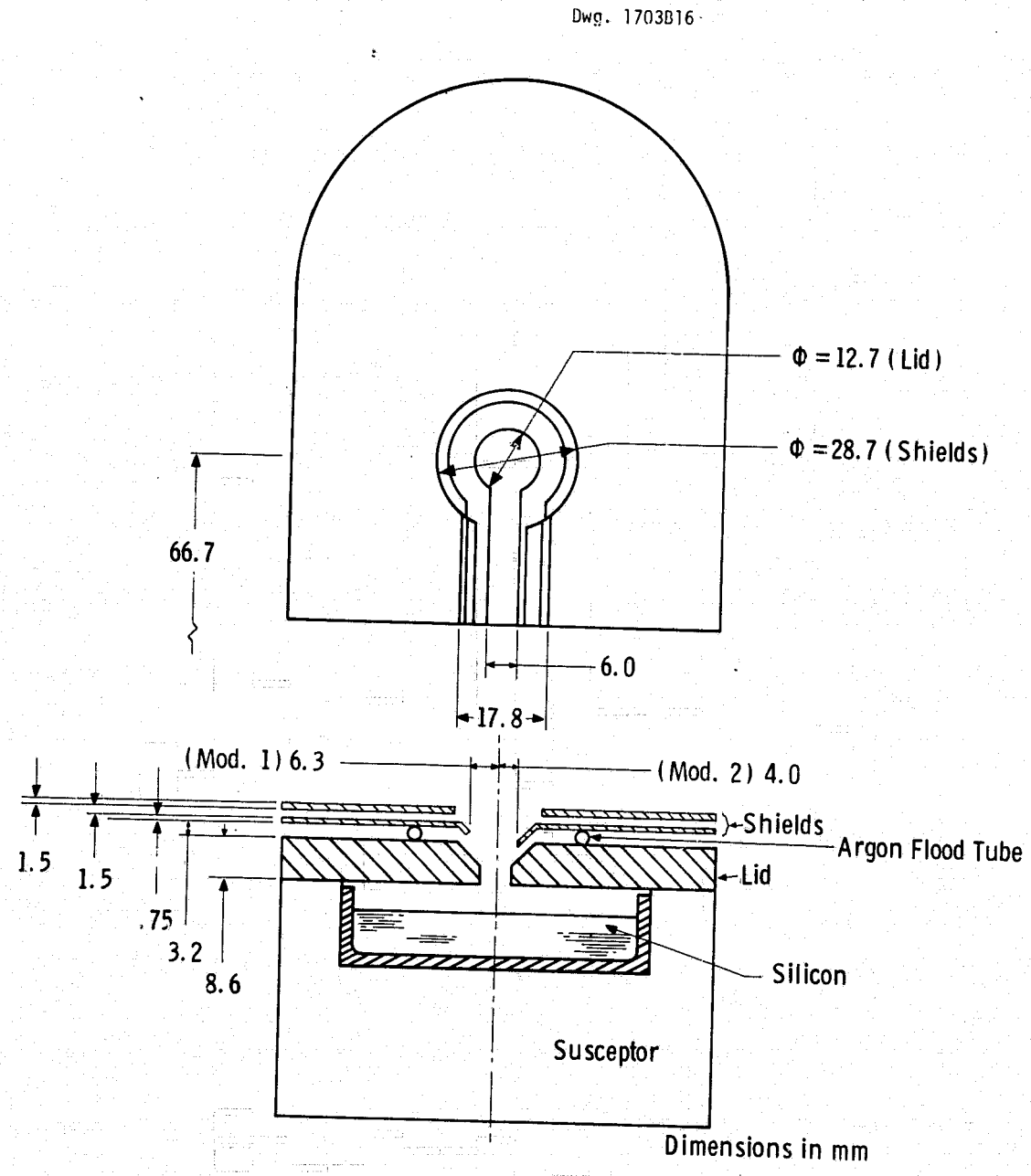

Figure 10 Examples of a growth lid which is beveled to increase radiative heat loss from the web. Mod. 1 and Mod. 2 depict different shield arrangements. The 2-dimensional slot geometry is the same as in Figure 4 and the resulting melt temperature profile is essentially the same.

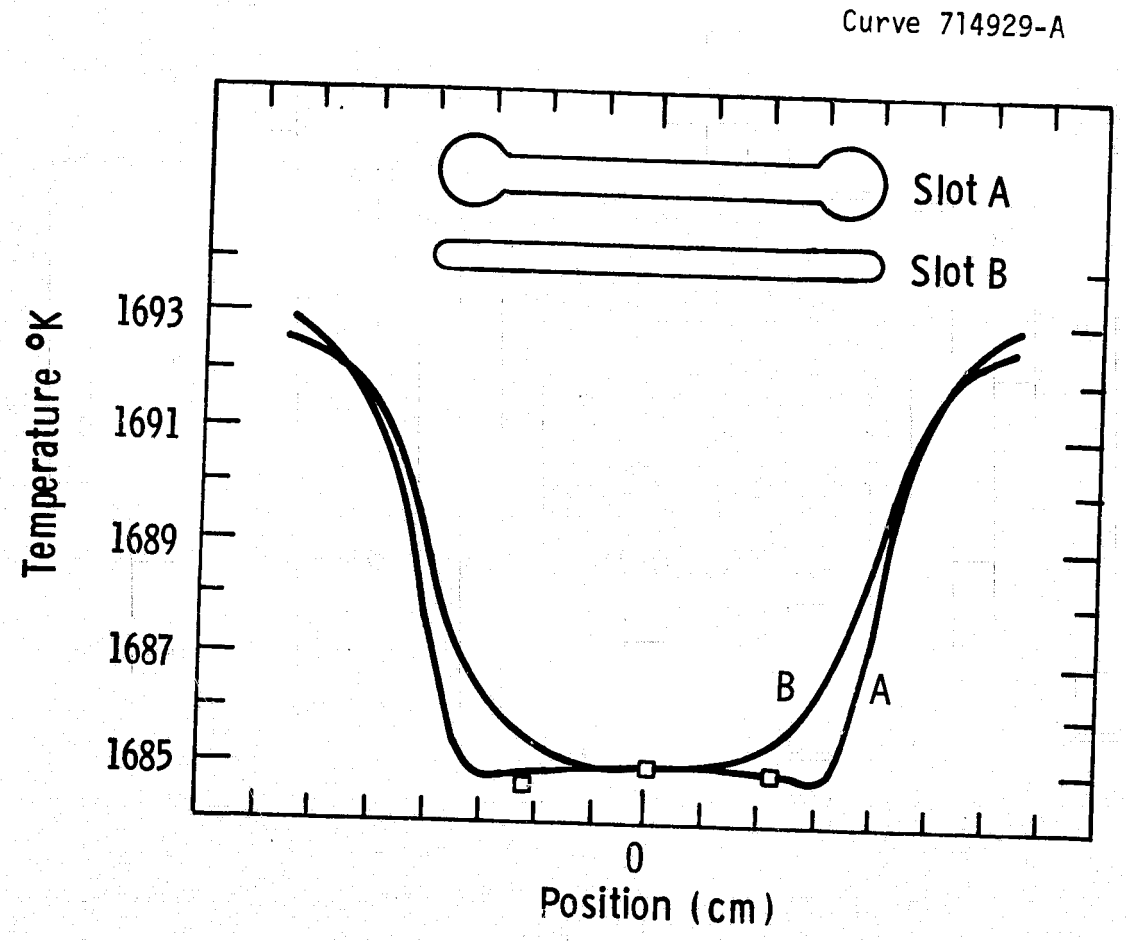

Figure 11 Computed and measured melt temperature profiles for different lid slot geometries.

Another slot geometry tested to improve web width was 114 mm x 6 mm, with a 3x3 mm bevel in a 7.5 mm thick lid. The rationale here was to provide a more uniform environment for the dendrites as the web widened (compared with the shorter dogboned slot) while the increased slot length compensated for the lack of dogbone holes. Indeed, dendrite probes indicated the melt profile to be flat to about 1°C in the growth region, although the measurements were somewhat erratic. Although harder to grow with than the aforementioned configurations, a 3 cm wide crystal was produced. The main difficulty with this configuration was the nucleation of floating ice in the melt. Overall, this configuration did not seem to offer any advantage over the configurations in Figures 4 and 10, so the latter were chosen as base lines for the application of thermal trimming to reduce stress-induced deformation.

Some important conclusions can be drawn from these experiments. First, in terms of melt profile, the maximum width capabilities of the RE-1 type slot geometry have not yet been approached. In all cases, the growth of wide webs are terminated because of the onset of stress-induced deformation. Modifications in lid and top shield configurations, discussed in the next section, have moved the initiation of deformation out to 4 cm, where the web still continues to widen. Second, the ability to control the melt temperature profile with small variations in slot geometry while maintaining high quality growth conditions has future implications with respect to width control for long period, continuous growth. (See, for example, discussion of width control in Section 3.3).

3.1.2.2 Stress Reduction for Web Width Enhancement

In the present phase of this program, a parallel experimental and analytical approach was taken to identify the sources of and to control the stress in dendritic web crystals. The results of the modeling study were presented in Section 3.1.1. In this section we describe the concurrent experimental work.

The major factor involved in stress reduction is management of the temperature profile in the growing web. Three approaches have been and/or are being tested experimentally: 1) after heater, 2) cold after trimmer, and 3) lid and top shield configurations. Although the afterheater experiments were negative they are covered here for sake of completeness. The most promising results have been the application of new lid/shield configurations.

After Heater Development. During the first quarter of the present development phase, several forms of integral afterheaters were tried with little success.[2] These trimmers were heated by induction coupling and by conduction from the lid to which they were attached. The lack of both independent temperature control and heater positioning were obvious deficiencies with the approach, so a new and more flexible apparatus was designed and constructed. This afterheater, whose function was based on concepts developed on other ribbon growth programs,[11,12] is depicted schematically in Figure 12. The upper and lower heaters on each side of the web are specially designed immersion heaters capable of operation at more than 1000°C. The upper and lower heater are joined by a thin nickel/chrome alloy sheet to generate a vertical temperature gradient along the length of the web. Each of the four heaters is equipped with its own power supply and temperature measurement and control so that a range of temperatures and temperature gradients can be obtained in practice. The vertical position of the entire assembly is also adjustable to supply an additional control parameter for experiments. All chamber penetrations required to position and power the afterheater are vacuum tight.

The operating range of the equipment was sufficient for the initial experiments.[4] These tests were carried with the afterheater positioned above a susceptor with an "RE-1" lid assembly (Figure 4). This lid was chosen as a baseline since it produced a flat melt temperature like Figure 11A and because a wealth of growth data had been accumulated against which to compare the performance of the afterheaters.

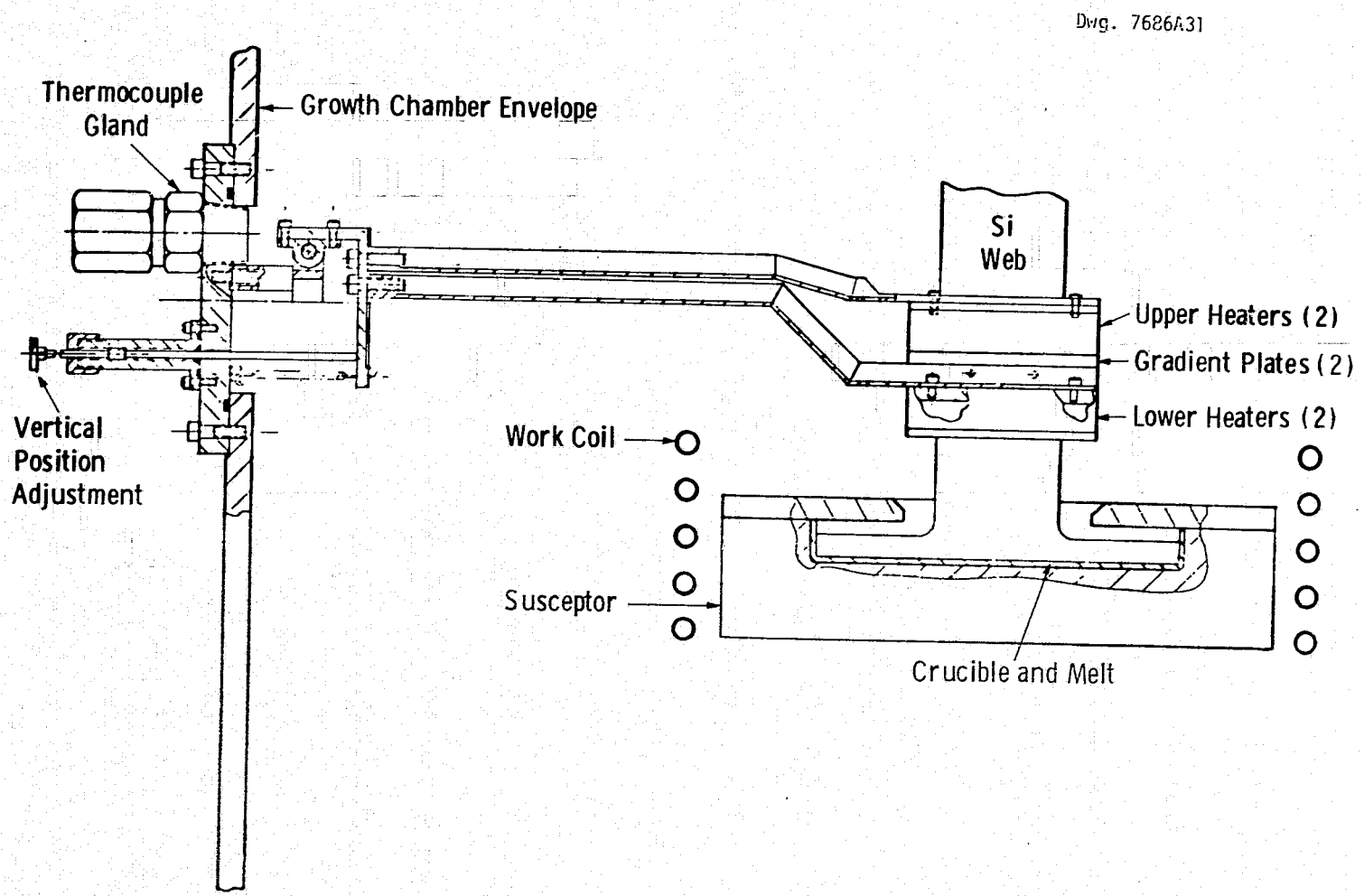

Figure 12 Schematic drawing of afterheater system used to modify vertical profile of a growing web crystal.

The most compelling results of the study were that stresses, especially the residual stresses, in the web crystals increased markedly for every combination of afterheater operating conditions that was tried. For example, from previous measurements[4], the characteristic residual stress for the RE-1 configuration was $\sigma/W^2 = 2.1 \pm 1.0 \times 10^7$ dynes/cm, a factor of about 20 greater than without the afterheater. (Table 1). Some of the reasons for this behaviour were clarified by the modeling results which became available about the time these initial afterheater tests were run, and are reviewed in Section 3.1.1. These results clearly indicated that the desired vertical temperature profile required a cooler rather than hotter ambient above the growth lid to reduce thermal stress.

Cold Aftertrimmer Studies. The first version of the cold aftertrimmer, Figure 13, was comprised of two water cooled copper plates about 4x8x.3 cm mounted at a 45° angle above the susceptor assembly. Perforated tubing which was brazed to the bottom edges of the plates provided an argon flow curtain to prevent any accumulation of oxide on the aftertrimmer.

Webs grown in the first few runs of this apparatus were subject to frequent pull outs; and the formation of third dendrites. The temperature distribution on the melt surface was then carefully measured by determining the melting point of a thin dendrite at several melt positions. This test revealed that the temperature profile had been drastically altered by the presence of the aftertrimmer. Since the aftertrimmer itself was essentially at the chamber wall temperature, this perturbation should not have been the result of changes in the heat loss from the liquid. Rather, the presence of the copper plates perturbed the induction heating field.

For this reason a second version of the aftertrimmer, Figure 14 was constructed. In this design the copper plates were arranged vertically above the susceptor to have a much smaller effect on the induction field. Indeed, dendrite probes indicated that the melt

Dwg. 7686A30

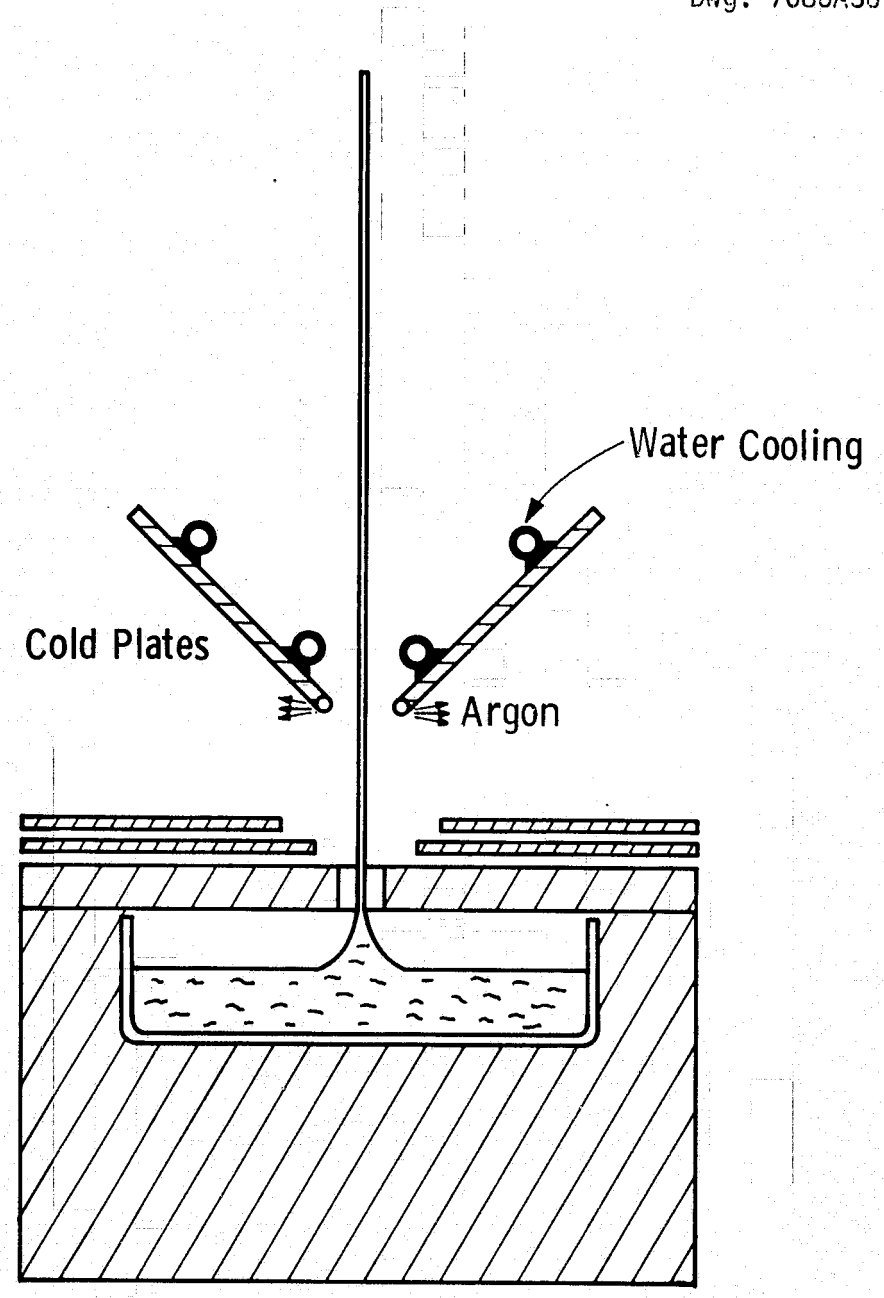

Figure 13 Schematic drawing of cold aftertrimmer with cold shield plates mounted 45° to the vertical axis.

Figure 14 Photograph of cold aftertrimmer with parallel cold plates.

temperature profile was flatter, although a slight right-left asymmetry still existed. Reversing the trimmer support arms so they no longer parallel the induction power leads (by remounting the aftertrimmer in the opposite side of the chamber), eliminated the asymmetry.

The first growth experiments with the cold aftertrimmer were very promising. Residual stress data from several crystals indicate that it is compatible with the stresses found with the RE-1 lid alone. Measurements of a number of webs, Table 1, gave a specific residual stress $\sigma/W^2 = 2.6 \pm 7.8 \times 10^6$ dynes/cm^2. (The large standard deviation of this data reflects the fact that various aftertrimmer conditions, e.g vertical position, were included in the measurements.)

These first experiments confirmed as predicted by the model, that the cold trimmer produces low residual stress. However, considerable difficulty was experiencedin further experiments aimed at producing a flat melt temperature profile in the presence of the aftertrimmer. Dendrite probe measurements indicated that the melt temperature profile was dipped several degrees, the amount of dip increasing as the trimmer was positioned closer to the lid. In addition, the dendrites bounding the web tended to be very non uniform in thickness, a condition usually associated with convectively induced thermal fluctuations in the liquid. Attempts were made to compensate for the melt profile perturbation by increasing the size of the dogbone holes, but this was unsuccessful. Changes in susceptor end shielding were also only marginally helpful. Dendrite probes showed melt temperature variations and growth conditions remained poor. It was finally deduced that the cause of the erratic growth behavior was gas convection induced by the chimney-like geometry of the aftertrimmer.

At this point, tests of the cold aftertrimmer were suspended so that a more favorable design could be formulated.

Lid/Top Shield Configurations. The stress modeling results implied that an alternative way to achieve the function performed by the cold aftertrimmer is by means of passive shielding. (This approach has the virtue of simplicity but clearly lacks the flexibility of the positionable trimmer.) By manipulating the number, position, and geometrical shape of the shields considerable adjustment in the web vertical temperature profile (and hence stress) was possible without the convective gas fluctuations attending the use of the cold trimmer.

The initial experiments have been extremely gratifying. For example, the addition of a third top shield to the lid configuration in Figure 10 increased the web width to over 4 cm. This result has been reproduced several times, viz Figures 15 and 16, with a maximum width of 4.2 cm achieved as of this writing.

Along with progress in width, there also has been an impressive improvement in the crystal quality of the wider web crystals. This is vividly illustrated in Figure 17. The lighting for this photograph was purposely arranged to clearly delineate the macrostructure of any surface defects. The rippled texture in the leftmost crystal (here and in Figure 15) is typical of the deformation mode observed in the widest webs grown at the end of the Phase I program. The other crystals shown, besides being wider than the earlier webs, are also free of the undulating surface features, and exhibit excellent crystal quality.

Combinations of improved lid shielding deployed with a redesigned aftertrimmer should increase the web width beyond the 4.2 cm maximum so far achieved.

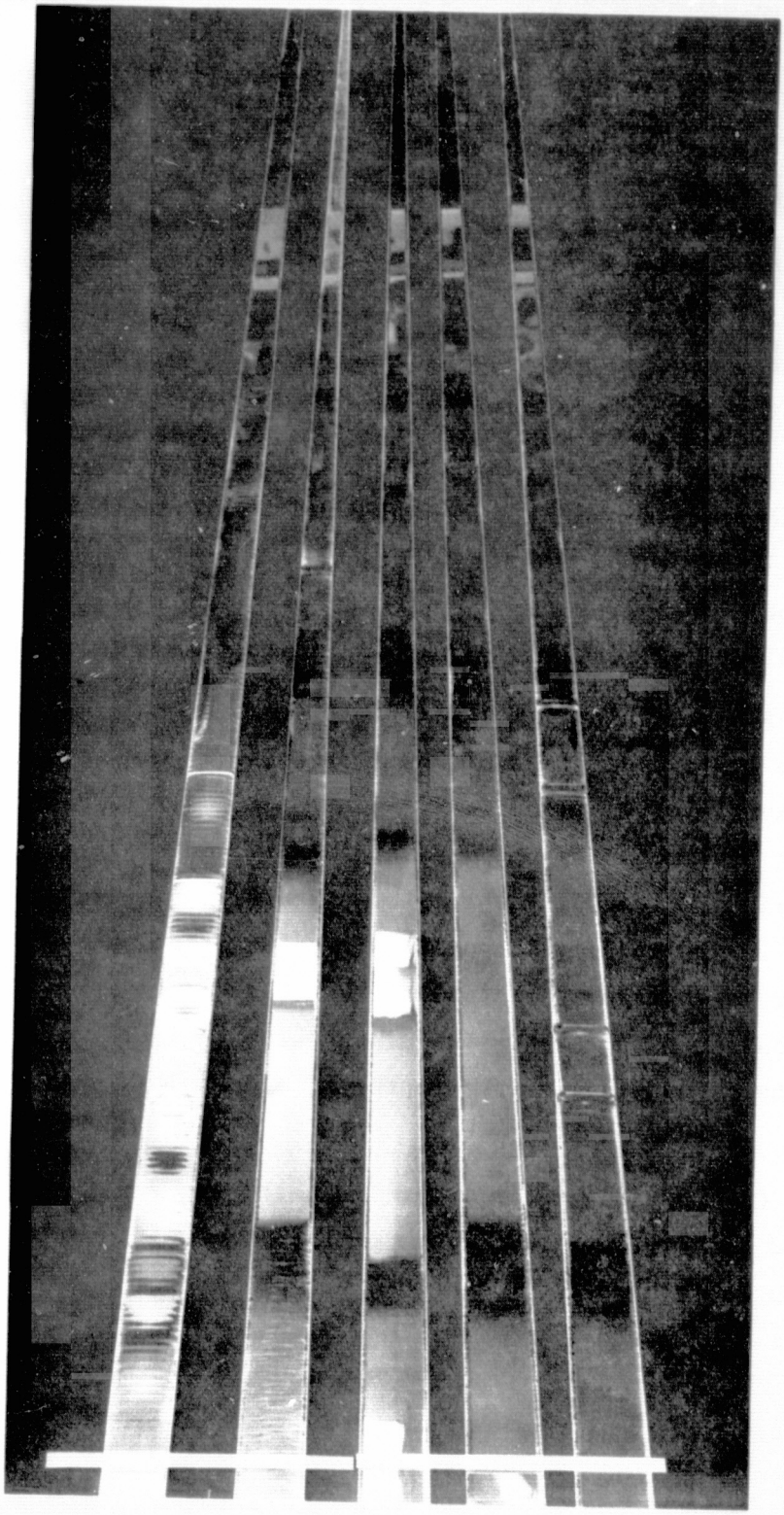

Figure 15 Wide web crystals produced by improvements to lid thermal shielding. Lights and laboratory surroundings are reflected in mirror-like surfaces.

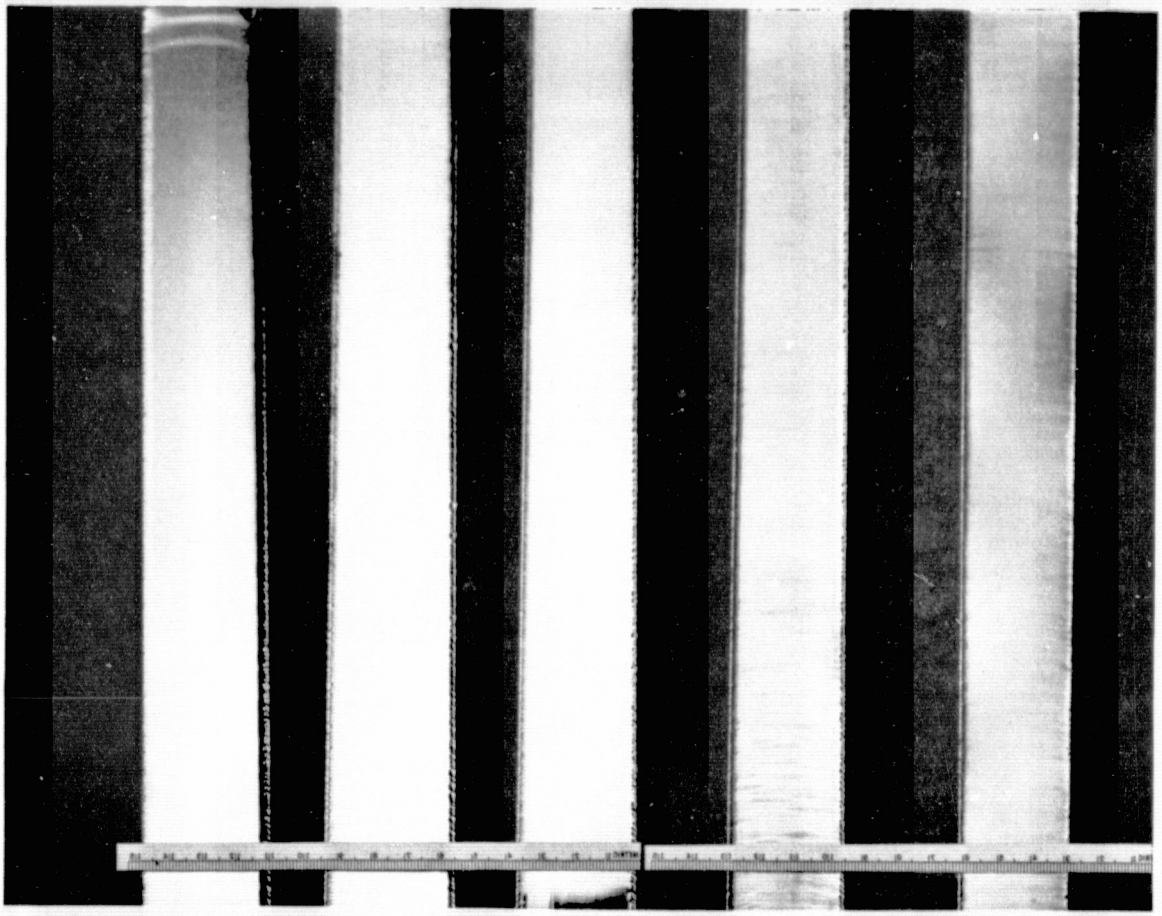

Figure 16 Close-up view illustrating smooth surfaces of as-grown web crystals. Faint striations are fine oxide particles deposited during growth.

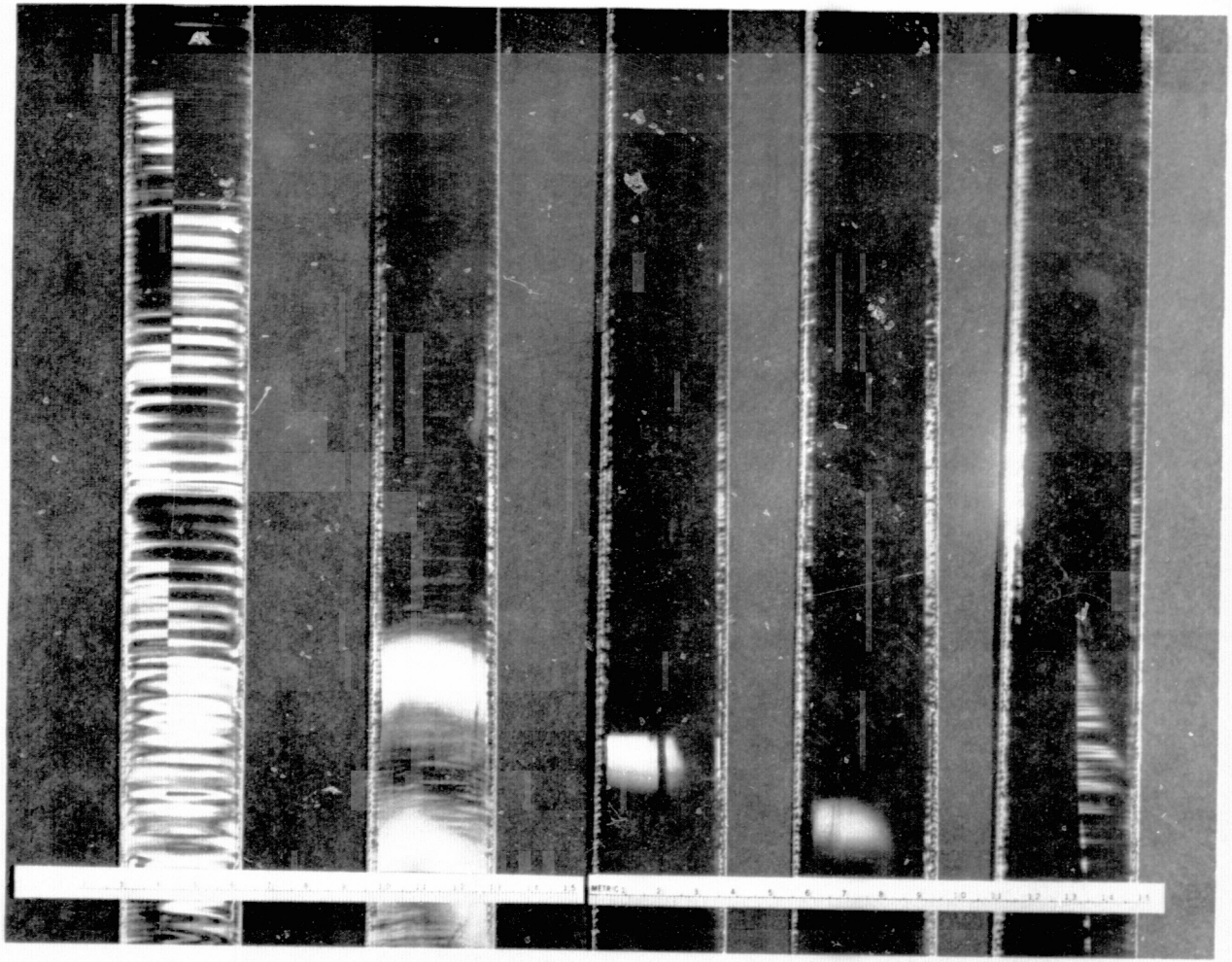

Figure 17 Wide web crystals photographed to highlight surface features. Rippled structure in lefthand crystal is characteristic of wider webs grown earlier in the program. Recent crystals are both wider and ripple free (Striations on remaining crystals are due to remnant surface oxide formed during growth.

3.1.3 Methods to Enhance Web Growth Velocity

3.1.3.1 Background

The maximum crystal growth velocity in general depends on how effectively the latent heat of fusion can be dissipated from the crystal-liquid interface. For dendritic web, unlike other ribbon techniques, the latent heat can be liberated in two ways:[1,4] to the supercooled liquid from which the crystal grows and to the crystal itself. Thus in principle higher growth speeds may be practical for web growth than for methods which do not employ liquid supercooling. To date growth velocities up to 10 cm/min have been achieved albeit on relatively thin ribbons;[4] 4-5 cm/min are more typical of the state of the art as we show below.

The experiments described in this section deal mainly with ways to improve radiative loss from the silicon web, the most direct route to improve practical growth speed. We used the mathematical model described in Appendix 1 to assess the effects of furnace parameters, e.g susceptor lid thickness, growth slot width, shield and aftertrimmer temperatures, on web growth rate. The situation can be visualized with the aid of Figure 18 from an earlier report. As the model analyses, and intuition would suggest, radiative loss from the web can be improved in the following ways:

(1) Reduce the temperature of the top radiation shield, e.g. use extra radiation shields above the susceptor lid;

(2) Increase the growth slot width;

(3) Increase the view angle in the susceptor lid (bevel the slot);

(4) Raise the web-liquid interface closer to the susceptor lid, and

(5) Reduce the susceptor lid thickness.

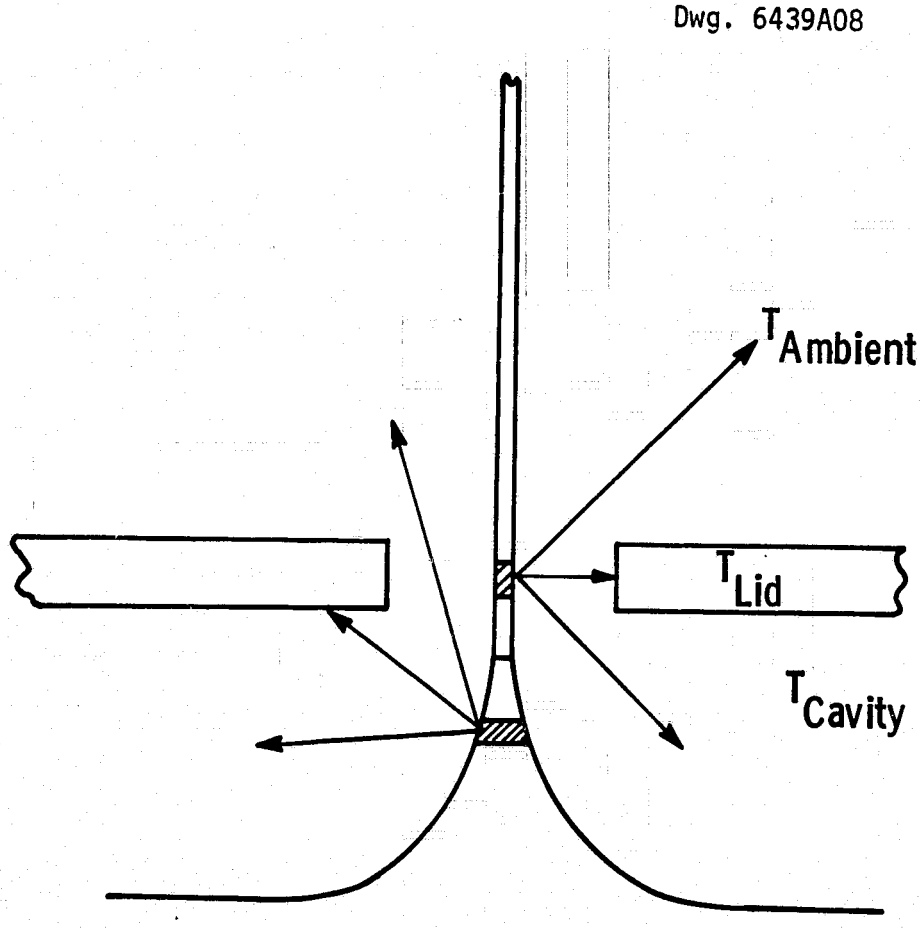

Figure 18 Paths for heat loss from the web crystal and adjacent liquid meniscus.

We have successfully applied a number of these approaches during Phase II, routes (1), (2), and (4) having been most effective so far. The thermal model for the web system predicts that for a given furnace geometry the relationship between web thickness and velocity will be of the form:

$$v = a + \frac{b}{t} \tag{13}$$

where t is the web thickness and a and b are constants specific to the growth configuration (for a given t, a system which more effectively dissipates heat will produce a higher growth velocity). Thus by measuring the thickness of webs grown from a fixed furnace condition as a function of the pull speed, a velocity-thickness plot is developed which is characteristic of that condition. We used this method to determine the effectiveness of specific growth geometries to increase web growth speed.[4] The model output was used to guide the choice of the initial configuration to be tested. The following sections highlight the results of these studies; details of the specific runs, most of which were carried out primarily in the J furnace, are tabulated in the Appendix 2, and discussed in Reference 4.

3.1.3.2 Increasing Growth Speed Via Lid Slot Design

We carried out a series of experiments to evaluate how beveled lids and slot width affected growth speed. Melt to lid height was also investigated by employing a lid which was recessed into the cavity above the melt.

Briefly, if a thick (9 mm), flat lid is considered a base case or slow growth geometry considerable improvement in growth speed is attained simply by introducing a beveled profile along the lid, (for example as shown in the left side of Figure 10.) In this way, speed increments of 2 to 3 times the base case were reached. That is, the velocity-thickness curve for a beveled lid shifts vertically up the

speed axis as the amount of bevel section is increased. Speeds up to 5 cm/min have been achieved this way.

By shielding the hot lip of the growth slot from the growing web, a further speed increase is gained. This situation is depicted by Mod 2 (right side) of Figure 10. The drawback to this approach is that an overhanging lid like that shown in the figure can collect oxide. To circumvent this problem, we introduced a pair of argon flow tubes (also shown in the Figure) parallel to the growth slot. Argon purged between the lid and shield can then be employed to prevent oxide deposits. A series of runs in the RE furnace, (Appendix 2) proved the validity of the approach (two other argon flow techniques have also been tested on the W furnace, viz. Section 3.3.3, but the best method is still undecided). This now makes possible the use of high speed lid configurations previously unfeasible. It also provides a means to introduce convective cooling of the web, an approach we have not previously explored.

A further evolution of the beveled lid concept is shown in Figure 19. The bevel is recessed with only a small straight lip over the liquid. Radiative transport was increased so that growth rates over 6 cm/min could be achieved on webs over 2.5 cm wide. By increasing the slot width of this design growth speed was further raised to 7 cm/min.

While we can achieve speeds commensurate with high overall output rates there are two difficulties which must be overcome to make such procedures routine and to stabilize growth conditions for longer periods. One of these is to better control the seeding operation for "fast" lids which provide greater radiative heat transport. Typically, during seeding both melt undercooling and growth speed are adjusted during a short transient to produce the button and initiate web growth. The added heat loss in a fast lid makes this adjustment more difficult for the operator to reproduce. Thick buttons may result. Within these buttons, extra twins (Figure 20) form, causing lineage structure to propagate into the web.[4] Improved parameter readout and control should resolve this difficulty; and this activity will form part of the future web development program.

Dwg. 7686A09

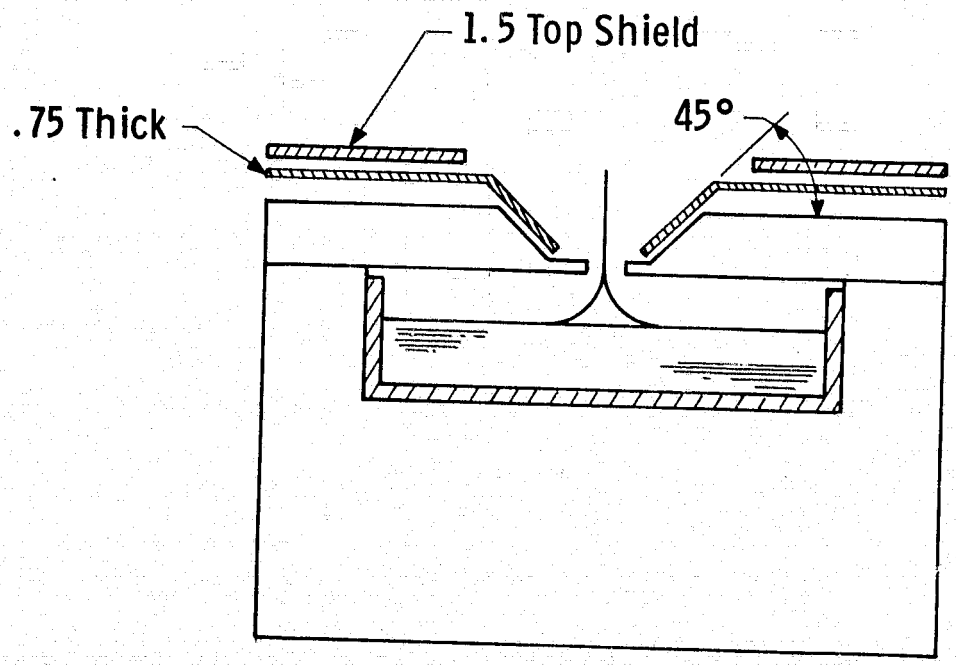

Figure 19 Lid slot design with large radiative view factor.

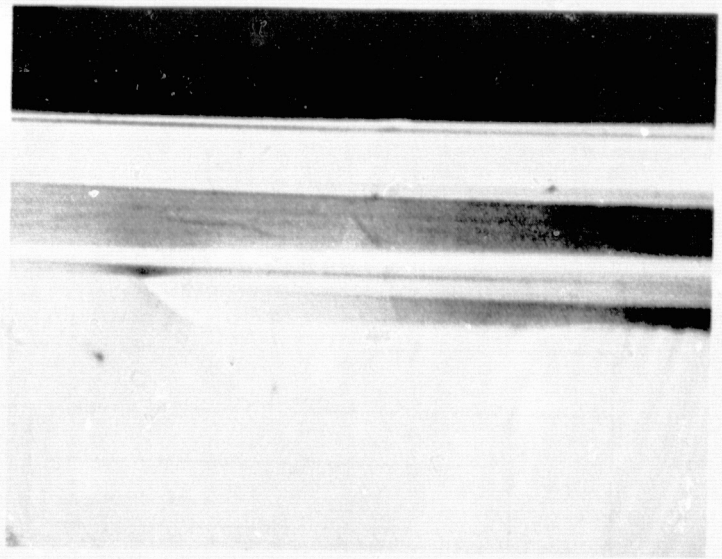

Figure 20 Extra twins formed during the seeding process when the crystal is excessively cooled.

Another way to increase web growth velocity is to raise the melt level closer to the lid slot. This may be accomplished by recessing the lid itself or by feeding silicon to the melt. One set of experiments conducted with a recessed lid produced speeds over 5 cm/min.

3.1.4 Combined Output Rate

Because techniques to increase web width and growth speed can be investigated in tandem, parallel efforts have been carried out as discussed in the preceeding sections in order to utilize program resources effectively. By this approach, speeds (8 cm^2/min) and widths (4.2 cm) have been independently demonstrated and if achieved simultaneously, would exceed the web output rate goal of 25 cm^2/min.

Recently we coupled the developments for width and speed, employing lid designs with relatively flat melt temperature profiles and good radiative loss. In this way we were able to achieve an output rate of 23.6 cm^2/min, very close to the target value for the program. Output rates above 18 cm^2/min have been reached on a number of occasions, Table 2. These improvements in output rate may be compared with the maximum value of 8 cm^2/min demonstrated by the end of the Phase I program.

We have not yet been able to sustain high output rate growth for prolonged periods.This isbecause in our present system, as the web crystal grows and widens, silicon is consumed and the melt level falls. There are two serious impacts. First, heat loss from the web is reduced causing the web to thin. Second, web stress levels are increased so that deformation is promoted. These observations (which are consistent with our computer simulation results) are described in detail in Appendix 2. The implication is that high growth rates and optimum web widths obtainable with proper lid design, can only be sustained for short periods in a run unless some control action is taken. Melt replenishment, in fact, is a far more elegant and necessary way to solve the problem. The status of melt replenishment technology development is covered in Section 3.2.

TABLE 2

RECENT WEB OUTPUT RATE RESULTS

RUN NO.	THROUGHPUT RATE cm^2/min	WIDTH mm	GROWTH VELOCITY cm/min
J-95	12.3	23.0	5.35
J-123	11.4	22.4	5.1
	8.8	30.8	2.9
J-125	14.7	25.0	5.9
J-126	12.2	14.7	8.3
RE-98	11.2	26.2	4.3
	12.7	25.5	5.0
J-129	12.3	24.2	5.1
RE-99	12.7	23.2	5.5
	14.8	27.9	5.3
RE-100	12.8	21.3	6.0
J-131	12.7	26.5	4.8
	13.7	29.3	4.7
	14.3	26.0	5.5
	12.3	24.2	5.1
RE-101	10.4	27.5	3.8
RE-102	11.9	23.9	5.0
	13.4	26.7	5.0
J-133	15.7	29.1	5.4
	13.9	32.3	4.3
J-135	12.2	24.0	5.1
RE-105	19.8	33.0	6.0
RE-107	15.1	35.5	4.25
RE-108	16.4	31.6	5.2
RE-113	14.3	30.4	4.7
RE-120	14.7	25.1	5.85
RE-122	13.5	27.5	4.9
RE-123	14.8	35.2	4.2
RE-124	17.0	31.7	5.35
RE-126	14.3	25.0	5.7
	15.3	29.2	5.25
RE-127	18.7	30.5	6.1

TABLE 2 (Cont.)

RECENT WEB OUTPUT RATE RESULTS

RUN NO.	THROUGHPUT RATE cm^2/min	WIDTH mm	GROWTH VELOCITY cm/min
RE-128	12.4	31.1	4.0
RE-130	18.7	32.5	5.75
	12.8	34.5	4.0
RE-131	21.9	34.2	6.4
RE-132	20.1	36.6	5.5
RE-133	23.6	40.6	5.8
RE-134	16.5	39.9	4.15
RE-135	12.8	34.1	3.75
	14.3	37.2	3.85
J-163	21.7	32.5	6.75
J-164	20.0	34.9	5.74

3.1.5 Summary

Web widths over 4 cm have been produced on several occasions by employing thermal shield designswhich limit radiation from the hot growth lid to the web. The material is free from structural ripples encountered in the widest web crystals grown previously. Bending of the web still remains an obstacle to further width increase, although our recent successes suggest the experimental directions for future improvements in width.

By suitable design of the growth slot width, slot profile, and adjustment of melt height, web growth speeds up to 8 cm/min have been achieved although rates to 5 cm/min are more common. For some of the high speed lid configurations, stable seeding conditions are difficult to maintain. This situation can be improved with signal indicators to give real time output of undercooling and pull speed during the seeding transient. With this information, to be developed during the next phase of the program, appropriate seeding conditions can be controlled and reproduced.

Combining the techniques evolved to improve web width and speed produced a demonstrated web output rate of 23.6 cm^2/min, very close to the goal of 25 cm^2/min. These rates are significant improvements over the 8 cm^2/min accomplished a year ago. The need for a constant melt and stable thermal conditions to sustain high output rate operation has been clearly identified.

Melt depletion during growth significantly alters heat loss from the web; high speed growth can then no longer be maintained without web thinning. Continual, thermal adjustments are required for thermal stability as the melt drops. If improperly carried out, this corrective action may actually destabilize growth at high output rates. An operational melt replenishment system with level control is the most effective solution to this problem, both for technical and economic reasons.

3.2 Melt Replenishment

3.2.1 Background

It is now well established that melt replenishment (or some equivalent procedure) will be required to achieve process economics for almost all of the ingot, sheet, and ribbon growth technologies if the 1986 LSA wafer cost objectives are to be met. For web growth melt replenishment is mandatory not only for cost reasons, but to sustain conditions for high output operation as described in the foregoing sections of the report.

As part of this program, our objective has been to demonstrate the feasibility of simulatneous web growth with melt replenishment. Silicon feedstock in the form of pellets 2 to 4 mm in diameter was chosen for our development because this approach offers several advantages:

(1) The pellets cause only slight temperature perturbations when fed to the melt.

(2) Additional system power requirements are small.

(3) The pellets are readily metered with simple, inexpensive equipment to replace the silicon consumed in growth.

(4) The approach lends itself to subsequent automation.

(5) Polycrystalline silicon produced by the LSA Task 1 is very likely to be in pellet form.[13,14]

Our initial experiments in melt replenishment included tests with manual and mechanized pellet feeders, design and test of a pellet injection system, development of a compartmented crucible to separate the injected pellet from the growing web, and a successful demonstration of web growth with simultaneous replenishment. The highlights of this work are described here; reference 4 may be consulted for further details.

3.2.2 Melt Replenishment Equipment

Two types of feed systems were utilized. Initially,a manual feed arrangement was employed in conjunction with an elongated susceptor system (RE furnace) to develop baseline data on pellet injection, crucible design, and growth parameters for feeding. Later a mechanized feeder was designed, built and operated in conjunction with a round susceptor system (W-furnace). These studies provided information on susceptor shielding, lid design, feed tube design, feed rates, and operation of the feeder itself which could then be applied to the standard elongated susceptor. This approach was taken to expedite output rate studies which required the use of the elongated susceptor in the RE furnace.

Manually-activated System. The manually-activated pellet feeder is depicted in Figures 21 and 22. The functional parts of the manual feed system are (1) a chamber for storing a supply of silicon pellets, (2) a manipulator mounted on top of the storage chamber which enables the operator to drop pellets into a funnel topped feed tube, and (3) a feed tube assembly. The feed tube assembly incorporates a valve so that the storage chamber may be isolated from the furnace growth chamber for reloading.

A susceptor lid and set of top shields were modified to allow penetration of a quartz feed tube at a position near one end of the crucible. A quartz barrier was positioned 16 mm from one end of the crucible with a nominal 1.6 mm spacing from the crucible bottom so as to provide a "leaky" replenishment compartment (see also Section 3.2.3). The purpose of the barrier is to prevent unmelted feed material from floating into the growth region of the melt and interfering with web growth. Feed stock consisted of 3 mm polysilicon cubes. The size was selected as convenient for manual feeding at a reasonable rate for evaluation purposes, but not to be construed as ideal for a practical automated melt replenishment system.

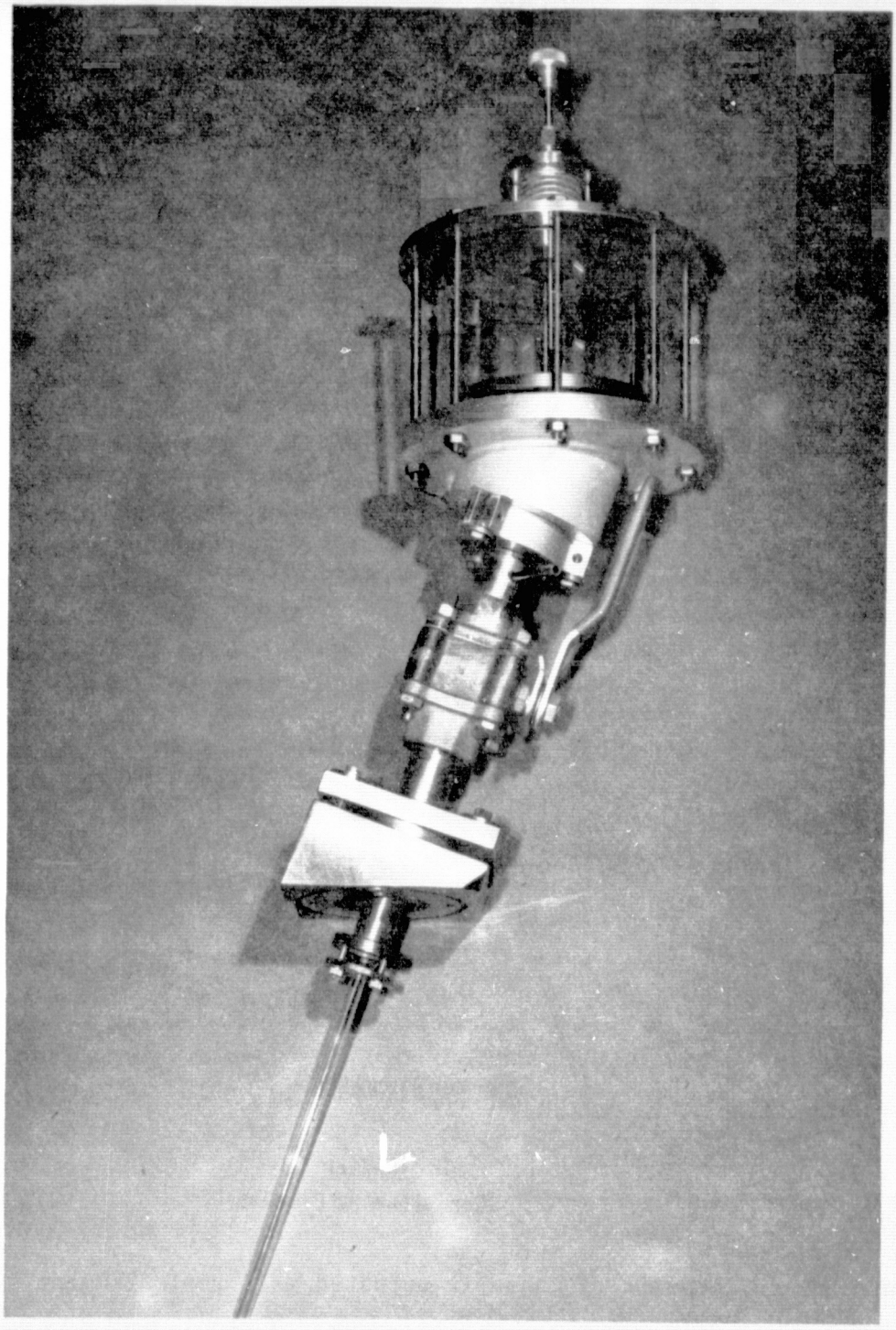

Figure 21 Photograph of manually actuated melt replenishment system.

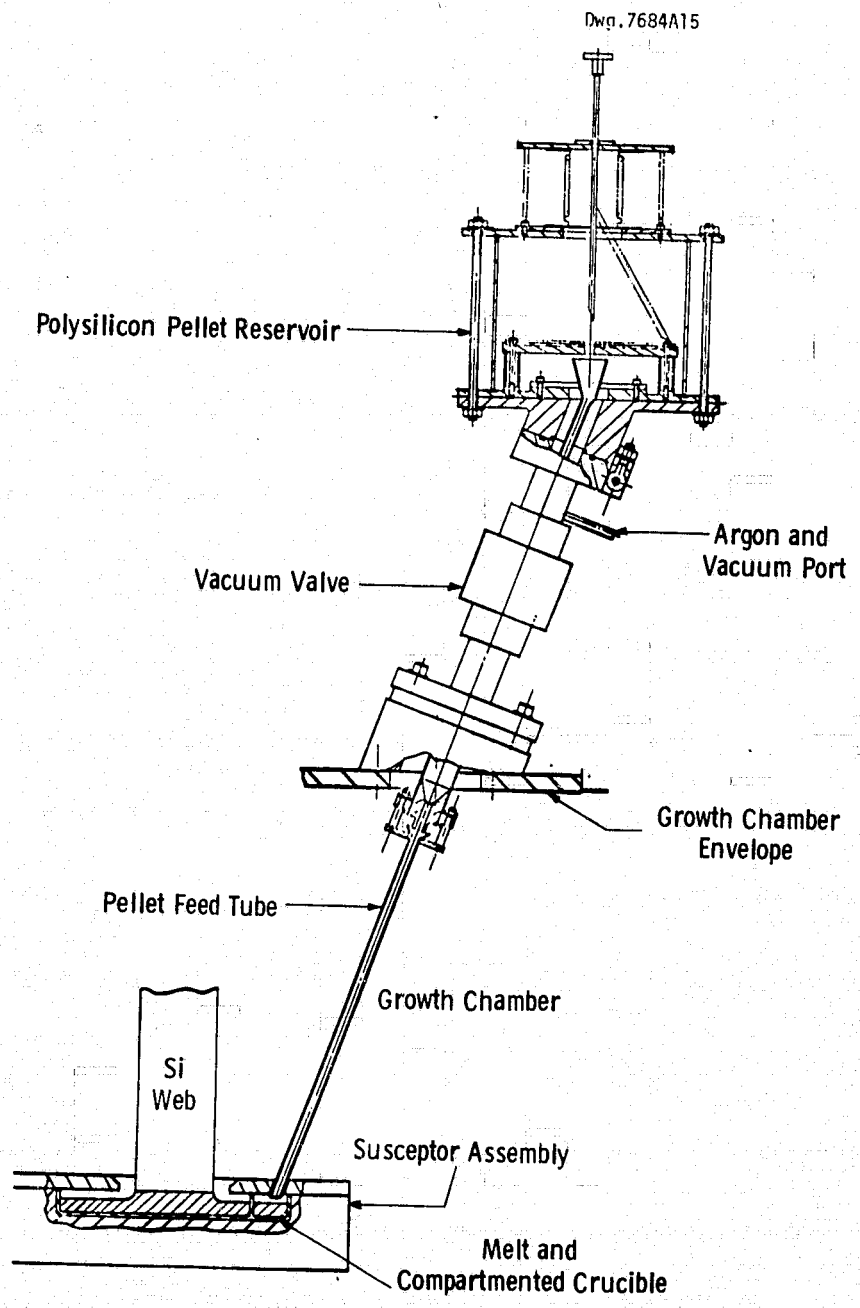

Figure 22 Schematic of manually actuated melt replenishment system.

Mechanically-activated System. A mechanically-operated pellet feeder was developed and built to replace the manually operated system. The mechanically-activated melt replenishment system provides all of the function of the manually operated system and, in addition, pellets can be fed on command and at a programmable rate. This improves experiment efficiency since the operator is freed from the laborious task of feeding individual pellets while monitoring web growth. Since the pellets can be fed at a variety of rates it is considerably easier to approximate and replenish silicon consumed during growth. Finally, with appropriate level sensing a truly operational replenishment system can be implemented with this pellet feeder as its basis.

The heart of the system is a slowly rotating dish called a separator, Figure 23 . It is presently made of polished stainless steel and is turned at the same rate as the pellets are fed. Its job is to separate one pellet from the load of pellets in the dish. The dish is inclined at 35 degrees from the horizontal so that the pellets tend to flow, not tumble, to the lower side. In the bottom of the dish near the vertical wall is a 4.2 mm hole. The hole diameter is just slightly larger than the maximum pellet dimension (e.g, the diagonal of a 2.4mm cube is 4.15 mm). With the dimensions chosen, only one pellet fits into the hole, so that as the dish turns, a pellet falls into the hole, and is separated from the mass of pellets remaining.

The bottom of the hole in the dish is covered with a spring loaded gate, actuated by a fixed cam which releases the captured pellet once every revolution of the dish. In the present model, the maximum rate is 30 pellets/minute. To double the rate a second hole can be added, etc. The release point is determined by the location of the cam. The present concept calls for the pellet to be released or dropped into a small funnel which leads through a tube directly into the melt.

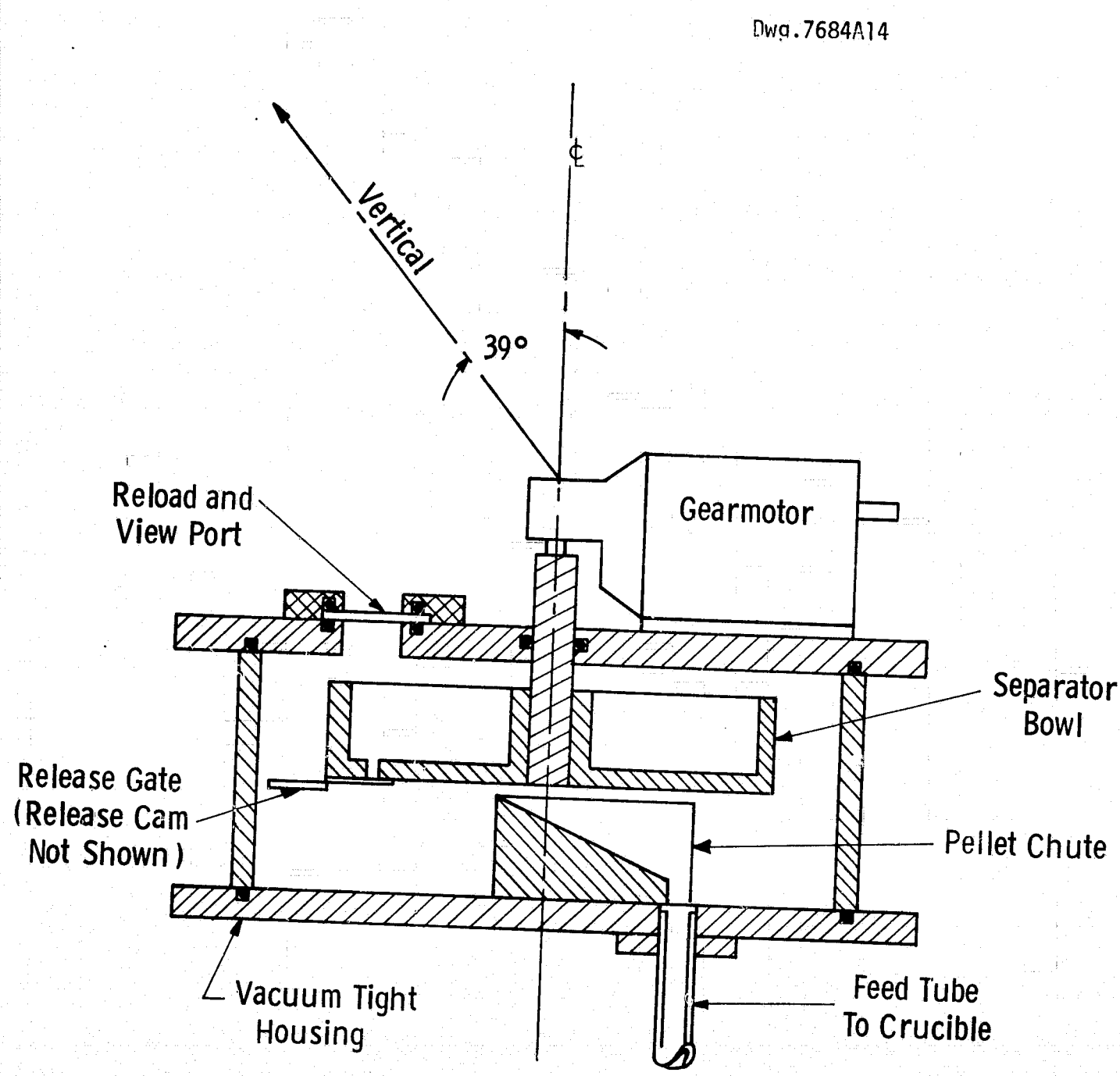

Figure 23 Mechanically-activated pellet reservoir and feeder.

Some important features of this system are:

(1) Capable of feeding both cubes and spheres

(2) Feed a single pellet at a constant rate up to 30 per minute

(3) Does not contaminate or abrade the pellets

(4) Low vibration level so the growing web and surrounding liquid are undisturbed

(5) Capable of operation with inert gas or vacuum

(6) Reservoir can be reloaded without impact on crystals being grown.

Since the pellets can be fed at a variety of rates it is simple to balance the feed rate with the silicon consumption rate during web growth. Clearly, with appropriate level sensing a truly closed loop replenishment system is possible with this approach.

Testing of the system commenced using the round susceptor of the W-furnace. The pellet feeder is shown installed on the furnace, Figure 24 , as it was operated for the experimental runs.

3.2.3 Melt Replenishment Results

Web Growth With Manual Feeding.

The first melt replenishment experiments employed the manual feed system in the RE furnace and were largely concerned with crucible barrier designs and gas flow management.

The first step in feeding was the development of a compartmented crucible to separate the feed and growth chambers, viz Figure 25. The crucible used a quartz barrier which prevents pellets injected into the feed chamber from floating into the growth region where they may cause crystal degradation or termination of growth.

The barrier must also permit molten silicon to pass between the feed chamber to the growth chamber, so that some form of opening was required as well. Several designs were tested;[4] the most effective was a rectangular "mouse hole" like that shown in Figure 25. This barrier design was used regularly, but at first did not give reproducible behavior.

Figure 24 Mechanically-activated feeder mounted for experimental operation on the W-furnace.

Dwg. 7695A07

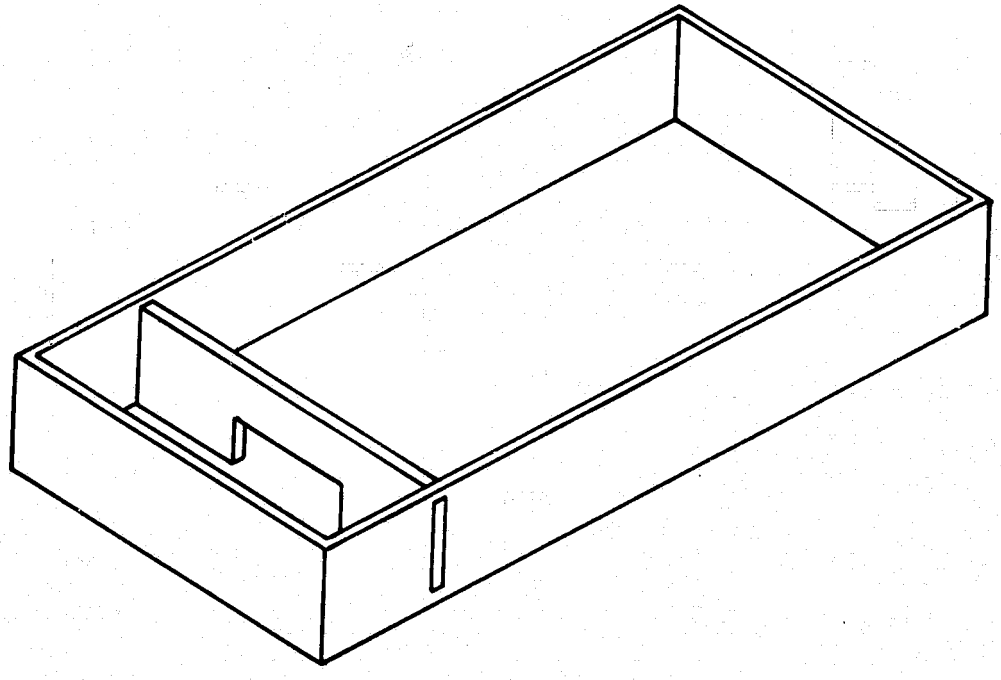

Figure 25 Type "C" barrier in quartz crucible.

During several runs the feed chamber was observed to empty completely, but at other times it remained full. It was determined empirically that the proper melt-down procedure was the key to keeping silicon in the feed chamber of the crucible.[4] When the material in the feed chamber is melted first (by shifting the coil position), the feed chamber remained filled with silicon throughout a run. This procedure is reproducible and has been adopted with success in all subsequent runs.

Another difficulty in the initial replenishment experiments was the clogging of the feed tube with a thin layer of silicon monoxide which interfered with pellet injection. To prevent oxide buildup, an argon flow system incorporating a flow meter was installed in an entry tube. A metered flow of argon then could be maintained down the feed tube. Tests with flow rates between 25 and 500 cm^3/min indicated that a flow rate of about 100 cm^3/min was adequate to prevent feed tube clogging. This procedure has also been adopted in all subsequent runs. Finally, from time to time as pellets are fed, tiny particles of silicon nucleate on the surface of the melt, float to the web, and either terminate growth or impair crystal quality. The occurrence was sporadic, sometimes occurring at the initiation of feeding, and sometimes much later in a run. This problem, also encountered with runs in the W-furnace, has been alleviated to a large extent by gas flow management and improved thermal shielding as discussed in later sections.

Web Growth with the Mechanically-activated Feeder. Figure 26 illustrates the components of the feed system employed on the W-furnace: (1) mechanized feeder with pellet reservoir, (2) feed tube assembly (3) compartmented crucible and (4) modified susceptor lid and shields. This figure will serve as a convenient reference for the discussion to follow.

As noted above, intermittent interruption of web growth by free-floating silicon particles occurred during the first feeding experiments. Two hypotheses were advanced to explain the behavior: (1) blow over of minute oxide specks from material deposited in the feed tube and (2) remelting and subsequent floating of

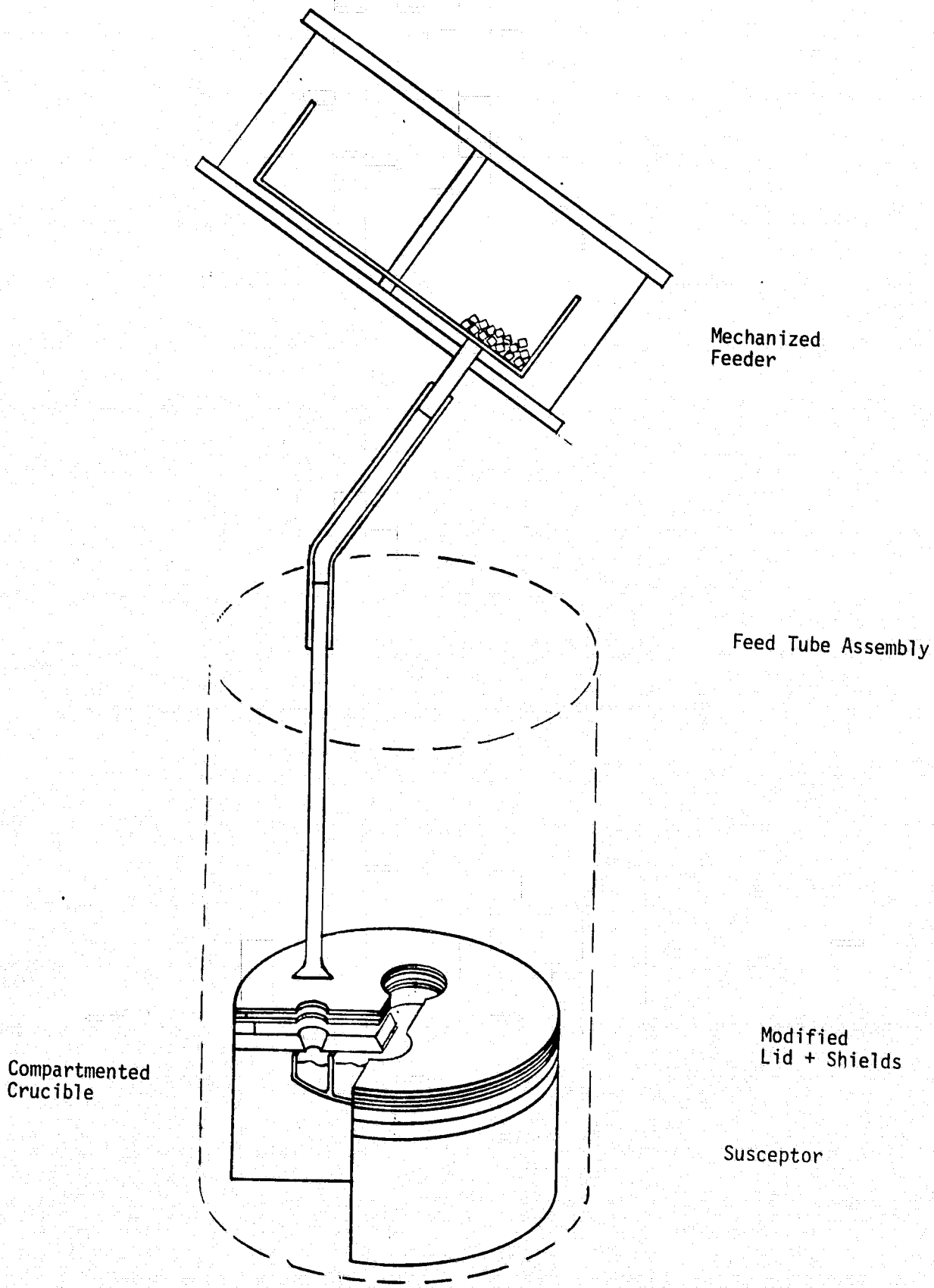

Fig. 26 SCHEMATIC OF AUTOMATIC FEEDING SYSTEM

dendritic silicon crystallized on the quartz barrier during temperature excursions in the system. Each possibility is depicted in Figure 27. As the W-furnace is equipped with a venturi system (see section 3.3) for controlling and directing gas flow, it was logical place to carry out experiments to eliminate mechanism number (1) as the cause of the sporadic ice particles. The venturi effect produces a counter flow of gas away from the growth region which should hinder particle carry over. (One disadvantage we recognized in the W-furnace is its round susceptor system which is not as well-suited thermally as an elongated susceptor is for feeding. The dimensions of the round susceptor place the feeding chamber very near the growth region.) Application of the W-furnace to melt replenishment studies also expedited use of the RE and J furnaces for improving web output rate technology as described earlier.

The first replenishment runs were plagued by the formation of dendrite spikes which developed as the melt was supercooled,and grew from the crucible edge toward its center. Thus attempts were made at once to minimize heat losses from the feed chamber. The first such experiment involved the addition of a molybdenum heat shield to the rear of the susceptor. This proved very effective for melting of pellets without the intrusion of ice fronts. Initial feeding periods up to 35 minutes were obtained.

Longer runs were hampered by the type of floating ice originally observed in the manual feeding experiments. The suspected cause was oxide carry-over from the feed tube which usually became coated during operation. To reduce oxide accumulation a flared feed tube, raised above the top shielding, Figure 28, was installed. This significantly reduced the build-up of oxide on the tube and underlying shields. For example, compare the oxide-free condition of the flared feed tube(center of Figure 28) with that of the straight tube after a days run.

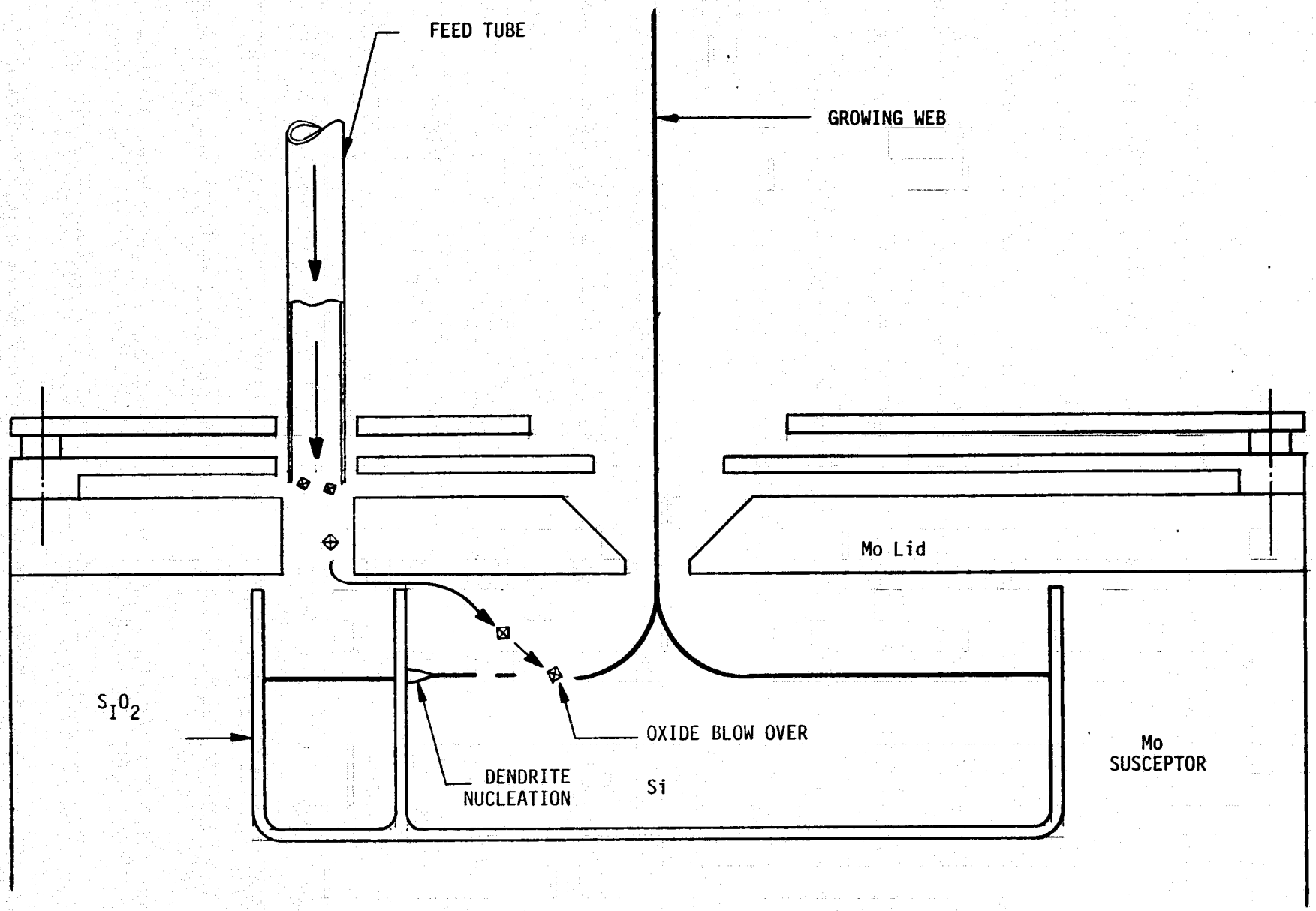

Figure 27 Mechanisms for the formation of free-floating silicon "ice" during melt replenishment.

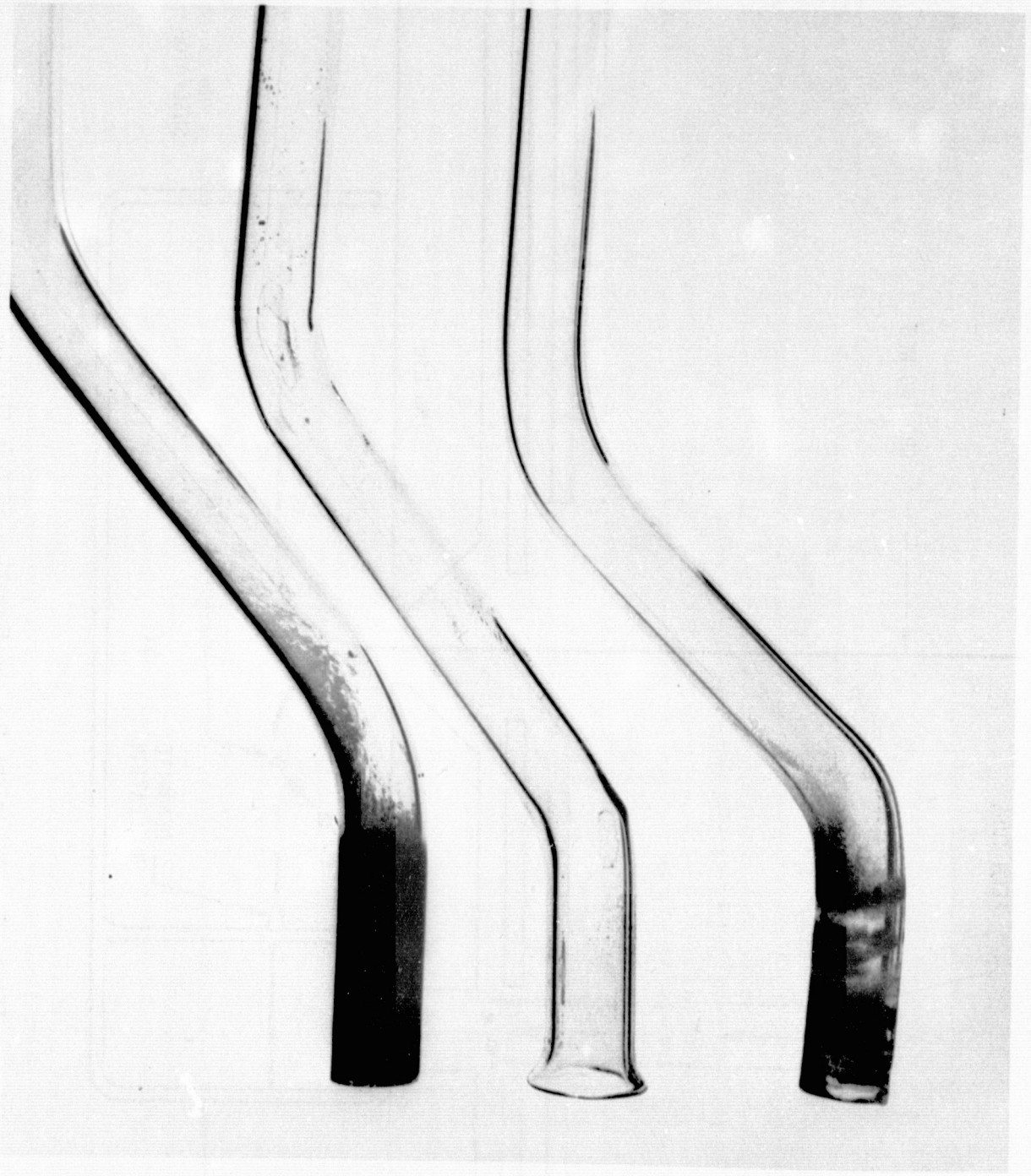

Figure 28 Flared feed tube (center) remains free from oxide buildup after one day run; straight tubes contain heavy oxide build-up.

With the reduction of oxide accumulation the replenishment results again improved considerably simultaneous growth and feeding for periods up to 50 minutes being achieved. In these experiments web growth was again terminated by floating ice. However, this time the silicon particles were in the form of small dendrite spikes. We believe that these spike-like particles were generated by dendrite nucleation on the quartz barrier as depicted in Figure 27. The dendrites once formed then melt off as the temperature of the feed chamber cycles with the injection and melting of the pellets.

The use of a tapered feed hole, Figure 29, (which diminished radiative loss in the vicinity of the hole and barrier by a factor of four) reduced, but did not completely eliminate, the incidence of dendrite spikes. Growth periods with replenishment over an hour were, however, readily attained before any spike formation took place.

3.2.4 Summary

We have demonstrated the feasibility of growing web while concurrently replenishing the consumed silicon. The replenishment technique, pellet feeding, is relatively simple, inexpensive and lends itself to closed loop control. A mechanically-activated, programmable pellet feeder has been successfully tested. Most important as we show in section 3.4, solar cells made on replenished material give excellent conversion efficiency. Apparently the melt replenishment technique we employ does not adversely effect material quality.

So far replenishment for extended periods has been hampered by the formation of free-floating silicon particles, or ice, which attach to the growing web, terminating growth in some cases. Two causes for the ice were identified, nucleation by oxide from the pellet injection tube and dendritic freezing from the quartz barrier in the crucible. The former was essentially eliminated by means of gas flow management (venturi system) and tube design. The latter condition could not be completely circumvented in the small, round susceptor of the W-furnace. We believe that with proper thermal shielding dendrite nucleation will be eliminated in the elongated susceptor system.*

* Experiments conducted as this report was being prepared confirm this conclusion.

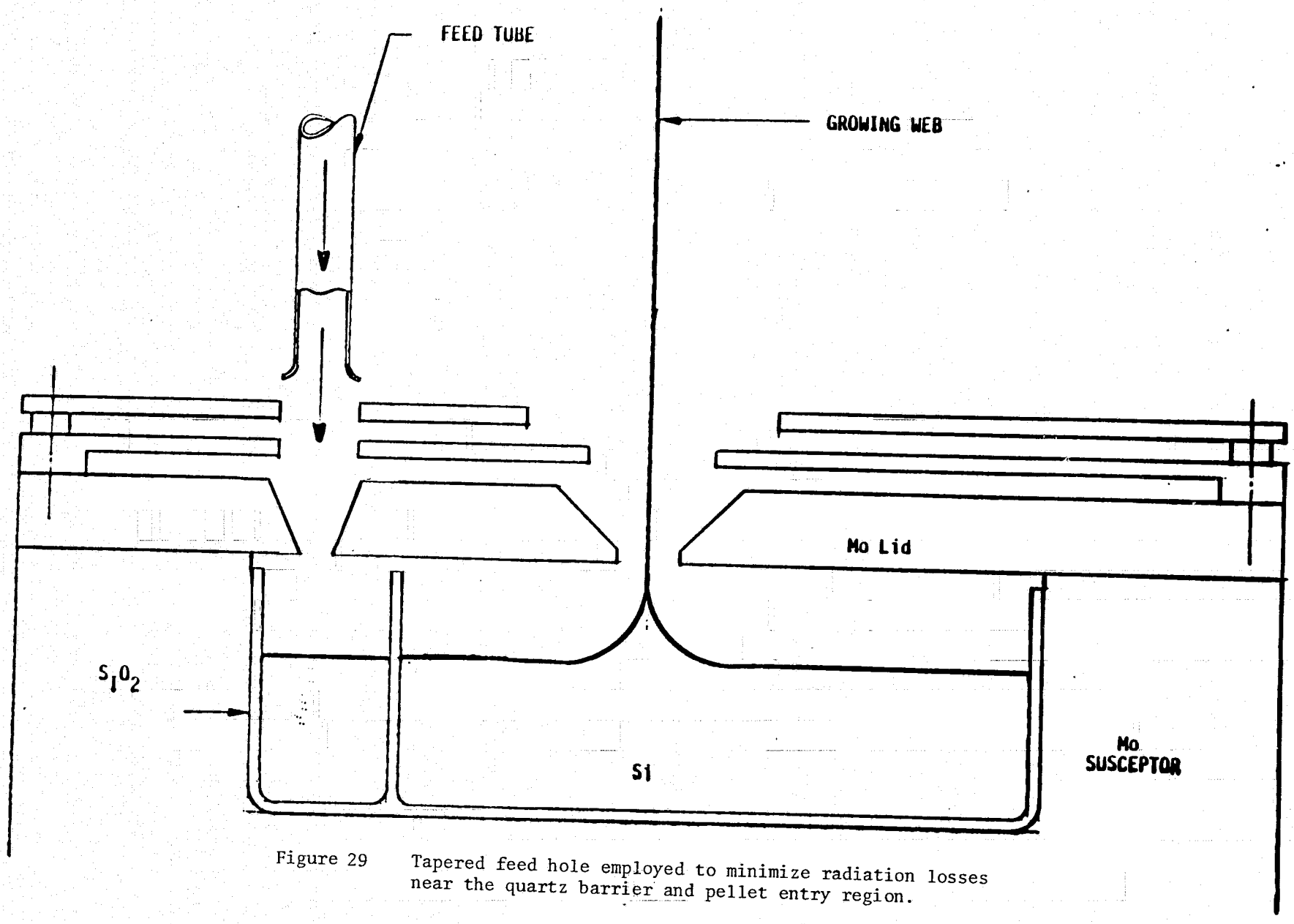

Figure 29 Tapered feed hole employed to minimize radiation losses near the quartz barrier and pellet entry region.

3.3 Techniques to Improve Process Control

Besides the improvement in web output rate and the development of melt replenishment techniques, both of which are central to the objectives of this program, we have also carried out studies to further improve our control over ancillary process variables. These activities have included, for example, the development of methods to (1) improve run to run reproducibility, (2) control and eliminate oxide accumulation on furnace components (3) improve web width control and (4) eliminate extra or "third" dendrites occasionally formed during growth.

3.3.1 Factors Affecting Run Reproducibility

Experimental runs are designed to test the impact of variables such as lid, shield, and aftertrimmer design on resultant web width, speed and structure. It is, therefore, important that no hidden variables be inadvertently introduced which might mask the true experimental results. Moreover, in a practical sense, day to day production operations when they begin must be highly reproducible in order to assure good product yield. Two factors, lid and crucible preparation were identified in our studies as requiring control for day to day run reproducibility.

Lid Preparation. It was discovered that the surfaces of the lid slot and its edges must have a slightly different preparation from the bottom surface of the lid which is exposed above the liquid silicon. Nicks or scratches on the slot faces nucleate silicon monoxide which may grow out changing the thermal distribution over the melt, or worse fall into the melt terminating web growth. Spalling of oxide occasionally collected on the lower lid surface can also have the same effects.

Empirically, procedures were developed which when implemented eliminate both these problems. The lid slot surfaces are carefully prepared when new to remove any machining marks. Between runs they are buffed. Following this approach the slots remain oxide-free indefinitely. In contrast, the bottom surface of the lid is sandblasted. The roughening apparently causes any oxide which forms to adhere tightly so that none falls into the melt. The procedures are simple, not overly time-consuming and appear satisfactory.

Crucible Preparation. Two aspects of crucible fabrication may affect reproducibility and uniformity of heat transfer from the susceptor to the crucible, and therefore reproducibility of growth behavior for a given lid and shield configuration. These are the shape, or fit, of the crucible in the susceptor, and crucible surface uniformity.

We have found that both of these potential difficulties could be circumvented fairly simply. First, proper dimensional specification and quality control provided crucibles which fit well in the susceptor cavity thus avoiding run to run variance. Second, we found that crucible surface finish, whether smooth or ground, must be uniform across the crucible bottom if heat transport from susceptor to melt is itself to be uniform. Again proper quality control must be implemented to eliminate crucible to crucible variations.

3.3.2 Management of Oxide Deposition by Gas Flow Control

As pointed out in Section 3.1, we found that some combinations of growth lids and shields gave improvements in web width and speed, but because of their geometry collected oxide and were thus impractical to use. The initial melt replenishment work was also hindered (Section 3.2) by potential oxide collection and dispersal problems. For this reason, we carried out experiments to devise a system based on directed gas flows which could be used to control and minimize oxide collection on furnace components. Some of our results are alluded to earlier in the report; details are given here and in Reference 4.

Three types of systems were tested; two employed argon purged directly over the lid and shields; the third was a novel venturi arrangement which appears very promising especially in conjunction with melt replenishment hardware.

Argon Jet System. Certain configurations involving shields which overhang the lip of the lid slot, e. g. Figure 10, Section 3.1.2, collect oxide along the edge of the shield no matter how carefully the shield edge is prepared. Since these configurations are extremely attractive in terms of web stress reduction and growth velocity, elimination of this oxide deposition assumes considerable importance.

To accomplish this, an argon jet flow system was designed fabricated, and tested. In essence, the system consists of a pair of perforated tubes which lie on either side of the slot betwen the lid and the overhanging shield (See Figure 10). A flow meter is used to control the argon flow. A total flow of about 30 cm^3/min is sufficient to keep the overhanging shield clean throughout the run, and does not interfere with web growth. (The optimal flow rate varies somewhat with the particular shield configuration). The system appears to be very useful and has been employed to grow web crystals 4 cm wide. Some potential to improve web speed by convective cooling is also likely.

Argon Flooding. An alternative to the argon jet system was tested in the W-furnace. The main difference in the approach was that the cavity between lid and shield was flooded with argon (rather than injecting the argon through individual jets.)

The basic components of the flooding system are depicted in Figure 30. Argon is introduced at the edge of the cavity formed between the hot susceptor lid and the intermediate shield. The argon flows through the cavity, and then over the web as indicated in the figure. A variety of positions of the feed tube and gas flow rate were tried. Extremely stable growth conditions were achieved with the opposed flow geometry. Lengths of web several meters long with widths controlled to $\pm$ 1mm were grown. Subsequent characterization of the web (Section 3.4) indicated, however, that solar cell efficiency was impaired in material grown this way. The characterization data suggested that surface contamination had occurred, probably by Mo transport in the hot argon gas. This effect was not seen with the jet system. Further work on the flooding arrangement was discontinued because of the adverse effect on material quality and the highly promising results with the jet and venturi systems.

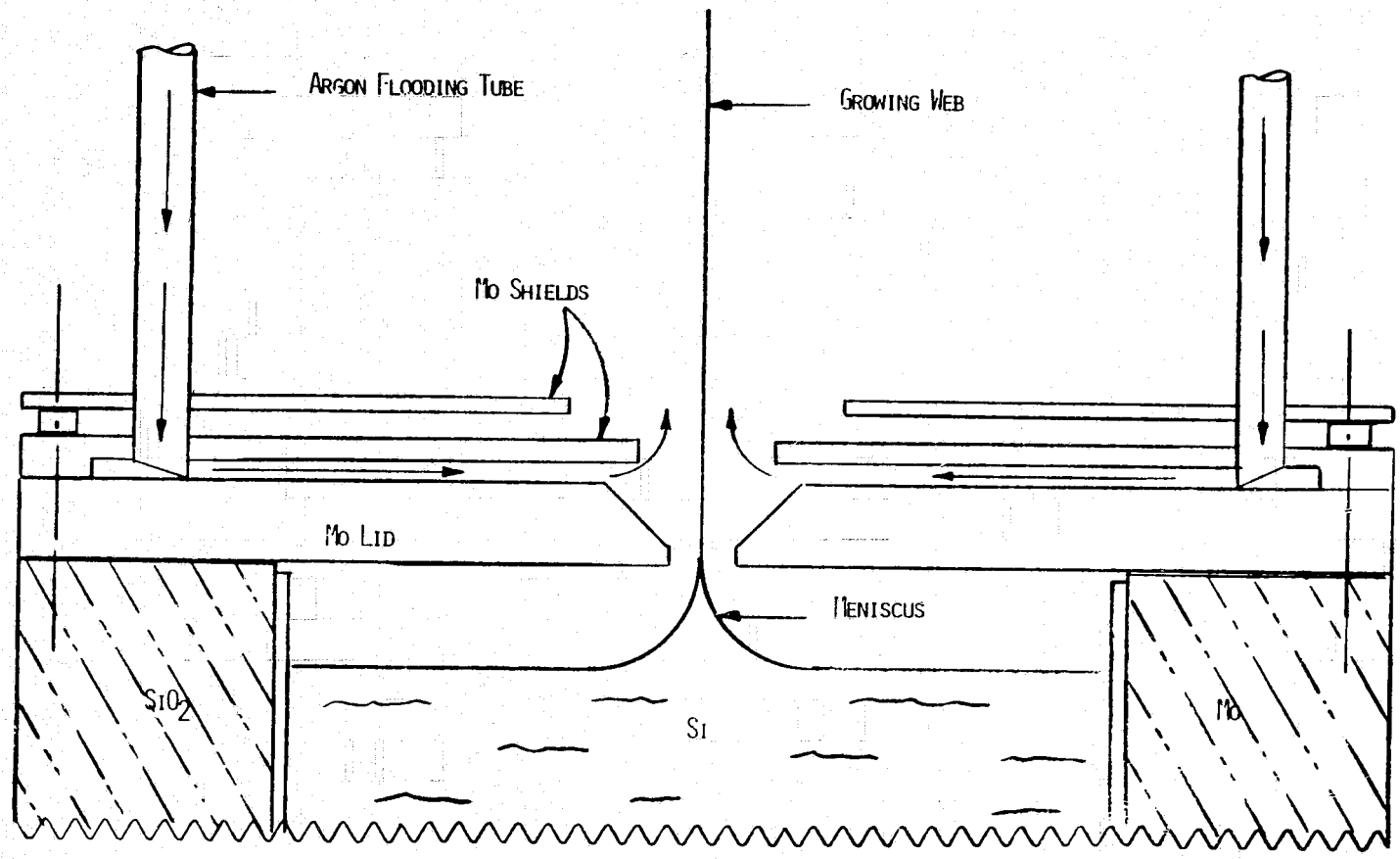

Figure 30 Argon flooding system used to eliminate oxide collection in the W-furnace.

Venturi Systems. Several venturi designs were tested in the W-furnace;[4] the most successful from the standpoint of growth stability and oxide control is illustrated in Figure 31. In the venturi method, argon gas is forced into a pair of venturi flow tubes (chimneys). This aspirator effect creates a suction which drains argon into the cavity between the lid and shield where it is then exhausted out the chimneys. A flow of clean gas passes over the web drawing oxide with it. The venturi arrangement is extremely effective. For example, no oxide deposited on the overhanging shields in the W-furnace even after an eight hour run.[4] The web surface is also kept clean and oxide free as well, Figure 32. Moreover, efficiencies measured on the webs grown this way are excellent ($\eta_{AR} \sim 14\%$).

We believe the venturi system has direct applicability in web systems designed for melt replenishment. In fact, preliminary experiments conducted on a system designed specifically for the elongated susceptor in the RE furnace have shown considerable improvement in melt replenishment and growth time.

3.3.3 Web Width Control

As the development of methods to grow web wide and fast comes to fruition it will become important to control width at a fixed value to facilitate melt replenishment automation and to meet eventual size specification on devices. Some preliminary experiments have been carried out to understand the factors controlling web width.

Figure 9 depicts how the web will eventually achieve a steady-state width dictated by the thermal profile in the melt. In principle, then, by choosing the correct lid slot design and fine tuning the temperature, one should be able to control web width. In our first experiments a target web width of 22 to 25 mm was chosen. For this width no web deformation should occur and with proper control long lengths of uniform width could be grown (no replenishment was used in these tests).

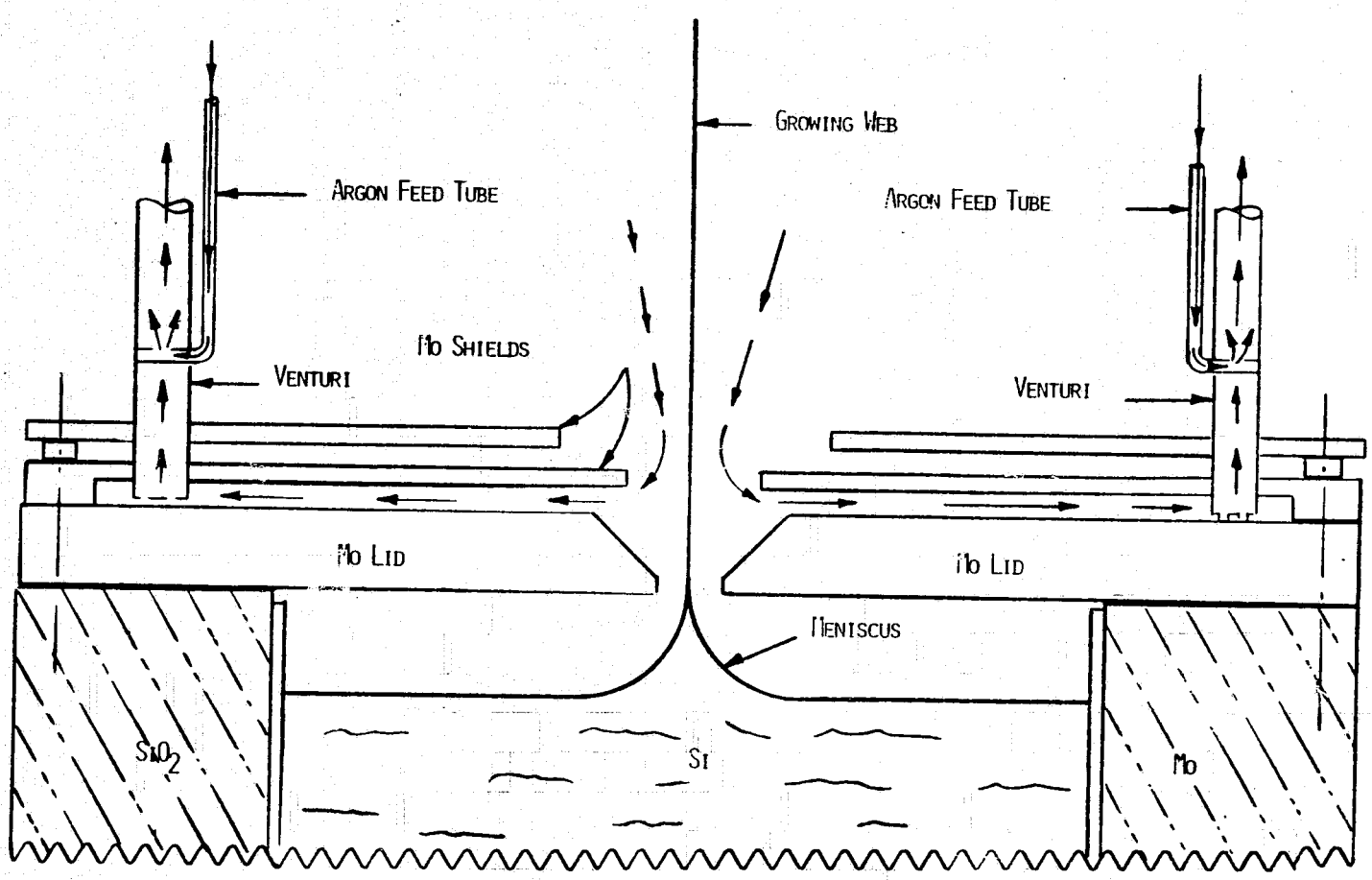

Figure 31 Venturi system used to control oxide accumulation in the W-furnace.

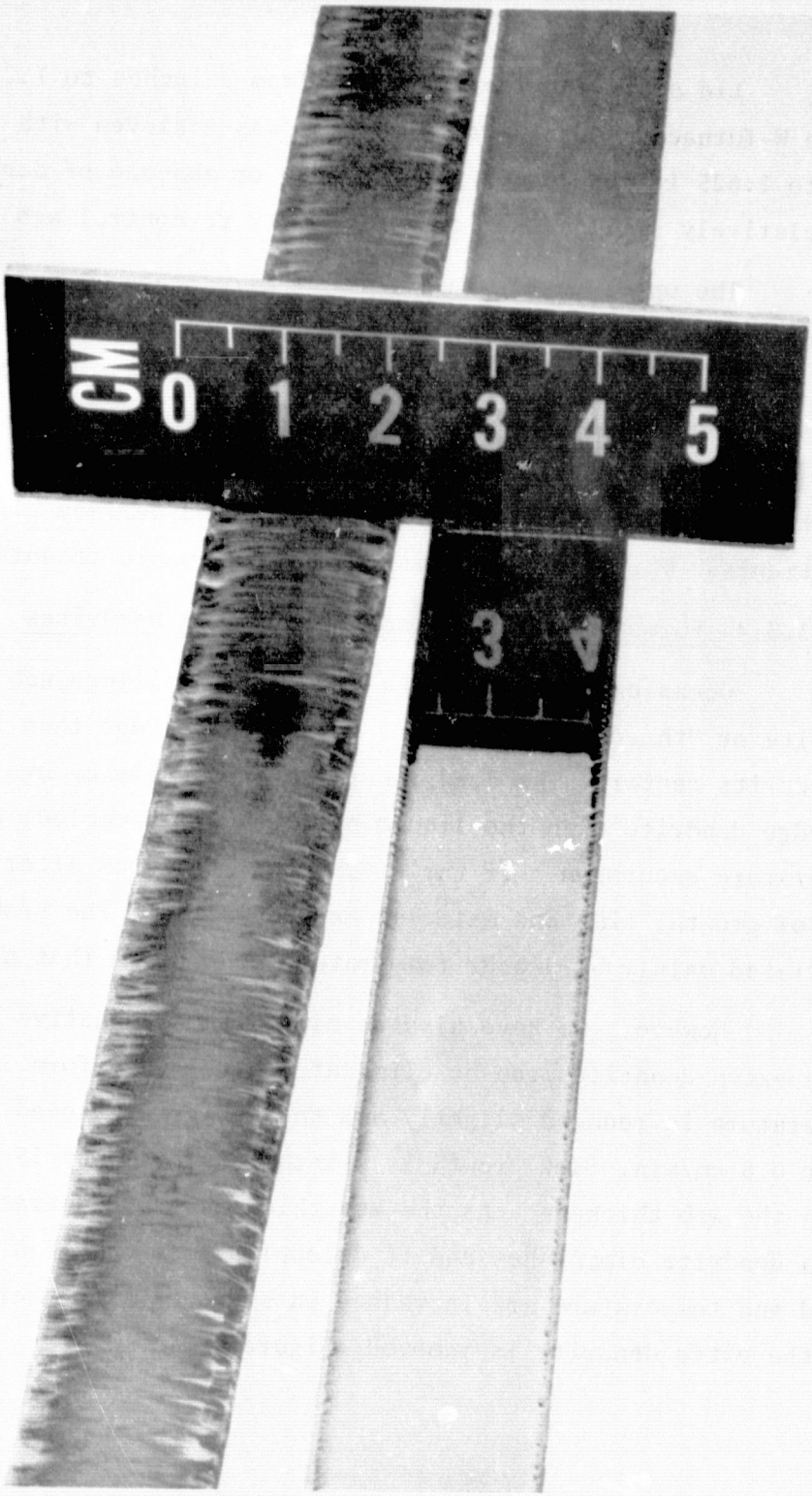

Figure 32 Web crystals grown with (right) and without gas flow control. As-grown crystal has mirror like surface when the venturi system is employed.

Lid slots ranging in length from 2 inches to 1.25 were tested in the W-furnace. Considerable success was achieved with shorter slots, 1.25 to 1.625 inches long. The presence or absence of dogbone holes had relatively small effect on the ability to control web width.

The upper curves in Figure 33 illustrate webswhich were controlled to 1 to 2 mm on an average width of about 23 mm. The lower curve in Figure 33 is for a web grown from a wider slot; the crystal widened uncontrollably eventually deforming at about 3 cm wide. Lengths up to 6 m were grown with good width control by employing short slots and utilizing an operator to view the webs and perform slight temperature adjustments. This manual process appears amenable to automation.

3.3.4 Formation and Elimination of Extra Dendrites

Occasionally during the growth of a silicon web an extra dendrite or "third" will nucleate near the web edge then grow slowly towards its center. The dendrite forms apparently by braching from the edge dendrite when the liquid becomes overly cooled, e.g by a temperature excursion. If the extra dendrite forms after a meter or more of growth, time and material may be wasted. The problem is alleviated mainly by proper temperature control so that no thirds form.

However, we have also developed an alternative procedure by which extra dendrites can be eliminated after they form. The melt temperature is reduced slightly and the web growth speed lowered to about 0.8 cm/min. Slow growth is maintained for about 15 seconds during which the web thickens. As the web thickens the penetration of the extra dendrite diminishes and it decouples from the liquid. The growth speed and temperature are increased in steps back to their initial values and the extra dendrite is removed, Figure 34 .

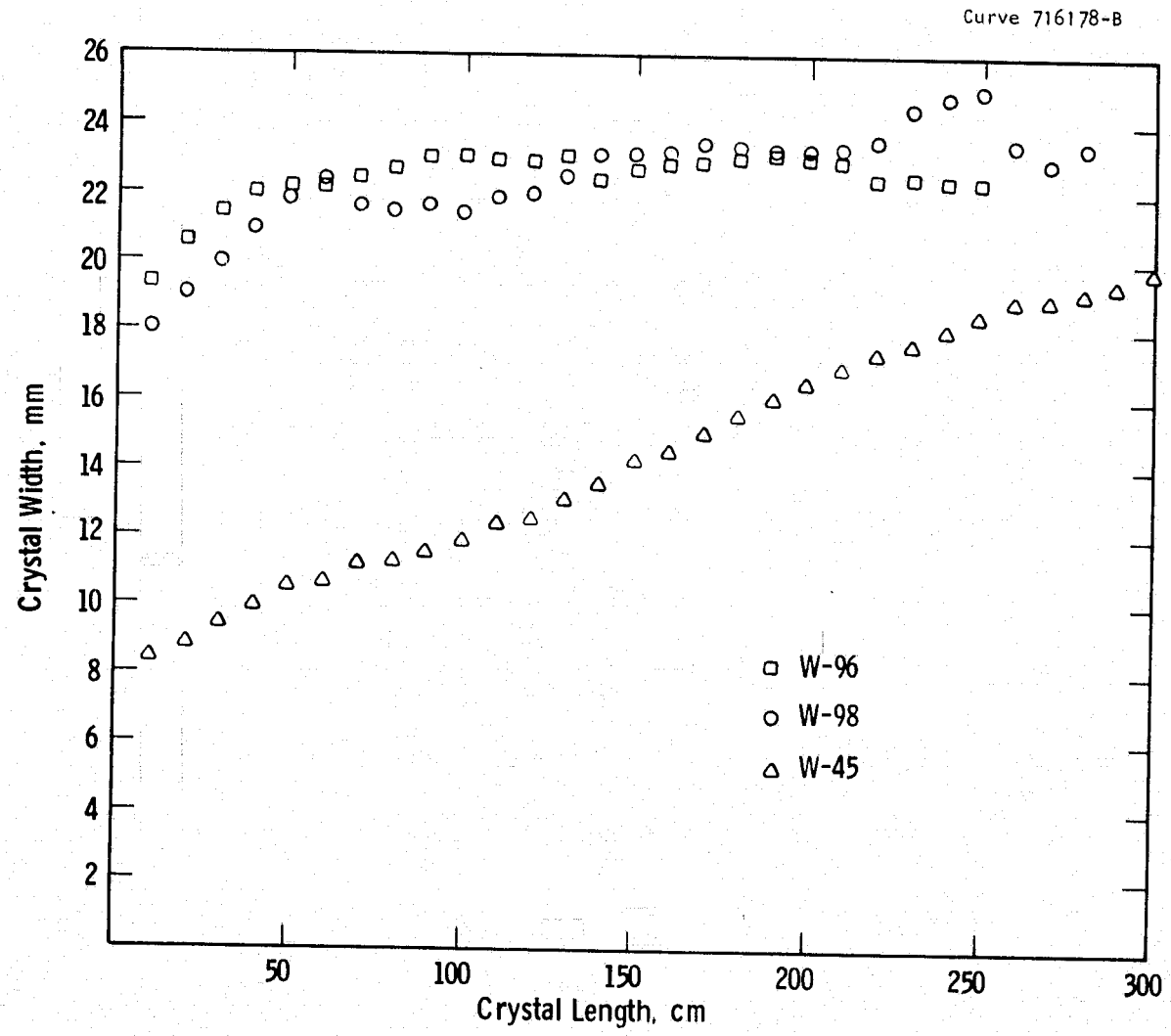

Figure 33 Variation in web width with length. Upper curves illustrate web width control by operator temperature adjustment and proper design of growth lid slot. Lower curve illustrates behavior of webs which widen uncontrollably.

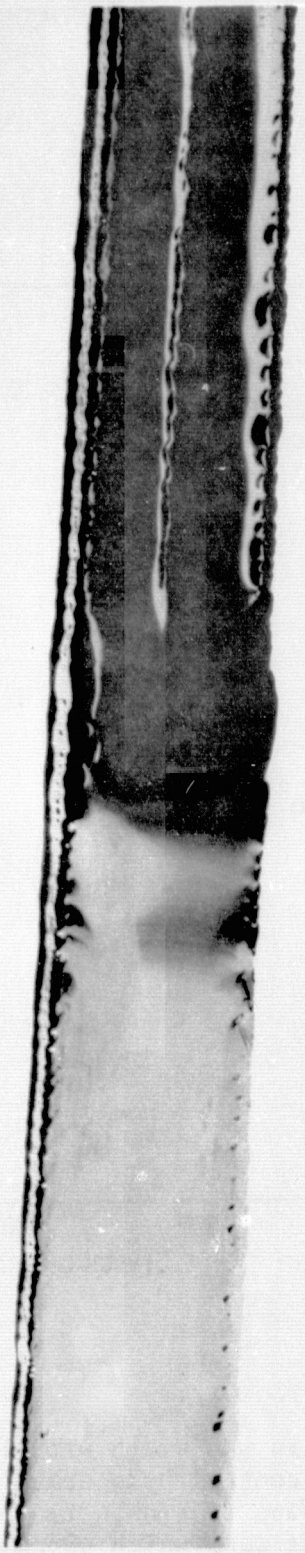

Figure 34 Silicon web in which an extra dendrite. Web was thickened by reducing pull speed. Extra dendrite is eliminated (lower portion of web).

3.4 Material Characterization

During the course of this program, the material produced has been characterized dimensionally, mechanically, electrically, and structurally. The dimensional characteristics used to correlate growth condition and output rate data are tabulated with the run summaries, Appendix 2. The principal mechanical parameter evaluated was the residual stress in the crystals; this topic has been covered in the section 3.1.1 on stress measurement and modeling. In the present section we discuss the electrical characterization of the material in terms of the properties of solar cells fabricated from web and also some recent information on the relationship between the electrical resistivity of the material and the boron doping added to the melts. A brief discussion of the web structural properties in the context of the relation between residual stress and the dislocation density is also included for completeness.

3.4.1 Solar Cell Properties

The intended application of dendritic web is photovoltaic devices, so the most meaningful test of the material quality is the performance of a standard solar cell. During Phase II of the dendritic web development program over 200 crystals (more than 800 test solar cells) have been fabricated and evaluated. The data are compiled in Appendix 3.

Standard Solar Cell: Design and Fabrication: Two 25 mm long samples are cut from each crystal to be evaluated and two 10x10 mm test cells are then fabricated on each piece. The basic p^+pn^+ cell design, fabrication procedure, testing and data analysis were discussed in detail in the previous annual report on this contract.[1] For the present web testing, the same fabrication procedure is followed with some slight modifications: (1) a cotton swab with HF is used to remove any oxide deposits; (2) an H_2SO_4 cleaning is included to remove any possible molybdenum deposit on the wafer; and (3) a SILOX masking procedure is used to restrict the p^+ layer to the back of the wafer and the n^+ layer to the front. The entire processing sequence is given in Figure 35. The dendrites are left on the blanks during processing and the cells themselves are defined by a mesa etch.400x.400 in. giving a total cell area of $1.032 cm^2$; the grid pattern reduces the active area by about 7.5%. The total cell area is used for the efficiency calculations.

Figure 35 Solar cell process sequence for web characterization

Start Date:		PROCESSING LOG	Page	Run or Sample Web Qual Run No.
Material:				
Quantity:	Engr.			

Date Tech.	Process	Special Instructions, Measurements etc.	Disp. C	Disp. E
	IDENTI-FICATION	Scribe serial numbers on either side of web near one end to identify P+ side of structure - (Swab HF rinse D.I. H_2O		
	CLEAN (1)	HF:H_2O (1 to 10 ratio) dip 15 sec. 4 min. H_2SO_4 - 160°C H_2O - NH_4, H_2O_2 - HCl		
	SILOX (2)	Silox side not numbered 420°C; 5000Å TK; Speed = 100		
	BORON DIFF. (3)	Boron Deposition, BBr_3 @ 960°C 2-20-2 min. Numbered side up. Very slow pull (5 min/2 inches)		
	REMOVE OXIDE (4)	3:1 (H_2O:HF) until all oxide is removed R_s = _____ Ω/ (Target value = 60 Ω/□		
	SILOX (5)	Silox numbered side 420°C; 5000Å TK; Speed = 100		
	CLEAN (6)	HF:H_2O (1 to 10 Ratio) dip 5 sec. H_2O_2 - NH_4, H_2O_2 - HCl		
	$POCl_3$ DIFFUSION (7)	Diffusion Temp. 850°C Time 35 min. Source Temp. = 0° Flow Rates 200 cc/min - N_2 Source; 1560 cc/min - N_2 Carrier 62.5 cc/min O_2 Slow cool by pulling 3 inches/5 min.		
	REMOVE OXIDE (8)	Strip deposition oxide 3:1 (H_2O:HF) Measure, R_s = _____ Ω/ (Target value = 60 Ω/□)		
	CLEAN (9)	H_2SO_4:H_2O_2 87°C, 5 min. Strip all oxides in darkness with buffered HF. 10/1 H_2O/HF Dip 10 sec		
	METAL (10)	Top Side (side not numbered) only Ti 1500 Å 20 Å/sec Pd 500 Å 10 Å/sec Ag 20000 Å 40 Å/sec		
	PHOTO RESIST (11)	Mask #1 (contact grid) Waycoat IC, 4000 rpm, h = 1.7 μm Exposure time = 3 sec (I_d = 0.2 μa)		
	ETCH METAL (12)	Ag-20-60 H_2O_2 & Ammonium Hydrox.-10-15 sec. Pd + 30 cc HCl + 10 cc HNO_3-5 sec. Ti-150 cc H_2O + 60cc HCl + 30cc Ammonium Fl. 5 sec		
	CLEAN (13)	H_2SO_4 at 75°C - 3 min HF Dip Rinse in D.I. H_2O		
	METAL BACK (14)	Ti 1500Å - Pd 500Å Back side is numbered Ag 20 KA		
	SINTER (15)	Temperature 550 °C Time 15 Min. Atmosphere = H_2, 500cc/min.		
	PHOTO-RESIST (16)	Mask #2 (Mesa) Waycoat SC, 7000 rpm, h - 4.0 μm Exposure time = 15 sec (I_2 = 0.6 μa), Apiezon wax back side		
	ETCH SILICON (17)	44 cc HF + 26 cc HNO_3 + 29 cc Acetic 5°C, Etch time = 5-10 sec Etch silicon between 5 to 8 μm deep, Talystep _____ μm.		
	TEST (18)			

Rev. #2 - EJS

The measurement and analysis procedures are discussed in detail in Reference 1, but may be summarized briefly as follows. A quartz-iodine lamp is used to simulate an AM1 spectrum at 91.6mW/cm^2 as determined by reference to a standard solar cell. Five current-voltage pairs are then used to evaluate I_{01}, R_s and n in the single exponential equation

$$I = I_{SC} - I_{01}\left[\exp\left\{\frac{q(V+IR_S)}{nkT}\right\} - 1\right], \qquad (14)$$

and the cell parameters are calculated from the equation. The data management program automatically flags any cells not having an acceptable fit to this model.

Summary of Results. The solar cell data for all the crystals tested in the report period are included as Appendix 3. Each entry represents the average of several test cells, typically four from each crystal. In some cases, as noted, a process variation such as chemically polishing the samples, was tested. The cell efficiency data for the majority of the crystals listed in the appendix are summarized as a histogram in Figure 36. The average efficiency of these cells (AR coated, AM-1) has a mean of about 13% with a few cells in the 15 to 16% range. This value can be compared with a weighted average of about 12% for cells reported in the previous annual report.[1]

Although the test cells are only 10x10 mm, they are a good representation of the performance which might be expected from larger devices. For example Figure 37 presents the distribution of cell efficiencies for a group of cells 16x70 mm which were fabricated in the course of a recent Westinghouse funded program.[15] The mean efficiency for this group of cells is very close to the mean efficiency of the smaller cells; a slight downward shift is due to a non-uniformity in the illumination source used to test the devices which was discovered later.

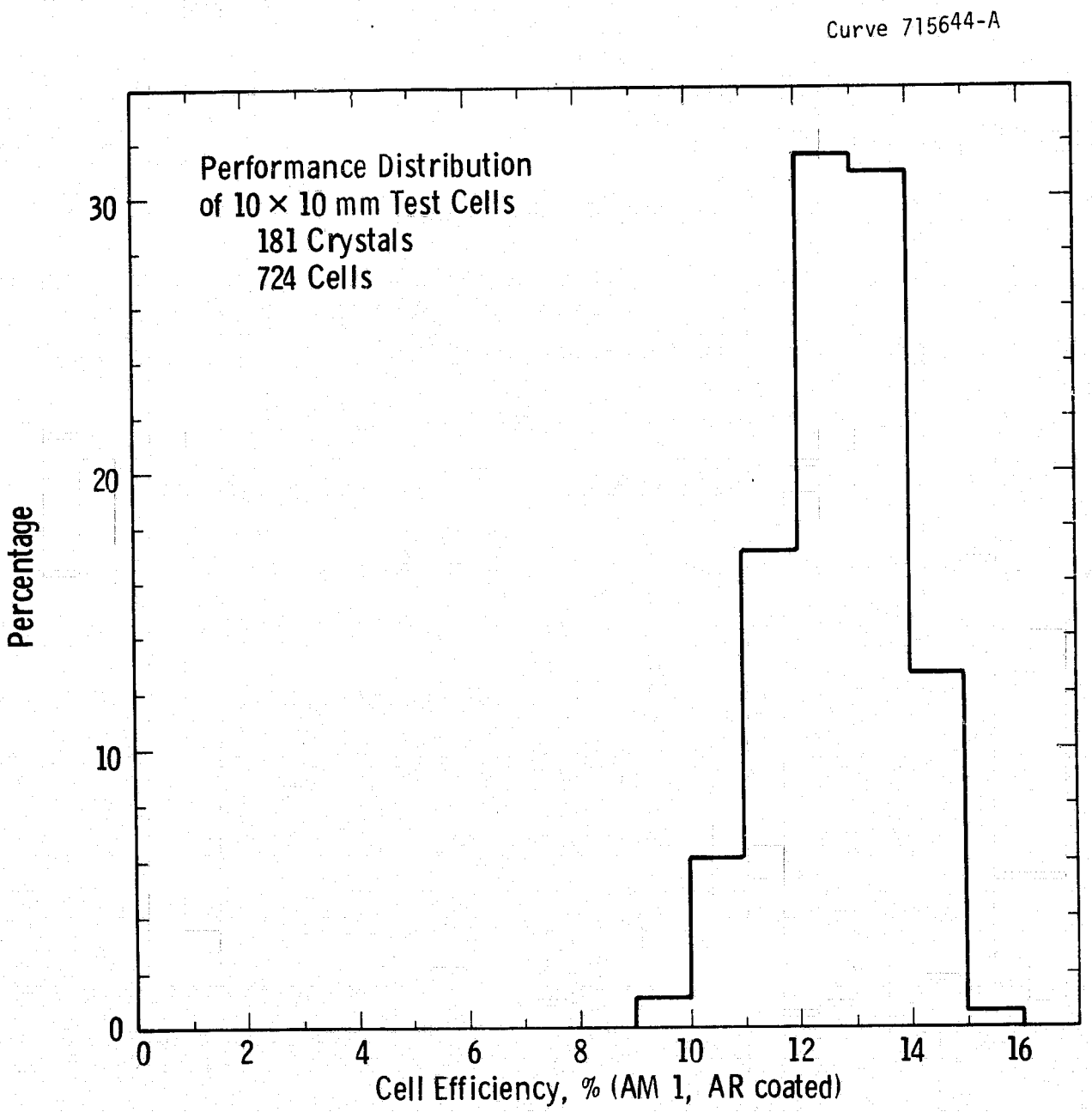

Figure 36 Performance distribution of web test solar cells for crystals grown during Phase II of the web development program.

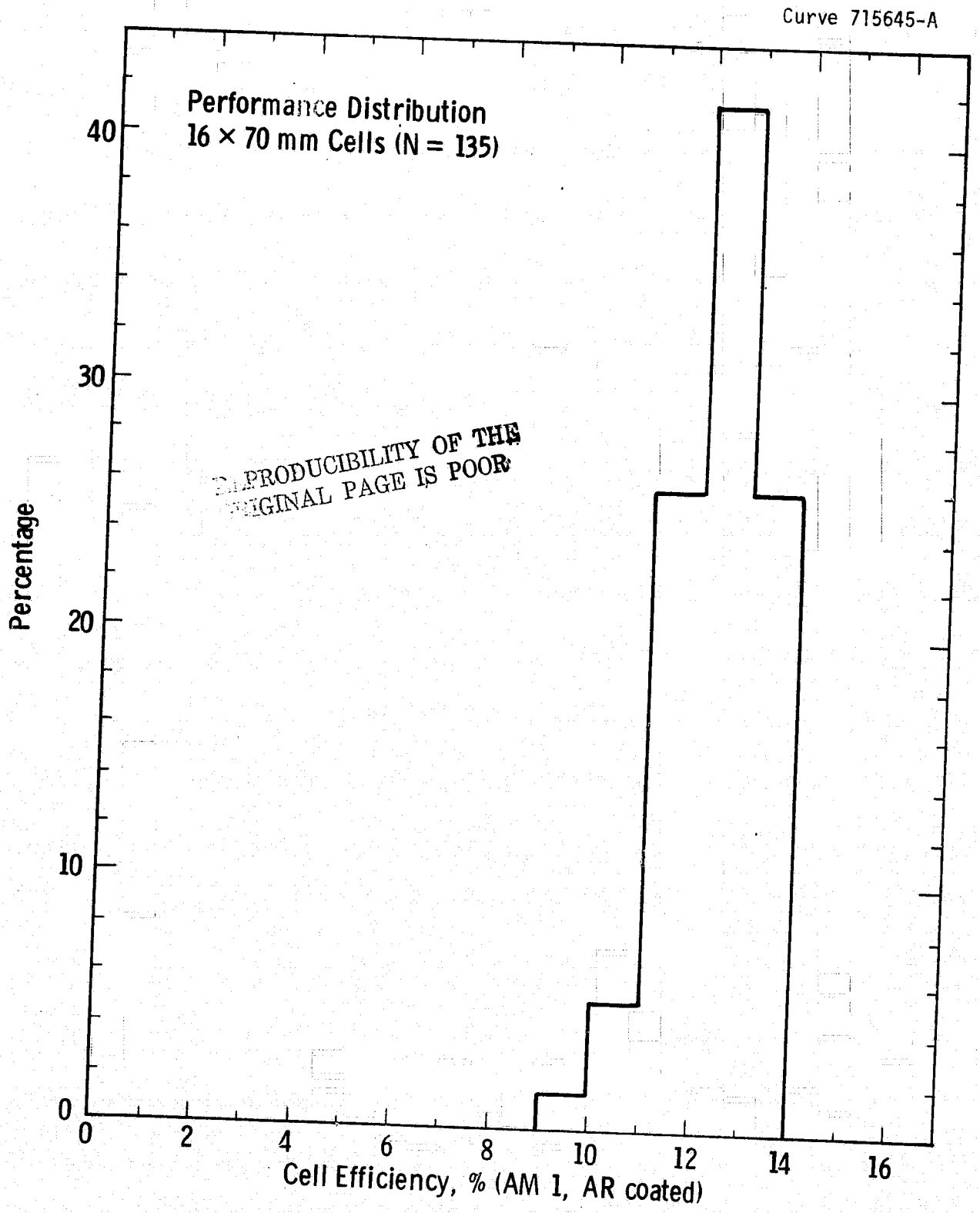

Figure 37 Performance distribution for large 1.6x7mm solar cells.

Not included in the histogram, Figure 36, are cells from a group of crystals which were badly contaminated during growth; the efficiencies of these cells averaged about 2.5% and they were clearly not members of the population represented by the other data. These contaminated crystals were grown from a geometry in which a large volume of argon was passed over the hot molybdenum lid assembly and then flooded on the growing web as described in Section 3.3.3. A detailed discussion of this contamination problem, its solution and auxiliary experiments is given in a recent quarterly report on this contract.[4] Briefly, however, once the gas flow was changed, the same lid geometry produced web giving solar cells of normal properties. This leads to the important conclusion that growing ribbon crystals can be seriously degraded by impurities deposited on the crystal surface by a gas stream.

Melt Replenishment Data. Perhaps one of the most significant groups of cell data in the compilation are those from crystals grown while simultaneously adding new silicon to replenish the melt, Section 3.2. Most of this material was evaluated in the WQ20 fabrication run as noted by the asterisks in Table 3 (crystals W151-1.2, W154-1.4 and W153-2.3). The twelve cells from these crystals had an average efficiency, $\eta_{AR} = 12.9\%$ compared with an average $\bar{\eta}_{AR} = 12.6\%$ for the 32 other cells measured in the run. Thus the replenishment of the melt with small pellets has no deleterious effect on the crystals.

3.4.2 Resistivity.

Although resistivity measurements have not been made routinely on webs grown during the present phase of the contract, a number of four probe measurements and re-analyses of previous data have been performed recently. This renewed interest arose from the requirement of a knowledge of N_A for DLTS measurements[4] as well as a desire to ascertain the effect of resistivity on solar cell performance. The present results indicate that some precautions are necessary to obtain accurate data for rectangular web samples and also suggest some possibly unusual solute partitioning effects in dendritic web growth.

TABLE 3

SOLAR CELL DATA FROM THE WQ20 FABRICATION RUN INCLUDING CRYSTALS GROWTH WITH SIMULTANEOUS MELT REPLENISHMENT

CRYSTAL	NO. CELLS	I_{SC} mA	V_{OC} VOLT	FF	η_o %	$\eta_{AR}{}^{+}$ %	τ_{OCD} μsec
RE12-3.2	4	22.18	.548	.737	9.47	13.5	11.4
RE102-2.2	4	20.18	.520	.734	8.15	11.7	3.8
J131-2.2	4	20.98	.537	.746	8.88	12.7	6.3
J131-3.4	4	19.40	.513	.733	7.73	11.1	2.8
J134-2.2	4	21.70	.536	.749	9.21	13.2	6.7
W141-1.2	4	21.90	.569	.738	9.73	13.9	6.3
*W151-1.2	4	22.18	.543	.738	9.35	13.4	8.6
*W154-1.4	4	21.58	.542	.722	8.92	12.8	7.5
*W154-2.3	4	21.35	.531	.734	8.79	12.6	5.4

* Grown with melt replenishment

\+ AM1 illumination @ 91.6mW/cm^2; cell area 1.032cm^2

An inconsistency in the resitivity data first appeared when measurements taken at different times on the same material, and even on the same sample, gave resistivities differing by 20 percent or more. After some study it became apparent that the discrepant results arose from the factor used to convert the current and voltage measurements to resistivity. The usual four-probe resistivity apparatus is calibrated in terms of round wafers which are the almost universal sample geometry. The dendritic web samples, however, are rectangular and require a different calibration factor which is a function of both the length and width. If the sample dimensions are large enough compared with the probe spacing, then the rectangular and circular factors are nearly the same; this condition was met for some web samples. In other cases, however, the rectangular sample had a very different correction factor. Since the samples are generally very thin compared with the probe spacing, no correction is necessary for the thickness.

The appropriate analysis for the four probe measurements has been given by Smits.[16] The bulk resistivity, ρ_B is related to the sheet resistivity, ρ_S by

$$\rho_B = \rho_S \, t \tag{15}$$

where t is the sample thickness. The sheet resistivity in turn is given by

$$\rho_S = C \frac{V}{I} \tag{16}$$

where V and I are the measured voltage and current respectively and C is the correction factor. For a rectangular sample, C is given by the equation

$$C = \pi \left\{ \ln \left[\sinh(2u)/\sinh(u) \right] + \sum_{m=1}^{\infty} \frac{2}{m} \frac{\exp(-amu)\ \sinh(3mu)\ \sinh(mu)}{\cosh\ (amu)} \right\}^{-1} \tag{17}$$

where $u = \pi s/d$ and $a = 2/s$ and where w is the sample dimension along the line of the probe contacts, d is the dimension normal to the line of the probe contacts, and s is the probe spacing. Generally, only the first term of the series is necessary to give an accuracy better than 0.1 percent. This equation is readily programmed on a hand calculator and evaluated for each sample.

One of the reasons for checking the web resistivity was that values reported during some cell processing experiments, both at these laboratories and elsewhere[17] differed from the values expected on the basis of the boron doping added to the melts. Where a value of about 15 Ω-cm was anticipated, values of 20 to 25 Ω-cm were reported. The more precise evaluation of the correction factor brought the measured and anticipated resistivities into closer agreement, however, there was still about a 20% disagreement. Apparently less boron was being incorporated by the crystal than expected on the basis of a segregation coefficient, $k = 0.8$.[18]

Resistivity measurements were then made on a number of samples grown in a variety of furnaces with different silicon and doping sources. These resistivity data were converted to acceptor concentration using the mobility equation of Antoiadis et al.[19]

$$\mu_\rho = 47.9 + \frac{418}{1 + \left[\frac{N_A}{1.606 \times 10^{17}}\right]^{0.7}} \ \text{cm}^2/\text{volt-sec.} \quad (18)$$

The boron concentration in the melt was determined from the nominal doping concentration-either Dopesil pellets or a master doping alloy. Using this data, an effective segregation coefficient of $k = 0.59 \pm .05$ was found as representative for boron in dendritic web growth. On the basis of the accuracy of the measurements involved, this is a significant variation from the value commonly accepted for Czochralski pulling. The data suggest some small shifts in k depending on the source of the boron

dope, but these were generally less than 10%. There was also a trend for the resistivity of the material to decrease slightly during a given growth run and along the length of a long crystal. Again, this effect was 5 to 10 percent and was consistent with the buildup of boron in the melt due to a k of about 0.5 to 0.6. This factor will have to be considered eventually in any melt replenishment process.

Although the apparently significant decrease of the partition coefficient of boron in silicon dendritic web growth is surprising, it is not inconsistent with previous results. We have already reported partioning experiments in which the effective solute partition coefficients of several solutes were very close to k_o.[20] In that paper we showed that the geometry of the liquid near the growth front was conductive to dispersal of the rejected solute. Thus it is reasonable that $k_{eff} \approx ko$; what is surprising is that $k_{eff} < k_o$. We offer the following speculative explanation for this behavior.

There is reason to suspect that the growth interface of the web may be facetted with {111} planes; this faceting provides the stability of the interface against breakdown during growth from the supercooled liquid. If this is indeed the case, then the interface partition coefficient for boron on a (111) growth front may well differ from the value for a non-singular interface. Milvidskii and Berkova[21] report that boron does not exhibit such a facet effect in silicon; however, their conclusions were based on Czochralski growth where the interface velocities are much smaller. At the fast growth rates encountered in web growth, a facet effect may well exist for boron in silicon.

3.4.3 Microstructural Evaluation

To better understand the mechanisms of the structural degradation of web crystals by high stresses during growth studies were made of the dislocation density in dendritic web crystals having different residual stresses.[4] Etch pits were formed by immersing cleaned web samples in Sirtl etch. This preparation gave high contrast pits which were easily counted using automatic quantitative metallography.

C-2

The actual determination of etch pit density was done with a Leitz Classimat automatic image analyzer. The apparatus counted the number of pits in a 680 μm square area, then moved in programmed steps to adjacent areas; the process repeated until a total area 6.8x10.2 mm in size had been covered. When the etch pit density distribution across the width of the sample was examined, it exhibited a distinct central maximum. Plotting the value of this maximum (obtained by averaging the three highest individual values) against the measured residual stress in the crystal gave a direct relation between the two parameters, Figure 38.

Two important conclusions were drawn from these results. First, dendritic web with small residual stress also has very few dislocations; in fact, it is dislocation free over large areas. Second, the dislocation density is largestin the central regionof the web where the lateral stresses are predicted from our thermal model (Section 3.1.1) to be largest. This provides strong evidence that this is the stress component responsible for the observed residual stress.

3.5 Web Solar Cell and Module Development

Although not part of the present program we have conducted further solar cell development activity as part of a companion LSA program.[22] Fabrication of web cell demonstration modules has also been performed as part of this activity and on Westinghouse funds, as well. For completeness we report some of these results below and in Appendix 1.

3.5.1 Back Surface Field Solar Cell Development

Silicon web crystals as grown are thin, typically 0.01 to 0.02 cm, so the efficiency of a solar cell fabricated on web will be impaired unless carrier recombination at the back surface of the device is minimized. This can be accomplished by incorporating an acceptor gradient at the back surface of the n-p device to induce a back surface field (BSF). The acceptor gradient promotes (1) an increase in short circuit current, (2) an increase in cell votage, (3) increased long wavelength response, (4) reduced cell resistance, and (5) increased fill factor in the cells.

Curve 715028-A

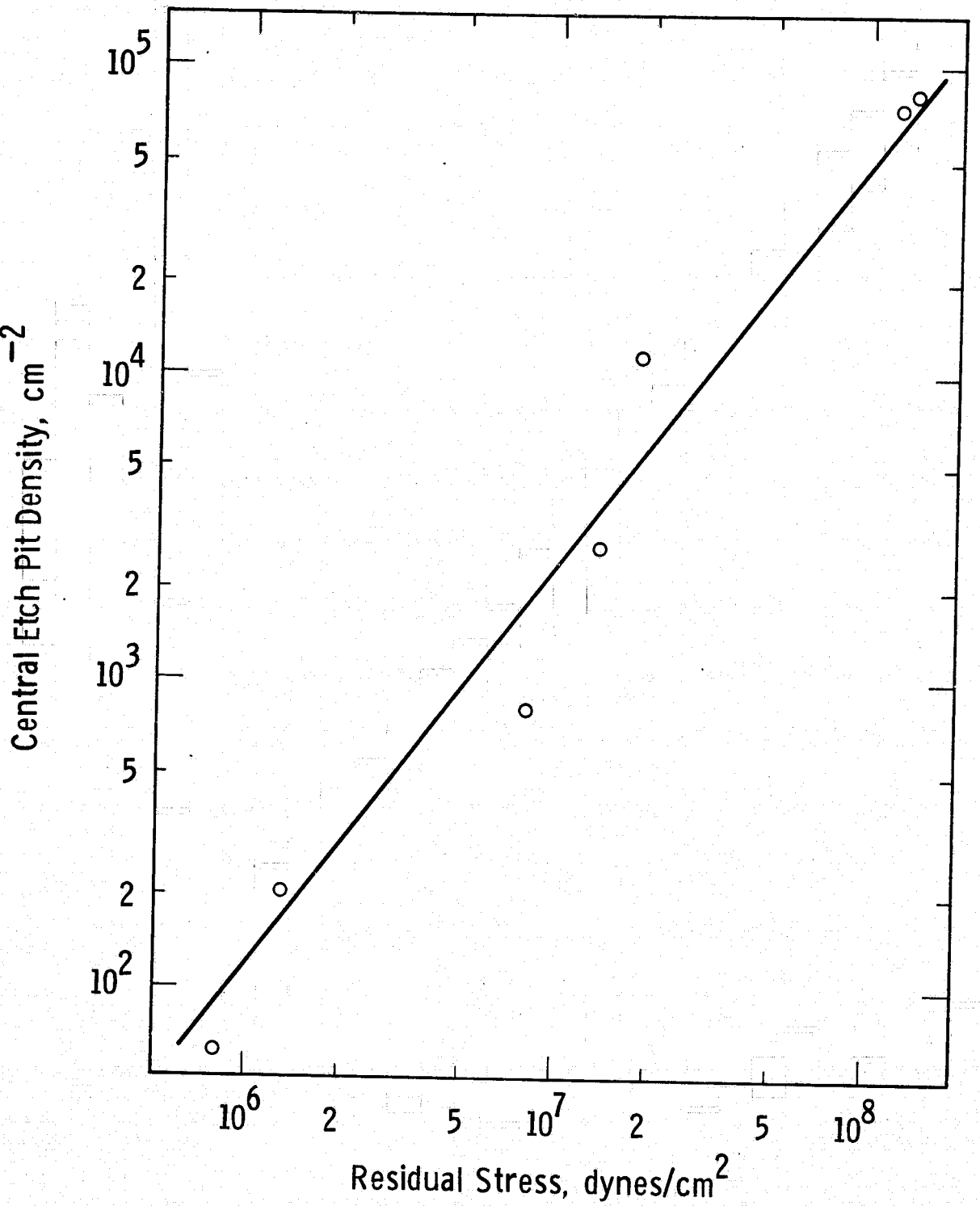

Figure 38 Relationship between etch pit (dislocation) density and residual stress in web crystals.

Web cells produced by our standard p^+pn^+ process using BBr_3 and $POCl_3$ diffusions have produced AM1 cell conversion efficiencies as high as 15.5% (AR coated). Although the performance of these devices is quite good, we found it sometimes difficult to maintain the required high base diffusion length with the BBr_3 diffusion sequence. Variations in cell to cell performance are one result of this.

To circumvent the limitations inherent in the BBr_3 process we investigated another boron BSF technique, diffusion from a CVD boron oxide, and also the formation of a BSF by aluminum doping.* Briefly, in the first case a 1 μm thick p^+ layer is formed by diffusion at 1000°C. In the second approach a 15 μm thick evaporated aluminum layer is heat treated at about 800°C to produce a p^+ layer about 7 μm thick. The front junctions of all the cells were made by $POCl_3$ diffusion at 850°C. Conventional Ti-Pd-Ag contacts were used on the front and back of the cells which were coated with TiO_2-SiO_2 to minimize surface reflection. Cell tests were performed with an AM1 illumination.[1,22] The web used was 15 Ωcm p-type; all experimental runs were accompanied by wafers of 10-12 Ωcm p-type float zone wafers for process control.

The device performance data (average values for several cells in a run), Table 4, indicate that the web solar cells behave in most respects like the baseline cells made on float zone wafers regardless of which process was used, a result consistent with earlier studies.[1] The data are too limited yet to distinguish which process produces the most efficient cells. The aluminum BSF technique, because it is a relatively low temperature process, holds considerable potential for maintaining good bulk recombination lifetime in the devices leading to both enhanced efficiency in the thin web cells and improved process reproducibility. The aluminum technique also appears amenable to automated processing for cost reduction. Experiments are underway to investigate the detailed time-temperature sequences for optimum device performance.[15]

*Work carried out as part of Contract 954873 (R. B. Campbell, et al.)

TABLE 4

PERFORMANCE OF WEB BACK SURFACE FIELD (BSF)
SOLAR CELLS MADE BY DIFFERENT TECHNIQUES

SAMPLE	J_{sc}(ma/cm^2)	V_{oc}(V)	EFF(%)	τ_{OCD}(μ sec)
BBr_3 Diff $X_j \sim 1$ μm web+ FZ Baseline	31.5 30.7	.573 .580	14.2* 14.2	36 35
Boron oxide CVD Drive - $X_j \sim 1$ μm web FZ BAseline	31.5 31.2	.566 .570	13.8* 14.3	35 15
Evap AL Drive $X_j \sim 7$ μm web FZ Baseline	31.8 31.5	.571 .597	14.6* 15.3	34 42

Web cells fabricated by identical sequences save for the absence of the BSF exhibit efficiencies lower by about 2%.

+ X_j is metallurgical junction depth.

NOTE: Cells are AR coated and measured under AM1 conditions (91.6 Mw/cm^2).

3.5.2 Module Fabrication

Several demonstration modules have been fabricated from 1.6x7 cm web cells to test assembly and interconnect techniques. For example, Figure 39 illustrates one module made on an internally funded effort. It is comprised of 72 cells, series connected by means of silver plated copper foil stops. The efficiency of the individual cells ranged from about 12% to 14%, distributed as indicated by the histogram of Figure 37. The cells were mounted in an aluminum plate, encapsulated with silicone, and covered with glass. Despite the presence of shorted cells in one string, the overall module conversion efficiency was 11.5%. We expect the module efficiency to improve with further fabrication experience and increased cell efficiency.

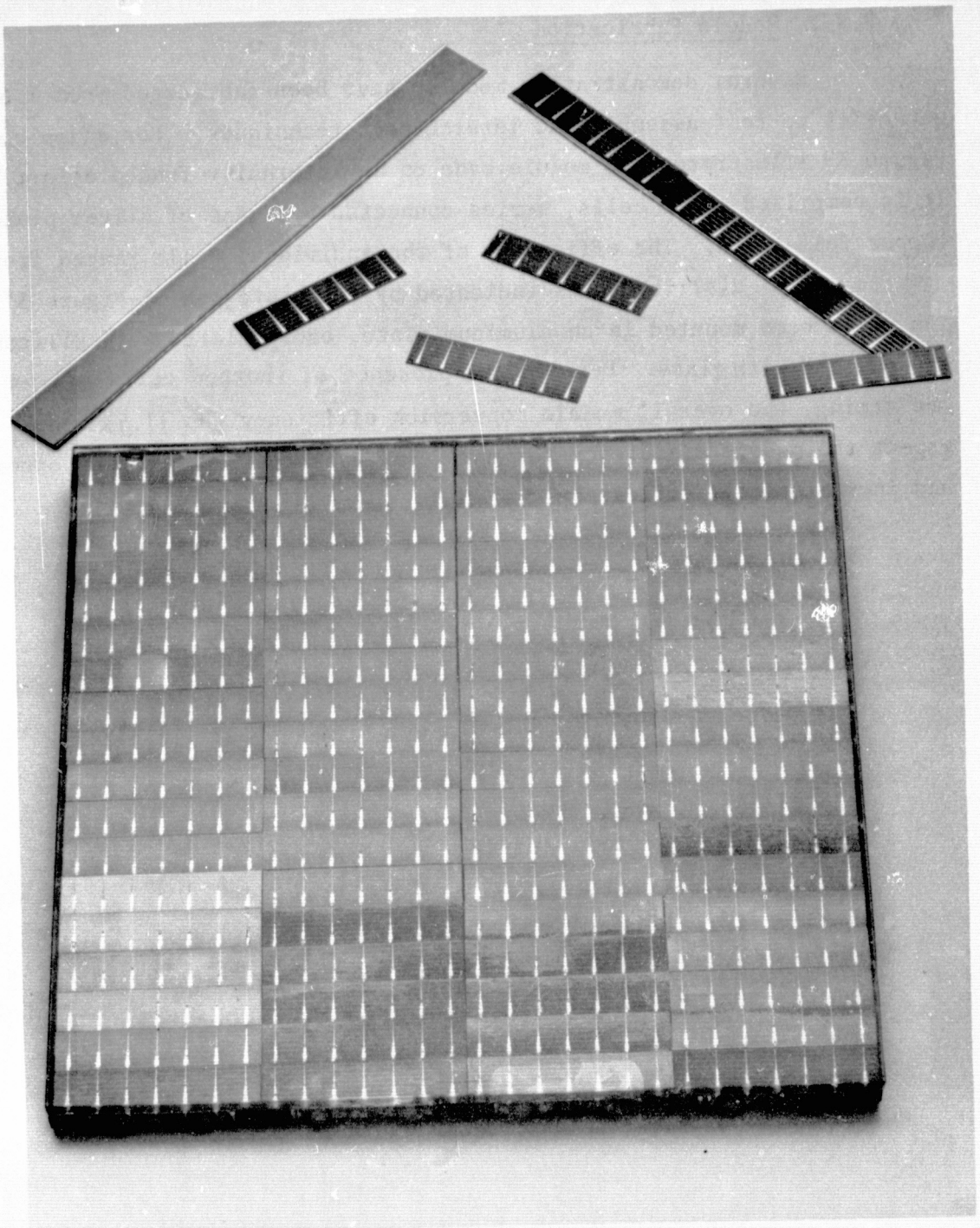

Figure 39 One foot square solar cell module constructed from 72 1.6x7 cm web solar cells connected in series. Also illustrated are web starting material and individual cells.

4. ECONOMIC ANALYSIS

An economic analysis of the silicon web process was previously prepared according to the JPL Interim Price Estimation Guidelines (IPEG).[1] This analysis provided a means to evaluate the status of the effort at that time and to identify the most productive directions for further development. An update of this analysis recently has been performed as part of the Phase II program. The results show both the current state of development and its relation to the JPL goals. As part of the analysis we have also determined, and illustrate below, some of the cost sensitivities of the process.

4.1 Status

The current status of silicon web process development may be put into perspective with the aid of Figure 40 which shows the maximum demonstrated output rate (area rate of growth), 23.6 cm^2/minute, and the cost sensitivity as related to varying output rates. These curves are taken from cost data prepared by the JPL SAMICS IPEG format based on 1975 dollars. The significance of the maximum demonstrated area rate of growth is clear: the intercept of the output rate with the cost curve falls below the JPL 1986 combined goal for polysilicon and wafer cost, assuming a polysilicon price of $10/Kg. For the 23.6 cm^2/minute rate and $10/Kg polysilicon the intercept occurs at 0.128 $/Wpk; for $25/Kg polysilicon the intercept is at 0.170 $/Wpk. These figures compare with the JPL 1986 goal of 0.160 $/Wpk for combined polysilicon and wafer cost. That is, even with $25/Kg silicon the projected web cost is within $0.01 of the cost goal.

Curve 713010-A

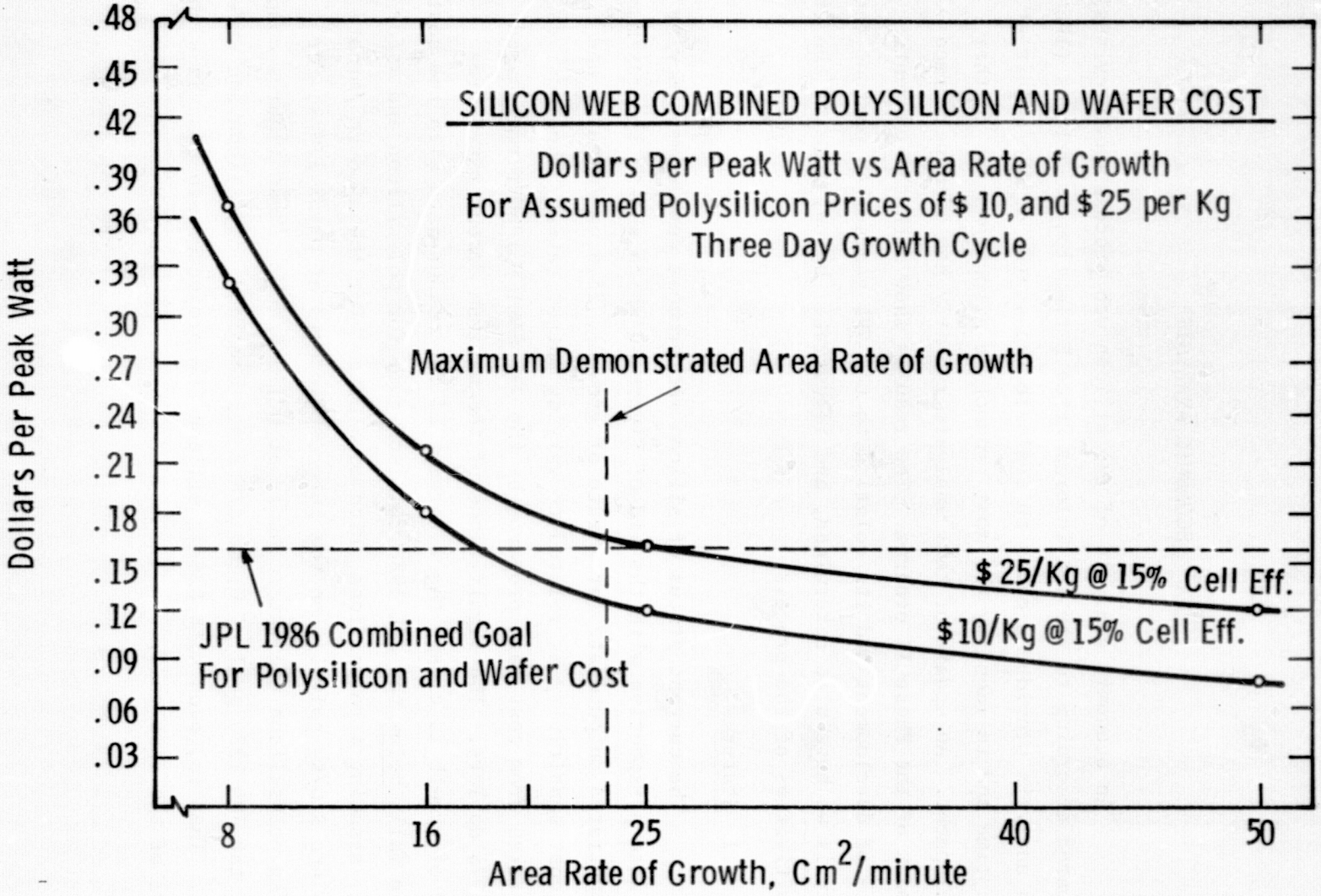

Figure 40 Effect of web output rate on combined wafer plus polysilicon cost.

Several assumptions were originally made in deriving the cost curves of Figure 40 . Some of these estimates have been verified during Phase II and should no longer be considered as assumptions. For example, cell efficiency was assumed at 15% AM1, which has been surpassed, the maximum demonstrated efficiency now being 15.5%.[22] Web ribbon (wafer) thickness was assumed to be 6 mils. In actual growth experience a ribbon thickness of range of 4 to 6 mils is typical. Thus the assumptions for cell efficiency and ribbon thickness, as represented by the cost curve, are conservative and overstate the cost to a small degree. For polysilicon price, the JPL 1986 price goal was assumed in our analysis. Calculations were also made on the basis of a polysilicon price of $25/Kg. In view of price forecasts of below $10/Kg by Task 1 contractors, it appears that our price assumption of $10/Kg is probably somewhat high.

Other assumptions represented in the curves <u>including</u> capital costs are based on process requirements which identify the required features of web growth equipment. The labor content used in the cost analysis is based on the belief that, with the fully developed process, growth will be automatically controlled and labor will thus be largely limited to starting, clean-up and reloading activity within a three day growth cycle.[1]

The three day growth cycle is the least proven assumption included in the economic analysis. The key development necessary to achieving long cycle automated growth is continuous melt replenishment simultaneous with web growth. During Phase II considerable progress was made toward that end. Simultaneous web growth and melt replenishment for periods greater than one hour produced web and solar cells of high quality. However, much longer sustained periods, of days rather than hours, are required. This development will be a basic part of the continuing program.

4.2 Cost Sensitivities.

Perhaps the first step to putting the various cost factors of the silicon web process into perspective is to review the distribution of those individual costs relative to the total costs as calculated by the JPL SAMICS IPEG format. Using growth parameters which, in our judgement, will enable the silicon web process to more than satisfy the JPL 1986 combined cost goal for polysilicon and wafers, we find the following distribution of costs:

TABLE 5

DISTRIBUTION OF COSTS FOR SILICON WEB PROCESS

GROWTH PARAMETERS			COST DISTRIBUTION ¢/Wpk						TOTAL COST ¢/Wpk
Area Rate cm^2/min	Silicon $/Kg	Cycle Days	Si	EQPT	SQFT	DLAB	MATS	UTIL	
25	10	3	2.77	3.30	1.78	2.74	1.27	0.44	12.3

(JPL 1986 Combined Goal for Silicon and Wafers = 16.0¢/Wpk)

Note that none of the costs are dominant. The largest cost contributor, capital equipment (EQPT) is just 26.8% of the total cost. Silicon and direct labor comprise another 22.5% and 22.3%,respectively.

Another consideration of cost sensitivity is the character of each cost. For example, does a particular element of cost have strong leverage on the total cost if the assumption for that element of cost is not attained? These sensitivities are addressed in the following discussion and figures.

The sensitivity of the web cost to the area rate of growth was illustrated in Figure 40, discussed earlier in this section. The present maximum demonstrated rate is below the steep portion of the curve in a region where a further improvement in output rate does not result in a comparable reduction in cost.

The characteristic of the capital cost of equipment is seen from Figure 41 as a non-critical linear relationship. Doubling of the equipment cost would still leave the total cost in $/Wpk slightly below the 1986 combined goal for polysilicon and wafer cost at a $10/Kg polysilicon price.

The cost of direct labor, Figure 42, also exhibits a non-critical characteristic. The cost of labor could be more than doubled without exceeding the 1986 goal all other costs remaining fixed. The characteristic cost of polysilicon, Figure 43, is non critical and by itself could be over 2 times higher without exceeding the 1986 goal.

The shape of curve relating web costs and growth cycle length, Figure 44, is very similar to that for output rate, Figure 44. Note that the assumed and expected growth cycle of 3 days falls below the steep portion of the curve. The 1986 goal would be satisfied with a growth cycle reduced to less than two days. Increases in the growth cycle length beyond 3 days result in a comparatively small improvement in cost.

4.3 Summary.

The economic analysis for silicon web indicates that the JPL 1986 combined polysilicon and wafer cost goal can be achieved or bettered. According to the analysis, the maximum demonstrated throughput rate of 23.6 cm^2/minute can provide a cost of 12.8¢/Wpk as compared to the JPL goal of 16.0¢/Wpk.

The economic analysis also indicates that no cost element is dominant and that none of the cost elements or assumptions have a strong leverage on total cost.

Finally, the analysis indicates that the requirement for long ($\sim$ 3 days) cycle growth is the only large cost assumption not yet completely verified. This requirement is strongly dependent on the completion of the development of technology for continuous melt replenishment.

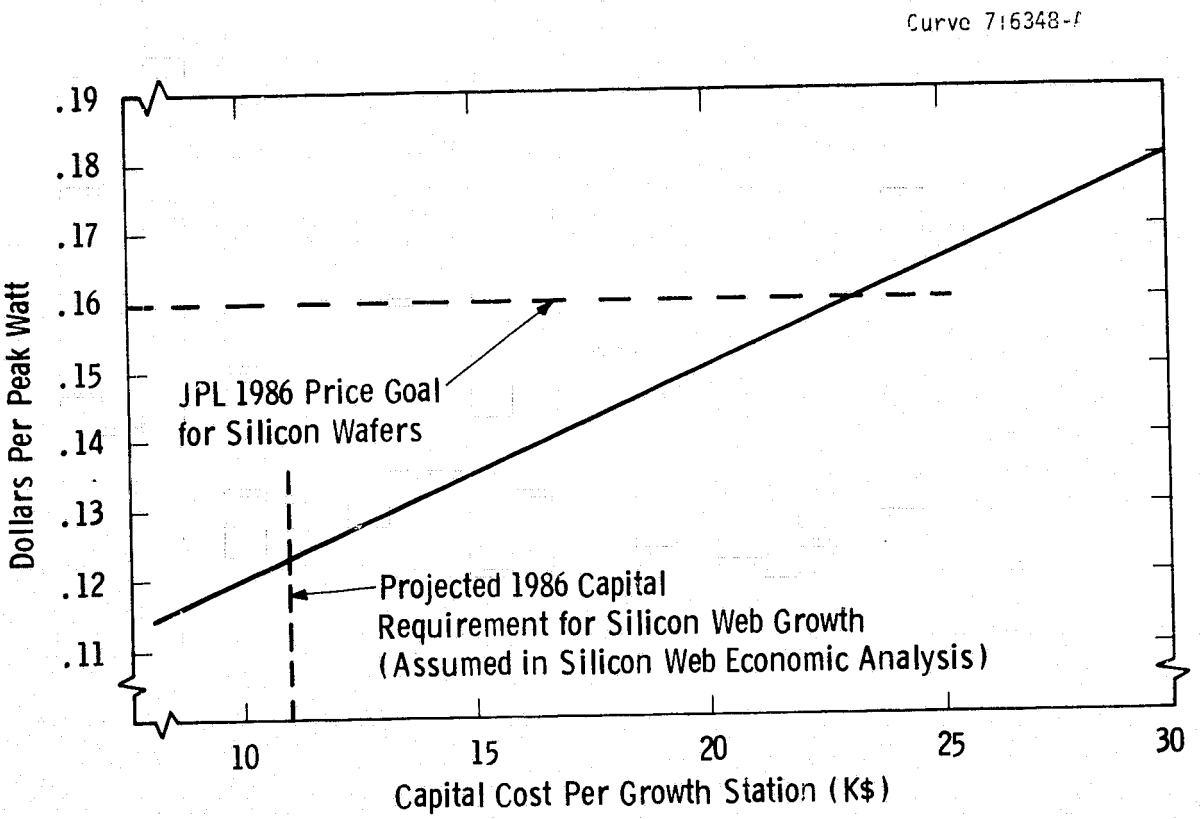

Figure 41 Silicon web combined polysilicon and wafer cost, dollars per peak watt vs capital cost per growth station, for three day growth cycle at 25 cm^2/min, \$10/kg polysilicon price, 6 mils thickness and 15% AM1 cell efficiency.

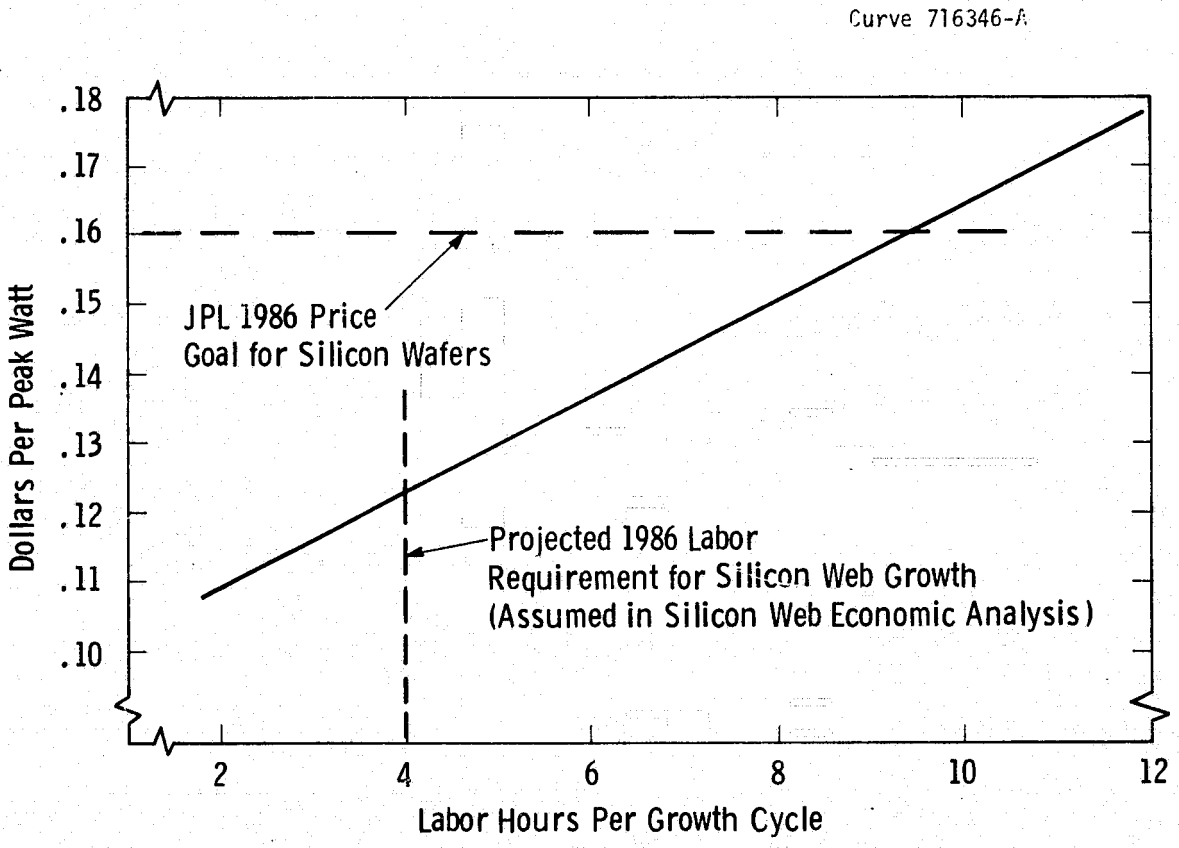

Figure 42 Silicon web combined polysilicon and wafer cost, dollars per peak watt vs. labor hours per growth cycle, for three day growth cycle at 25 cm^2/minute.

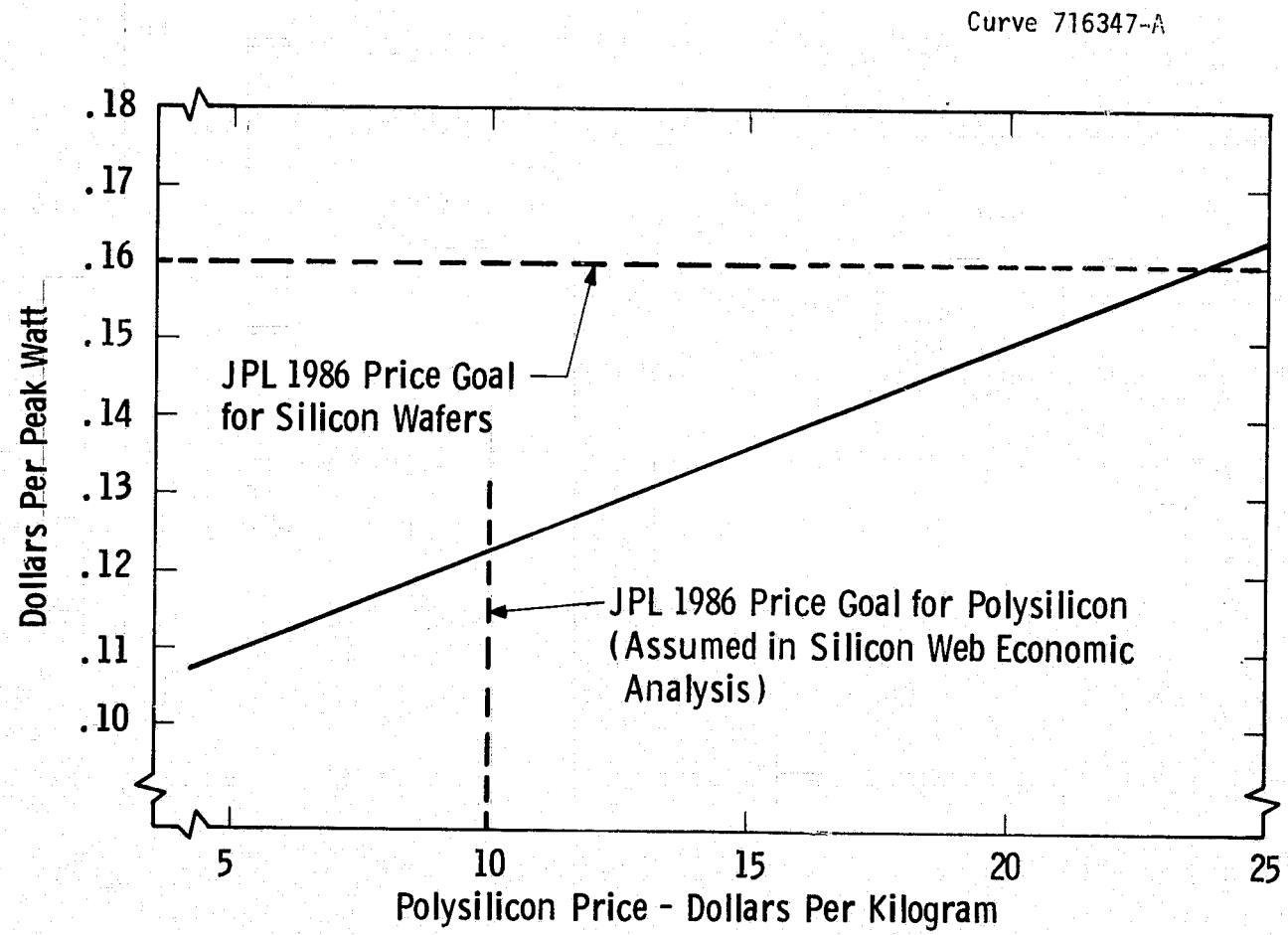

Figure 43 Silicon web combined polysilicon and wafer cost, dollars per peak watt vs polysilicon price, for three day growth cycle at 25 cm^2/minute, 6 mils thickness.

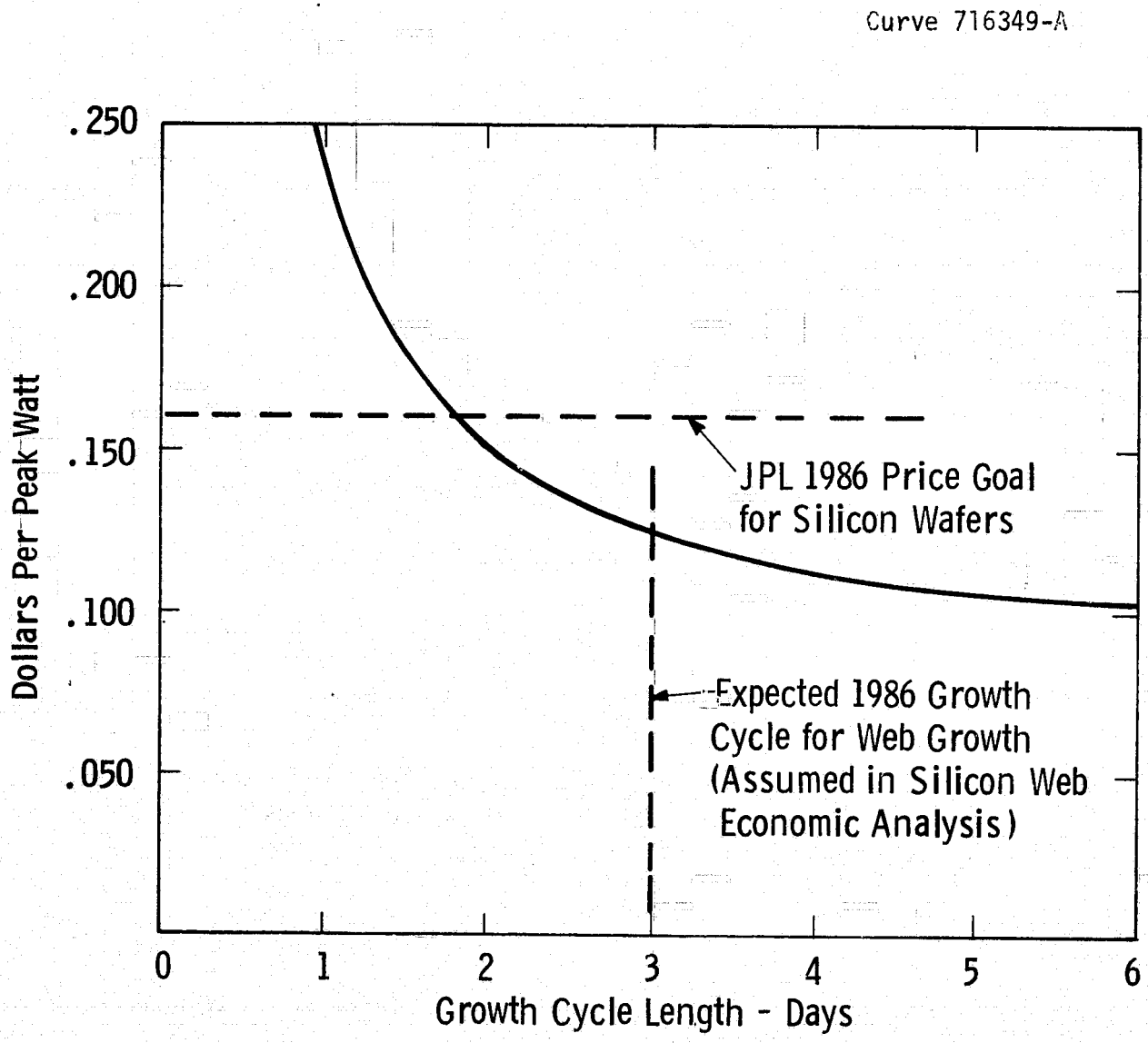

Figure 44 Silicon web combined polysilicon and wafer cost, dollars per peak watt vs growth cycle length (days), for 25 cm^2/min throughput, $10/kg polysilicon, 6 mils thickness, and 15% cell efficiency.

5. SUMMARY AND RECOMMENDATIONS

5.1 Summary of Phase II Progress

During this past year significant advances were made in silicon web technology, particularly in three areas: (1) web output rate, (2) melt replenishment techniques and (3) average solar cell performance.

For example, an output rate of 23.6cm^2/min--about triple the 8cm^2/min rate demonstrated at the end of Phase I--was recently achieved. This accomplishment was an outcome of new growth lids and shields designed on the basis of computer simulations of the web growth process. This approach has made it possible for the first time to achieve web widths over 4cm on long crystals.

Key developments in melt replenishment technology included the design, test and operation of a programmable, mechanically-activated pellet feeder, a pellet injection system and a compartmented crucible which permits pellet feeding without disturbing the growing web crystal. These components comprise the heart of a system by which it should be possible to feed silicon at a rate needed to replace the silicon transformed to web crystal during growth. So far solar cells made on replenished material have exhibited excellent cell conversion efficiency.

As part of the program, all web runs are subjected to some type of dimensional, mechanical, electrical and solar cell testing, or combination thereof. More than 700 solar cells fabricated on crystals grown under a variety of experimental conditions have been tested. The average web cell conversion efficiency on this experimental material was 13% AM1, AR coated. This is a full percentage point above the 12% average efficiency of Phase I material. Moeover, a maximum cell efficiency of 15.5% was demonstrated on a second program devoted to cell array development.[22] This is the highest efficiency so far achieved for a ribbon material and is comparable to that for cells made on Czochralski silicon.

Put in the perspective of our updated economic analysis, these results indicate that most of the key technology elements required to reach the 1986 JPL wafer cost goal have now been demonstrated for web. The following section outlines our recommendations with respect to future development that must take place if the full potential of web for low cost solar cells is to be realized in a timely manner.

5.2 Recommendations for Future Technology Development

As a consequence of the demonstrated web output rate of 23.6cm^2/min we project from our economic analysis, Section 4, that web wafer cost for a fully developed web process will fall well below the JPL 1986 goal. A sensitivity analysis indicates that no cost element is dominant with respect to web wafer cost. However, for the projected cost to be realized in actual production, high output rate must be attained on a sustained basis under the conditions assumed in the analysis.

Critical future developments have been identified and given priority on the basis of results from the economic model. Probably, the most obvious need is to develop continuous melt replenishment since it is a key component of sustained long term growth. Equally important, it has also been demonstrated that a specific, maintainable melt level position is critical to the attainment of maximum width and speed (hence output rate) and minimum thermally generated stress. Clearly, the development of continuous melt replenishment is of the highest priority. Furthermore, as this development is the prerequisite to the continued development of optimized thermal conditions for high throughput and low stress, it should take place first, chronologically.

The primary development and demonstration of simultaneous melt replenishment and growth is now complete. Continuing development should consist of two parts which at first can proceed independently. The development of thermal design and pellet injection already underway should continue as a sub-task in parallel with a new sub-task for the development of melt level sensing. Later, the results of the two sub-tasks would be joined for simultaneous operation.

Concurrently with work on melt replenishment, improvements in the thermal conditions to sustain high output rate should be continued. A large portion of this activity can take place pending the availability of an operational melt replenishment system. However, completion of the development will take place under conditions of optimal and sustained melt level control provided by melt replenishment.

When combined melt replenishment and melt level sensing have been demonstrated, the last major obstacle to automated web growth will have been removed. At this point implementation of closed loop controls for semi-automated web growth should be developed and demonstrated. In this context, semi-automated is defined as requiring some minimal operator intervention during the growth portion of the total start-to-finish web growth cycle.

At the completion of this next development phase semi-automated growth of silicon web for extended periods, a requisite for meeting the long run economic objectives, should be demonstrated.. Coupled with high output rate operation and some improvements in average cell performance all key technology elements for pilot production development will have, been, we believe, shown feasible.

6. NEW TECHNOLOGY

During Phase II of this program, two items of new technology were identified and reported to JPL.

The first item was the thermal design for growing wide dendritic web from silicon melts. In order to grow wide web crystals, it is necessary that the melt be uniformly supercooled over a region commensurate with the width of the crystal. Previous practice in web crystal growth was to use a round crucible system and to achieve the uniformity of the temperature distribution by a suitable slot shape in the crucible cover. This approach was suitable for crystals up to about 25 mm wide, however it is difficult to achieve thermal geometries suitable for wider growth this way. The new technology reported was the use of an elongated system where the whole/susceptor/lid system was compatable with the essentially two dimensional nature of the crystal. With this sort of geometry, flat temperature distributions 6 to 7 cm long could be established on the melt surface thus removing this limitation to the growth of wide dendritic web crystals.

The second item developed during this program was a new apparatus for the growth of silicon dendritic web. In order to satisfy the goals of the program it was necessary to provide a web growth apparatus having greater width capability than existed in prior technology. In addition to the width capability it was further necessary to incorporate other new concepts which contained provisions for the development and demonstration of high throughput, economical web growth.

7. REFERENCES

1. C. S. Duncan, et al., Silicon Web Process Development, Annual Report DOE/JPL-954654-78/2 April (1978).

2. C. S. Duncan, et al., Silicon Web Process Development, Quarterly Report DOE/JPL-954654-78/3 July (1978).

3. C. S. Duncan, et al., Silicon Web Process Development, Quarterly Report DOE/JPL-954654-78/4 October (1978).

4. C. S. Duncan, et al; Silicon Web Process Development, Quarterly Report DOE/JPL-954654-79/1 January (1979).

5. Yu, A. Burenkov and S. P. Nikanorov, Fiz. Tver. Tela 16, 1496 (1974) Translated in Soviet Phys. Sol. State, 16, 963 (1974).

6. R. H. Gallagher, "Finite Element Analysis," Prentice-Hall Inc., Englewood, NJ (1975) p. 100.

7. B. A. Boley and J. H. Weiner, "Theory of Thermal Stresses," John Wiley and Sons, NY (1960), p. 95.

8. C. S. Duncan et al., Ibid, Ref. 4, p. 23.

9. B. A. Boley and J. H. Weiner, Op. cit., p. 323.

10. C. D. Graham et al., "Final Report-Research and Development of Low Cost Processes for Integrated Solar Arrays, "No. ERDA/SE/EC(11-1)-2721/FR/76/1.

11. A. D. Morrison et al., Annual Report, "Large Area Silicon Sheet by EFG," ERDA/JPL 954355-76/11 (September 1976).

12. A. Baghdadi et al., Annual Report, "Laser Dope Growth in a Ribbon-to-Ribbon Process, etc. "DOE/JPL 954376-78/4 (September (1978).

13. J. M. Blocher, et al., Quarterly Report DOE/JPL-954339-78/10 April (1978).

14. W. C. Breneman, et al., Quarterly Report DOE/JPL-954334 April (1978).

15. R. B. Campbell, E. J. Semen, and P. Rai-Choudhury, Westinghouse R&D Center, unpublished results (1978).

16. F. M. Smits, Bell System Technical Journal, 37, 711 (1958).

17. H. I. Yoo, P. A. Isles and D. P. Tanner, "Silicon solar cell process development, fabrication and analysis; second quarterly report." DOE/JPL-955089-79/1, OCLI (1979).

18. F. A. Trumbore, Bell System Technical Journal, 39 205 (1960).

19. D. A. Antoniadis, A. G. Gonzalez and R. W. Dutton, J. Electrochem. Soc., 125, 813 (1978).

20. R. G. Seidensticker, A. M. Stewart and R. H. Hopkins, J. Crystal Growth, 46, 61 (1979).

21. M. G. Mil'vidskii and A. V. Berkova, Fiz. Tver. Tela, 5, 709, (1963) Translated: Sov. Physics-Solid State 5, 517 (1963).

22. R. B. Campbell, et al., Annual Report, DOE/JPL-954873, November (1978).

8. APPENDICES

8.1 APPENDIX 1

SILICON RIBBON GROWTH BY THE DENDRITIC WEB PROCESS

SILICON RIBBON GROWTH BY THE DENDRITIC WEB PROCESS

R. G. Seidensticker and R. H. Hopkins
Westinghouse Research Center
Pittsburgh, PA 15235

ABSTRACT

Silicon dendritic web is a unique mode of ribbon growth in which crystallographic and surface tension forces, rather than shaping dies, are used to control crystal form. The single crystal webs, typically 2-4 cm wide, have been made into solar cells which exhibit AM1 conversion efficiencies as high as 15.5%. During crystallization, silicon webs effectively segregate metal impurities to the melt ($k_{eff} \sim 10^{-5}$) so that the use of cheaper, less pure silicon as feedstock for crystal growth appears feasible. Recent studies described here indicate that higher growth output rates can be achieved by control of the thermal profiles in the web itself and in the melt from which the crystal grows. The improvements stem from an enhancement in the dissipation of latent heat and a reduction in stress within the crystals. To sustain high output rates for prolonged periods will require melt replenishment during growth.

1. INTRODUCTION

The dendritic web growth mode produces a ribbon crystal whose form is controlled by crystallography and surface tension forces rather than shape-defining dies. Ribbons of indium antimonide[1,4], gallium arsenide[2], germanium[3,4] and silicon[5] have been produced this way, though silicon has attracted the greatest interest due to its potential as base material for efficient, low cost solar cells[6]. In the latter context the overiding concern is to produce large areas of efficient devices as cheaply as possible. Thus the thrust of recent silicon web research has been to develop ways to (1) increase web output rate (the product of web width and growth speed), (2) minimize raw material cost and (3) raise solar cell conversion efficiency as high as possible. The results of several of these studies are reported in this paper.

2. THE DENDRITIC WEB PROCESS

Detailed descriptions of web growth have been given elsewhere[5,6] but it is worth reviewing here the basic features of the process. This can be accomplished with the aid of Figure 1 which illustrates what happens when the liquid surrounding a fine silicon dendrite seed is supercooled by a few degrees. As the melt temperature falls, the seed first spreads laterally to form a button; when the seed is then raised, two secondary dendrites propagate from each end of the button into the melt. The button and dendrites form a frame supporting a liquid film

which crystallizes to form a silicon web typically 0.1 to 0.2 mm thick. The twins shown in the figure provide reentrant corners for dendrite growth but do not appear necessary for growth of the web itself[6].

The web and bordering dendrites can be propagated indefinitely by replenishing the liquid silicon as it is transformed to crystal. As we will see below, the ultimate web width and growth velocity are determined by the thermal conditions in the surrounding melt and furnace ambient.

3. SILICON WEB GROWTH

Figure 2 depicts the essential features of a silicon web growth furnace. Heat is introduced to the system by induction coupling to a molybdenum susceptor. The outflow of heat is controlled by a slotted molybdenum susceptor lid and heat shields through which the growing web also passes. The lid and shields shape the isotherms in the liquid so the center region is supercooled while the periphery remains hot enough to prevent freezing at the quartz crucible-melt interface.

3.1 Web Output Rate

The rate at which liquid silicon is converted to web single crystal is determined by the attainable web width and growth velocity. Crystal width depends dominantly on the lateral temperature profile in the liquid, while the dissipation of the latent heat of fusion controls the growth velocity. Both processes are influenced strongly by system heat flow, but in different ways. For example, the growth slot width, bevel angle and lid thickness have profound effects on web growth

velocity, while the slot length, area and hole size are more important for controlling the melt temperature profile. For practical purposes, the two problems, (1) heat flow in the melt/crucible/susceptor system and (2) heat loss from the web and meniscus, can be decoupled and treated separately. We have done this by means of two thermal models which were used to guide the design of furnace geometries for higher web output rates.

3.1.1 Web Width

Figure 3 suggests the way in which the temperature distribution across the melt surface fixes the ultimate web width. The web grows from a meniscus 6 or 7 mm above the melt surface; however, the high liquid curvature required at the edges of the bounding dendrites limits the meniscus height there to only 1 or 2 mm. Crystallographic and heat flow factors cause the growth direction of the dendrites to be very nearly a [211] direction. Heat loss from the meniscus, however, perturbs the thermal field near the tip of the dendrite so that there is slightly more growth on the outer edge than on the inner edge. This causes a small deviation of the growth direction from [211] and the crystal widens so long as there is a uniform temperature profile in the melt. When the widening web reaches a region of increasing melt temperature, as shown in the figure, the intrinsic lateral temperature gradient in the liquid counteracts the temperature gradient created by the meniscus heat loss. The web then ceases to widen and continues to grow at steady state.

Thus a necessary condition for growing wide web is a temperature profile on the melt surface which is essentially flat over a distance commensurate with the desired width of the web. This surface temperature distribution is a strong function of the shape of the slot in the susceptor cover. As the number of potential slot geometries which could be tried experimentally to obtain a flat temperature profile is large, computer analysis was employed to guide the empirical effort.

To compute the temperature distribution in the susceptor-crucible-melt assembly, we constructed a three dimensional finite element model of the system. Most of the 4184 elements in the model are three dimensional and represent conductive heat transfer in the solid or liquid regions of the assembly; however, a number of one dimensional links are used to represent radiative heat transfer from the liquid to the surroundings. Each node on the melt surface is radiatively connected with the slot, the lid and the exposed susceptor via linkages which account for the various view factors and emissivities. In a usual network representation of a radiative transfer problem[7], separate elements are used to represent the emissivity and view factor; in the present model some efficiency in computation was achieved by a wye-delta like transformation so that only three direct linkages result at each melt surface node:one to the slot, one to the lid and one to the wall. Figure 4 schematically illustrates the type of model used. The model was evaluated using a general purpose computer code.[28]

Numerous slot profiles were modeled in this way and the most promising were subjected to experimental verification. An example of the results for two similar designs is shown in Figure 5; a long straight slot and a similar slot terminated by end holes (sometimes called a "dog-bone" slot). The addition of the end holes has almost doubled the length of the thermally flat region. The data points in the figure, obtained by determining relative temperatures for equilibrium between the melt surface and a fine silicon dendrite, are in good agreement with the model predictions.

Perhaps the most striking verification of the model's predictions is the increase in web width with successive iterations in the slot geometry. Figure 6 illustrates webs grown from slots typical of the geometries in Figure 5; slot A with a flat profile over 6 cm long produced webs up to 4.2 cm wide. Further increase in width was not limited by the flatness of the melt temperature but by thermal stresses which deformed the crystals, a subject discussed later.

3.1.2 Growth Velocity

Thermal transport also plays a dominant role in the relationships between the web growth velocity, web thickness and the furnace geometry. As with any solidification process, the critical factor in such a relationship is the dissipation of the latent heat. For dendritic web, there are two modes of heat loss from the interface: to the solid ribbon and to the supercooled melt.[6] Since the growth front is at a constant temperature, presumably the melting temperature, the analysis can be broken into two problems which can be solved separately.

Both the web crystal and the meniscus are relatively long and wide compared with the thickness; the problem reduces to a one dimensional analysis so numerical integration rather than finite element techniques were used for the solution. A detailed analysis of the approach is given in Reference 27. Briefly, at any point along the length of the crystal (or meniscus), several heat transfer processes must be evaluated as suggested in Figure 7. Expressions were developed for the radiation view factors used for the heat transfer term in the moving frame heat flow equation. This differential equation was then solved numerically using a 500 step, fourth order, Runge-Kutta procedure. In the case of the ribbon, the melting temperature of silicon at the growth front provided one boundary condition, while a second boundary condition was supplied by requiring the numerical solution to match an analytical solution far from the growth front. A somewhat similar, simplified approach has been reported by Harrill et al.[8]

The model has been used to assess directly the effects of furnace parameters such as susceptor lid thickness, growth slot width, heat shield temperature and melt depth (interface position) on the web growth rate.[25] A set of typical temperature profiles is shown in Figure 8 which illustrates the effect of interface position on web temperature for a given growth geometry. Data like this can also be used as input information to calculate thermal stress fields in the growing web crystals (Section 3.2).

In general,the trends predicted by our calculations are in agreement those of Harrill et al.[8] As Figure 7 and intuition would suggest, growth velocity can be increased by increasing the radiative heat loss from the web. This can be accomplished in several ways:

(1) Lower the temperature of the top of the radiation shield, e.g. by using stacks of radiation shields above the susceptor lid;

(2) Increase the width of the growth slot;

(3) Raise the position of the growth front closer to the susceptor lid;

(4) Increase the view angle in the susceptor lid, e.g. by beveling the slot; and

(5) Reduce the thickness of the susceptor lid

Experimentally, approach (2) is somewhat less viable than the others because it may induce undesirable secondary effects. For example, if the growth slot is too wide (> 7 mm) the melt temperature profile steepens and web widening is restricted.

Examples of the calculated and measured velocity-thicknesss relationships for two of the numerous slot geometries studied are depicted in Figure 9. Agreement between theory and experiment is excellent. The data were obtained by measuring the thickess of webs grown from a fixed furnace condition but with incrementally varied growth speed. Growth velocities in excess of 5 cm/min can be obtained with rather simple combinations of bevel angle and lid thickness.

As Harrill, et al.[8] suggested and our calculations confirm, a given growth rate can only be sustained so long as the melt level remains fixed. As liquid silicon is removed by crystal growth the freezing front drops lower into the hot cavity below the susceptor lid. Less heat can be dissipated so that the web must thin if the velocity remains constant. The experimental data from a "slow" growth lid, Figure 10, demonstrate that this prediciton is in fact realistic. In the figure, we plot web thickness as a function of growth time (which is inversely proportional to melt height). As the melt is depleted the web becomes thinner and thinner.

One can compensate for this effect somewhat by adjusting the melt temperature and hence supercooling. This is because, unlike other ribbon processes, latent heat of fusion can be dissipated to the melt as well as the surroundings during web growth. Of course growth velocity variations, which change the latent heat output, can also be used to maintain constant thickness. Neither approach is entirely satisfactory since careful attention by a skilled operator would be required for prolonged growth periods, and also because adverse stresses develop in the web as the melt level falls. Melt replenishment in fact is a far more elegant and practical solution to the problem.

3.2 Generation and Control of Thermal Stress During Web Growth

As the melt temperature profile became flatter making possible the growth of wide webs, deformation of the crystals by twisting or curling was encountered. Similar effects have been observed for other ribbon growth techniques such as EFG and laser-melted ribbon to ribbon crystals where the principal cause of this deformation was reported to be thermal stress generated by curvature of the vertical temperature profile in the ribbon.[9,10] Even when observable deformation of the crystals did not occur during growth, residual stresses sometimes remained making it difficult to handle during subsequent device fabrication steps.

Residual stresses can be measured in ribbons by splitting the crystals lengthwise and measuring the split divergence as a function of length. By analogy with the stress distribution in a uniformly curved beam, the residual stress in the ribbon crystal is given by

$$\sigma_{res} = \frac{EW}{8} \frac{d^2\eta}{d\xi^2} \qquad (1)$$

where E is Young's modulus (1.9×10^{12} dynes/cm^2), W is the width of the crystal before splitting, η is the split width and ξ is the distance along the crystal. In practice, with the web crystals, measurements of η were made with a microscope eyepiece micrometer every centimeter for 15 to 25 cm. The resulting data was then used to generate a least squares value for the coefficients in a quadratic equation; $d^2\eta/d\xi^2$ was computed from the quadratic coefficient. This procedure gives a good fit to the data and has a sensitivity limit of about 1×10^6 dynes/cm^2 ($\sim$ 15 psi).

Residual stresses in the dendritic web crystals were found to vary from as much as 2 to 3×10^8 dynes/cm^2 to $\leq 10^6$ dynes/cm^2, depending on the specific slot and shield configuration. The preliminary data suggested that wider slots tended to generate lower stresses than the narrower slots, however the data was scattered and hard to interpret. Rather than follow a purely empirical development approach, analytical modeling was used to identify the source of stresses and guide the development of lid designs which would generate low stress material.

Since the origin of the thermal stress was presumably the ribbon temperature profile, the thermal model developed for the thickness-velocity analysis (Section 3.1.2) was used to provide an input to a finite element stress model. The stress model was then evaluated using the WECAN code. The output of this analysis was an evaluation of σ_{ZZ} (the longitudinal stress), σ_{YY} (lateral stress) and σ_{ZY} (shear stress) as well as principal stresses and stress intensity for each element, both numerically and as isostress plots.

Several interesting results were obtained from test cases used to verify the stress model. First, no thermal stresses result from a linear temperature profile in the web if the thermal expansion coefficient is constant. Second, as expected, only longitudinal stresses of constant magnitude were present away from the growth front when a parabolic temperature profile was imposed.[11] Third, significant thermal stresses were present even with a linear profile, when a temperature dependent expansion coefficient was used in the calculation. Finally, the traction-free boundary conditions at the growth front and at the ribbon

edges were important. Longitudinal stresses (σ_{ZZ}) were significant several centimeters away from the growth front, but they were small in the hot, plastic, region near the liquid. Conversely, the lateral stresses (σ_{YY}) were largest in this plastic region and decreased away from the growth front.

For practical reasons, quantitative results were desired from this analysis; however we realized that uncertainties in the physical parameters preclude a strict interpretation of the results. The data used for the analysis were Young's modulus, $E = 1.9 \times 10^{12}$ dynes/cm^2,[12] Poisson's ratio, $\nu = .20$ [12] and thermal expansion coefficient $\alpha = 2.552 \times 10^{-6} + 1.95 \times 10^{-9} T - 9.0 \times 10^{-15} T^2$.[13] Of several choices for α, this data is in best agreement with the independent lattice parameter measurements of Logan and Bond.[14] A final parameter needed for interpretations of the residual stress measurements is an estimate of the effective yield stress; an operational estimate can be obtained from the results of Graham et al.[15] Their results for visco-elastic flow can be expressed as

$$\sigma_{YP} = 2.57 \times 10^{-5} \exp (49459/T) \text{ dynes/cm}^2.$$

The initial analysis of several slot profiles indicated that the lateral stress components are probably responsible for most of the residual stresses found in dendritic web crystals. Figure 11 shows σ_{YY}, σ_{ZZ}, and σ_{YP} for one such design, and although the longitudinal stresses reach larger values than the lateral stresses, the ribbon temperature drops so rapidly that only the lateral stresses exceed the estimated yield stress. The analysis is supported by experimental results:

crystals grown from this lid generally have small residual stresses in the range of 1 to $3x10^6$ dynes/cm^2, although the stress is occasionally larger as noted below.

Because the liquid level falls during growth without melt replenishment, we investigated what effect the changing position of the growth front would have in the residual stress in the web. The most significant change was in the lateral stress in the sensitive region near the growth front. Figure 12 illustrates the magnitude of the lateral stress when the interface is at the lid, and 1, 2 and 4 mm below the lid. In two cases, σ_{YP} is exceeded and plastic deformation might be expected; in the other two cases little residual stress should result. This is consistent with our observation that the residual stress increased after several meters of crystal were grown from this furnace geometry without melt replenishment.

When growth geometries giving low residual stress were employed, the width of undeformed crystals increased from about 20 to over 35 mm. However, deformation was still observed at greater widths. Samples taken just before the deformed regions showed typical low stress values and concommitant low dislocation densities, typically 10^2 to 10^3 cm^{-2}. After the deformation event, the residual stress and dislocation density increased by several orders of magnitude. These precipitous changes suggested that web bending was due to elastic buckling of the ribbon by large longitudinal stress fields well above the growth front.

The proposed process is illustrated schematically in Figure 13. Initially the crystal grows without deformation as in Figure 13a, although stress fields are present. The largest lateral stresses are at "P" where plastic flow can occur, and the largest longitudinal stress is at E where only elastic deformation is possible. As the crystal widens, the magnitude of the stresses increases[11] and the resistance of the ribbon to buckling decreases so that at some critical point in growth (Figure 13b) the ribbon buckles with the greatest (elastic) deformation at "E", and with some lesser deformation at "P"; in addition to the curvature shown by the sections, there would also be a curvature out of the plane of the figure.

At this point, the deformation may be purely elastic, or some plastic flow may also occur at "P". In any case, the twin planes in the material must also curve and remain locally parallel to the crystal faces. However, as the ribbon continues to propagate, the new material will tend to grow in a straight line between the bounding dendrites due to surface forces in the meniscus as shown in Figure 13c. This new material cannot contain the twin plane which will emerge as a roughly parabolic trace on the ribbon surface as shown in Figure 13d; the dislocation density and slip will also increase. These "wishbone" configurations are in fact frequently observed in deformed web crystals as is the increase in dislocation density and slip. Further, once the dislocation pinning effect of the twin planes is gone, the deformation mode of the ribbon frequently changes to the rippled morphology shown in Figure 14. Other modes which are seen include a twist, probably the result of lateral thermal asymmetry, and a long period waviness.

Current design studies are directed to develop growth configurations having lower longitudinal stresses away from the interface as well as low lateral stresses. Qualitatively, this will require "straighter" temperature profiles in the crystal for several centimeters above the growth front; apparatus for this purpose is being tested.

4. FEEDSTOCK PURITY CONSIDERATIONS FOR WEB GROWTH

The development of production methods for a cheaper, less pure "solar" grade of silicon is underway in a number of places.[16] This material used as feedstock for crystal growth could reduce significantly the overall cost of silicon solar cells. Since it is likely that solar grade silicon will have contaminant levels higher than usual, or acceptable in current semiconductor silicon, we carried out a series of experiments to assess the tolerable impurity levels for (1) the web growth process itself and (2) solar cells made on webs grown from contaminated feedstock. (Analogous studies were carried out earlier for Czochralski growth.[17])

4.1 Stability of Crystal-Liquid Interface

It is well known for ingot growth,[18,19] that under fixed growth conditions a planar crystal-liquid interface cannot be sustained when the liquid impurity concentration exceeds a critical value C_ℓ^*. The phenomenon, called constitutional supercooling, leads to inclusion entrapment and the termination of single crystal growth. No such phenomenon has been experimentally identified for silicon web, although it has been

postulated that sufficient contaminant levels might promote some form of instability during web growth.[20]

To search for such effects silicon webs were grown from melts purposely doped with 1 to $6x10^{18}cm^{-3}$ (20 to 120 ppm) of either Cu, Ni, Cr, Mn, Fe, Ti, V or Mo, impurities expected to be encountered in solar grade material.[21] The elemental metals (> 99.99% pure) were dissolved in silicon along with $4x10^{15}cm^{-3}$ boron to provide subsequent electrical activity. Webs were then pulled from a crucible/susceptor arrangement like Figure 2 at rates between 1.5 and 5 cm/min (web deformation, viz. section 3.2 precluded meaningful analysis of crystals grown at speeds above 3 cm/min for the thermal geometry of these experiments).

Briefly, the key results of the experiments were as follows: neither the Ni, Cu or Mn-doped specimens showed any unusual microstructural features. Etch pit densities fell in the range normally encountered for uncontaminated material. In contrast, when the other metals were present in the melt, numerous outcrops of roughened surface formed intermittently along the length of otherwise smooth webs. The morphology of the outcrops, a system of nearly parallel ridges and valleys (illustrated for a Ti-doped web in Figure 15), was a common feature of all the impurities which induced structural degradation.

Material near the outcrops etched preferentially with respect to the adjacent smooth face of the web. Infrared micrographs and x-ray topographs, Figure 16, confirmed the presence of second phase inclusions in the web beneath the outcrops. Perhaps the most striking aspect of growth from the impure liquids was the complete breakdown of the smooth

web-liquid interface to an array of parallel dendrites for the higher velocities and impurity concentrations, Figure 17. As in Figure 15 the dendrite array appears to initiate immediately below a ridged outcrop. The exact origin of the surface corrugations is yet obscure but the dendritic breakdown in the material appears to be a true case of interface instability. The approximate concentrations at C_ℓ^*(struct) at which outcrops developed for each impurity are listed in Table 1.

4.2 Effect of Impurities on Web Solar Cells

Ten to fifteen specimens from each doped web were processed to 1cm x 1cm solar cells via the standard fabrication sequence described elsewhere.[21] (Samples from the material which exhibited outcropped structure were avoided). Webs containing no added contaminant were processed concurrently to obtain baseline values.

The performance of solar cells can be related directly to the contaminant level in the silicon.[17, 21] The impurity concentration in the silicon is determined by the liquid impurity concentration C_ℓ and the effective distribution coefficient, k_{eff}, for impurity partitioning during crystal growth. We have shown for web growth that k_{eff} depends on growth velocity (v_o) and thickness (t) according to the relation[22]

$$k_{eff}(\text{web}) = k_o \left(1 + \frac{v_o t}{2D \sin\theta} \right) \qquad (2)$$

where k_o is the equilibrium partition coefficient, D is the solute diffusivity in the liquid, and θ approximates the meniscus half angle. We used the growth conditions and liquid impurity concentrations for these experiments to calculate k_{eff} and hence C_s. With C_s and the previously determined impurity concentration-cell performance relations,[21] we estimated the expected performance of cells made on the doped webs. These data are compiled in Table 2 along with the measured values of cell performance.

The measured and calculated values of cell performance are in excellent agreement. Of all the impurities studied Ti, V, and Mo are most detrimental to the devices made upon contaminated web. This result is consistent with data gathered on solar cells fabricated from metal-doped Czochralski crystals.[17,21]

4.3 Impurity Tolerance for Continuous Web Growth

The tolerable feedstock contaminant level for web growth will be determined by the liquid impurity concentration at which either (a) structural breakdown or (b) cell performance degradation first occurs. We denote these impurity levels by C_ℓ^* (struct) and C_ℓ^* (cell), respectively. By comparing the breakdown data and cell performance results we may deduce for each metal species which impurity level, C_ℓ^* (struct) or C_ℓ^* (cell) will control the feedstock purity. For web growth the data in Table 1 indicate that C_ℓ^* (cell) < C_ℓ^* (struct) for all impurities (save perhaps Cu and Ni) a result similar to the previous analysis of Czochralski growth. If however, the cell performance requirements were relaxed, e. g. if one allowed the contaminated devices

to be 90% as efficient as the baseline cells ($\eta = 0.9\ \eta_B$) then for some impurities like Fe structural breakdown would be the critical consideration dictating feedstock purity.

In reality the "critical" concentration values in Table 1 define an upper boundary for melt impurity content. In a practical situation some form of melt replenishment will be required to effect process economics and to maintain stable growth conditions for prolonged periods (see section 3). Under these conditions impurities will be continually rejected from the crystal to the liquid as growth proceeds, and melt impurity concentration will rise as the amount of crystal grown increases. Thus the initial feedstock impurity concentration C_o must be less than C_ℓ^*. How much smaller C_o must be depends on the material throughput and whether the melt is sequentially or continuously replenished.

We expect to adopt continuous replenishment for web growth. For this approach the instantaneous melt impurity concentration when a volume of crystal V_c has been grown is given by[17]

$$C_\ell/C_o = 1 + \frac{V_c}{V_o} \qquad (3)$$

when $k \leq 10^{-3}$. In equation 3, C_o is the initial or feedstock impurity content and V_o is the melt volume. Thus we may determine the feedstock impurity content corresponding to $C_\ell = C_\ell^*$ from Eq. 3 by specifying the throughput rate and the growth cycle period. For example, if 5 cm wide by 0.015 cm thick web grows at 5 cm/min about 52.4 gm of silicon web

will be produced in an hour. Then for a three day growth cycle (65 hours of actual growth), as now looks attractive from an economic standpoint, $V_c/V_o \sim 17$ when the melt volume $V_o \sim 200g$. From Equation 3

$$C_o = \frac{C_\ell}{1 + 17} = \frac{C_\ell}{18} \tag{4}$$

Thus if the values of C_ℓ^* (cell) are assumed to define the maximum impurity content that may be reached by the end of the run, then

$$C_o = \frac{C_\ell^* \text{ (cell)}}{18} \tag{5}$$

for a three day cycle. The values of C_o calculated this way appear in the last column of Table 1.

From the table it is evident that with continuous replenishment under the conditions assumed above, most impurities can be tolerated in the web feedstock at a 1 to 3 ppma level. Major exceptions are Ti and V whose concentrations must be considerably lower if cell performance is to remain completely unimpaired. Again these results are similar to the Czochralski growth case.

In our calculation we assumed no reduction in cell performance would be tolerable. Relaxation of these requirements to say $\eta = 0.9\eta_B$ increases impurity tolerance by factors from about 2 to 10 depending on the impurity. Further, if melt volume were increased above that assumed, impurity buildup would be slower and larger C_o's would be acceptable.

Typical semiconductor grade feedstock contains impurities at concentrations of parts per billion or less. We estimate that parts per million concentrations of impurity will be tolerable for web growth. Thus the use of a cheap solar grade feedstock appears quite feasible for continuous web growth.

5. SILICON WEB BACK SURFACE FIELD SOLAR CELLS*

Silicon web crystals as grown are thin, typically 0.01 to 0.02 cm, so the efficiency of a solar cell fabricated on web will be impaired unless carrier recombination at the back surface of the device is minimized. This can be accomplished by incorporating an acceptor gradient at the back surface of the n-p device to induce a back surface field (BSF).[23,24] The acceptor gradient promotes (1) an increase in short circuit current, (2) an increase in cell voltage, (3) increased long wavelength response, (4) reduced cell resistance, and (5) increased fill factor in the cells.

In our initial studies a standard BBr_3 diffusion at 960°C was employed to form the p^+p back junction of the cells. The n^+ front junction was then introduced by $POCl_3$ diffusion at 850°C. The process sequence and geometry of the test cells has been described previously.[25] Web solar cells produced this way have exhibited AM1 conversion efficiencies as high as 15.5% with 12.5% being average for the anti-reflection coated devices.[26] Although the performance of these devices is quite good, we found it sometimes difficult to maintain the required high base diffusion length with the BBr_3 diffusion sequence. Variations in cell to cell performance are one result of this.

*These studies were carried out by R. B. Campbell, E. J. Semen, P. Rai-Choudhury and J. R. Davis.

To circumvent the limitations inherent in the BBr_3 process, we have recently investigated the utility of another boron BSF technique, diffusion from a CVD boron oxide, and also the formation of a BSF by aluminum doping. Briefly, in the first case a 1 μm thick p^+ layer is formed by diffusion at 1000°C. In the second approach a 15 μm thick evaporated aluminum layer is heat treated at about 800°C to produce a p^+ layer about 7 μm thick. The front junctions of all the cells were made as described above. Conventional Ti-Pd-Ag contacts were used on the front and back of the cells which were coated with TiO_2-SiO_2 to minimize surface reflection. Cell tests were performed with an AM1 spectrum simulator (see reference 25 for details). The web used was 15 Ωcm p-type; all experimental runs were accompanied by wafers of 10-12 Ωcm p-type float zone wafers for process control.

The device performance data (average values for several cells in a run), Table 3, indicate that the web solar cells behave in most respects like the baseline cells made on float zone wafers regardless of which process was used. This result is consistent with earlier studies which found web devices comparable in performance to control samples made on Czochralski wafers.[6] The data are too limited yet to distinguish which process produces the most efficient cells. However, the CVD oxide technique offers an advantage over the BBr_3 diffusion for process automation. The aluminum BSF technique, because it is a relatively low temperature process, holds considerable potential for maintaining good bulk recombination lifetime in the devices leading to both enhanced efficiency in the thin web cells and improved process

reproducibility. The aluminum technique also appears amenable to automated processing. Future experiments will investigate the detailed time-tempeature sequences to achieve optimum device performance.

6. CONCLUSIONS

The dendritic web technique is a unique method to grow ribbon single crystals of diamond lattic semiconductors. The method applied to silicon, produces high purity, low dislocation density crystals which are excellent substrates for the fabrication of efficient solar cells. For example, efficiencies up to 15.5% AM1 (the highest reported value for ribbon crystal) have been achieved with cell structures employing a BBr_3-diffused back surface field. Back surface fields produced by aluminum alloying or CVD oxide diffusion appear to work equally well and show advantages for cost reduction via process automation.

For commonly encountered metal impurities the effective segregation coefficients during web growth are small, typically within a factor of two to three of k_o. Thus the use of a cheaper, solar grade silicon containing on the order of a part per million of impurity, appears feasible for web growth even with melt replenishment.

Web output rates can be enhanced by manipulation of the thermal environment of the growth system. For example, extending the susceptor lid slot and introducting "dogbone" holes flattens the melt profile so that web widths over 4 cm can be achieved. By increasing the radiation loss from the web higher growth velocities can be attained. By reducing

the top heat shield temperatures and beveling the lid slots, growth speeds of 5 cm/min are readily produced. Sustained growth at high output rates, however, has been hampered by depletion of the melt which (1) reduces latent heat dissipation and thus speed and (2) increases ribbon thermal stress causing deformation of the ribbon. At low output rates melt depletion evolves slowly enough that temperature corrections can be made by the operator. Ribbons 6 to 8 meters long have commonly been grown this way.

To sustain high output rates for long growth periods will require melt replenishment to maintain the melt level, and hence thermal conditions invariant. We have recently demonstrated a system by which pelletized silicon can be fed to maintain a uniform melt level while web simultaneously grows. Future development will combine melt replenishment with thermal trimming to grow low stress material at larger output rates.

ACKNOWLEDGEMENT

This work was performed for the California Institute of Technology Jet Propulsion Laboratory under the Low Cost Solar Array Project by agreement between the National Aeronautics and Space Agency and the Department of Energy. We are deeply indebted to our colleagues on the silicon web development program for providing the technical data and expertise on which this paper is based: J. P. McHugh, C. S. Duncan, P. Piotrowski, A. M. Stewart, H. Foust, W. A. Stickel, E. P. Metz, H. Wehrli, J. M. Driggers, M. E. Heimlich, J. Pollito, V. DiMarchi, T. Hovanek, F. E. Hill, R. B. Campbell, J. R. Davis, E. J. Semen, D. N. Schmidt, C. F. Seiler, J. C. Neidigh, H. F. Abt, W. Cifone, B. F. Westwood, S. Gabrielse, and E. Mitsch.

REFERENCES

1. R. G. Seidensticker and D. R. Hamilton, J. Phy. Chem. Solids, 24, 1585, (1963).

2. R. G. Seidensticker, Westinghouse R&D Center, Unpublished work (1962).

3. S. O'Hara and A.I. Bennett, J. Appl. Phys. 35, 686, (1964).

4. S. O'Hara, J. Appl. Phys. 35 409, (1964).

5. D. L. Barrett, D. R. Hamilton, and E. H. Meyers, J. Electrochem Soc. 118, 952, (1971).

6. R. G. Seidensticker, J. Crystal Growth, 39 6, (1977).

7. H. C. Hottel and A. F. Sarofin, Radiative Heat Transfer; McGraw-Hill, NY, (1967).

8. M. D. Harrill, C. A. Rhodes, J. W. Faust, R. B. Hilburn, J. Crystal Growth, 44, 34, (1978).

9. B. H. McIntosh, et. al. Conference Record, 13th IEEE Photovoltaic Specialists Conference; IEEE, NY, 350 (1978).

10. R. Gurtler, et al., Conference Record 13th IEEE Photovoltaic Specialists Conference; IEEE, NY, 363 (1978).

11. B. A. Boley and J. H. Weiner, Theory of Thermal Stresses; John Wiley, NY, 323 (1960).

12. Yu. A. Burenkov and S. P. Nikanorov, Fiz. Tver. Tela 16, 1496, (1974). translated Soviet Phys. Sol State 16, 963, (1974).

13. R. O. A. Hall, Acta Cryst. 14, 1004, (1961).

14. R. A. Logan and W. L. Bond, J. Appl. Phys. 30, 322, (1959).

15. C. D. Graham et al., "Final Report-Research and Development of Low Cost Processes for Integrated Solar Arrays", No. ERDA/SE/EC(11-1)-2721/FR/76/1.

16. See for example, L. P. Hunt, V. D. Dosaj, J. R. McCormick and A. W. Ravchholz, Conference Record 13th IEEE Photovoltaic Specialists Conf., IEEE, NY, 333; (1978) W. C. Breneman, E. G. Farner and H. Morihara, Ibid, 339; W. H. Reed, T. N. Meyer and M. G. Fey, Ibid, 370.

17. R. H. Hopkins, R. G. Seidensticker, J. R. Davis, P. Rai-Choudhury, P. D. Blais, and J. R. McCormick, J. Crystal Growth 42, 493, (1977).

18. D. T. J. Hurle, Solid St. Electronics 3, 37, (1961).

19. W. W. Mullins and R. F. Sekerka, J. Appl. Phys. 35, 444, (1964).

20. S. O'Hara, J.A.P. 37, 3783 (1966).

21. J. R. Davis, P. D. Blais, R. H. Hopkins, P. Rai-Choudhury, A. Rohatgi, and J. R. McCormick, Conference Record 13th IEEE Photovoltaic Specialists Conf; IEEE, New York, 490, (1978).

22. R. G. Seidensticker, R. H. Hopkins, and A. M. Stewart, J. Crystal Growth 46, 5, (1979).

23. M. P. Godlewski, C. R. Baraona, and H. W. Brandhorst,Conference Record, 10th IEEE Photovoltaic Specialists Conf. IEEE, New York, 70 (1970).

24. M. Wolf, Proc. IEEE, 51, 675, (1963).

25. R. G. Seidensticker, R. E. Kothman, J. P. McHugh, C. S. Duncan, R. H. Hopkins, P. D. Blais, J. R. Davis and A. Rohatgi, Conference Record, 13th IEEE Photovoltaic Specialists Conf; IEEE, NY, 358, (1978).

26. R. B. Campbell, P. Rai-Choudhury, E. J. Semen, and M. H. Hanes, Westinghouse R&D Center, unpublished results, (1978).

27. C. S. Duncan, et al, Annual Report, Silicon Web Process Development, DOE/JPL-954654-78/2, 195 (1978).

28. O. C. Ziekiewicz and Y. K. Chung, The Finite Element Method in Structural and Continuum Mechanics, McGraw Hill Ltd, London, 228 (1967).

TABLE 1

FEEDSTOCK IMPURITY CONCENTRATIONS FOR WEB GROWTH
(see text for nomenclature)

Impurity	C_ℓ^* (struct) 10^{18} cm^{-3}	ppma*	C_ℓ^*(cell), $\eta/\eta_B \tilde{\sim} 1.0$ 10^{18} cm^{-3}	ppma	C_o 10^{18} cm^{-3}	ppma
Cu	> 1.4+	28	1.1 (est)	22	.06 (est)	1.2 (est)
Ni	> 1.0	> 20	≥1.1	≥ 22	≥.06	≥1.2
Cr	6	120	≥1.6	≥ 32	≥.09	≥1.5
Mn	> 2.6	52	≥2.6	≥ 52	≥.14	≥2.8
Fe	3	60	≥1.3	≥ 26	≥.07	≥1.4
Ti	4	80	0.05	1	.003	.06
V	4	80	0.04	0.8	.002	.04
Mo	2.5	50	0.8	16	.04	.8

+ > indicates no breakdown observed at this concentration

≥ indicates no measured cell degradation at this concentration

* 1 ppma $\sim 5 \times 10^{16}$ cm^{-3}

TABLE 2

PERFORMANCE OF CONTAMINATED SILICON WEB SOLAR CELLS

Impurity	k_{eff}(web*)	C_ℓ (10^{18} cm^{-3})	C_s (10^{13} cm^{-3}	η/η_B^+(calc)	η/η_B^+(meas)
Mo	1.2 (10^{-7})	2.5	.03	.91	0.85
Ni	8 (10^{-5})	1.1	8.8	.98	1.01
Cr	2.75 (10^{-5})	1.6	4.4	.97	1.03
Mn	3.25 (10^{-5})	2.6	8.5	.97	1.07
Fe	1.6 (10^{-5})	1.3	2.1	.97	1.01
Ti	9 (10^{-6})	2.2	1.9	.77	.73
V	1 (10^{-5})	1.5	1.5	.79	.80

* Calculated from Equation 2 with D = 5×10^{-4} cm^2/sec, $\theta = 20°$ (See Ref. 22).

\+ η_B is the efficiency of an uncontaminated device, about 12.5% AM1 with AR coatings in these studies.

TABLE 3

COMPARISON OF BACK SURFACE FIELD (BSF) FORMATION TECHNIQUES ON DENDRITIC WEB SILICON SOLAR CELLS

SAMPLE	J_{sc} (ma/cm^2)	V_{oc} (V)	EFF(%)	τ_{OCD} (μ sec)
BBr_3 Diff $X_j \sim 1$ μm web+ FZ Baseline	31.5 30.7	.573 .580	14.2* 14.2	36 35
Boron oxide CVD* Drive - $X_j \sim 1$ μm web FZ Baseline	31.5 31.2	.566 .570	13.8* 14.3	35 15
Evap AL Drive $X_j \sim 7$ μm web FZ Baseline	31.8 31.5	.571 .597	14.6* 15.3	34 42

* Web cells fabricated by identical sequences save for the absence of the BSF exhibit efficiencies lower by about 2%.

+ X_j is metallurgical junction depth.

NOTES: 1) AR Coated

2) Measured at AM1 (91.4 MW/cm^2)

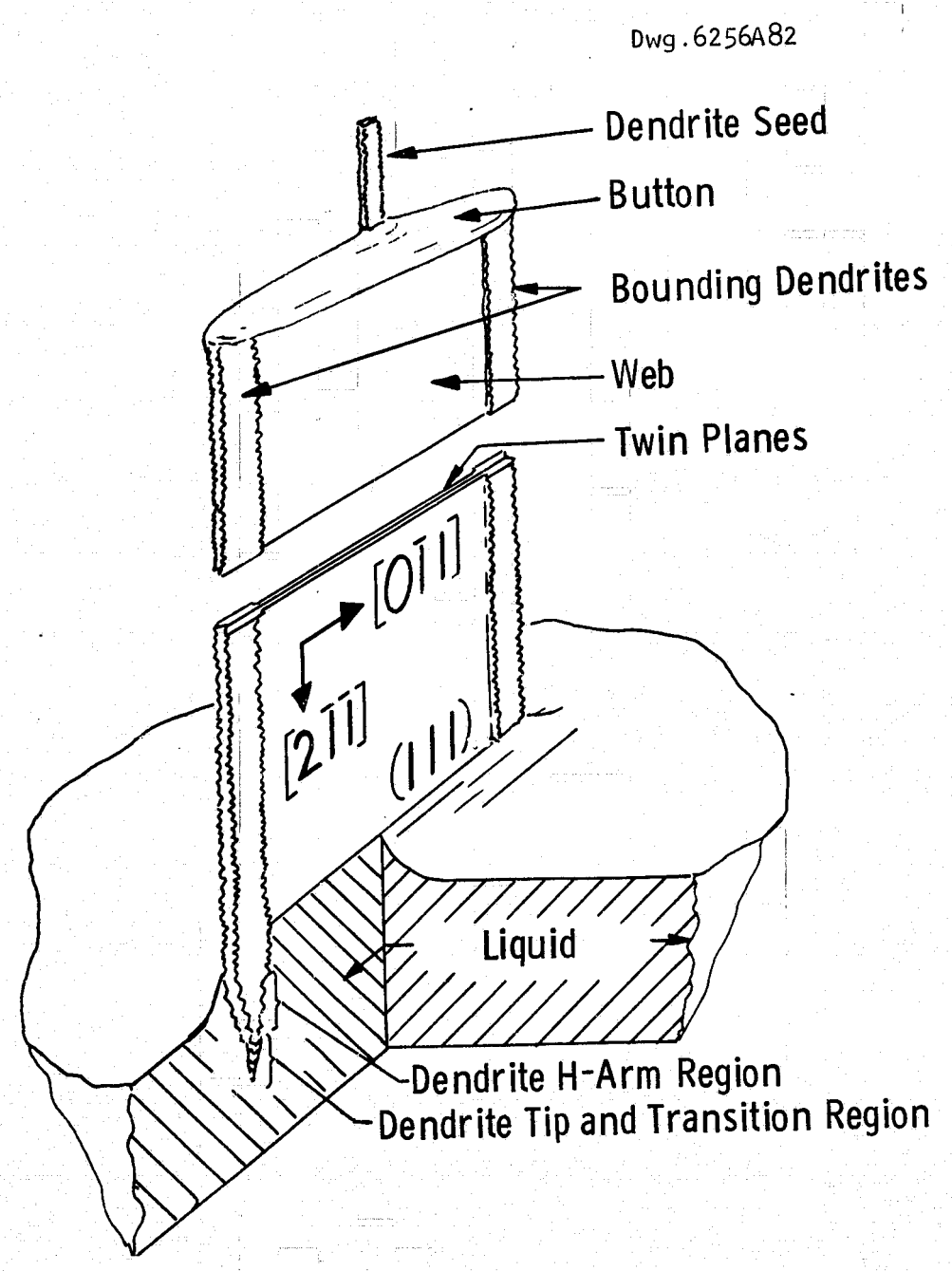

Figure 1 Schematic depiction of dendritic web growth. Seed button, bounding dendrites and crystallographic orientation of the ribbon are illustrated.

Dwg. 7686A17

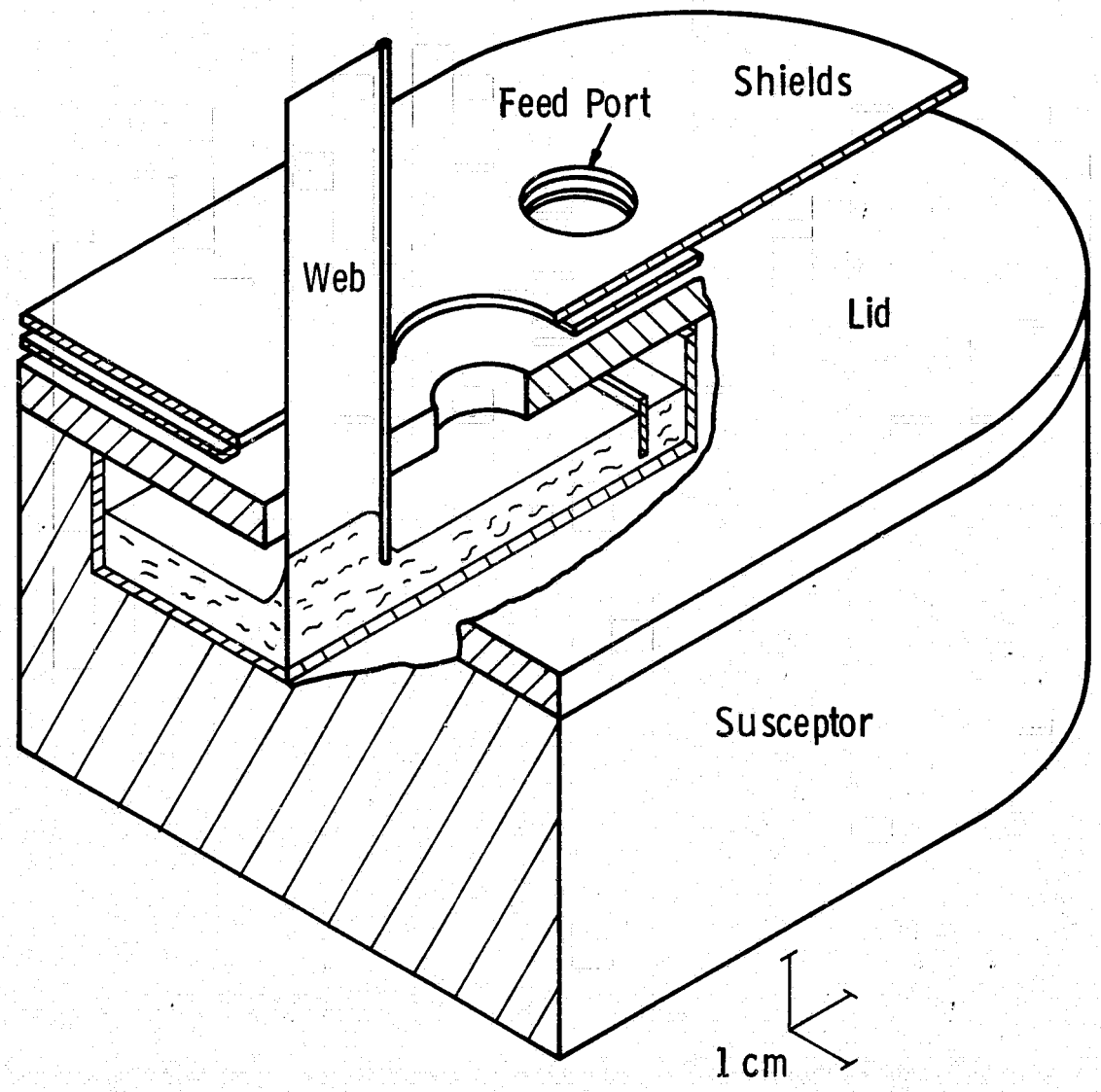

Figure 2 Sectional view of susceptor-crucible-lid assembly for dendritic web growth; low frequency induction coil not shown.

Dwg. 6438A24

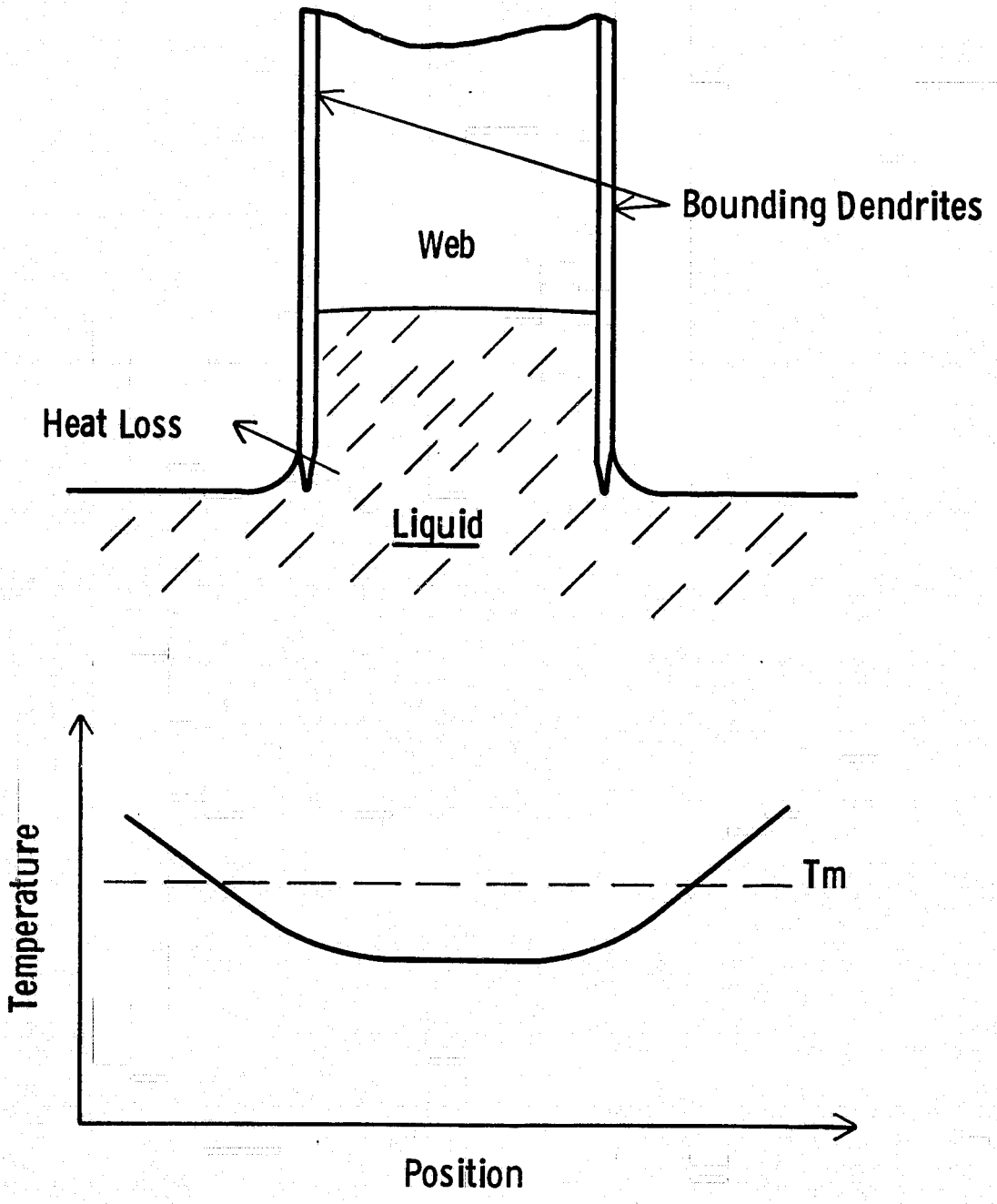

Figure 3 Illustration of the way the lateral temperature distribution in melt and lateral heat loss from the ribbon influence the dendritic web widening process.

Dwg. 7686A16

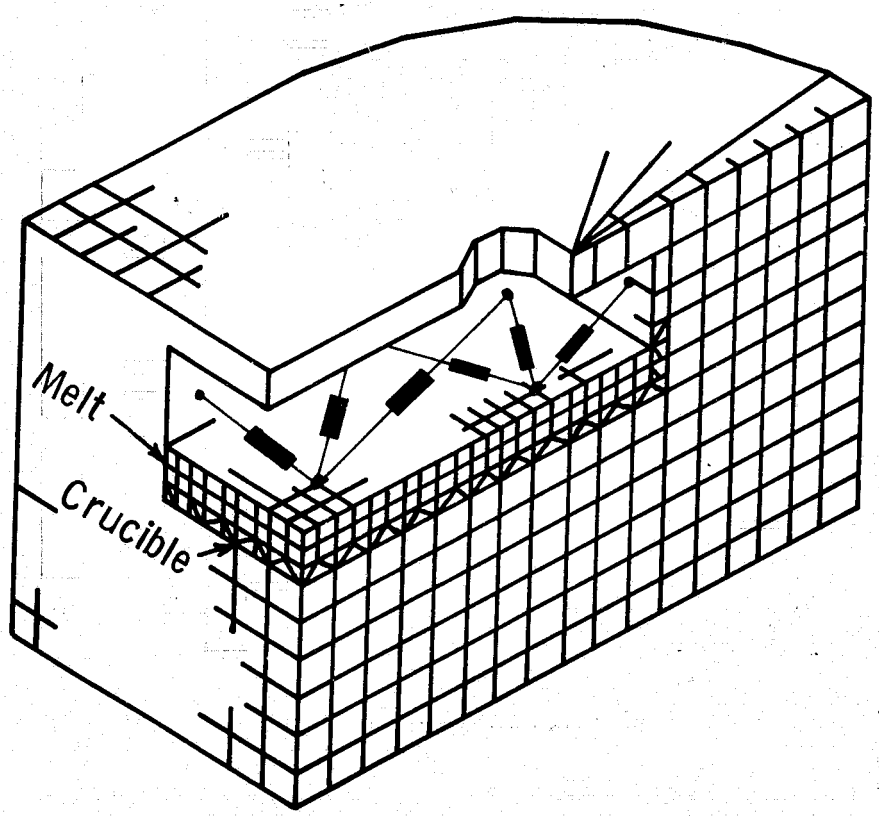

Figure 4 Schematic representation of finite element model for susceptor-crucible-melt assembly.

Curve 714929-A

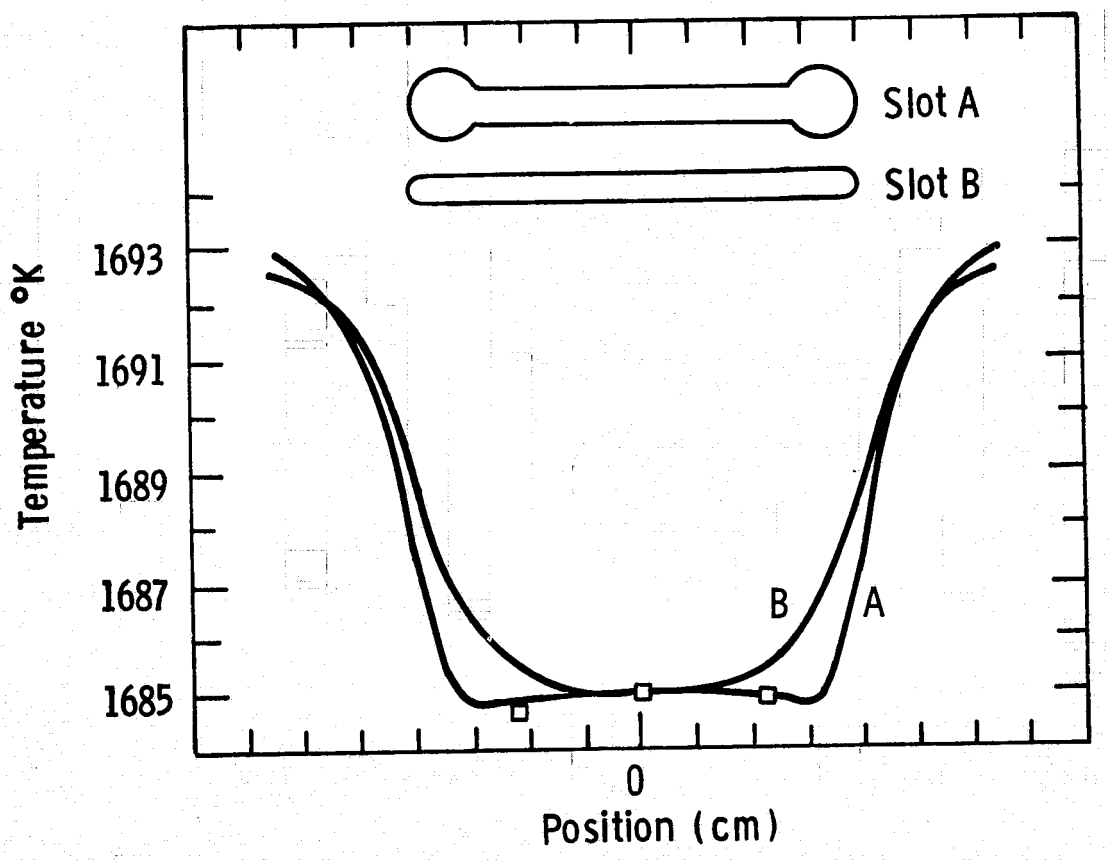

Figure 5 Lateral melt temperature profiles computed for a long slot terminated by end holes (A) and a similar straight slot (B) Data points were determined from the melting temperature of a fine dendrite seed.

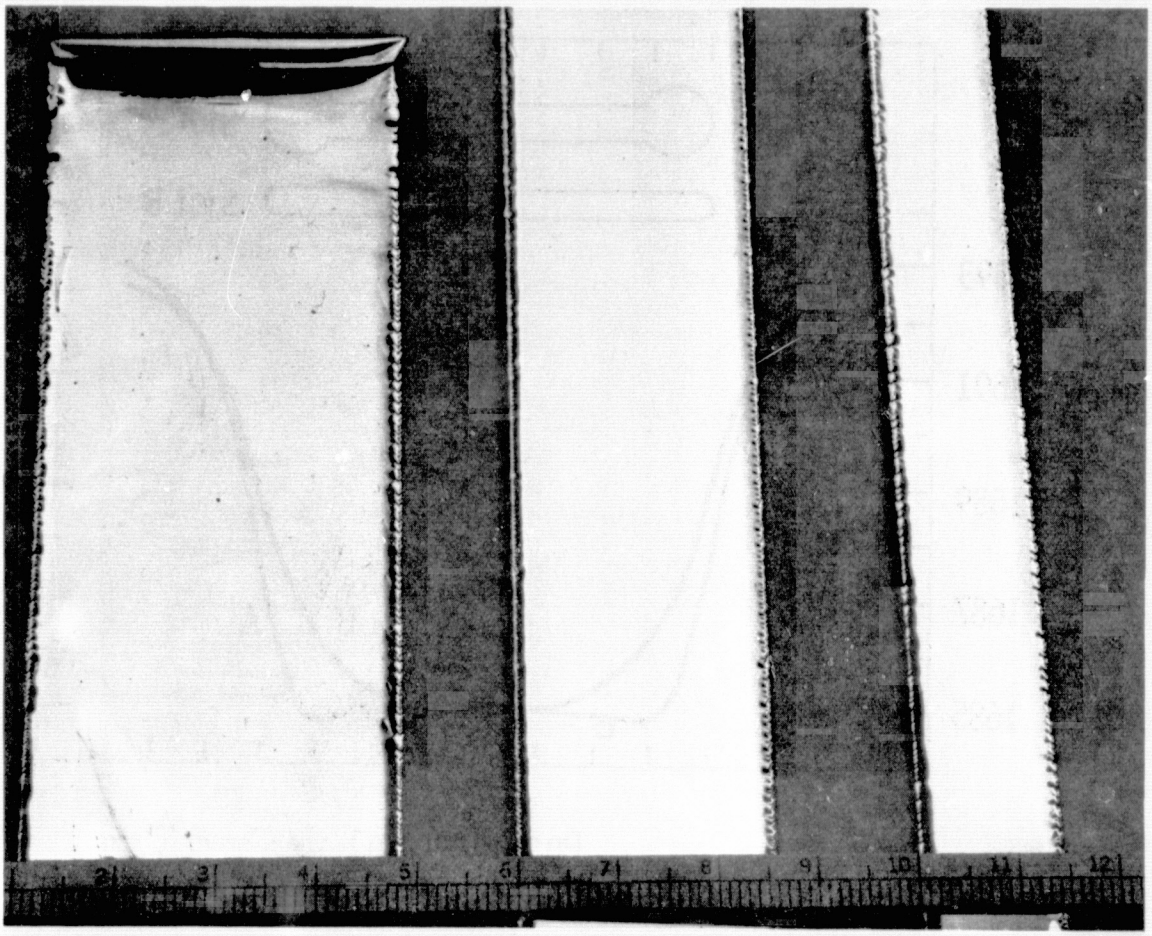

Figure 6 Increase in actual web width obtained with successively flatter melt temperature profiles. The 4 cm wide crystal was grown with slot A illustrated in Figure 5.

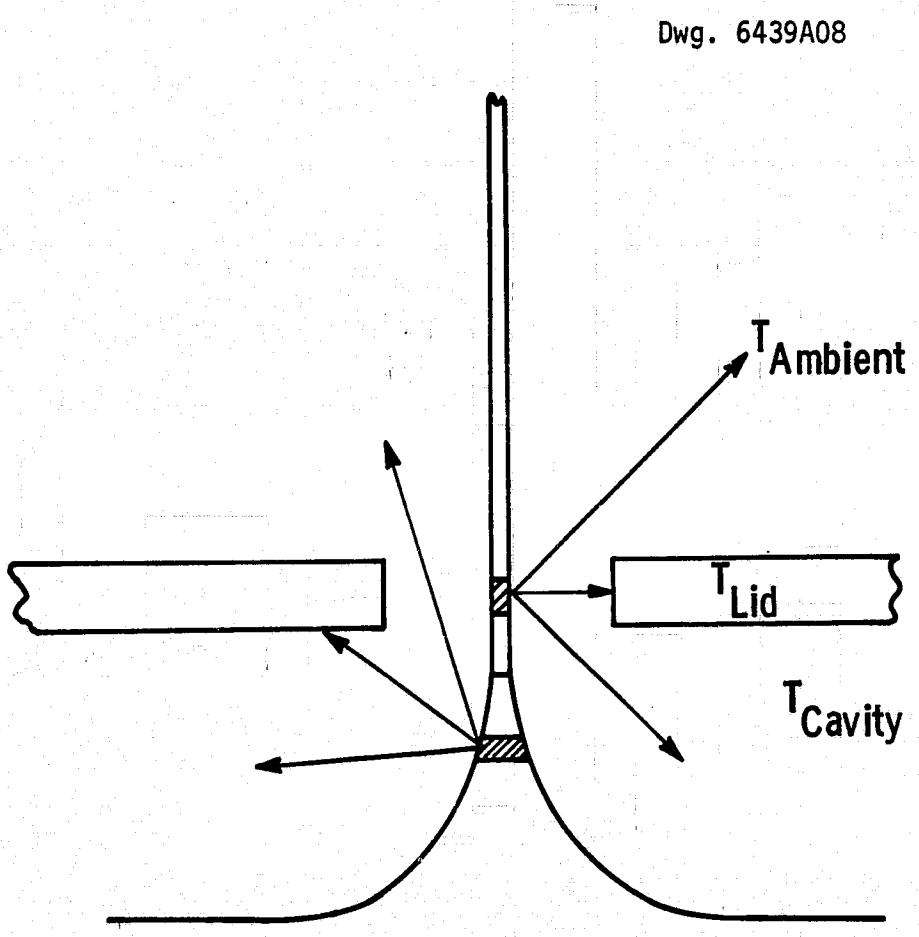

Figure 7 Heat transfer paths for modeling temperature profiles in the meniscus and in the web.

Curve 714927-A

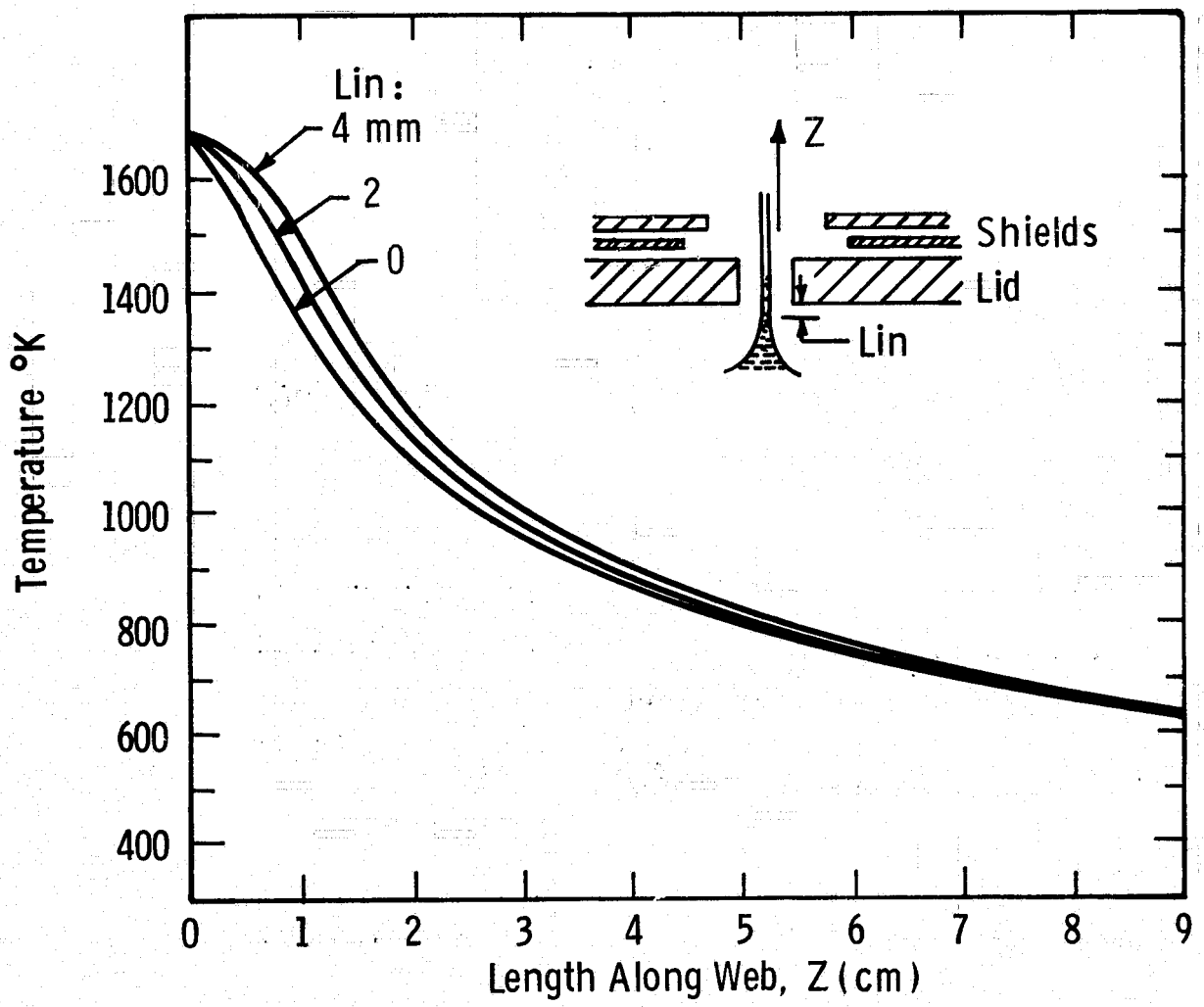

Figure 8 Calculated longitudinal temperature profiles in a 150 μm thick web crystal grown from the lid in Figure 2. The exact profile depends on the distance of the crystal-liquid interface below the lid, identified by LIN in the Figure.

Curve 714924-A

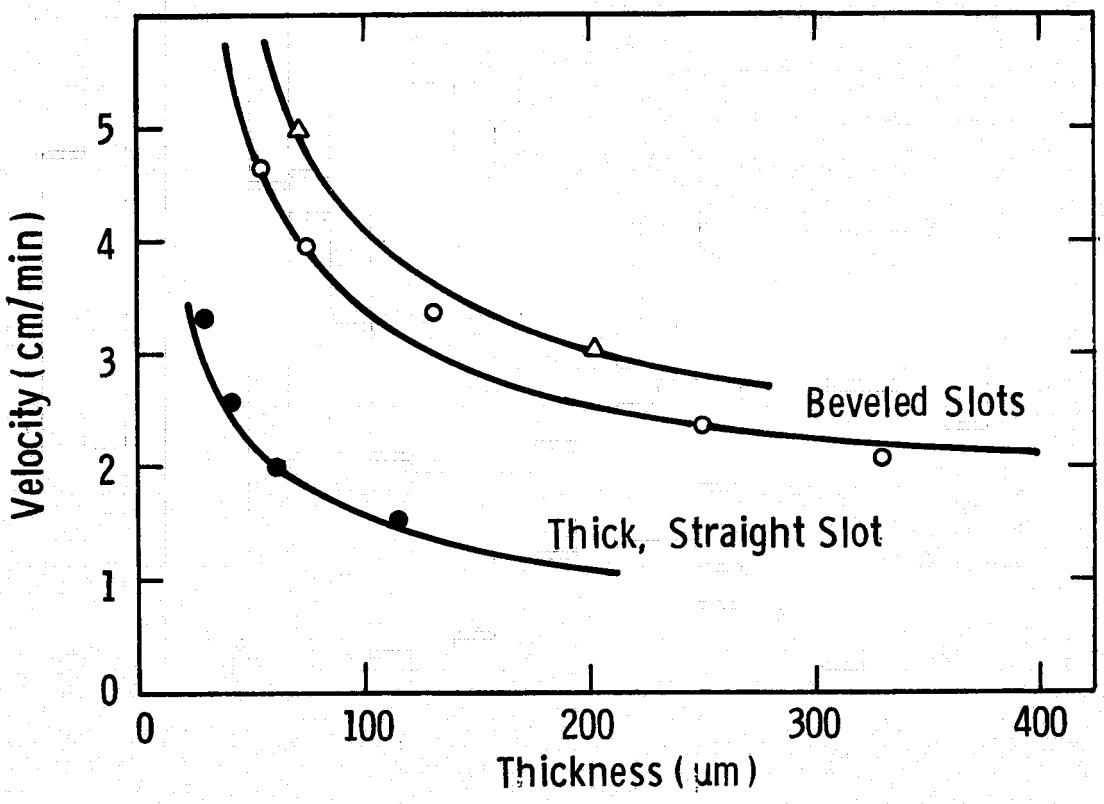

Figure 9 Growth velocity as a function of web thickness for different lid slot profiles. Curves are calculated from theory, data from thickness measurements on web crystals.

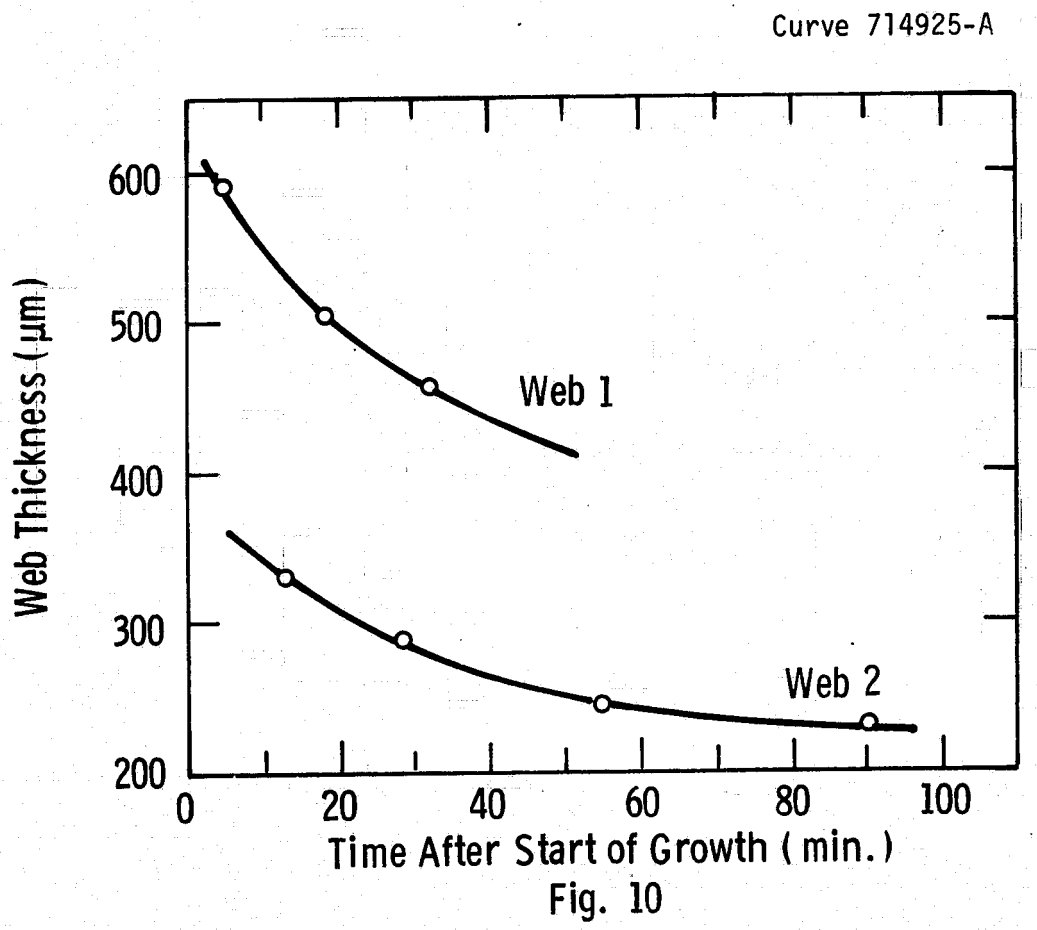

Figure 10 Web thickness as a function of growth time. The decrease in thickness at constant speed is caused by the drop in melt level.

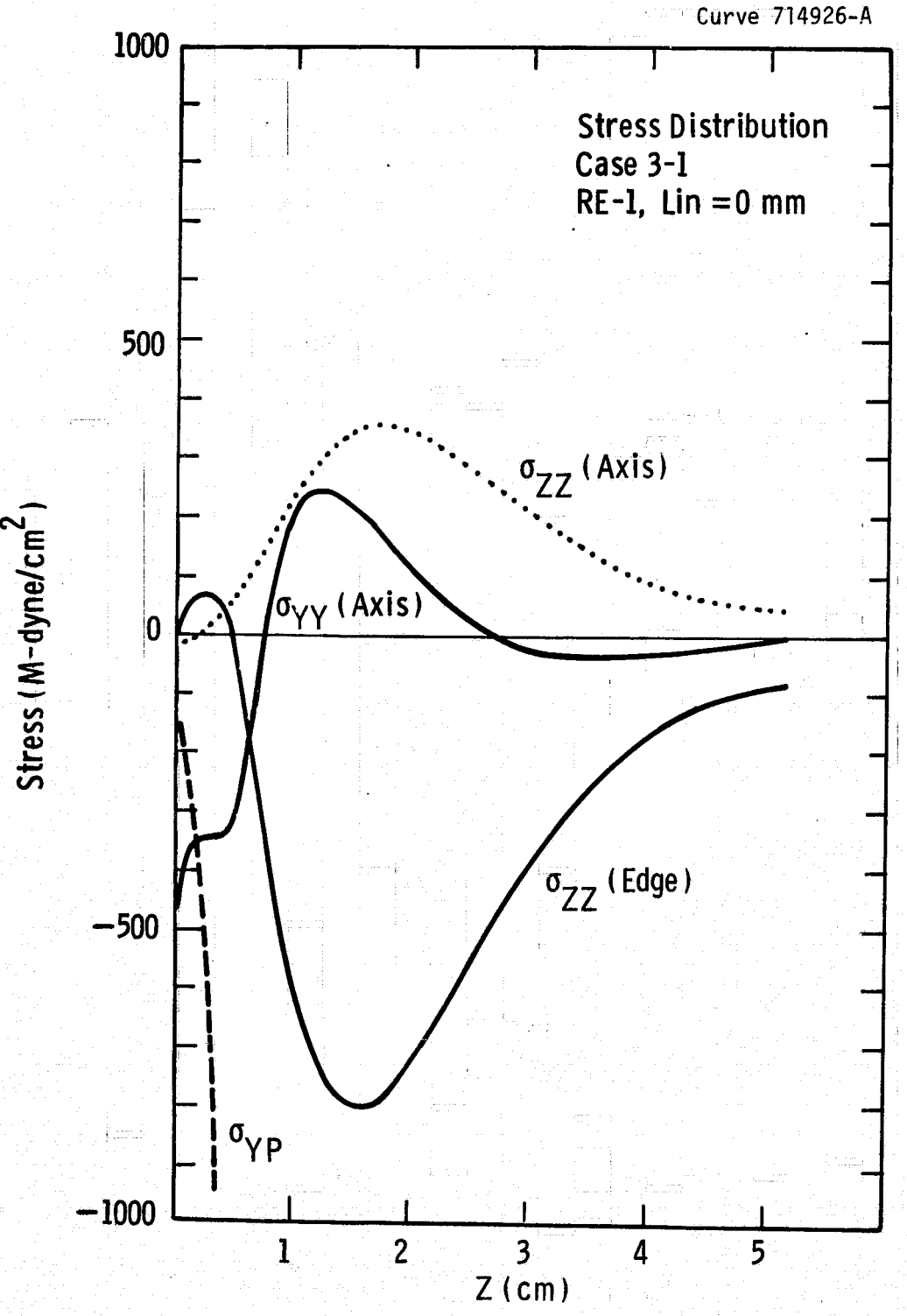

Figure 11 Calculated variation of longitudinal (σ_{ZZ}) and lateral stress (σ_{YY}) components along the length of a ribbon grown from the slot illustrated in Figure 2.

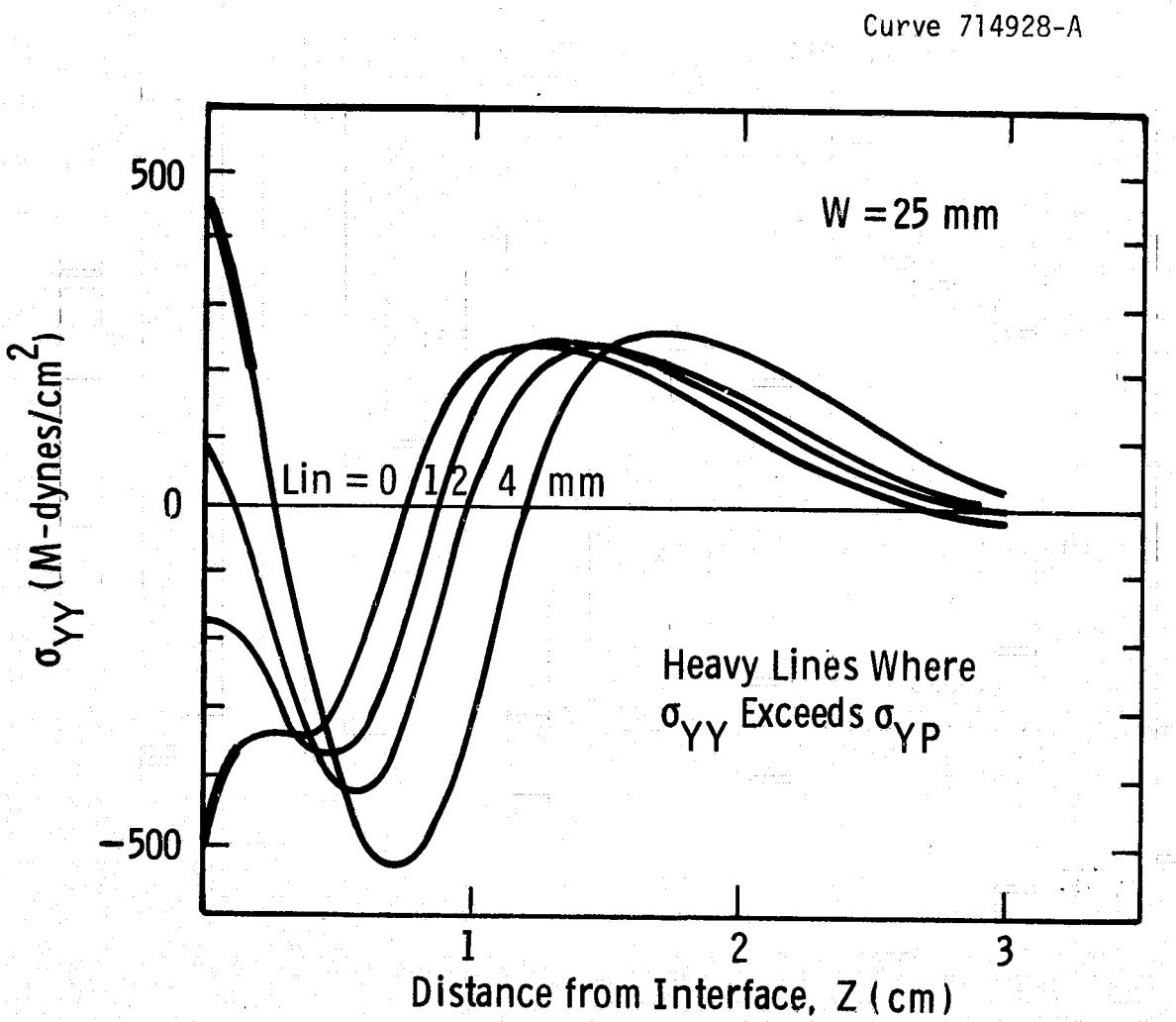

Figure 12 Lateral stress (σ_{YY}) at center of 25 mm wide web for different crystal-liquid interface locations below the lid; see Figure 8 for corresponding temperature profile.

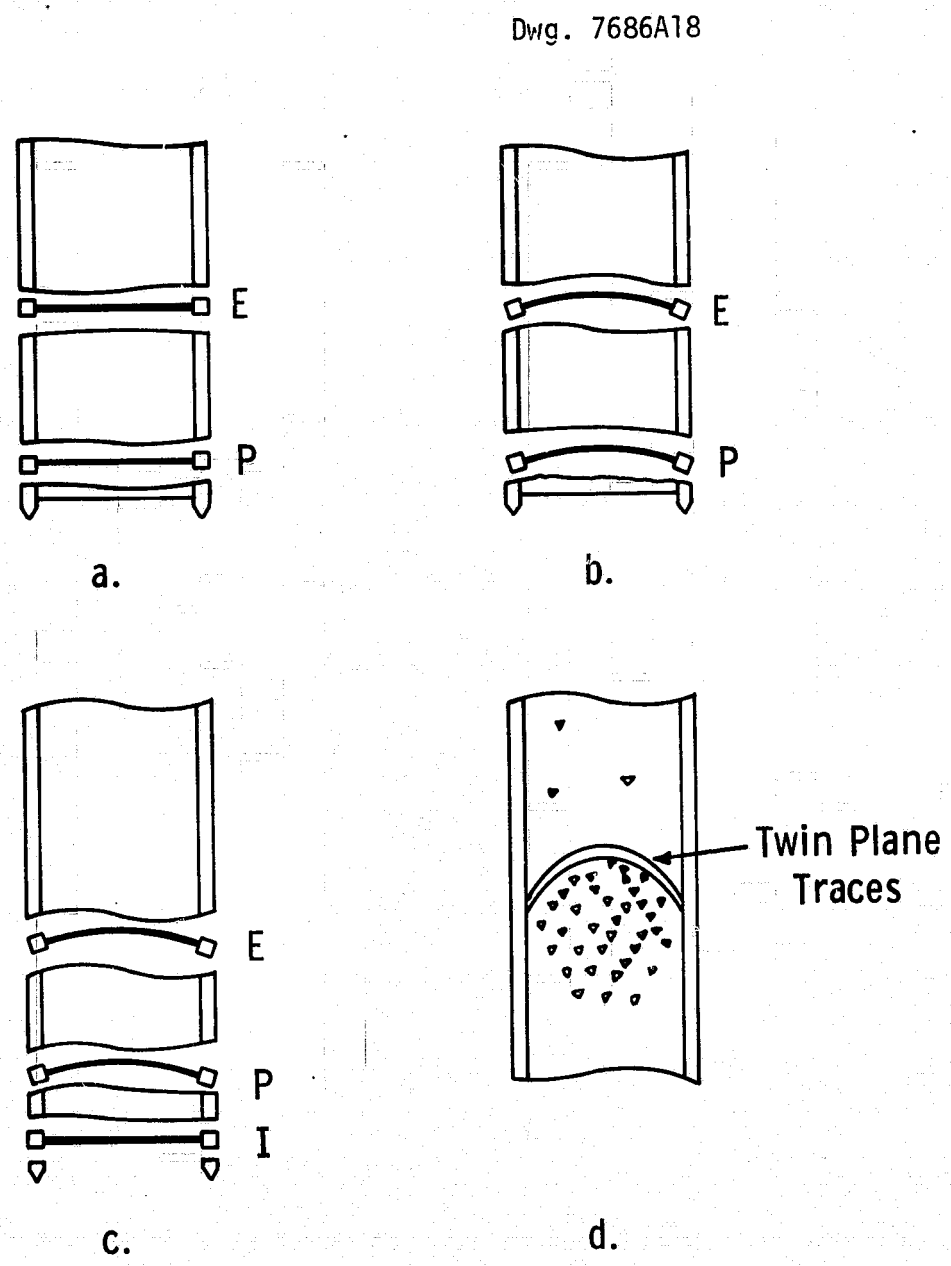

Figure 13 Model for elastic deformation process: a) initial condition; b) start of deformation; c) continued growth with straight growth front; d) web surface illustrating twin planes traces and slip bands after outcrop on surface.

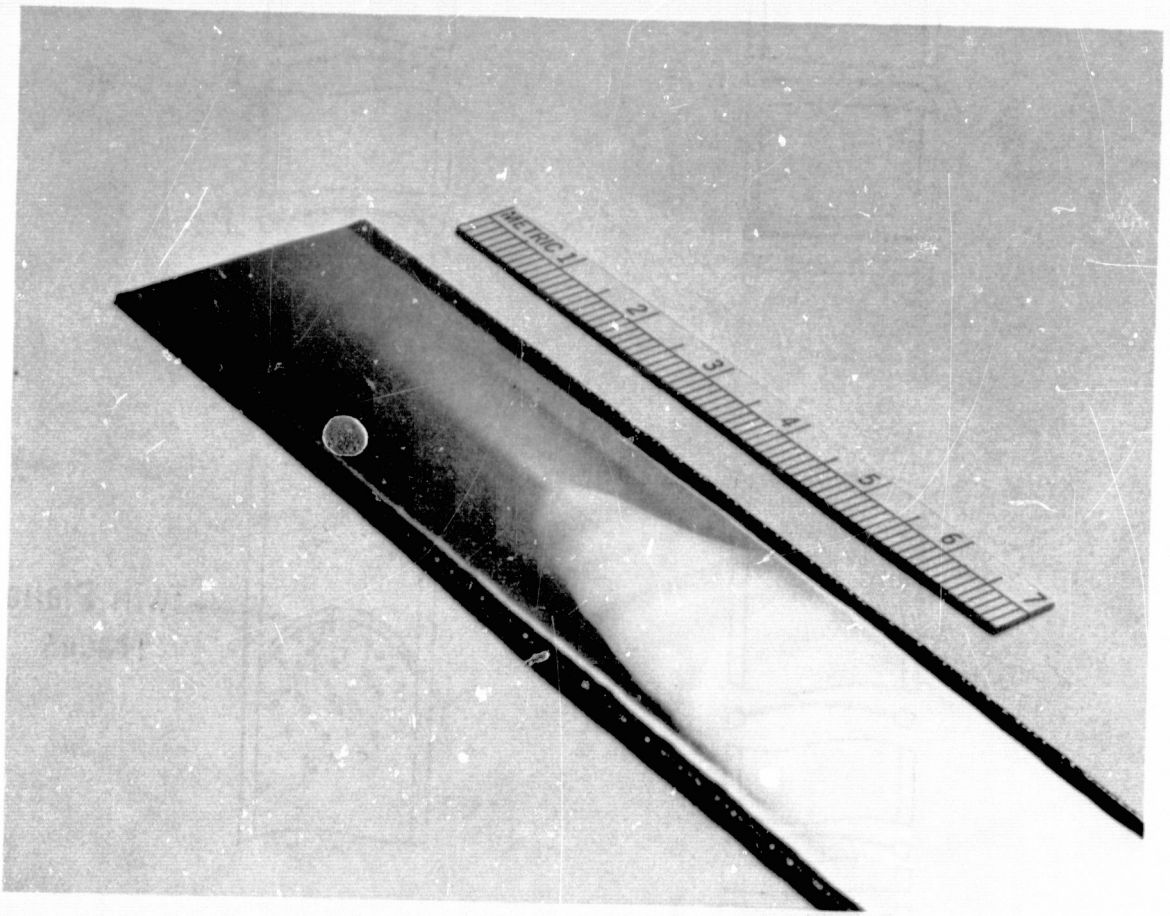

Figure 14 Rippled deformation mode which develops in a web after the twin plane outcrops due to elastic bending.

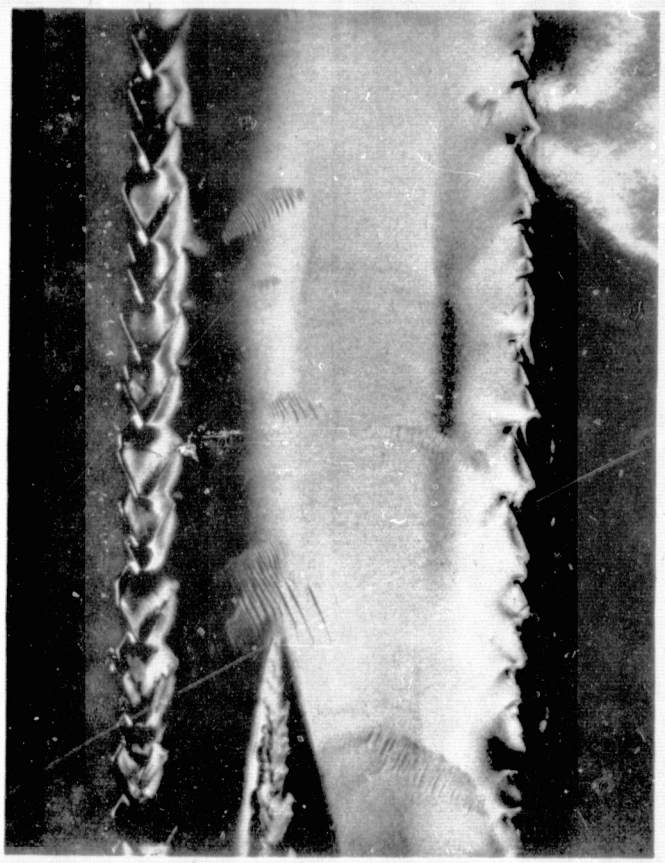

Figure 15 Patches of corrugated surface which developed in webs grown from a melt containing > $4 \times 10^{18} cm^{-3}$ titanium. Extra dendrites often nucleate in the vicinity of such patches as indicated in the figure.

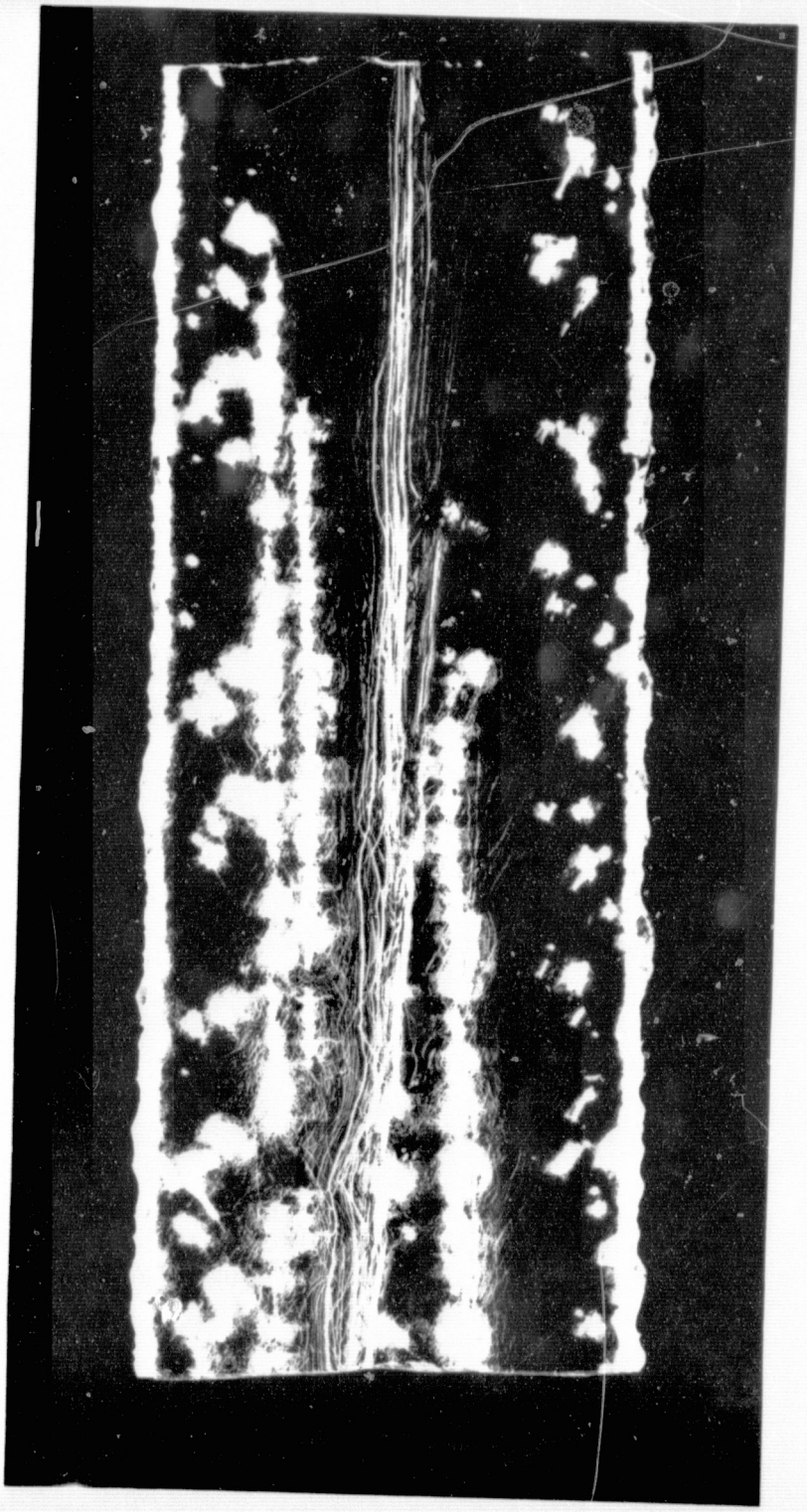

Figure 16 X-ray topograph of a silicon web grown from a heavily metal-doped melt. Individual bright spots in the typograph are strain fields surrounding the positions of inclusions entrapped within the crystal during growth.

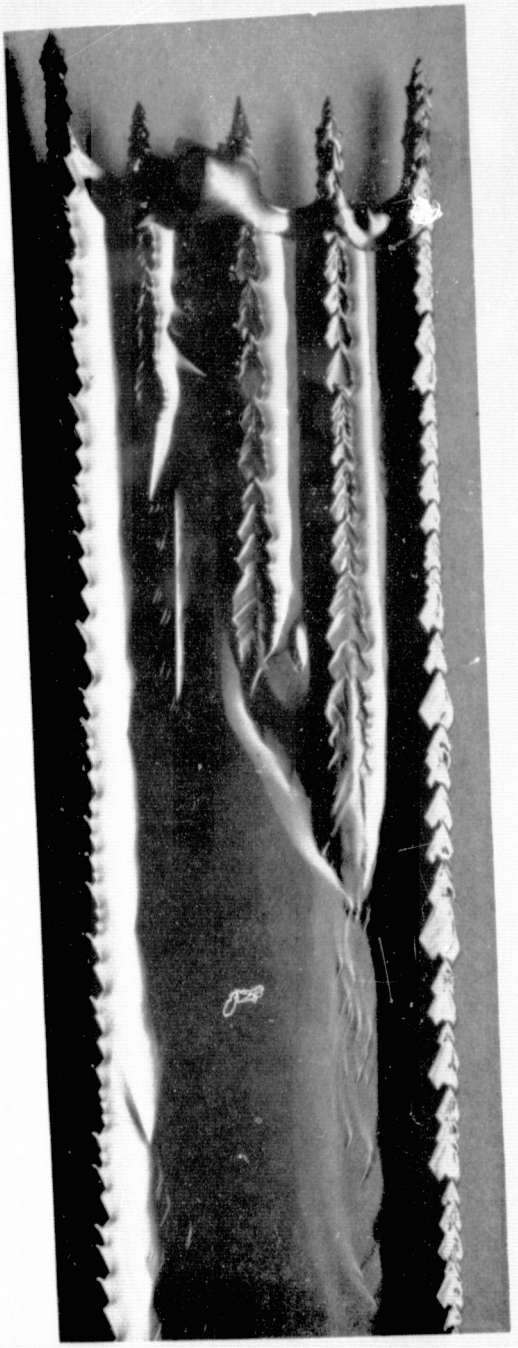

Figure 17 Breakdown of the smooth web-liquid interface to a dendritic array. Melt contained about $3 \times 10^{18} cm^{-3}$ of molybdenum.

8.2 APPENDIX 2

GROWTH RUN SUMMARIES

GROWTH RUN SUMMARY

Preface to RE Furnace Runs

The majority of runs in the RE-furnace fall into three broad categories: 1) extensive repeated runs using a fixed configuration in order to establish base line growth characteristics, study reproducibility, develop operator technique, optimize growth procedures and supply web material for characterization and cell fabrication. 2) Develop melt replenishment techniques and hardware. 3) Combine width and speed technology for high output rates. In addition, some runs were devoted to testing lid designs for width or speed and an argon flow system for oxide control.

The first 31 runs in the RE furnace (except RE-19) used the same general configuration (the "RE-1" lids). Problems associated with crucible fit, oxide deposition, and lid preparation were identified and steps were taken to understand and control these variables.

Feed system tests were begun with run RE-38 and continued, with a few interruptions, through run RE-79. A variety of crucible barrier designs and slot configurations were tested. Problems requiring further study were identified, and this work was continued in the W-furnace.

At this point, the RE furnace was largely dedicated to studies to obtain higher output rates, testing configurations for higher growth speed and greater web width.

GROWTH RUN SUMMARY

RUN	NO. OF CRYSTALS	LENGTH (cm)	MAX. WIDTH (mm)	MAX. VELOCITY (cm/min)	DESCRIPTION/RESULT
RE-1	2	278	28.0	2.1	R-furnace modified to use elongated susceptor (J-type)/ 6.3 mm thick lid, 80x6 mm slot, 12.7 mm dogbone holes. Two top shields, lower shortened. Configuration grows well in both furnace facilities.
RE-2	3	315	28.9	1.9	To prepare n-type base material for cell fabrication. $1.2x10^{18}$ phosphorus doping (0.86 gms) RE-1 configuration.
RE-3	7	469	22.6	2.4	Rerun RE-1 configuration. After some problems in morning, grew well in afternoon.
RE-4	1	69	156	2.4	Repeat RE-1 configuration. Difficult to start growth. Concern about argon purity. Change in operator.
RE-5	3	170	20.8	2.1	Argon purification train installed. Same configuration as RE-1. Some problems with thirding and ice.
RE-6	4	310	19.5	2.1	RE-1 configuration. Melt unstable in a.m., some floating ice.
RE-7	2	327	32.0	1.7	RE-1 configuration. Problems with oxide deposition on lid.
RE-8	4	404	25.5	1.8	RE-1 configuration. Some oxide and ice problems.
RE-9	5	438	25.0	1.8	RE-1 configuration. Most crystals terminated by pullout.
RE-10	2	462	30.7	1.7	RE-1 configuration. generally good growth behavior. One crystal was 290 cm long.
RE-11	4	368	28.6	1.5	RE-1 configuration. Some floating ice in a.m.
RE-12	3	299	28.4	1.6	RE-1 configuration. Some problems with oxide growth on lid slot.
RE-13	7	530	24.7	1.5	RE-1 configuration. Unstable melt, oxide.
RE-14	3	382	30.4	1.8	RE-1 configuration. Starting problems in a.m. better in p.m.
RE-15	3	445	35.8	3.05	RE-1 configuration. 285 cm long crystal. 10.9 cm^2/min. thruput.

GROWTH RUN SUMMARY

RUN	NO. OF CRYSTALS	LENGTH (cm)	MAX. WIDTH (mm)	MAX. VELOCITY (cm/min)	DESCRIPTION/RESULT
RE-16	3	103	16.7	1.8	RE-1 configuration. Plagued by oxide in slot falling into melt, terminating growth.
RE-17	2	83	16.1	1.7	RE-1 configuration. Ice problems.
RE-18	3	410	29.5	1.7	RE-1 configuration. Doped to produce lower resistivity than normal.
RE-19	Not Productive of Web				Test new lid configuration. Lid 8.7 mm thick, slot 80x6 mm, 12.7 mm dogbones, 5x5 mm bevel all around. Two top shields. Large piece of oxide fell into melt early and went to crucible wall, caused ice problems all day.
RE-20	5	548	18.5	2.6	Repeat RE-19. Take thickness-velocity data. Growth behavior generally good.
RE-21	7	510	26.3	1.8	Same configuration as RE-19. Many short crystals decanted because they went poly early.
RE-22	4	305	26.9	1.7	RE-1 configuration. Crucible bottom ground flat in hopes of improving reproducibility.
RE-23	7	498	33.2	1.8	RE-1 configuration. Crucible bottom ground flat.
RE-24	4	284	29.7	1.8	RE-1 configuration. Crucible bottom ground flat, now becoming standard procedure.
RE-25	6	546	35.0	1.8	RE-1 configuration. Melt pulled free from crucible wall during growth of last crystal.
RE-26	5	420	30.0	1.8	RE-1 configuration. Melt partially replenished with Si rods. Oxide in slot late in day.
RE-27	4	357	26.3	1.8	RE-1 configuration. Some oxide problems late in day.
RE-28	6	430	36.0	1.9	RE-1 configuration. Occasional ice.
RE-29	4	365	25.8	1.9	RE-1 configuration. Oxide in dogbone hole.
RE-30	2	264	28.1	1.9	RE-1 configuration. Oxide in dogbone hole.
RE-31	2	132	18.4	1.9	RE-1 configuration. Ice problems all day.

GROWTH RUN SUMMARY

RUN	NO. OF CRYSTALS	LENGTH (cm)	MAX. WIDTH (mm)	MAX. VELOCITY (cm/min)	DESCRIPTION/RESULT
RE-32	5	326	25.2	1.9	Change configuration. 80x6 mm dogboned slot with 5x5 mm bevel all around in thick lid, 3 top shields, 2 lower formed to lap bevel 3 mm. Excessive oxide build up on lip of formed shields prevented growth of long crystals.
RE-33	5	529	27.9	1.9	RE-32 lid, 3 top shields, only lower one formed over lid bevel. Much better growth behavior.
RE-34	6	448	23.2	2.1	Repeat RE-33 configuration. Some oxide.
RE-35	Not Productive of Web Crystals				RE-32 lid with 3 flat top shields. Excessive oxide and ice problems. Melt too cold at ends.
RE-36	Not Productive of Web Crystals				RE-32 lid, 2 full top shields, plus one over ends only. Crystals consistently started poly. Melt too hot at ends.
RE-37	Not Productive of Web Crystals				RE-36 lid and shield configuration, except lower half of susceptor side shields removed in effort to trim melt profile consistent poly starts.
RE-38	Not Productive of Web				First test of manual feed system. Lid 66.6x6.3 mm dogboned slot with feed hole, 2 top shields. Crucible with barrier to separate feed and growth regions. Bottom of feed tube became blocked with oxide.
RE-39	Not Productive of Web				Test use of argon flow through feed tube to prevent oxide deposition in tube. Problem with floating ice.
RE-40	3	290	17.8	2.1	RE-1 configuration.
RE-41	3	350	24.6	2.1	RE-1 configuration. Oxide problems.
RE-42	1	85	16.6	1.9	Test behavior of lid with straight slot beveled 5x5 mm, 2 top shields Ice repeated nucleated by oxide apparently spalling off bottom of lid.
RE-43	2	146	22.4	2.2	Feed system test, RE-38 configuration. Feed tube blocked early. Insufficient oxide flow in feed tube.

GROWTH RUN SUMMARY

RUN	NO. OF CRYSTALS	LENGTH (cm)	MAX. WIDTH (mm)	MAX. VELOCITY (cm/min)	DESCRIPTION/RESULT
RE-44	5	255	17.8	2.1	Feed system test, RE-38 configuration. Fed pellets for 8 min. and 11 min., while growing then floating ice particle observed, which attached to web causing breakdown. After run, crucible feed compartment empty except for a few frozen drops.
RE-45	1	67	16.8	2.4	Repeat RE-44. Feed tube clogged with oxide before feeding initiated. Crucible feed compartment empty after run.
RE-46	2	169	17.2	2.2	Repeat RE-33 configuration. Oxide build up on lower shield. Icing.
RE-47	1	90	23.3	1.8	Feed system test. RE-38 configuration. Oxide and ice problems, even without feeding pellets.
RE-48	Not Productive				RE-1 configuration. Aborted during melt down. Si touched lid, immediate and catastrofic reaction.
RE-49	4	577	25.0	1.9	New susceptor and new lid configuration tested 50x4 mm straight slot beveled 5x6 mm, 2 top shields. Test behavior of shorter slot, to be later used in feed experiments. Crystal went poly at about 2 meters.

GROWTH RUN SUMMARY

RUN	NO. OF CRYSTALS	LENGTH (cm)	DESCRIPTION/RESULT
RE50	2	170	Feed system test. Run to evaluate Type A crucible barrier (vertical, narrow slot). Fed and grew web simultaneously. Growth terminated by floating ice in melt. Noted melt rippling during feeding; did not disturb growth. Silicon remained in feed reservoir.
RE51	4	473	Test effect of narrow straight (80x4 mm) slot on web stress. Two full top shields 5mm x 5mm bevel. Web deformed at about 2 cm maximum width and went polycrystalline.
RE52	3	170	Feed system test. Test shorter growth slot(50x4mm) to raise temperature at feed position. Type A barrier in feed reservoir. Oxide collected on right of growth slot. Argon feed rate appeared too high; reduce flow reduced oxide deposition. Silicon remained in feed reservoir.
RE53	3	214	Feed System Test. Initially no silicon in feed chamber to test: (1) thermal symmetry in system (2) melting behavior of pellets. Type A barrier. Dendrite probe indicated thermal asymmetry-feed side hot. Pellets melted in empty reservoir and some flowed over to growth chamber.
RE54	4	470	Test new RE-1 lid to replace damaged lid. Buttoning and growth behavior normal for this lid. Widths 23-28 mm easy to achieve. Lid appears useable in future experiments.
RE55	3	162	Test effects of 80x6mm slot, 5x5mm bevel (12.7 mm dogbone) on melt profile, web stress and width. Dendrite profile indicated temperature is slightly humped in center of melt and some asymmetric. Crystals widened poorly 20mm max. Oxide collected on shield assembly caused ice in melt.

GROWTH RUN SUMMARY

RUN	NO. OF CRYSTALS	LENGTH (cm)	DESCRIPTION/RESULT
RE56	4	372	Verification run on new RE-1 lid. Maximum width 28.5 mm. Melt profile relatively flat as expected. Plan to run lid in after-trimmer experiments.
RE57	6	350	Test effect of vertical coil position on seeding and growth with RE-1 lid. Problems with ice formation negated experiment. Note oxide on bottom of lid after run. Apparently spalled during run. Test new lid cleaning procedure installed.
RE58	3	305	Test effect of directed argon flow to minimize oxide buildup on overlapping shields. Beveled lid, 80mm slot. Considerably reduced oxide laid down on shield. Harder to seed at high flow rates-third dendrites.
RE59	4	464	Verification test of directed argon flow system. Good oxide control. Grew maximum width of 28mm. Good seeding.
RE60	4	389	Test 5cm, beveled lid for subsequent feeding runs. Dendrite probe fairly flat over center 2-3cms. Feed hole clogged in absence of argon flow. Flow is mandatory for this configuration.
RE61	Not Productive of Web		Feed system test with RE60 lid. Type B barrier no silicon in feed chamber. Large amounts of ice. Shields oxidized suspect system leak. Clean and tighten fittings before next run.
RE62	1	96	Test RE58 lid configuration. Lid overhang extended to reduce radiation from hot lid to web. Used argon flow between shields. Excessive oxide accumulation.
RE63	1	88	Feed system test. Beveled lid, 5cm slot, dogbones. Addition of argon flow tubes to minimize oxide accumulation. Type B crucible barrier (60° slant). No silicon in feed reservoir. Fed and grew web; growth terminated by floating ice.

GROWTH RUN SUMMARY

RUN	NO. OF CRYSTALS	LENGTH (cm)	DESCRIPTION/RESULT
RE64	1	70	Retest RE62 configuration (80mm slot, beveled large overlapping shields) without argon flow tubes. Excessive oxide. Conclude cannot run this arrangement without argon purge.
RE65	5	325	Feed System Test. Beveled lid, 5cm slot, dogbones (RE63) without argon purge through shields. Large (6mm) gap below feed barrier. Assess containment characteristics. Got ice when feeding pellets. Some oxide toward end opposite feed tube. Silicon remained in feed reservoir.
RE66	1	95	Test dished growth lid (design to vary radiation view angle along slot length) two top shields. Evaluated widening characteristics Only 21mm width. Excessive oxide on shield made result ambiguous.
RE67	3	264	Feed System Test. 5cm, beveled slot with dogbones (RE63). Test use of $A\ell_2O_3$ ceramic argon flow tubes under shield to replace Mo tubes. Type A barrier. Fed pellets without perturbing growth. Feed chamber empty of silicon after run. Growth slot free of oxide.
RE68	2	88	Rerun test of dished lid (RE66). Still have problem with oxide deposition on shields. Conclude must alter shield configuration or use argon purge.

GROWTH RUN SUMMARY

RUN	NO. OF CRYSTALS	LENGTH cm	DESCRIPTION/RESULT
RE69	5	282	Feed system test. Test type C barrier (6x10 mm hole) as partition for feed reservoir. Crystal growth terminated repeatly by formation of ice in melt during feeding.
RE70	3	203	Feed system test. Feed tube itself submerged in melt to act as pellet insertion mechanism as well as in situ barrier. Feed and in situ grow for periods up to 10 min. Pellets only partially melted and blocked tube to further feeding.
RE71	3	158	Feed system test. Retest of submerged tube with argon flow adjusted. Both oxide and unmelted pellets terminated feeding eventually. Conclude submerged tube ineffective feeding technique.
RE72	4	228	Feed system test. Test type C barrier with extended height to minimize oxide transport to growth chamber. Again grew and fed for short periods but ice formation terminated growth. Conclude higher barrier ineffective solution to oxide problem.
RE73	Unproductive		Test of reversed argon flow through lid shields (away from slot) to minimize oxide. Produced temperature fluctuations. Seeding and growth difficult to control. Abort run.
RE74	Unproductive		Feed system test. Type C barrier. Systematic test of argon purge rate through feed tube to control oxide buildup. Unable to grow due to ice throughout run. Suspect furnace leak. After run found that no silicon remained in feed chamber.

GROWTH RUN SUMMARY

RUN	NO. OF CRYSTALS	LENGTH cm	DESCRIPTION/RESULT
RE75	5	350	Feed system test. Repeat of previous run after furnace checkout. No major ice problem. Grew and fed simultaneously for periods over 1 hour. Growth of longer crystal terminated by oxide speck.
RE76	3	98	Feed system test. Test of methods to eliminate outflow of silicon from feed chamber during run: larger hole (7x15 mm) in type C barrier. Result ambiguous due to oxide. Height of hole too close to melt surface to act as effective barrier.
RE77	Unproductive		Feed system test. Test effects of melt down procedure to prevent outflow of silicon from feed chamber. Melt charge from feed end toward center. Silicon in feed chamber at end of run. Oxide and ice in melt made run unproductive for growth.
RE78	4	416	Feed system test. Verification of effects of directional charge melt down procedure. Melt from center to feed end by repositioning coil. Feed reservoir empty at end of run. Conclude must melt material in feed chamber first during start up to keep silicon there during run. Fed and grew during run.

GROWTH RUN SUMMARY

RUN	NO. OF CRYSTALS	LENGTH (cm)	DESCRIPTION/RESULT
RE79	2	273	Feed Run Test. Evaluate melt down procedure on silicon retention in feed chamber. RE-1 type lid. Melt down from feed end first. Silicon remained in feed reservoir throughout run. Web width up to 24mm.
RE80	Not Productive of Web		Test lid for high speed growth. Recessed bevel, ∿ 3mm thin lip (see text, section 3.1.3). Speed to 6cm/min in short lengths. Excessive oxide accumulation on shields. Oxide fell in, run aborted.
RE81	7	471	Retest high speed lid of RE80 but with argon purge to reduce oxide. Speeds up to 4.5 cm/min. Widths 12.3-17.5mm. Lineage.
RE82	2	209	Retest high speed lid (RE81). Evaluate effect of coil height on seeding and growth. Max. speed 3.5cm/min; Max. width 15mm. Problem with lineage structure formed during seeding; limits widening.
RE83	2	123	Test effect of lid-melt distance on speed. Full beveled, dogboned lid recessed 2mm to bring melt level close to growth slot. Collect thickness velocity data. Maximum speed 5cm/min. Hard to control seeding.
RE84	1	42	Test effect of slot width on speed and seeding. Slot configuration. as in RE81. Slot widened from 4.6 to 5.5mm. Tendency for web to go polycrystalline near start of seeding. Harder to control seeding.
RE85	Not Productive of Web		Rerun RE84 configuration. Obtained thickness-velocity data but no long web lengths (due to vibration in melt). Speeds to 5cm/min.
RE86	4	280	Test effect of melt height on growth velocity. Reduced melt height with RE84 lid configuration. Better control of seeding but growth speed reduced.
RE87	Run aborted		Test beveled, recessed lid as used in RE83. Argon flow tubes to minimize oxide. Melt wetted lid; run aborted.

GROWTH RUN SUMMARY

RUN	NO. OF CRYSTALS	LENGTHS (cm)	DESCRIPTION/RESULT
RE88	Not productive of Web		Clean up lid wetted in RE87. Attempt rerun of that configuration. Vibration on melt surface prevented stable growth.
RE89	4	498	Retest of configuration attempted in RE87 and 88. Lower initial melt level to improve melt stability. Growth stability good. Width up to 24mm.
RE90	1	68	Grow crystal for resistivity check; doping level $3x10^{17}$ DOPESIL compared to $1x10^{17}$ usually employed.

GROWTH RUN SUMMARY

RUN	NO. OF CRYSTALS	LENGTH (cm)	MAX. WIDTH (mm)	MAX. VELOCITY (cm/min)	DESCRIPTION/RESULT
RE-91	4	407	30.8	2.0	The purpose of this run was to provide crystals with double the usual doping level for characterization studies. RE-1 type lid and top shield configuration.
RE-92	Not Productive of Web				Purpose: web for characterization studies. Very erratic buttoning behavior and temperature drifts. After run, shields were found to be oxidized. Leaks were found in the growth chamber and repairs made.
RE-93	1	95	20.3	1.9	Test of new set of RE-1 Type lids for aftertrimmer experiments. Top shields and side shields. Icing problems all day. Growth initiation difficult. Some leaking may still be occurring.
RE-94	Not Productive of Web				Test of lid configurations for high speed growth. Test full beveled lid, recessed 2mm in order bring lid closer to melt surface. Purpose, higher speed. Starts were consistently poly. Conclude view factor too open, i.e. excessive heat loss at start.
RE-95	1	124	23.4	1.9	Feed system test. Attempt to prevent ice nucleation in growth region by modification of feed configuration RE-1 type lid and top shields with feed holes. Bottom of feed tube 1 cm above shields so that gas flow is decoupled from melt. Feeding caused freezing in crucible feed compartment because of excessive heat loss. Oxide build up on shield feed holes. Not a viable feed configuration.

GROWTH RUN SUMMARY

RUN	NO. OF CRYSTALS	LENGTH (cm)	MAX. WIDTH (mm)	MAX. VELOCITY (cm/min)	DESCRIPTION/RESULT
RE-96	3	198	24.0	2.0	Test behavior consistency of RE-1 configuration in RE facility. There was a tendency to either third or pullout, unstable melt condition.
RE-97	Not Productive of Web				Repeat previous experiment. Erratic buttoning behavior and tendency to third readily; even though melt probe indicated a relatively flat profile.
RE-98	6	197	25.5	5.0	Test thick lid with straight slot, beveled 45°x4mm, 80mm long. Try high speed growth, and wide (>2.5cm) starts. Reached thruput rate of 12.7cm^2/min. Easy to start at 2.5cm or less, difficult to drop dendrites with longer buttons. Melt profile dipped ∿ 1°C over 3cm.
RE-99	5	124	27.9	5.5	Attempt to achieve higher thruput. RE-1 type configuration. Maximum thrupout of 14.8 cm^2/min.
RE-100	1	45	21.3	6.0	Attempt at high speed growth. 6mm thick lid, 80mm dogboned slot, 3mmx45°bevel, RE-1 top shields crystals consistently poly. This slot geometry has highly unfavorable thermal geometry for starting and maintaining high crystal quality.
RE-101	3	152	27.5	3.8	Attempt to flatten melt profile by addition of 2nd partial top shield to RE-1 configuration. Melt probe indicated extra shield not effective, melt dipped in center. Max. thruput only 9.5cm^2/min.
RE-102	2	191	26.7	5.5	Run purpose was to provide data for thermal modeling. Lid with straight 6x80mm slot, 6.2mm thick. RE-1 top shield configuration. Melt profile measured. and thickness velocity data obtained. Reached thruput of 13.4 cm^2/min.

GROWTH RUN SUMMARY

RUN	NO. OF CRYSTALS	LENGTH (cm)	MAX. WIDTH (mm)	MAX. VELOCITY (cm/min)	DESCRIPTION/RESULT
RE-103	2	125	18.1	1.6	Purpose: confirm behavior of straight slot lid of RE-102. Slow melt down and high coil voltage suggested susceptor shields partially oxidized; confirmed after run. Poor growth behavior, choppy dendrites, melt profile dipped.
RE-104	3	149	23.6	1.9	Purpose: increased thruput. RE-1 configuration. Excessive nucleation of floating ice caused growth termination before widths of significance for thruput purposes could be achieved.
RE-105	3	248	33.0	6.0	Purpose: Increased thruput. RE-1 configuration. Icing problems in late afternoon. Reached thruput of 19.8 cm^2/min.
RE-106	Not productive of web				Purpose: Test modified fast lid configuration. Lid shown in Figure 18, Dec. 1978 quarterly with lower top shield modified with 5 mil moly vertical shield along slot, 8 mm separation. Attempt to improve quality of growth initiation with small sacrifice in growth velocity. Rapid oxide buildup on edges of thin shields prevented growth of web.
RE-107	1	226	35.5	4.25	Purpose: Data for thermal modeling and test growth behavior. 9.5 mm dia. dogbone hole added to lid of RE-102, 103, Slot 83x6 mm, RE-1 type top shield: Melt profile still dipped, but less than straight slot. Max. thruput 15.1 cm^2/min.

GROWTH RUN SUMMARY

RUN	NO. OF CRYSTALS	LENGTH (cm)	MAX. WIDTH (mm)	MAX. VELOCITY (cm/min)	DESCRIPTION/RESULT
RE-108	3	385	31.6	5.2	Repeat RE-107 configuration, attempt increased thruput max thruput 16.4 cm^2/min.
RE-109	Not Productive of Web				Argon blow tubes added to RE-106 configuration in effort to control oxide. Not effective. Oxide grew too fast to permit web growth. Growth potential of lid cannot be assessed unless oxide can be controlled in this geometry.
RE-110	2	210	26.7	2.6	Check baseline RE-1 configuration. Some problems with floating ice.
RE-111	4	399	26.5	4.0	Purpose: obtain thermal and thickness velocity data On modified slot. 1 mmx45° bevel added to RE-107 lid. Max. thruput 10.6 cm^2/min.
RE-112	2	288	24.0	5.2	Repeat RE-111, gather additional thermal data Max. thruput 12.5 cm^2/min.
RE-113	2	322	30.4	4.7	Purpose: additional thruput data RE-1 configuration. Max thruput 14.3 cm^2/min.
RE-114	4	436	25.7	5.0	Repeat RE-111 configuration, attempt high speed growth. Max thruput 11.3 cm^2/min. Conclusions: The small bevel on this lid does not interfere with seeding, and yields a small gain in growth velocity. The melt profile is significantly dipped, restricting web width. In future experiments the dogbone holes and bevel will be systematically increased and width and growth velocity related to both measured and theoretical thermal configurations.

GROWTH RUN SUMMARY

RUN	NO. OF CRYSTALS	LENGTH (cm)	MAX. WIDTH (mm)	MAX. VELOCITY (cm/min)	DESCRIPTION/RESULT
RE-115	3	198	16.4	3.1	Test new lid configuration with elongated slot. 114x6 mm straight slot, 3x3 mm bevel, 7.5 mm thick lid. Melt profile flat to 1°C. Velocity-thickness data. Ice problems all day. Oxide spalling from bottom of lid. Underside of lid roughened by sand-blasting in preparation for next run.
RE-116	6	513	29.8	3.8	Repeat RE-115 configuration. After early poly starts and thirding problems, grew well in afternoon.
RE-117	1	46	17.5	-	To obtain baseline data on susceptor and melt profiles. RE-1 type lids, no end shields. Susceptor ends down 16°C. Melt profile dipped about 1° over 4.4 cm.
RE-118	1	60	14.3	3.2	Test new lid and shielding configuration. RE-102, 103 lid has dogbone holes increased from 9.5 mm to 14.3 mm. Perforated susceptor end shields, 75% coverage.
RE-119	No Significant Web Production				Continue to gather temperature data with variations on lid and susceptor shield configurations. Dogbone holes in RE-118 lid opened to 15.9 mm dia. Perforated susceptor end shields. Susceptor profile flat end to end to about 3°C. Melt profile dipped about 2° over 4 cm.

GROWTH RUN SUMMARY

RUN	NO. OF CRYSTALS	LENGTH (cm)	MAX. WIDTH (mm)	MAX. VELOCITY (cm/min)	DESCRIPTION/RESULT
RE-120	2	286	25.1	5.85	Repeat RE-119 configuration without end shields. Some floating ice problems early in day. Melt profile dipped about 1.5° over 4 cm. Max. thruput of 14.7 cm^2/min.
RE-121	No Significant Web Production				Test thermal effects of 114 mm long straight slot with bevel on bottom, with susceptor end shields. Susceptor profile flat to ± 2°, but melt profile badly dipped. Thermal measurements took most of day.
RE-122	3	361	27.5	5.0	Repeat RE-121 configuration to check growth behavior. Some icing. Reached thruput 13.5 cm^2/min.
RE-123	5	635	35.2	5.0	Change in lid configuration. 80x6 mm slot, 12.7 mm dogbone holes, 5x5 mm bevel all around. 9.5 mm thick lid. Lower of two top shields laps lid bevel slightly. (Figure 17, Dec. 1978 Quarterly Report). Argon flow tubes in place. Max. thruput of 14.8 cm^2/min. This configuration will be repeated several times in order to test maximum thruput capabilities.
RE-124	2	348	31.7	5.35	Repeat RE-123 configuration. Reached thruput of 17.0 cm^2/ minute.
RE-125	3	220	23.6	5.35	Repeat RE-123 configuration. Some oxidation of shields early in day deleterious to growth behavior. Ice problems. Max. thruput 12.6 cm^2/min.
RE-126	5	455	29.2	5.7	Repeat RE-125, with system leaks repaired: some ice problems. Thruput rate of 14.3 cm^2/min reached.

GROWTH RUN SUMMARY

RUN	NO. OF CRYSTALS	LENGTH (cm)	MAX. WIDTH (mm)	MAX. VELOCITY (cm/min)	DESCRIPTION/RESULT
RE-127	2	325	30.5	6.15	Repeat RE-123 configuration attempt high thruput rates. Rached thruput rate of 18.75 cm^2/min.
RE-128	5	377	31.1	5.0	Repeat RE-123 configuration. Max. thruput 12.4 cm^2/min.
RE-129	6	470	27.4	5.75	Repeat RE-123 configuration. Ice problems early in day.
RE-130	2	419	34.5	5.75	Repeat RE-123 configuration. Thruput rates of 18.7 and 12.8 cm^2/min.
RE-131	4	584	34.2	6.4	Repeat RE-123 configuration. Thruput rates of 16.7 and 21.9 cm^2/min.
RE-132	2	388	36.65	5.5	Repeat RE0123 configuration. Oxide and ice problems until late in day. 19.96 cm^2/min. max. thruput.
RE-133	2	421	40.6	5.8	Repeat RE0123 configuration with edition of third top shield max thruput 23.55 cm^2/min. Third shield seems to reduce stress build up, allowing increase in web width.
RE-134	2	372	39.9	4.15	Repeat RE-133 configuration. Max thruput 16.6 cm^2/min.
RE-135	3	550	37.2	3.9	Repeat RE-133 configuration. Early starts poly, grew well in afternoon.
RE-136	2	310	29.9	4.5	Repeat RE0133 configuration. Tendency to pull out. Thickness velocity data obtained.
RE-137	3	315	28.5	4.0	Test addition of fourth shield to RE-133 configuration did not grow as well. Floating ice during afternoon.

GROWTH RUN SUMMARY

Preface to J-Furnace Runs

The majority of runs in the J-furnace were devoted to testing a variety of lid and shield configurations to improve width and speed and to reduce stress. Extensive measurements of melt and suceptor temperature profiles were made. Some tests of output capabilities were also carried out.

Several types of ancillary hardware were tested in an effort to reduce stress levels in the web crystals so that greater web width could be achieved. Passive afterheaters proved totally unsatisfactory. A dynamic afterheater system was constructed and tested, beginning with run J-69. The afterheater had deleterious effects on thermal geometry and increased web stress levels. Tests with a cold after trimmer were begun in run J-106. The cold trimmer produced low residual stress but in its present design compromises the growth system.

A series of runs largely dedicated to gathering thermal data, melt profiles, and testing the effects of susceptor shielding modifications were begun with run J-141. This data was used to correlate growth behavior with thermal behavior. Web growth was not a primary objective in these runs and output was generally low.

GROWTH RUN SUMMARY

RUN	NO. OF CRYSTALS	LENGTH (cm)	MAX. WIDTH (mm)	MAX. VELOCITY (cm/min)	DESCRIPTION/RESULT
J-29	Not Productive of Web				Test thick passive afterheaters, 5.2 cm long x 3.8 cm x .63 cm thick, Placed 1cm apart parallel to slot; 1.3 cm radiation gap above lid. Slot has 3x3 mm bevel. Single Top Shield. Oxide Deposition. Afterheater effected thermal geometry, web poly, thirds.
J-30	1	53	9.7	-	Repeat J-29 with second top shield. Oxide problems, growing from afterheater-lid interface.
J-31	3	277	26.6	1.9	To produce material for evaluation. RE-1 configuration.
J-32	6	490	23.8	2.1	Report J-31, slot not polished. Some oxide growth on slot.
J-33	2	54	15.3	2.3	Test new lid with shorter slot, 66.1x6.3 mm, 12.7mm dia. dogbone holes, 6.3mm thick, single top shield. Poor growth, dendrites choppy, pullouts.
J-34	4	504	26.4	2.0	Repeat J-33 configuration with the addition of a second, partial top shield. Second shield improved growth substantially. Will repeat several times to establish reproducibility of growth behavior.
J-35	7	618	22.1	2.3	Repeat J-34. Good growth.
J-36	2	131	23.0	1.9	Repeat J-34, new operator.
J-37	Not Productive of Web				Repeat J-34. Severe problem with oxide growth on slot, falling into melt and causing icing.
J-38	5	520	26.0	2.0	Repeat J-34. Good growth behavior.
J-39	2	154	25.9	1.9	Repeat J-34. Trouble starting growth during afternoon.
J-40	6	468	31.7	1.9	Repeat J-34. Most crystals terminated by pullout after beginning to twist.
J-41	4	331	30.5	1.6	Repeat J-34. 3 cm wide crystal decanted because of twisting.
J-42	4	200	15.4	1.9	Test of thick passive afterheaters. New lid, 80x6mm slot, 12.7 mm dogbone holes, 6.3 mm thick. Two top shields. Oxide collected on lower top shield. Problems with pull out.

GROWTH RUN SUMMARY

RUN	NO. OF CRYSTALS	LENGTH (cm)	MAX. WIDTH (mm)	MAX. VELOCITY (cm/min)	DESCRIPTION/RESULT
J-43	1	41	12.7	1.9	Repeat J-42. Severe oxide collection on lower top shield forced early shutdown.
J-44	2	88	15.2	2.0	J-42 configuration with lower top shield set back on additional 1.5 mm. This eliminated oxide deposition on lower top shield, but oxide collected on lid slot. Melt profile dipped in center.
J-45	2	93	15.1	6.7	Repeat J-44 configuration.
					Conclusion on passive afterheater: Introduces such severe perturbations in thermal geometry that the effect if any, on stress can not be assessed.
J-46	Not Productive of Web				Return to J-34 configuration. Melt unstable, difficult to start.
J-47	4	196	17.1	1.7	Repeat J-46 configuration, New Tank Argon. Problems with oxide and ice.
J-48	1	36	19.2	1.9	Repeat J-46, crucible bottom ground flat. Difficulty dropping dendrites, consistent pull out. Ice during afternoon.
J-49	4	487	28.8	1.6	Repeat J-46, crucible bottom ground flat crystals terminated by decanting because of twisting.
J-50	2	318	24.0	1.8	Repeat J-46 configuration. Growth terminated by twisting and pull out.
J-51	4	207	14.8	2.9	Test new configuration. 6.3 mm thick lid, 80x6 mm slot, 12.7 mm dogbones. 3x3 mm bevel along slot. Single top shield with 2.6 cm wide slot. To test effect on growing web of more exposure to hot lid. This is to partially simulate effect on web of hot after-trimmer. Web very thick (to 400 μm), tendency to third.

GROWTH RUN SUMMARY

RUN	NO. OF CRYSTALS	LENGTH (cm)	MAX. WIDTH (mm)	MAX. VELOCITY (cm/min)	DESCRIPTION/RESULT
J-52	Not Productive of Web				Repeat J-51 with higher coil position. Thick web, pullouts and thirds.
J-53	4	391	27.0	2.0	New lid configuration. Lid 8 mm thick, 80x6 mm slot, 12.7 mm dia. dogbones. 3 top shields, lower two .5mm thick bent to partially lap slot bevel. Upper shield flat 1.5 mm thick. Oxide deposition caused some growth difficulties, but growth behavior is encouraging.
J-54	2	224	23.9	2.0	Repeat J-53, to further evaluate growth characteristics, oxide.
J-55	3	406	29.9	2.0	Repeat J-53. Growth behavior good, but problems with oxide on slot region all day.
J-56	2	99	18.0	1.9	Repeat J-53, except one of formed top shields removed. Air got into system when trying to remove oxide. Run aborted.
J-57	3	368	27.9	2.0	Repeat J-53. Oxide problems. This type of configuration appears promising if oxide deposition on top shields and slot can be eliminated.
J-58	6	381	29.8	1.9	RE-1 configuration, to produce web material.
J-59	Not Productive of Web				Test behavior with no Top shields; to partially simulate effect of hot aftertrimmer on web. Could not grow;ice formed near ends of slot. Dendrite probe indicated center of melt profile hot by at least 2°C. Susceptor profile also hot in center.
J-60	Not Productive, run aborted during melt down				Try J-59 configuration with susceptor side shields removed coil water boiled when attempting melt down.
J-61	Not Productive of web.				Same as J-59, except single top shield open over entire crucible area. Could not grow. Oxide deposition on slot a constant problem. Conclusion: configurations with largely unshielded lids cause substantial problems with no redeeming virtues.

GROWTH RUN SUMMARY

RUN	NO. OF CRYSTALS	LENGTH (cm)	MAX. WIDTH (mm)	MAX. VELOCITY (cm/min)	DESCRIPTION/RESULT
J-62	2	105	20.1	2.1	Test 80x6.1 mm dogboned slot, two identical top shields with 4.7 mm set back. Difficult to initiate growth, pull out.
J-63	2	105	19.6	2.1	Alter J-62 configuration by increasing set back of upper top shield. Hard to grow,choppy dendrites, pull out.
J-64	4	829	27.3	1.9	New lid. Straight slot (no dogbones) 80x4 mm 5x5mm bevel all around, 8 mm thick. Two top shields with 1 mm set backs. Webs terminated because of twisting and going poly. Otherwise, growth easy and stable.
J-65	5	474	27.0	1.9	
J-66	2	221	18.3	1.9	Repeat J-64 configuration. Similar growth behavior.
J-67	3	159	18.1	1.9	Repeat J-64 configuration. Ice problems all afternoon.
J-68	3	209	17.8	2.1	Repeat J-74 configuration. Ice problems all day.
J-69	2	103	16.3	2.0	Repeat J-64 configuration. Ice nucleated all day. Source of ice nucleation not clear. Problem seems to have gotten worse with each run of J-64 lid.
J-70	3	121	18.0	2.1	First test of dynamic afterheaters, bottom of heater 23 mm above lid.With no input power, heaters 770°C bottom, 550°C top, 100% power, lower only,930°C bottom, 570°C top. RE-1 type lid configuration.
J-71	4	137	20.8	2.1	Repeat J-69 configuration. Consistent problems with floating ice.
J-72	Not Productive of Web				Repeat J-69 configuration. Ice problems. Apparently, oxide is flaking from afterheater, falling into melt.
J-73	6	224	26.8	2.0	Test J-64 lid configuration with afterheater. Excessive oxide deposition and ice nucleation prevented growth.
J-74	5	234	32.1	2.0	Test crucible from new supplier. RE-1 configuration, no afterheater. Crystals terminated by pullout.
J-75	4	321	19.0	2.1	Repeat J-64 configuration. Crystals twist and go poly.
					Change configuration by addition of 12.7 mm dogbone holes to J-64 lid geometry, 2 full top shields. Crystals tended to go poly.

GROWTH RUN SUMMARY

RUN	NO. OF CRYSTALS	LENGTH (cm)	MAX. WIDTH (mm)	MAX. VELOCITY (cm/min)	DESCRIPTION/RESULT
J-76	3	198	18.0	2.1	Test J-75 configuration with afterheaters 25 mm above lid. Vary afterheater temperatures. Crystal went poly. Similar to J-75 growth behavior.

C3

GROWTH RUN SUMMARY

RUN	NO. OF CRYSTALS	LENGTH (cm)	MAX. WIDTH (mm)	MAX. VELOCITY (cm/mm)	DESCRIPTION/RESULT
J77	2	70	18.1	2.1	Afterheater Test. Full beveled lid, 80x6mm slot, dogbones, 5x5mm bevel. Continue test of afterheater. Vertical position: 1.5cm above lid. Lineage structure limited widening. Oxide collection on lid shields.
J78	3	292	25.5	2.2	Test effect of shield on oxide accumulation for lid used in J77. Lower shield bent upward. Widening fair but still some oxide accumulation.
J79	2	137	21.3	1.9	Retest of shield configuration in J78. Similar result. Conclude no improvement in oxide control, web speed or width with this shield arrangement.
J80	5	538	30	2.0	Test behavior of new RE-1 lid. for later experiments with afterheater. Baseline behavior verified.
J81	2	148	16.1	2.3	Test shield arrangement to minimize oxide accumulation on long beveled, growth slot. Lower top shield bent up along slot. New top shield. Oxide well controlled but difficult to seed without third dendrities or pull out. Conclude not a useful configuration.
J82	3	123	22	2.0	Afterheater test with RE-1 lid. Evaluate effect of heater vertical position on growth: 2.5cm above lid. Dendrite probe revealed slightly cupped profile in liquid limited widening.

GROWTH RUN SUMMARY

RUN	NO. OF CRYSTALS	LENGTH (cm)	MAX. WIDTH (mm)	MAX. VELOCITY (cm/min)	DESCRIPTION/RESULT
J83	2	114	19.6	2.0	Test effect of 3rd top shield to flatten melt temperature profile with long, beveled lid. Profile flattened but not sufficiently to increase width. Adjust shielding.
J84	4	385	34.7	2.0	Retested 3 shield configuration used in J83. Produced web to 34.7 mm.
J85	2	274	22.9	1.9	Afterheater test. RE-1 baseline lid. Heater 1.5cm above. Remove outside shields on afterheater to raise available ΔT. Very little improvement in ΔT or widening of web.
J86	1	41	14.4	1.9	Afterheater test. RE-1 lid. Lower heater temperature raised (increase ΔT by $\sim$ 100°C) Web did not widen. Run terminated by oxide collection on afterheater.
J87	1	42	14.5	1.9	Ran RE-1 lid without afterheater to check if melt profile was flat. Conclude profile flat enough to get wide web. Failure of afterheater not due to effect in RE-1 lid. Icing terminated run.
J88	5	463	24.0	2.7	Test of dished lid (variable bevel angle across slot length) 8mm thick. 76x5mm slot, 12.7mm dogbones. Center of lid dished to 4mm thickness. Evaluate effect of lid on web widening. Width up to 24mm. Dendrite probe gave flat profile. Webs deformed due to stress.
J89	1	84	17.4	2.0	Test of dished lid (J88) with 2 top shields instead of three. Attempt to reduce web stress. Dendrite profile showed asymmetric temperature profile. Could not widen.

GROWTH RUN SUMMARY

RUN	NO. OF CRYSTALS	LENGTH (cm)	MAX. WIDTH (mm)	MAX. VELOCITY (cm/min)	DESCRIPTION/RESULT
J90	4	423	19.4	5.4	Test shorter lid slot for width control in feeding experiments. Collect velocity-thickness data. Dendrite probe reveals dished profile. Width kept below 20mm. Some oxide accumulation.
J91	3	298	23.5	1.9	Retest of dished lid. Use narrower slots in top shield to reduce stress in web and test widening behavior. Web still deformed.
J92	1	48	13.9	1.7	Retest short slot of Run J90. Argon flow added to reduce oxide. Unstable growth. Tended to produce third dendrites on seeding.
J93	3	444	31.8	2.0	80x6mm, beveled, dogbone lid. Two top shields, bottom large overhang. Argon flow along slot. Test effect of argon flow rate (30 to 100 cm^3/min) on oxide accumulation. Higher flow rate gave better results.
J94	4	309	15.5	2.0	Retest of short slot for feed runs. Difficult to control growth: pullout or third dendrites.
J95	4	295	24.6	5.5	Retest of beveled lid for high speed growth. Less overhang on lower top shield to reduce oxide. No oxide problems. Combined output rate over 12 cm^2/min.
		Output >	12cm^2/min.		

GROWTH RUN SUMMARY

RUN	NO. OF CRYSTALS	LENGTH (cm)	MAX. WIDTH (mm)	MAX. VELOCITY (cm/min)	DESCRIPTION/RESULT
J96	5	329	28.3	2.7	Test new lid bevel. Several crystals run to get velocity-thickness characteristics. Lid employs directed argon flow to minimize oxide accumulation in overhanging shield. Data collected. No oxide accumulation.
J97	2	177	21.5	> 5 cm/min	Use same slot-shield configuration as previous run. Raise melt level to improve speed characteristics. Take velocity-thickness data to characterize thermal geometry. Crystals consistent with increased speed attained.
J98	3	156	16.3	2.7	(Runs 98 to 100 were tests of a shorter slot length designed to keep the width smaller for subsequent feed experiments in RE facility). Test 3.8 cm long slot for width control in feeding-target width 2.5cm. Crystals did not widen well enough. Dendrite probe revealed steep dip in melt temperature profile.
J99	2	86	14.2	2.3	Test of 3.8 cm slot with lower melt level to flatten melt profile. Melt temperature profile showed some improvement but still not enough to get to desired constant width. Some temperature fluctuations during growth run.

GROWTH RUN SUMMARY

RUN	NO. OF CRYSTALS	LENGTH (cm)	MAX. WIDTH (mm)	MAX. VELOCITY (cm/min)	DESCRIPTION/RESULT
J100	No Significant Web Production.				Test of 3.8 cm slot. Argon flow to top shields reduced to minimize any temperature fluctuations. Temp profile remained dipped. Conclude this lid design ineffective for width control in feeding experiments.
J101	2	138	23 (> 12 cm^2/min output)	7	Test new lid bevel with argon flow under top shields for increased growth speed. Achieved 7 cm/min maximum velocity. Some instability in seeding control, repeatability
J102	1	83	18.5	2.1	Retest of lid used in 101 with slightly lower melt level to improve seeding. Run relatively unproductive. Vibration in melt (cause undetermined) and some temperature control problems.
J103	2	182	21	2.0	Replace thermocouple in system. Reran configuration of J102 with larger shield overhang (cooler shields improve heat transfe Tests restricted by free floating ice in melt
J104	2	241	27.6	2.0	Retest of larger shield overhang as per J102 and J103. Width improved. Melt pulled away from crucible before speed test complet meltlevel too low.
J105	2	170	18.6	2.2	Raised melt level to more stable regime. Retest shields used in J102-J104. Some oxide collection and icing. Conclude shield lid configuration improves speed and output rate but results are not sufficiently reproducible to achieve goals.

GROWTH RUN SUMMARY

RUN	NO OF CRYSTALS	LENGTH (cm)	MAX. WIDTH (mm)	MAX. VELOCITY (cm/min)	DESCRIPTION/RESULT
J106	3	477	27.7	2.1	First test of cold after trimmer designed to reduce elastic bending of web. Test conducted with RE-1 lid, a baseline configuration. Initial trimmer position 2.5 cm above lid. Widest crystal decanted spontaneously. No bending.
J107	2	442	19	1.9	Second test of cold after trimmer. Position 2.0 cm above lid. Oxide collection on trimmer later in day reduced run effectivenes:

GROWTH RUN SUMMARY

RUN	NO. OF CRYSTALS	LENGTH (cm)	MAX. WIDTH (mm)	MAX. VELOCITY (cm/min)	DESCRIPTION/RESULT
J108	3	190	23	2.0	Test repeat J106 Cold aftertrimmer (angled plates,45°) Evaluate any effects of aftertrimmer melt temperature profile with RE-1 lid. Mounting of trimmer modified to improve vision during seeding. Melt probe indicated temperature dipped in liquid, asymmetric also.
J109	1	78	23.8	1.7	Test cold aftertrimmer. Evaluate effect of trimmer vertical position on melt profile. Melt dipped with trimmer at extreme lower and higher position. Also asymmetric.
J110	2	91	17.4	2.0	Test cold aftertrimmer. Evaluate effect of coil position on melt profile with afterheater 1.6cm. Temperature profile dipped and asymmetric in low position. Slightly dipped in high position.
J111	2	86	15.1	2.1	Evaluate melt profile for RE-1 lid with cold after-trimmer removed. Melt profile flat. Melt vibration limited growth.
J112	7	716	26.3	2.1	Retest melt profile and growth with RE-1 lid, aftertrimmer removed. Flat profile. Concluded angled plates on aftertrimmer interact with induction field and perturb melt temperature profile.
J113	Not productive of web				Cold aftertrimmer modified to vertical parallel plate configuration to reduce inductive effects. Probe melt as a function of coil height. Profile flatter but asymmetric atcoil positions tested. Conclude trimmer should be inserted at end of furnace opposite coil leads.

GROWTH RUN SUMMARY

RUN	NO. OF CRYSTALS	LENGTH (cm)	MAX. WIDTH (mm)	MAX. VELOCITY (cm/min)	DESCRIPTION/RESULT
J114	3	125	19.8	2.1	Cold aftertrimmer test. Trimmer inserted at end of furnace opposite cool to reduce inductive effects further. Melt profile nearly flat and symmetric.
J115	3	464	23.7	1.9	Cold aftertrimmer test. Evaluate position of trimmer above lid on melt profile and growth. Trimmer 2.1cm above RE-1 lid. Crystals under better than previous run. Growth ended by pullout.
J116	5	433	26.4	2.0	Cold aftertrimmer test. Trimmer set 1.0 cm above RE-1 lid. Width improved. Lineage in widest crystal due to bad start.
J117	3	247	23.4	1.9	Cold aftertrimmer test. Retest conditions of run J116 trimmer 1.0 cm above lid. Run dendrite probe at low and medium coil positions. Slight asymmetry at medium position; slight dip no asymmetry at low position. Conclude slight dip still limiting widening.
J118	2	276	24.1	2.0	Cold aftertrimmer test. Run at higher coil position to reduce thermal dip.
J119	Abort run				Cold aftertrimmer test. Continue evaluation of aftertrimmer vertical position on melt profile and web growth. Melt wet lid.
J120	5	549	31.3	2.0	Cold aftertrimmer test with new RE-1 lid. Continue evaluation of trimmer vertical position. Trimmer 1.6cm to 2.1cm above lid.

GROWTH RUN SUMMARY

RUN	NO. OF CRYSTALS	LENGTH (cm)	MAX. WIDTH (mm)	MAX. VELOCITY (cm/min)	DESCRIPTION/RESULT
J-121	3	194	16.7	1.9	Test of cold aftertrimmer. RE-1 type lid and shield configuration. Trimmer set 1.3cm above lid. Thirding, pull out and icing problems again consistent with dipped melt temperature profile.
J-122	2	242	24.9	1.9	Test of cold after trimmer. RE-1 type lid and shield configuration. Trimmer set 1.8cm above lid. There were some icing problems and a drifting thermal profile. Axial thermocouple exhibited erratic behavior. Check out thermocouple and electronics.
J-123	2	30	30.8	5.1	Test of thruput capabilities of RE-1 type lid and shield configuration. Cold aftertrimmer 1.5cm above lid. Thruput rate of 11.4cm^2/min reached.
J-124	Not Productive of Web				Repeat of J-123 configuration. This run was not productive because of very erratic seeding behavior, which was not consistent with the results of a dendrite profile of the melt surface. Button symmetry was only obtained when ice formed on the right.
J-125	1	32	25	5.9	Another test of thruput capabilities of RE-1 configuration with cold aftertrimmer. Unsuccessful attempts were made to start with long buttons (3 to 4 cm). Growth speed up to 5.9 cm/min was obtained. A thruput of 14.7cm^2/min was attained in short lengths. It was noted that some defects had developed in the susceptor

GROWTH RUN SUMMARY

RUN	NO. OF CRYSTALS	LENGTH (cm)	MAX. WIDTH (mm)	MAX. VELOCITY (cm/min)	DESCRIPTION/RESULT
J-126	2	132	19.0	8.2	Test of cold aftertrimmer with RE-1 lid configuration, for thruput capabilities. Erratic starting behavior was a problem. A growth velocity of 8.2cm/min was reached on one crystal.
J-127	Not productive of web				Repeat previous run configuration. Free-floating ice nucleation was a problem all day, even though lid and shields remained free of oxide.
J-128	1	50	15.9	2.0	There has been a problem of reproducibility and erratic behavior in the above series of runs with the cold after trimmer. In order to determine whether this is due only to the trimmer configuration or to other cause, a series of runs with the RE-1 type configuration, but without the after trimmer was begun. This run was to test growth behavior as a function of coil height. Oxide deposition on the slot and falling into the melt prevented significant crystal growth.
J-129	3	78	24.2	5.1	Repeat of above run. Test thruput capabilities. Melt jumpy, but no oxide or icing. Attempts to start wide buttons not successful due to erratic drift in thermal symmetry. Dendrite probe of melt surface gave dip of about 1°C over 4cm. Reached thruput of 12.3cm^2/min.

GROWTH RUN SUMMARY

RUN	NO. OF CRYSTALS	LENGTH (cm)	MAX. WIDTH (mm)	MAX. VELOCITY (cm/min)	DESCRIPTION/RESULT
J-130	2	72	22.9	6.8	The susceptor was replaced in effort to reduce erratic run to run growth behavior. RE-1 lid configuration. Buttoning behavior continued to be variable, and there was some problem with ice nucleation. 12cm of crystal were grown at 6.8cm/min. before ice caused pull out.
J-131	5	309	29.3	5.5	Suspect variable thermal transport between susceptor and crucible. Therefore to improve growth behavior reproducibility the ground surfaces of the crucible were fire polished in hopes of improving uniformity of heat transfer. RE-1 type lids. Behavior improved significantly thruput rates of 12.6, 12.7, 13.7, and 14.3 cm^2/min were reached on four crystals. Dendrite probe-indicated flat melt temp. profile.
J-132	2	186	21.7	1.9	Repeat previous run. Crucible fit not quite uniform on bottom. Some icing. Melt profile dipped. Conclusion: Both bottom surface preparation and flatness are important to uniform and reproducible heat transfer.

GROWTH RUN SUMMARY

RUN	NO. OF CRYSTALS	LENGTH (cm)	MAX. WIDTH (mm)	MAX. VELOCITY (cm/min)	DESCRIPTION/RESULT
J-133	2	313	32.3	5.4	Run purpose: increased thruput. RE-1 type configuration with fire polished crucible. Reached thruput of 15.7 cm^2/min.
J-134	3	386	32.4	1.6	Test of cold after trimmer. RE-1 type lid configuration Trimmer 1.1 cm above lid. Generally easy to grow. Crystal termination by pullout. Dendrite probe indicated melt dipped 1.7°C over 4 cm, while susceptor probe indicated ends of susceptor 14°C lower than center.
J-135	1	86	24.0	5.1	Purpose: measure melt temperature profile at different cold after trimmer heights. Melt dipped 1.4°C over 4 cm with trimmer 1.1 cm above lid; 1.1°C at 2.1 cm above lid. Appears that some fine tuning of shielding needed to minimize temperature dip. Maximum thruput 12.2 cm^2/min.
J-136	3	97	17.6	1.6	Purpose: test effect of additional susceptor side shielding on melt surface temperature profile in presence of cold after trimmer. Additional side shields 5 cm wide added at center of susceptor. Dendrite probe gave less than 1° dip over 4 cm. Growth terminated by oxide nucleation at one point on lid slot, then falling into melt, causing ice nucleation.
J-137	1	25	15.2	2	Repeat J-136. Same oxide and icing problems as J-136. Subsequently, a very small crack was discovered on lid, which acted as nucleation site. Will be corrected for future runs. However, during this run there were additional icing problems independent of oxide.
J-138	No significant crystal production due to icing.				Repeat J-137 in attempt to pin down causes of icing. Dendrite probe indicated ends colder, not consistent with J-136 probe results.

GROWTH RUN SUMMARY

RUN	NO. OF CRYSTALS	LENGTH (cm)	MAX. WIDTH (mm)	MAX. VELOCITY (cm/min)	DESCRIPTION/RESULT
J-139	Not productive of web due to repeated icing.				Repeat J-138 in effort to resolve inconsistencies. Melt probe erratic. Conclude 5 cm extra side shields not effective in improving growth behavior.
J-140	3	243	27.5	2.0	Purpose: recheck base line RE-1 configuration with respect to growth behavior. Conclusion: Though melt was somewhat "jumpy" and unstable, icing was not a problem. Suspect that added central shielding causes cold regions in crucible corners not accessible to the dendrites used for thermal probing.
					The purpose of the following series of runs is to flatten the temperature profile in the susceptor by modifications in the susceptor shielding. Subsequently, lid slot modifications will be made to improve melt profile. This will facilitate use of the after trimmer for the growth of wider web crystals. Web production is secondary to the thermal measurements.
J-141	1	95	20.3	2.0	RE-1 lid configuration with the addition of susceptor end shields slotted to give 50% shield coverage. Susceptor probe measurements indicate susceptor still cold at ends relative to center, but not symmetrical because of offset coil position. Melt profile dipped.
J-142	1	80	16.0	2.0	Repeat J-141, adjusting coil until thermal symmetry is reached. Susceptor ends cold by about 4°C, center dipped about 2°C. Melt profile dipped.

GROWTH RUN SUMMARY

RUN	NO. OF CRYSTALS	LENGTH (cm)	MAX. WIDTH (mm)	MAX. VELOCITY (cm/min)	DESCRIPTION/RESULT
J-143	No significant web growth.				Test shielding modification. Ends of side shields perforated to increase losses in effort to eliminate central dip in susceptor profile noted in previous run. Same end shields. Measurements showed that this modification overcompensated, increasing end drop and producing ∿ 4°C hump in center.

GROWTH RUN SUMMARY

RUN	NO. OF CRYSTALS	LENGTH (cm)	MAX. WIDTH (mm)	MAX. VELOCITY (cm/min)	DESCRIPTION/RESULT
J-144	Not Productive of Web Crystals				Test susceptor shielding modification. End shield coverage increased to 70%. RE-1 type lid configuration susceptor profile fairly flat, slightly asymmetric. Melt profile dipped and very asymmetric. Very choppy dendrites.
J-145	1	56	12.4	2.0	Test susceptor shielding modification. Perforated side shields replaced by solid ones. Susceptor ends hot by about 5°C. Melt profile very dipped and asymmetric.
J-146	1	110	18.2	1.9	Test susceptor shielding modification. 7 4mm dia. holes each end of side shields. 114x6 mm straight slot, 3 mm bevel. Susceptor ends cold by 5°C. Melt flat to within about 1°. End shields deformed; suspect reproducibility of shielding not good enough.
J-147	1	83	18.9	4.0	Test new end shields, perforated to provide 75% coverage. 114 mm straight slot. Shields are much stronger mechanically than slotted shields used previously susceptor profile flat to + 0.7°C. Melt dipped and asymmetric.
J-148	4	223	20.4	2.0	Repeat J-147 with addition of cold aftertrimmer 1.1 cm above lid. 114 mm straight slot. Susceptor profile flat. Melt flat to about 1°C. Considerable oxide deposition on aftertrimmer.
J-149	2	207	16.9	-	Repeat J-148. Problems with oxide on aftertrimmer and ice formation. Oxide accumulation is much greater than observed in past with RE-1 lids.

GROWTH RUN SUMMARY

RUN	NO. OF CRYSTALS	LENGTH (cm)	MAX. WIDTH (mm)	MAX. VELOCITY (cm/min)	DESCRIPTION/RESULT
J-150	2	138	15.7	-	Test lid with enlarged dogbone, with aftertrimmer. Slot 83x6 mm, 15.9 mm dia. dogbone holes. Icing and oxide problems. Melt profile flat.
J-151	1	20	22.0	7.3	Test J-150 configuration without cold aftertrimmer in order to determine if trimmer is source of problems. Icing problems all day. Floating ice from left, while buttons long to right. Dendrite probe indicates melt cold left, consistent with ice location, but inconsistent with buttoning behavior. Suggests non-uniform heat transfer in crucible.
J-152	3	104	11.6	6.75	Cold aftertrimmer modified so that argon blows outside rather than between vertical cold plates. Floating ice, choppy dendrites. Melt probe indicated melt surface slightly crowned in center. Unstable melt and starting behavior.
J-153	3	190	21.4	-	Repeat J-152 configuration. Choppy dendrites, susceptible to pullout.
J-154	2	167	24.5	1.6	Repeat J-152 configuration, with the addition of end shields on the susceptor in effort to improve melt stability and reduce thermal convection. End shields are perforated to give 76% shield area coverage. Melt profile dipped about 1.5°C over 4.5 cm.
J-155	2	102	17.2	1.9	Repeat J-154 with susceptor end shield coverage reduced to 60%. Still difficulty with pull out.

GROWTH RUN SUMMARY

RUN	NO. OF CRYSTALS	LENGTH (cm)	MAX. WIDTH (mm)	MAX. VELOCITY (cm/min)	DESCRIPTION/RESULT
J-156	3	286	19.6	2.0	Modify J-155 configuration by removing 0.8 cm from bottom of end shields. Growth behavior improved.
J-157	4	260	25.7	1.7	Modify J-156 configurations by removing an additional 0.8 cm from bottom of end shields. Choppy dendrites, pullouts.
J-158	2	120	14.6	-	An additional 0.8 cm was removed from the bottom of the end shields as modification of J-157 configuration difficult to initiate growth.
J-159	1	86	15.5	-	Repeat J-158, with varying coil heights. Difficult to initiate growth choppy dendrites.
J-160	2	206	18.5	2.0	Repeat J-159 with cold aftertrimmer raised to 1.3 cm above lid. Hard to grow, choppy dendrites, pullouts.
J-161	No Significant Web Production				Repeat J-160, higher coil position. Dendrites very choppy, pull out. Dendrite probe indicated melt profile flat to 0.5°C.
J-162	1	62	17.5		Same lid and shielding arrangement as J-161, except cold aftertrimmer removed. Test whether choppy dendrite caused by chimney effect of trimmer. Dendrites still choppy, but not as bad as with trimmer. However melt profile now dipped nearly 2°C. Conclude that trimmer in its present configurations interferes excessively with ability to grow.

GROWTH RUN SUMMARY

PREFACE TO W-FURNACE RUNS

In large measure the W-furnace experiments fall into three catagories (1) experiments to develop run to run reproducibility (2) design and test of systems to minimize oxide deposition during growth (thus facilitating long cycle growth) and (3) evaluation of melt replenishment concepts. Subheadins within the summaries indicate the various stages of the work.

GROWTH RUN SUMMARY

Runs 21 through 39 were used to determine the effects of melt height and lid shield configurations on growth conditions such as widening rates, total length, maximum width, stress levels, etc. Some runs were not productive as new, inexperienced operators were trained and also some malfunctions in the furnace controls occurred.

RUN	MAX. WIDTH (mm)	TOTAL LENGTH (cm)	DESCRIPTION/RESULT
W-21	16.4	88.9	195.3 gm Si, $1x10^{17}$ DOPESIL Lid 3U, Shield 4.
W-22	26 0	211	Purpose: study effect of melt level on stresses 120.2 gm Si, $1x10^{17}$ DOPESIL LID 3U, Shield 4.
W-23	16.2 18.6	235	Purpose: evaluate melt level 121.4 gm Si, $1x10^{17}$ DOPESIL Lid 3U, Shield 4.
W-24	18.1	69	Lid 3U, Shield 4 Low argon flow rate 120.3 gm Si; $1X10^{17}$ DOPESIL.
W-25	Not Productive of Web		Repeat W-23.
W-26		350	Repeat W-23 120.3 gm Si; $1x10^{17}$ DOPESIL.
W-27	30.7	207	Repeat W-23 121.0 gm Si; $1x10^{17}$ BORON
W-28	Not Productive of Web		New Lid 8U Shield 4.
W-29	Not Productive of Web		Repeat W-23.
W-30	22.4	104	Lid 8U, Shield 4 120 gm Si; $1x10^{17}$ DOPESIL.
W-31	Not Productive of Web		Lid 8U, Shield 1 120 gm Si; $1x10^{17}$ DOPESIL Lower Coil.
W-32	Not Productive of Web		Lid 8U, Shield 1 120.8 gm Si; $1x10^{17}$ DOPESIL.
W-33	Not Productive of Web		Lid 8U, Shield 1 Lower coil position 119.8 gm Si; $1x10^{17}$ DOPESIL.
W-34		230	Repeat W-33 119.6 gm Si; $1x10^{17}$ DOPESIL
W-35	Not Productive of Web		Lid 8U, Shield 1 Lower Coil
W-36	Not Productive of Web		Lid 8U, Shield 1 space between lid and susceptor; raised coil 121.8 gm si: $1x10^{17}$ DOPESIL.

GROWTH RUN SUMMARY

RUN	MAX. WIDTH (mm)	TOTAL LENGTH (cm)	DESCRIPTION/RESULT
W-37	20.2	181	Repeat W-36 122.8 gm Si; $1x10^{17}$ DOPESIL.
W-38	Not Productive of Web		Repeat Lids of W-36 closed holes in susceptor 119 gm si: $1x10^{17}$ DOPESIL.
W-39	Not Productive of Web		Lid 8U Shield 2 Shield 1 119.2 gm Si; $1x10^{17}$ DOPESIL.
	Runs 40 through 72 were designed to determine effects of lid configuration melt height and coil position on various growth parameters such as stress levels, width, speed, widening rates, etc. Experiments in width control were also performed.		
W-40	16.4	106	Evaluate Lid 8U with shields-S (1+2) 119.2 gm Si; $1x10^{17}$ DOPESIL.
W-41	21.4	368	Evaluate Lid. 8U and shields S(1+2) at lower coiled height. 119.8 gm Si; $1x10^{17}$ DOPESIL.
W-42	21.5	245	Repeat Run W-41
W-43	19.8	280	Repeat Run W-41 123 gm Si; $1x10^{17}$ DOPESIL.
W-44	20.3	420	Repeat Run W-41 119.1 gm Si; $1x10^{17}$ DOPESIL.
W-45	21.8	520	Evaluate short, unbeveled slot lid 14S, shield S (1+3) 121.8 gm Si; $1x10^{17}$ DOPESIL.
W-46	Not Productive of Web		Repeat Run W45 120.6 gm Si; $1x10^{17}$ DOPESIL.
W-47	20.0	500	Repeat Run W45. Web Split when unreeled 118.9 gm Si; $1x10^{17}$ DOPESIL.
W-48	15.8	62	Repeat W-45 120.6 gm Si; $1x10^{17}$ DOPESIL.
W-49	16.4	237	Repeat W-45 120.7 gm Si; $1x10^{17}$ DOPESIL.
W-50	14.9	194	Evaluate Lid 14T with shields S (1+3) 121.8 gm Si; $1x10^{17}$ DOPESIL.
W-51	22.1	237	Repeat W-50 122.6 gm Si; $1x10^{17}$ DOPESIL.
W-52	22.0	389	Repeat W-50 119.7 gm Si; $1x10^{17}$ DOPESIL.

GROWTH RUN SUMMARY

RUN	MAX. WIDTH (mm)	TOTAL LENGTH (cm)	DESCRIPTION/RESULT
W-53	Not Productive of Web		Evaluate lid 3U with S (1 and 3), oxide problems on lids.
W-54	Not Productive of Web		Repeat W-53, had oxide problems.
W-55	22.6	305	Repeat W-50 126.7 gm Si; $1x10^{17}$ DOPESIL.
W-56	22.5	450	Repeat W-50 124.2 gm Si; $1x10^{17}$ DOPESIL.
W-57	18.0	230	Repeat W-50 127.1 gm Si; $1x10^{17}$ DOPESIL.
W-58	22.0	217	Repeat W-50 127.1 gm Si; $1x10^{17}$ DOPESIL.
W-59	14.0	187	Repeat W-50 127.1 gm Si; $1x10^{17}$ DOPESIL.
W-60	21.9	210	Repeat W-50 131.1 gm Si; $1x10^{17}$ DOPESIL.
W-61	18.6	340	Repeat W-50 127.1 gm Si; $1x10^{17}$ DOPESIL.
W-62	Not Productive of Web		Lid 14+ Shields 1 and 3.
W-63	Not Productive of Web		Lid 14+ Shields 1 and 3.
W-64	21.9	583	Lid 14+ Shields 1 and 3 125.1 gm Si; $1x10^{17}$ DOPESIL.
W-65	Not Productive of Web		Repeat W-64, had problems with oxide in melt.
W-66	21.4	270	Lid 14U Shields 1 and 3 121.5 gm Si; $1x10^{17}$ DOPESIL.
W-67	22.0	640	Lid 14U Shields 1 and 3 118.1 gm Si; $1x10^{17}$ DOPESIL.
W-68	16.8	110	Repeat W-67, determine effects of bigger bevel on stress levels.
W-69	11.6	85	Repeat W-67 using a lower coil position.
W-70	Not Productive of Web		Repeat W-67, temperature control problems resulted in early shut down.
W-71	22.0	720	Lid 14T + S (1+3), using a smaller bevel to determine effects on stress levels.
W-72	16.2	200	Repeat W-71 with coil moved toward rear of susceptor.

GROWTH RUN SUMMARY

Runs W-73 through 97 were used to experiment with gas flow redirection and oxide management. Difficulties with temperature control and oxide management resulted in some non-productive runs.

RUN	MAX. WIDTH (mm)	TOTAL LENGTH (cm)	DESCRIPTION/RESULT
W-73			Lid-4mm slot, beveled; shields 1&3.
W-74	16.7	221	Lid-4mm slot, beveled; shields 1&3.
W-75	18.2	279	Lid-4mm slot, beveled; shields 1&3.
W-76	21.4	139	Lid 8U, shields 1&5.
W-77	Not Productive of Web		Lid 8U, shields 1&2.
W-78	19.7	298	Lid 8U, shields 1&2.
W-79	Not Productive of Web		Lid 8U, shields 1&4.
W-80	Not Productive of Web		Lid 8U, shields 1&4.
W-81	Not Productive of Web		Lid 8U with chimney, shields 1&2.
W-82	Not Productive of Web		Lid 8U with chimney, shields 1&2.
W-83	Not Productive of Web		Lid 8U with chimney, shields 1&2.
W-84	Not Productive of Web		Lid 8U with chimney, shields 1&2.
W-85	17.2	82	Lid 8U with chimney, shields 1&2.
W-86	13.1	114	Lid 8U with chimney, closed.
W-87	15.1	115	Lid 8U with chimney, shields 1&6.
W-88	25.8	330	Lid 8U; 1/4" ring; LID 8U with chimney.
W-89	Not Productive of Web		Lid 8U; 1/4" ring; cut back chimney lid.
W-90	22.7	400	Lid 8U; 1/4" ring; shield 6; cut back chimney lid.
W-91	22.0	320	As in W-90.
W-92	16.0	92	Shield 5, 1/4" ring; shield 6, cut back chimney.
W-93	21.2	270	As in W-90, except 1/8" ring.
W-94	Not Productive of Web		As in W-93.
W-95	24.7	154	Lid 8U, 1/8" ring; shields 1&2.
W-96	22.4	353	As in W-95
W-97	Not Productive of Web		As in W-95.

GROWTH RUN SUMMARY

RUN	MAX. WIDTH (mm)	TOTAL LENGTH (cm)	DESCRIPTION/RESULT
W98	23.3	390	Test argon flooding system to keep shields clean. System clean throughout run. Width of web maintained constant to ± 1 mm over 220 cm length.
W99	25	323	Test argon flooding system. Examine flow rate effects. System clean throughout run. Good width control.
W100	16.4	120	Test argon flooding system and controls. Severe vibration in melt precluded good growth.
W101	28.2	381	Test of argon flooding system with inner quartz baffle removed to monitor effects on total system flow (observation of asymmetric oxide deposition on webs after last runs) Result: no effect on oxide on web but produced oxide accumulation on shields. Higher coil position needed for growth but stability maintained.
W102	20	200	Test argon flooding system. Quartz baffle replaced; shields remain clean. Conclude baffle required for system cleanliness.
W103	24.8	374	Argon flooding system. Longer slot in lid used to increase target width for constant growth. Oxide accumulated at start of run. It was removed and shields stayed clean.
W104	18.5	309	Argon flooding system. Attempt to introduce width control with longer lid slot. Width controlled for one meter. Shields remained clean.
W105	22.2	192	Argon flooding system. Returned to shorter slot to obtain more experience with procedures to control width. Width control more difficult with longer slot.
W106	23.7	220	Argon flooding test. Increase gap in flow cavity between shields from 1/8" to 1/4" to reduce flow velocity. Oxide collected on lower shields.
W107	Unproductive of Web		Argon flooding system. Return to 1/8" cavity. Shields clean but icing problem throughout run.
W108	24.1	403	Repeated run W107. Tested effect of tank argon supply vs. liquid argon for flooding. Oxide collected on shields during run although growth was stable.

GROWTH RUN SUMMARY

RUN	MAX. WIDTH (mm)	TOTAL LENGTH (cm)	DESCRIPTION/RESULT
W109	13.8	168	Argon flooding system; 1/8" gap, short slot. Return to liquid argon supply. Width control difficult because of poor visibility through new quartz tube used to replace one broken after a previous run.
W110	23.3	190	Argon flooding system. Test effects of coil position on growth rate and width control. Lower coil positions caused freezout. Return to higher positions.
W111	16.8	116	Argon flooding system. Further test of coil position. Uppermost positions evaluated. Tendency to extra dendrites at extreme positions. Coil position optimized at mid range for this system.
W112	Unproductive of Web		New venturi, system (2 in. aspirator) tested for first time. Flooding system worked well for growth but surface contamination of web reduced cell efficiency. Reversal of gas flow with venturi should keep shields clean but leave web unaffected. First run to debug flow system; little growth.
W113	18.4	241	Venturi system test. Short growth lid. Small amount of oxide on shield. Initial conditions for web growth identified.
W114	16.1	120	Venturi system test. Test effect of coil position on ability to control web growth. Some oxide collected and inhibited growth.
W115	Unproductive of Web		Venturi system test. Leak in piping caused oxidation of furnace parts. Run aborted.
W116	20.4	196	Venturi system test. Retest of system employed in W115 The lid and shields remained clean. Some tendency for web pullout.

GROWTH RUN SUMMARY

RUN	MAX. WIDTH (mm)	TOTAL LENGTH (cm)	DESCRIPTION/RESULT
W117	19.5	241	Venturi system test. The lid and shields as in W115. Parts remained clean. The coil was raised to improve stability of crystal growth.
W118	22.3	227	Venturi system test. The setup was the same as in W-115. Continue the study of cool position on growth. Lower position. Stable growth.
W119	30.5	294	Venturi system test; set up as in W-115 with the short dogbone lid and the usual shields. Run to verify previous results. The lid and shields remained clean and the crystal grew well. Run terminated by pullout.
W120	25.4	145	Venturi system test, setup as in W-115. Test flow rate in aspirator. The lid and shield remained clean.
W121	22.1	256	Venturi system test, setup as in W-115. Test flow rate in aspirator. The lid and shields remained clean.
W122	23	396	Venturi system test, setup as in W-115. Test argon flow rate. Decreased flow-through aspirators. The shields remained clean to fairly low argon flow. When argon was totally turned off, oxide accumulation slowly initiated.
W123	23	102	Venturi system test; setup as in W-115. There was some oxide collection on the shield.
W124	23.5	218	Venturi system test; setup as in W-115. Test ability to control web width. The shields remained clean.
W125	25.7	202	Venturi system test; setup as in W115. Test ability to control width. There was some oxide collection on the shields, but it did not present a growth hazard. Temperature control was extremely stable.

GROWTH RUN SUMMARY

RUN	MAX. WIDTH (mm)	TOTAL LENGTH (cm)	DESCRIPTION/RESULT
W126	24.3	341	Venturi system test; setup as in W115. Test ability to control web width. There was some oxide growth on the shields. Generally good control.
W127	13.5	90	System test; setup as in W115. Test ability to control width. Trouble with extra dendrites.
W128	28.8	437	Aspirator system test using long dogbone lid to increase web target width. Width control was difficult. Either pullout or third dendrites with this lid, but wider crystals grow easily.
W129	26.8	307	Aspirator system, set up as in W128. There was some oxide collection on the shield.
W130	23.8	394	Aspirator system, using short dogbone lid. There was a significant amount of oxide collection on the shield.
W131	25.1	354	Aspirator system using short dogbone lid. The 2" chimneys have been replaced with 2 3/4" long chimneys to try to improve venturi effect. Both shields and web were clean in this run.

GROWTH RUN SUMMARY

Two types of experiments were carried out in runs W132 to 150: (1) further tests of parameters effecting growth stability with venturi lid configurations (argon flow, slot length, shield arrangement coil position, etc.) and (2) installation and preliminary testing of a melt replenishment system with mechanized feeder. Growth rate set at ∿ 2 cm/min. Target width about 2.5cm.

RUN	MAX. WIDTH (mm)	TOTAL LENGTH (cm)	DESCRIPTION/RESULT
W132	19.6	130	Venturi system test. Evaluate aspirator in conjunction with short dogbone slot plus two shields. Test stability of growth conditions. Problems with oxide on shields and formation of extra dendrites and polygrowth. Temperature stability poor. Conclude need for higher argon flow rate in aspirator to reduce oxide accumulation.
W133	19.0	170	Venturi system test. Rerun of 132 at higher argon flow rate. Clean shields. Temperature fluctuations still large and extra dendrities form. Possible flow rate effects due to aspirator are inducing variations with short slot. Try longer (medium) slot.
W134	27.2	190	Venturi system test. Evaluate medium length growth slot. Also test effect of lower coil position on seeding. Web grew wider without problem of extra dendrites. Elastic bending of widest webs.
W135	24.2	310	Venturi system test. Repeat of W134 to verify improved results. Seeding well controlled; no extra dendrites. Longer crystal pulled out Generally improved growth stability. Lower coil position beneficial.
W136	24.2	320	Venturi system test. Same configuration as W134. Verify repeatability and test effect of system parameters for routine operation. Crystals widen until elastic bending occurs. Difficult to grow long lengths due to pull out but system otherwise very clean and well behaved.

GROWTH RUN SUMMARY

RUN	MAX. WIDTH (mm)	TOTAL LENGTH (cm)	DESCRIPTION/RESULT
W137	27.2	227	Venturi system test. Continue evaluation of medium length growth slot. Crystals widen nicely but bend at width around 27mm. Difficult to sustain long pulls with argon flow at 4.0 setting.
W138	25.1	240	Venturi system test. Continue evaluation of flow rate effects in medium dogbone. Pull out or overthinning of dendrites hinders growth of long,wide crystals. Some temperature fluctuations.
W139	21.8	180	Venturi system test. Evaluation of growth parameters for routine operation, Pull out and choppy dendrites at most coil positions. Conclude need to further reduce argon flow through aspirators.
W140	28.4	250	Venturi system test. Evaluate lower argon flow rate on growth stability with medium length slot. Oxide collected, dendrites remain choppy with tendency for pull out. Conditions somewhat more stable but oxide buildup obscures result.
W141	25.4	270	Venturi system test. Continue evaluation of flow rate effects in aspirators. Again lower flow resulted in oxide collection. Some improvement in stability; dendrites smoother and less tendency to pull out. Conclude need for more data on flow rate effects.
W142	23.6	230	Venturi system test. Attempt to control width at 27mm. Still same tendency to pull out. Elastic bending of wide crystals consistent with results in RE and J furnaces when no aftertrimmer used. Continue flow rate and slot geometry experiments.
W143a	Not Productive of Web		Melt replenishment system test. Install mechanized feeder, feed injection system and modified growth lids. Test pellet injection. Ice grew in liquid when pellets fed. Argon setting of 4.0 kept feed tube clean. Conclude need for more heat to melt pellets during feeding.

GROWTH RUN SUMMARY

RUN	MAX. WIDTH (mm)	TOTAL LENGTH (cm)	DESCRIPTION/RESULT
W143b	24.0	185	Melt replenishment run. Test effects of barrier crucible on ability to grow web. No feed tube. Observe normal growth; no ice. Conclude icing in previous run due to pellet feeding not barrier. Test coil position changes in next runs to control pellet melting.
W144	19.1	125	Melt replenishment run. Try to feed and grow without argon in feed tube. Test rate of pllet melting. Oxide collection blocked feed tube, stopped pellet injection. Growth normal. Conclude need for argon flow to keep feed tube clean.
W145	Not Productive of Web		Melt replenishment system test. Purpose to test whether 0.4 setting of flow will permit feeding. Test time to melt pellets and effect of coil height changes in melting. Feed tube clean. Ice when pellets fed. Could not melt out easily. Raising coil not effective. Some oxide; suspect system leak.
W146	Not Productive of Web		Melt replenishment system test. Evaluate coil position to melt pellets and grow. Moving coil 0.2 in. increased ability to melt pellets without changing growth conditions. Could melt pellets fed at 2 min. intervals. Had icing due to oxide which terminated growth. Performed system leak check. Crack in teflon feed tube. Replaced for next run.
W147	Not Productive of Web		Melt replenishment system test. Purpose to evaluate minimum time to melt pellets. Coil 0.3 inches forward. Check effects of fixing teflon tube. Run clean and oxide free. No icing with pellets fed at 1 min. intervals for 10 min total. Growth difficult with coil displacement so great. Extra dendrites. Can melt pellets but hard to grow. Teflon tube functioned OK.

GROWTH RUN SUMMARY

RUN	MAX. WIDTH (mm)	TOTAL LENGTH (cm)	DESCRIPTION/RESULT
W148	Not Productive of Web		Melt replenishment system test. Added semi cylindrical heat shield behind pellet feed chamber. Evaluate effects on melting and growth. Feed at 20 sec. intervals. Easy to melt with shield. Front too cold and icing occured there. Difficult to grow in asymmetric thermal profile. Conclude shielding over-compensated. Try smaller shield.
W149	10	45	Melt replenishment system test. Evaluate shorter semi cylindrical shield. Floating ice possibly nucleated by oxide. Difficult to grow without ice. Source of icing must be determined.
W150	19	85	Melt replenishment system test. Evaluate higher coil positions to aid pellet melting. Fed and grew web; pellets injected 2 min. intervals. Icing when 1 min intervals used. Higher coil improved growth stability and ability to feed/ Conclude need to repeat experiments with assessment of origin of icing.

8.3 APPENDIX 3

AVERAGED SOLAR CELL DATA FOR WEB CRYSTALS

The tables in this appendix give the averaged solar cell performance for cells fabricated from the crystals listed. Each entry in the table represents the average value for approximately four cells. Measurement conditions were a simulation of an AM1 illumination at a power density of 91.6 mW/cm^2 as determined by a standardized solar cell. The cells were nominally 10x10 mm square (actual area 1.032 cm^2), and had an active area of about 92.5%. The cell efficiency with an anti-reflective coating η_{AR}, is an estimated value based on an average improvement factor of 1.43, typical of the results we obtain in practice with a TiO_2-SiO_2 coating.

RE-Crystals

Crystal	Run	I_{sc} mA	V_{OC} Volt	FF	η_0 %	η_{AR} %	τ_{OCD} µs	ρ Ω-cm	NOTES
RE1-1	WQ2	21.6	.553	.716	8.7	12.4	6.5		
RE1-2	WQ2	21.5	.550	.717	8.9	12.7	8.4		
RE3-6	WQ5	22.2	.560	.741	9.7	13.4	17.4		
RE3-7	WQ3	21.1	.536	.711	8.6	12.2	6.5		
RE7-2	WQ3	22.3	.542	.711	9.2	13.2	19.0		
RE8-3	WQ3	21.3	.532	.722	8.7	2.4	8.0		
RE9-3	WQ3	22.4	.543	.743	9.6	13.7	17.6		
RE10-2	WQ3	22.9	.554	.736	9.9	14.2	29.7		
RE11-4.3	WQ4	21.6	.529	.684	8.3	11.9	6.9		
RE12-3.1	WQ20	22.2	.548	.737	9.5	13.6	11.4	16.5	Std. Matl.
	WQ21	22.9	.535	.730	9.5	13.6	13.8		"
RE12-3.2	WQ6	22.7	.563	.749	10.1	14.4	41.0		
RE14-2.3	WQ4	21.4	.509	.661	7.6	10.9	4.4		
RE15-3.4	WQ4	20.6	.504	.700	7.7	11.0	3.3		
RE18-1.4	WQ4	20.9	.543	.726	8.7	12.4	4.9		
RE18-3.3	WQ4	19.4	.526	.740	8.0	11.4	0.9		
RE23-3.2	WQ5	21.1	.513	.719	8.2	11.7	7.0		
RE24-1.3	WQ6	23.4	.561	.727	10.1	14.4	43.9		
	WQ17	22.5	.553	.729	9.6	13.7	6.5		
RE25-2.2	WQ6	23.6	.553	.743	10.3	14.7	25.0		
RE25-3.1	WQ8	23.2	.569	.752	10.5	15.0	31.9		
RE26-3.3	WQ6	22.8	.564	.732	10.0	14.3	31.4		
RE26-5.2	WQ6	22.1	.545	.737	9.4	13.4	24.7		
RE28-5.1	WQ6	22.8	.567	.749	10.2	14.6	36.1	18	Std. Matl.
	WQ15	20.3	.554	.739	8.8	12.6	21.8		"
	WQ16	22.6	.564	.736	9.9	14.2	29.9		"
	WQ17	22.3	.557	.729	9.6	13.7	21.9		"
RE29-35	WQ7	21.6	.538	.724	8.9	12.7	12.0		
RE30-1.4	WQ7	22.4	.543	.746	9.6	13.7	23.0		
RE30-2.2	WQ7	21.6	.541	.737	9.1	13.0	14.6		
RE32-4.1	WQ8	22.6	.560	.745	10.0	14.3	33.8		
RE32-5.1	WQ8	22.6	.570	.751	10.2	14.6	23.7		Std. Matl
	WQ9	22.1	.564	.743	9.8	14.0	22.3		"
	WQ10	22.4	.566	.731	9.8	14.0	23.4		"
	WQ11	21.8	.555	.737	9.4	13.4	20.7		"
	WQ15	20.7	.548	.728	8.7	12.4	17.2		"
RE33-1.3	WQ8	22.6	.557	.740	9.8	14.0	35.4		
RE33-3.3	WQ8	22.1	.553	.734	9.5	13.6	21.5		
RE33-5.1	WQ8	22.3	.564	.748	10.0	14.3	21.1		
RE34-6.3	WQ8	22.8	.565	.748	10.2	14.6	22.8		

RE CRYSTALS (Cont.)

Crystal	Run	I_{sc} mA	V_{OC} Volt	FF	η_o %	η_{AR} %	τ_{OCD} μs	ρ Ω-cm	NOTES
RE49-3.5	WQ10	20.4	.526	.717	8.1	11.6	5.5		
RE49-4.4	WQ10	20.3	.506	.708	7.7	11.0	3.6		
RE50-1.3	WQ10	20.5	.522	.719	8.1	11.6	3.9		
RE50-2.1	WQ10	20.3	.519	.702	7.8	11.1	2.8		
RE54-1.2	WQ13	23.0	.550	.740	9.9	14.2	19,5		
RE54-1.3	WQ10	22.3	.555	.735	9.6	13.7	22.6		
RE54-2.1	WQ10	21.1	.530	.729	8.6	12.3	9.1		
RE56-3.2	WQ10	22.2	.570	.745	9.9	14.1	28.3		
RE78-3.3	WQ15	21.5	.542	.727	9.0	12.9	14.2		
RE78-4.3	WQ15	21.1	.533	.731	8.7	12.4	9.0		
RE79-1.4	WQ16	22.0	.526	.719	8.8	12.6	5.8	15.2	
RE89-2.3	WQ17	20.9	.532	.707	8.3	11.9	5.5	19.3	
RE91-2.3	WQ18	21.0	.549	.733	8.9	12.7	7.0	7.6	
RE91-3.2	WQ18	20.7	.548	.726	8.7	12.4	5.6	7.9	
RE101-3	WQ21	21.4	.529	.717	8.6	12.3	3.2		
RE102-2.2	WQ20	20.2	.520	.734	8.2	11.7	3.8	9.1	
RE105-3	WQ21	21.7	.540	.747	9.3	13.3	6.2		
RE107-1.3	WQ21	21.4	.539	.742	9.0	12.9	4.6		
RE108-2	WQ21	20.2	.516	.738	8.1	11.6	1.1	10.1	

J-CRYSTALS

Crystal	Run	I_{sc} mA	V_{OC} Volt	FF	η_0 %	η_{AR} %	τ_{OCD} μs	ρ Ω-cm	NOTES
J9-4	WQ1	20.2	.540	.714	8.5	12.2	5.0		
J10-1	WQ1	19.0	.514	.699	7.5	10.7	2.6		
J10-2	WQ1	18.5	.507	.709	7.3	10.4	1.5		
J11-3	WQ1	19.9	.511	.715	7.6	10.9	2.0		
J14-2	WQ1	21.7	.553	.724	9.5	13.6	14.0		
J16-1	WQ1	21.5	.534	.720	8.5	12.2	6.5		
J16-3	WQ1	17.3	.496	.686	6.5	9.2	0.6		
J16-4	WQ1	17.9	.510	.709	7.1	10.0	0.6		
J17-2	WQ1	19.8	.517	.708	7.9	11.3	4.0		
J21-5	WQ1	21.2	.545	.695	8.8	12.6	10.5		
J24-2.2	WQ5	20.3	.518	.704	7.8	11.2	2.1		
J31-3.1	WQ5	20.7	.526	.718	8.3	11.9	5.5		
J34-2.5	WQ5	21.8	.489	.690	7.8	11.2	4.1		
2.4	WQ6	21.8	.535	.724	8.6	12.3	8.0		
J49-1.2	WQ5	20.1	.485	.680	7.0	10.0	1.5		
J53-2.1	WQ8	22.6	.512	.709	8.7	12.4	7.1		
J53-4.4	WQ8	21.9	.516	.714	8.5	12.1	3.9		
J55-2.4	WQ7	21.9	.535	.721	8.9	12.7	10.4		
J55-3.1	WQ7	21.1	.514	.713	8.2	11.7	5.2		
J57-1.2	WQ7	22.3	.546	.728	9.4	13.4	23.7		
J57-2.2	WQ7	21.7	.547	.726	9.1	13.0	17.6		
J57-3.3	WQ7	21.3	.549	.737	9.1	13.0	14.3		
J73-5.1	WQ10	20.4	.514	.710	7.9	11.3	2.4		
J78-3.2	WQ10	21.0	.526	.734	8.6	12.3	3.7		
J80-4.2	WQ11	19.6	.510	.740	7.8	11.2	2.1		
J80-5.1	WQ10	20.1	.518	.725	8.0	11.4	2.6		
J84-4.3	WQ10	22.1	.550	.736	9.5	13.6	12.1		
J84-4.7	WQ10	21.6	.542	.728	9.1	13.0	10.0		
J95-2.2	WQ15	20.9	.532	.739	8.7	12.4	12.5		
J95-3.2	WQ15	19.1	.513	.735	7.6	10.9	3.0		
J96-5.2	WQ15	21.1	.537	.739	8.9	12.7	12.5		
J97-1.3	WQ15	21.2	.548	.743	9.1	13.0	14.7		
J101-1.4	WQ16	22.6	.554	.725	9.6	13.7	21.5	25.0	
J104-2.1	WQ15	21.2	.548	.743	9.1	13.0	22.5		
J106-1.6	WQ15	20.1	.533	.745	8.4	12.0	9.4		
J106-3.4	WQ15	20.3	.522	.741	8.3	11.9	6.0		

J-CRYSTALS (Cont.)

Crystal	Run	I_{sc} mA	V_{OC} Volt	FF	η_o %	η_{AR} %	τ_{OCD} μs	ρ Ω-cm	NOTES
J112-3.3	WQ16	22.1	.546	.697	8.9	12.7	13.7		
J112-4.2	WQ16	22.1	.540	.708	8.9	12.7	13.1		
J112-5.3	WQ16	21.1	.523	.711	8.3	11.9	5.5	24.3	
J115-2.4	WQ16	23.0	.555	.729	9.8	14.0	25.1	20.2	
J115-3.4	WQ16	22.8	.558	.730	9.8	14.0	19.5		
J120-3.1	WQ16	21.6	.542	.725	9.3	13.3	5.8	6.1	
J120-4a	WQ17	20.3	.532	.729	8.4	12.0	2.9	6.3	
J120-4b	WQ17	19.9	.539	.724	8.2	11.7	3.4	6.3	Chem. Pol.
J120-5.2a	WQ17	18.6	.512	.713	7.2	10.3	1.3	6.4	
J120-5.2b	WQ17	18.9	.520	.711	7.4	10.6	1.4	6.4	Chem. Pol.
J122-2.4	WQ18	21.6	.542	.725	9.0	12.9	12.4	20.0	
J131-2.2	WQ20	21.0	.537	.746	8.9	12.7	6.3	8.4	
J131-3.4	WQ20	19.4	.513	.733	7.7	11.0	2.8	9.7	
J133-2.4	WQ20	19.8	.513	.726	7.8	11.2	2.5	10.6	
J134-2.2	WQ20	21.7	.536	.749	9.2	13.2	6.7	10.7	
J140-3.2	WQ21	21.9	.538	.741	9.3	13.3	6.1		

AVERAGED SOLAR CELL CHARACTERISTICS
W-CRYSTALS

Crystal	Run	I_{sc} mA	V_{OC} Volt	FF	η_o %	η_{AR} %	τ_{OCD} µs	ρ Ω-cm	NOTES
W13-1.4	WQ4	20.5	.515	.711	7.9	11.3	2.0		
W19-1.4	WQ5	21.6	.539	.742	9.1	13.0	10.9		
W22-5.5	WQ5	22.2	.540	.749	9.5	13.6	10.9		
W26-2	WQ5	21.7	.543	.746	9.3	13.3	8.0		
W27-5	WQ5	22.1	.539	.751	9.5	13.6	16.3		
W37-2.4	WQ8	22.6	.548	.743	9.7	13.9	27.3		
W37-2.4	WQ8	21.6	.539	.728	8.7	11.4	7.6		Chem. Polished
W41-1.8	WQ8	22.6	.562	.749	10.0	14.3	22.4		Chem. Polished
W41-1.8	WQ7	21.1	.562	.749	9.4	13.4	24.4		
W41-1.12	WQ7	20.8	.559	.745	9.2	13.1	18.2		
W43-1.4	WQ8	22.0	.542	.741	9.4	13.4	14.1		Chem. Polished
W78-1.5	WQ13	20.9	.555	.746	9.1	13.0	13.7		
W87-2.3a	WQ11	20.2	.540	.749	8.6	12.3	2.7		Std. Clean
W87-2.3b	WQ11	20.4	.541	.759	8.9	12.7	2.3		No HF
W87-2.3c	WQ11	20.3	.546	.763	8.9	12.7	2.8		25 µm CP
W88-2.3	WQ11	20.9	.510	.693	7.8	11.2	1.1		"Clean" Web
W90-3.3	WQ11	20.1	.531	.749	8.4	12.0	4.4		
W91-4.8a	WQ11	20.8	.549	.749	9.0	12.9	8.1		Std. Clean
W91-4.8b	WQ11	20.6	.534	.743	8.6	12.3	5.3		No HF
W91-4.8c	WQ11	20.4	.548	.747	8.8	12.6	7.4		25 µm CP
W94-2.1	WQ15	20.9	.541	.754	9.0	12.9	12.7		
W94-3.2	WQ15	20.5	.532	.747	8.6	12.3	8.2		
W96-1	WQ11	11.4	.361	.590	2.6	3.7	-		
W98-1	WQ13	11.8	.374	.601	2.8	4.0	0.9		
W99-1	WQ13	10.3	.313	.545	1.8	2.6	0.5		
W103-2	WQ13	12.9	.363	.588	3.0	4.3	0.5		
W104-2a	WQ13	10.2	.322	.558	1.9	2.7	0.8		Jcn on clean side
W104-2b	WQ13	12.3	.339	.558	2.5	3.6	0.8		" " " "
W105-1a	WQ13	10.2	.315	.547	1.9	2.7	0.4		" " " "
W105-1b	WQ13	11.9	.377	.600	2.9	4.1	0.8		" " " "
W106-1a	WQ13	11.6	.347	.577	2.5	3.6	0.4		" " " "
W106-1b	WQ13	11.2	.332	.563	2.2	3.1	0.4		" " " "
W108-1	WQ13	13.2	.346	.543	2.6	3.7	0.4		
W108-1.3	WQ13	10.8	.330	.558	2.1	3.0	0.4		
W113-1	WQ13	22.3	.563	.738	9.8	14.0	17.9		

W-CRYSTALS (Cont.)

Crystal	Run	I_{sc} mA	V_{OC} Volt	FF	η_0 %	η_{AR} %	τ_{OCD} µs	ρ Ω-cm	NOTES
W114-2	WQ13	22.2	.564	.744	9.8	14.0	24.7		
W116-1	WQ15	19.9	.516	.735	8.0	11.4	2.9		
W116-1	WQ16	21.4	.522	.726	8.6	12.3	3.7		
W118-1.3	WQ16	22.2	.558	.743	9.7	13.9	21.2		
W120-1.2	WQ16	20.9	.534	.714	8.4	12.0	5.3		
W121-1.4	WQ17	20.9	.542	.704	8.4	12.0	5.2		
W122-1.5	WQ16	21.9	.557	.728	9.4	13.4	16.9		
W124-1.4	WQ16	22.2	.558	.725	9.5	13.6	12.4		
W125-1.3	WQ16	22.2	.559	.730	9.6	13.7	13.1		
W126-1.4	WQ17	21.6	.548	.721	9.0	12.9	9.0	12.3	
W126-2.3	WQ17	21.7	.560	.728	9.4	13.4	10.6	11.8	
W128-2.3	WQ17	23.3	.532	.699	9.6	13.7	32.4	787	
W128-3.3	WQ17	22.5	.532	.707	8.6	12.3	20.0	290	
W129-1.4	WQ19	20.3	.528	.716	8.1	11.6	3.9	13.9	
W129-2.3	WQ19	21.3	.538	.723	8.7	12.4	3.9		
W130-1.5	WQ19	20.8	.526	.720	8.3	11.9	5.1	17.7	
W131-2.4	WQ17	21.6	.533	.748	9.4	13.4	11.1	11.0	
W132-2.3	WQ19	21.4	.553	.730	9.5	13.6	7.7	3.2	
W133-3.5	WQ17	22.6	.560	.718	9.6	13.7	15.6	15.6	
W134-1.4	WQ17	22.3	.560	.732	9.7	13.9	18.9	15.9	
W135-1.4	WQ18	21.8	.564	.734	9.5	13.6	18.6	16.0	
W135-2.2	WQ18	21.0	.556	.718	8.9	12.7	8.7	19.0	
W136-1.5	WQ18	21.0	.547	.714	8.7	12.4	9.8	17.0	
W136-2.3	WQ18	21.7	.568	.737	9.6	13.7	16.0	15.0	
W137-1.4	WQ18	21.5	.563	.725	9.3	13.3	15.5	15.0	
W138-1.2	WQ18	21.3	.557	.734	9.2	13.2	13.7	15.0	
W138-2.5	WQ19	20.7	.543	.733	8.7	12.4	6.9	15.0	
W139-2.4	WQ18	21.1	.564	.735	9.3	13.3	7.7	5.5	
W140-1.6	WQ18	21.0	.562	.737	9.2	13.2	7.8	5.5	
W141-1.2	WQ20	21.9	.569	.738	9.7	13.9	6.3	2.8	
W141-1.3	WQ19	19.6	.551	.751	8.6	12.3	2.6	3.0	
W141-2.4	WQ18	20.8	.578	.745	9.5	13.6	7.7	3.2	
W142-3.2	WQ19	21.6	.568	.748	9.7	13.9	7.6	2.9	
W143-1.4	WQ19	21.3	.559	.748	9.4	13.4	11.5	14.1	
W144-1.6	WQ19	20.1	.514	.709	7.8	11.2	4.3	12.8	
W146-1.5	WQ19	20.8	.509	.745	8.3	11.9	3.0	9.8	

W-CRYSTALS (Cont.)

Crystal	Run	I_{sc} mA	V_{OC} Volt	FF	η_o %	η_{AR} %	τ_{OCD} µs	ρ Ω-cm	NOTES
W147-1.3	WQ19	20.5	.532	.746	8.6	12.3	4.6	10.4	
W147-2.4	WQ19	21.4	.551	.677	8.4	12.0	6.5	13.2	
W151-1.2	WQ20	22.2	.543	.735	9.4	13.4	8.6	10.3	FEED
W154-1.4	WQ20	21.6	.542	.722	8.9	12.7	7.5	12.2	FEED
W154-2.3	WQ20	21.4	.531	.734	8.8	12.6	5.4	10.9	FEED
W158-1.1	WQ20	9.0	.313	.558	1.7	2.4	1.0		FLOOD
W164-1.1	WQ23	20.5	.504	.713	7.9	11.3	2.6		
W165-2.2	WQ21	20.7	.522	.729	8.4	12.0	5.7		
W165-2.2	WQ23	20.8	.530	.732	8.5	12.2	4.2	9.4	
W167-2.1	WQ23	20.7	.515	.719	8.1	11.6	3.7	10.2	